

Synthesis, physico-chemical properties and potential applications of colloidal gel particles

By

Reham Mohsen M. Momee

(B.Sc. Pharm. Sci, M.Sc. (Res))

A thesis submitted in partial fulfillment of the University of
Greenwich for the degree of Doctor of Philosophy

March, 2015

Department of Pharmaceutical, Chemical and Environmental Sciences

Faculty of Engineering and Science

University of Greenwich, Medway Campus Chatham

Maritime, Kent ME4 4TB, UK



UNIVERSITY
of
GREENWICH

DECLARATION

“I certify that this work has not been accepted in substance for any degree, and is not concurrently being submitted for any degree other than that of Doctor of Philosophy being studied at the University of Greenwich. I also declare that this work is the result of my own investigations except where otherwise identified by references and that I have not plagiarized the work of others”.

_____ (Reham Mohsen Momee) (Candidate)

_____ Date

_____ (Prof. Martin J. Snowden) (Supervisor)

_____ Date

_____ (Dr. Bruce Alexander) (Supervisor)

_____ Date

Quote

"All that I am or ever hope to be, I owe to my angel Mother."

~ Abraham Lincoln

ABSTRACT**Synthesis, physico-chemical properties and potential applications of colloidal gel particles**

Four new *N-isopropylacrylamide* (NIPAM) based particles have been synthesized and characterized. The first experimental chapter reports that fluorescent poly(*N-isopropylacrylamide-co-5% vinyl cinnamate*) microgels were deposited on different solid surfaces to produce new environmental responsive surfaces. The mass of microgel particles deposited on glass pre-treated with acid, glass pre-treated with base, quartz, stainless steel, gold and Teflon at 25°C and 60°C was determined using fluorescence spectroscopy. The factors affecting the adsorption/desorption of the microgel particles were also investigated. The study shows that the solid surface charge is the most significant factor, followed by that of surface roughness and temperature; meanwhile, the hydrophobicity/hydrophilicity of the surface was the least significant.

Fluorescent temperature/pH responsive p(NIPAM-*co-5% acrylic acid*)-rhodamine B particles were studied. The results confirm the attachment of rhodamine B to the microgel particles. The long chains attached to the particles caused the particles to be poly-dispersed which suggests non-uniformity of particle size and behavior.

Fluorescent temperature/pH responsive poly(*N-isopropylacrylamide-co-5% lucifer yellow*) (p(NIPAM-*co-5% LY*)) microgel particles were tested for toxicity. The particles were negatively charged, mono-dispersed and were approximately 250 nm in diameter at 15°C. The toxicity of different concentrations of p(NIPAM-*co-5% LY*), p(NIPAM) and NIPAM monomer was tested on two cell lines (HeLa and Vero). The results show that the two particles maintain cell viability over 80% (for both cell lines HeLa and Vero) up to a concentration of 3 mg/mL while NIPAM monomer showed a cell viability of over 80% at a concentration equal to or less than 0.3 mg/mL.

Abstract

The fourth experimental chapter explores the opportunity of using microgel particles as an emulsifier. p(NIPAM-co-5% acrylic acid)-hexenol particles with both hydrophilic and hydrophobic groups in their molecular structure were used to stabilize two emulsions (tricaprylin-in-water and hexadecane-in-water). The stability of the emulsions increased with increasing the concentration of the microgel. For the tricaprylin-in-water emulsion, a concentration of 0.3% w/v of the novel microgel particles managed to stabilize the emulsion for a week. In case of the hexadecane emulsion in water, 0.45% w/v microgel particles could show an increase in the emulsion stability and a decrease in the creaming.

Reham Mohsen (B.Sc., M.Sc. (Res), AMRSC)

v

Acknowledgements

ACKNOWLEDGEMENTS

I would like to express my deep thanks, appreciation and gratitude to my supervisors Prof. Martin Snowden and Dr. Bruce Alexander; they have always been very generous with their advice, time, care and support without which my project would not have been possible. I am also very thankful to Prof. John Mitchell, Prof. B. Z. Chowdhry and Dr. Simon Richardson for all their help and support throughout my work.

I was very lucky in having the chance to carry out my project in such an encouraging environment as Medway Sciences, where people are very co-operative and helpful. My thanks to Dr Joanna Thorne, Dr George Vine, Shashi Rudrangi, Ruchir Bhomia, Amanda Lewis and

Dr Vivek Trivedi. I also owe special thanks to Dr. Ian Slipper for his help with the SEM imaging in different parts of my project. Also special thanks to Dr. Samer El-Daher for his continuous support.

My genuine appreciation also goes to my family at MSA University in Cairo, to Mama Nawal El-Degwi, Dr. Khayri Abdel-Hamid, Dr. Heba Osman and Dr. Gehan Safwat for all their care. Special thanks to Dr. Ayman Diab for all his support and care.

I was blessed by being surrounded by very dear friends throughout my project, I appreciate all the care and encouragement that they have always shown to me, and they are: Samer Mouhandes, Bishoy Maher, Aicha Tigani, Mona Mokhatab and Hiba Hamidi.

I would also like to express my deepest thanks and love to my sisters Tasneem and Raghda, my brother in-laws Kareem Rashed and Asser Omar and my best friends Sarah Salah and Islam Mannaa who were always very loving, caring, encouraging and were always there for me whenever I needed them.

My deepest love, thanks and appreciation go to my dear Mum for everything she has done for me, without which I would have achieved nothing in my life. For all her love, care, encouragement, for all her sacrifices and efforts. My prayers are for my Mum's soul to rest in peace and enjoy heaven!

For her who will always be in my heart

For my MUM

For my lovely little family

CONTENTS

Title page	i
Declaration	2
Quote	3
Abstract	4
Acknowledgements	6
Dedication	7
Contents	ix
List of Figures	xvi
List of Tables	xxii
Abbreviations	xxiv
Conferences/Seminars and Publications	xxviii

Chapter One

Introduction

1.1 Microgels	1
1.1.1 <i>N</i> -isopropylacrylamide (NIPAM)	1
1.1.2 Types of microgels	2
1.1.3 Preparation of microgels	3
1.1.3.1 The mechanism of surfactant free emulsion polymerization	4
1.1.3.1.1 Thermal decomposition of the initiator	4
1.1.3.1.2 Initiation	4
1.1.3.1.3 Propagation	5
1.1.3.1.4 Termination	5
1.1.4 Properties of microgels	6
1.1.4.1 Swelling behaviour of microgels	6
1.1.4.1.1 The effect of temperature	6
1.1.4.1.2 The effect of pH	7
1.1.4.2 Electrophoretic mobility	8

Contents

1.1.5 Characterization of microgels	8
1.1.5.1 Dynamic light scattering	9
1.1.6 Colloidal stability and interactions of microgels	11
1.1.6.1 Electrical double layer	13
1.1.6.2 Origins of surface charge	13
1.1.6.3 Double layer interactions	14
1.1.6.4 Stern potential	14
1.1.6.5 Electrophoresis	14
1.1.6.6 DLVO theory	15
1.1.7 Fluorescent microgels	17
1.1.8 Applications of microgels	18
1.1.8.1 Microgels as drug delivery systems	19
1.1.8.1.1 Microgels and oral drug delivery	19
1.1.8.1.2 Microgels as transdermal drug delivery system	20
1.2 Environmental responsive surfaces	20
1.2.1 Deposition of microgels on surfaces	20
1.2.2 Applications of environmental responsive surfaces	22
1.2.2.1 Control of protein adhesion	22
1.3 Context	22
1.4 References	23

Chapter Two

Deposition of fluorescent poly(*N*-isopropylacrylamide-*co*-vinyl cinnamate) particles on solid surfaces: quantitative analysis and the factors affecting it

2.1 Introduction	30
2.1.1 Vinyl cinnamate	32
2.2 Materials and methods	33
2.2.1 Microgel synthesis	33
2.2.2 Microgel characterization	33
2.2.2.1 Dynamic light scattering	33

Contents

2.2.2.2 Fluorescence spectroscopy	34
2.2.3 Slide surface treatments	34
2.2.3.1 Glass and quartz	34
2.2.3.2 Stainless steel	34
2.2.3.3 Gold	34
2.2.3.4 Teflon	35
2.2.4 Surface deposition/desorption of microgel particles	35
2.2.5 Surface characterization	35
2.2.5.1 Fluorescence spectroscopy	35
2.2.5.2 Atomic force microscopy	36
2.2.5.3 Energy dispersive X-ray spectroscopy	36
2.3 Results and discussion	36
2.3.1 Characterization of p(NIPAM-co-5% VC) microgel particles	36
2.3.1.1 Size and VPTT	36
2.3.1.2 Fluorescence spectroscopy	37
2.3.2 Characterization of solid surfaces	38
2.3.2.1 Energy dispersive X-ray spectroscopy	38
2.3.3 Factors affecting the mass of p(NIPAM-co-5% VC) deposited on different surfaces	41
2.3.3.1 Effect of surface charge	41
2.3.3.2 Effect of surface roughness	46
2.3.3.3 Effect of hydrophilicity/hydrophobicity	48
2.3.3.4 Effect of temperature	49
2.4 Conclusions	51
2.5 References	51

Chapter Three Design, synthesis and characterization of poly(*N*-isopropylacrylamide-co-acrylic acid)-ethylene diamine-rhodamine B particles

3.1 Introduction	54
------------------	----

Contents

3.1.1 Rhodamine B	54
3.2 Materials and methods	55
3.2.1 Materials	55
3.2.2 Methods	56
3.2.2.1 Synthesis	56
3.2.2.2 Synthesis of p(NIPAM- <i>co</i> -5% AA)	56
3.2.2.3 Microgel-EDA coupling	56
3.2.2.4 Microgel-EDA-rhodamine B coupling	56
3.2.2.5 Characterization of microgel particles	57
3.2.2.5.1 Dynamic light scattering	57
3.2.2.5.2 Fluorescence spectroscopy	58
3.2.2.5.3 Infrared spectroscopy	58
3.2.2.5.4 Microscopy	58
3.2.2.5.4.1 Scanning electron microscopy	58
3.2.2.5.4.1 Fluorescence microscopy	59
3.3 Results and discussion	59
3.3.1 Particle size analysis	61
3.3.1.1 Effect of temperature	61
3.3.1.2 Effect of pH	63
3.3.2 Electrophoretic mobility	64
3.3.3 Fluorescence spectroscopy	66
3.3.3.1 Effect of addition of rhodamine B	66
3.3.3.2 Effect of temperature	67
3.3.3.3 Effect of pH	70
3.3.4 Infrared spectroscopy	72
3.3.5 Fluorescence microscopy	75
3.3.6 Scanning electron microscopy	75
3.4 Conclusions and future work	77
3.4.1 Conclusions	77
3.4.2 Future work	78
3.5 References	78
Chapter Four Design, synthesis, characterization and toxicity studies of poly(<i>N</i>isopropylacrylamide-<i>co</i>-lucifer yellow) for drug delivery applications	
4.1 Introduction	81

Contents

4.1.1 Lucifer yellow VS	82
4.2 Materials and methods	83
4.2.1 Materials	83
4.2.2 Methods	83
4.2.2.1 Synthesis of p(NIPAM-co-5% LY)	83
4.2.2.2 Dynamic light scattering	83
4.2.2.3 Fluorescence spectroscopy	83
4.2.2.4 Infrared spectroscopy	84
4.2.2.5 Microscopy	84
4.2.2.5.1 Scanning electron microscopy	84
4.2.2.5.2 Fluorescence microscopy	84
4.2.2.6 Toxicity studies	85
4.2.2.6.1 Sterilization	85
4.2.2.6.2 Preparation of media	85
4.2.2.6.3 Cell sub-culturing	85
4.2.2.6.4 Cell seeding	85
4.2.2.6.5 Sample preparation	86
4.2.2.6.6 Cell dosing	86
4.2.2.6.7 MTT assay	87
4.2.2.6.8 Growth curves	87
4.3 Results and discussion	88
4.3.1 Particle size	88
4.3.1.1 Effect of temperature	88
4.3.1.2 Effect of pH	89
4.3.2 Electrophoretic mobility	91
4.3.2.1 Effect of temperature	91
4.3.2.2 Effect of pH	92
4.3.3 Fluorescence spectroscopy	92
4.3.3.1 Effect of addition of lucifer yellow	92
4.3.3.2 Effect of temperature	95
4.3.3.3 Effect of pH	95
4.3.4 Infrared spectroscopy	96
4.3.5 Microscopy	100

Contents

4.3.5.1 Scanning electron microscopy	100
4.3.5.2 Fluorescence microscopy	101
4.3.6 Toxicity studies	101
4.6 Conclusions and future work	109
4.6.1 Conclusions	109
4.6.2 Future work	110
4.7 References	110

Chapter Five

Synthesis, characterization and emulsification properties of poly(*N*-isopropylacrylamide-*co*-acrylic acid)-hexenol

5.1 Introduction	118
5.2 Materials and methods	120
5.2.1 Materials	120
5.2.2 Methods	120
5.2.2.1 Synthesis of p(NIPAM- <i>co</i> -5% AA)-hexenol	120
5.2.2.2 Dynamic light scattering	121
5.2.2.3 Infrared spectroscopy	122
5.2.2.4 Scanning electron microscopy	122
5.2.2.5 Emulsification	122
5.2.2.6 Synthesis of microgelloosomes	122
5.2.2.7 Optical microscopy	123
5.2.2.8 Fluorescence microscopy	123
5.2.2.9 Scanning electron microscopy	123
5.3 Results and discussion	123
5.3.1 Characterization of p(NIPAM- <i>co</i> -5% AA)-hexenol particle	125
5.3.1.1 Particle size	125
5.3.1.1.1 Effect of temperature	125
5.3.1.1.2 Effect of pH	125
5.3.1.2 Electrophoretic mobility	127
5.3.1.2.1 Effect of temperature	127

Contents

5.3.1.2.2 Effect of pH	128
5.3.1.2 Infrared spectroscopy	128
5.3.1.3 Scanning electron microscopy	132
5.3.2 Characterization of the emulsion stabilized by p(NIPAM-co-5% AA)hexenol particles	133
5.3.3 Microgellosomes	138
5.3.3.1 Characterization of microgellosomes	138
5.3.4 Characterization of emulsions stabilized by microgellosomes	140
5.4 Conclusions and future work	141
5.4.1 Conclusions	141
5.4.2 Future work	141
5.5 References	142

Chapter Six

Conclusions and future work

6.1 Conclusions	145
6.2 Future work	149
6.3 References	151

LIST OF FIGURES

Chapter One

Introduction

- Figure 1.1** Structure of NIPAM monomer and structure of the polymer where “*n*” represents the number of monomer units **2**
- Figure 1.2** A schematic of the swelling-deswelling transition of a pH-responsive and a temperature-responsive microgel **3**
- Figure 1.3** Mechanism for the preparation of microgel particles by SFEP **5**
- Figure 1.4** Schematic illustrating the conformational change at the VPTT for thermoresponsive microgels **6**
- Figure 1.5** Schematic illustrating the conformational change at the pK_a of the monomer for pH-responsive microgels **7**
- Figure 1.6** Optical arrangement of the ZS for size measurements **10**
- Figure 1.7** Types of possible emulsion interactions in a colloidal system **12**
- Figure 1.8** A schematic representing the electrical double layer **13**
- Figure 1.9** A schematic representing the DLVO potential energy diagram showing interaction curves; van der Waals attractive forces (V_A) and electrostatic repulsive forces (V_R) and the net total interactive forces (V_T) **16**

Chapter Two Deposition of fluorescent poly(*N-isopropylacrylamide-co-vinyl cinnamate*) particles on solid surfaces: quantitative analysis and the factors affecting it

- Figure 2.1** Molecular structure of vinyl cinnamate **32**
- Figure 2.2** The effect of temperature (heating) on the particle size of p(NIPAM-*co*-5% VC) at pH 3 and 10 across temperature range (15-60°C) **37**
- Figure 2.3** Comparison between the emission spectra of 50 µg/mL of 100 % p(NIPAM) and p(NIPAM-*co*-5% VC) in water, excited at 300 nm at 25°C **39**

List of figures

Figure

Figure 2.4 Calibration curve of p(NIPAM- <i>co</i> -5% VC) in water at 25°C, excited at 300 nm and emitted at 350 nm	
Figure 2.5 Fluorescence intensity of 50 µg/mL 100% p(NIPAM) and p(NIPAM- <i>co</i> -5% VC) in water in response to heating/cooling from 15-60°C, excited at 300 nm and emitted at 350 nm	
Figure 2.6 Energy-dispersive x-ray analysis of stainless steel, quartz, glass and Teflon	40
Figure 2.7 AFM topography and line profile for glass, quartz, stainless steel, gold and Teflon before deposition of microgel particles	47
	50
60°C	

Chapter Three

Design, synthesis and characterization of poly(*N*-isopropylacrylamide-*co*-acrylic acid)-ethylene diamine-rhodamine B particles

Figure 3.1 The molecular structure of rhodamine B	55
Figure 3.2 The suggested molecular structure of p(NIPAM- <i>co</i> -5% AA)-EDA-RhB	60
Figure 3.3 The effect of temperature on the particle size of p(NIPAM- <i>co</i> -5% AA), p(NIPAM- <i>co</i> -5% AA)-EDA and p(NIPAM- <i>co</i> -5% AA)-EDA-RhB at pH 11.5	62
Figure 3.4 The effect of temperature on the electrophoretic mobility of p(NIPAM- <i>co</i> -5% AA)p(NIPAM- <i>co</i> -5% AA)-EDA and p(NIPAM- <i>co</i> -5% AA)-EDA-RhB at pH 11.5	65
Figure 3.5 The fluorescence spectra of 0.2 µg/mL p(NIPAM- <i>co</i> -5% AA)-EDA, p(NIPAM-	67

List of figures

Figure 2.8 AFM images of p(NIPAM-*co*-5% VC) particles deposited on glass at 25°C and at *co*-

5% AA)-EDA-RhB and RhB excited at 540 nm at 25°C at pH 6.5

List of figures

Figure

- Figure 3.6** Fluorescence emission spectra of 0.2 µg/mL p(NIPAM-*co*-5% AA)-EDA-RhB at, pH 2, pH 6.5 and pH 11.5 and 0.2 µg/mL RhB excited at 540 nm at pH 2, pH 6.5 and 11.5 at 25°C, 35°C and 45°C **69**
- 3.7** Fluorescence of 0.2 µg/mL RhB excited at 540 nm at 25°C at pH 2.5, 6.5 and 11.5 **70**
- Figure 3.8** Fluorescence of 0.2 µg/mL p(NIPAM-*co*-5% AA)-EDA-RhB excited at 540 nm at 25°C at pH 2.5, 6.5 and 11.5 **70**
- Figure 3.9** FT-IR spectra of p(NIPAM-*co*-5% AA)-EDA-RhB, p(NIPAM-*co*-5% AA)-EDA, p(NIPAM-*co*-5% AA) and RhB **74**
- Figure 3.10** Fluorescence microscopy images of p(NIPAM-*co*-5% AA)-EDA-RhB at 25°C **75**
- Figure 3.11** SEM images of p(NIPAM-*co*-5% AA), p(NIPAM-*co*-5% AA)-EDA and p(NIPAM-*co*-5% AA)-EDA-RhB at 25°C **76**

Chapter Four

Design, synthesis, characterization and toxicity studies of poly(*N*-isopropylacrylamide-*co*-lucifer yellow) for drug delivery applications

- Figure 4.1** Molecular structure of lucifer yellow VS dilithium salt **82**
- Figure 4.2** Structure and organization of the 96 well plates used for toxicity studies. **87**
- Figure 4.3** The effect of temperature on the particle size of p(NIPAM-*co*-5% LY) at pH 7 across temperature range (15-60°C) **88**
- Figure 4.4** The effect of pH on the hydrodynamic diameter of p(NIPAM-*co*-5% LY) at 25°C **89**
- Figure 4.5** The effect of temperature (heating) across a range (15-60°C) on the electrophoretic mobility of p(NIPAM-*co*-5% LY) and p(NIPAM) in 10⁻⁴ M NaCl at pH 7 **91**
- Figure 4.6** The effect of pH on the electrophoretic mobility of p(NIPAM-*co*-5% LY) in 1 x 10⁻⁴ M NaCl at 25°C **92**

List of figures

- Figure 4.7** Fluorescence spectra of 0.01 $\mu\text{g/mL}$ LY, 0.2 $\mu\text{g/mL}$ p(NIPAM-co-5% LY) and 0.2 $\mu\text{g/mL}$ p(NIPAM) excited at 430 nm at pH 7 at temperatures 25°C and 45°C **94**
- Figure 4.8** Fluorescence spectra of 0.01 $\mu\text{g/mL}$ LY, 0.2 $\mu\text{g/mL}$ p(NIPAM-co-5% LY) and 0.2 $\mu\text{g/mL}$ p(NIPAM) excited at 430 nm at 25°C at pH 3 and 7 **94**
- Figure 4.9** FT-IR spectra of p(NIPAM), p(NIPAM-co-5% LY) and LY in the region (3800-1400 cm^{-1}) **98**

List of figures

Figure 4.10 FT-IR spectra of p(NIPAM), p(NIPAM-co-5% LY) and LY in the region (1300-750 cm ⁻¹)	99
Figure 4.11 SEM pictures of p(NIPAM-co-5% LY) at pH 3	100
Figure 4.12 Fluorescence microscopy pictures of 2 µg/mL p(NIPAM-co-5% LY)	101
Figure 4.13 Growth curves of HeLa cells and Vero cells	102
Figure 4.14 percentage cell viability (after 72 hours) versus log concentration (across conc. range of 0.03 µg/mL to 3000 µg/mL) of dextran, NIPAM monomer, p(NIPAM), p(NIPAMco-5% LY) and PEI on 1 x 10 ⁴ HeLa cell/mL	102
Figure 4.15 percentage cell viability (after 72 hours) versus log concentration (across conc. range of 0.03 µg/mL to 3000 µg/mL) of dextran, NIPAM monomer, p(NIPAM), p(NIPAMco-5% LY) and PEI on 1 x 10 ⁴ Vero cell/mL	103

Chapter Five

Synthesis, characterization and emulsification properties of poly(*N*-isopropylacrylamide-co-acrylic acid)-hexenol

Figure 5.1 The suggested structure of p(NIPAM-co-5% AA)-hexenol	124
Figure 5.2 The hydrodynamic diameter of p(NIPAM-co-5% AA)-hexenol at pH 7 in response to increasing the temperature (15-55°C)	126
Figure 5.3 The hydrodynamic diameter of p(NIPAM-co-5% AA)-hexenol at 25°C in response to pH change	126
Figure 5.4 The electrophoretic mobility of p(NIPAM-co-5% AA)-hexenol in response to temperature change (15-55°C) at pH 7	127
Figure 5.5 The electrophoretic mobility of p(NIPAM-co-5% AA)-hexenol at 25°C in response to pH change	128
Figure 5.6 The FT-IR spectra of p(NIPAM-co-5% AA)-hexenol, p(NIPAM-co-5% AA) and 5 hexen-1-ol	131

Figure 5.7 SEM pictures of p(NIPAM- <i>co</i> -5% AA)-hexenol at 25°C with a magnification of (a) x25,000 and (b) x35,000	132
5.8 Emulsions of tricaprylin/water mixtures in the presence of different concentrations of p(NIPAM- <i>co</i> -5% AA)-hexenol, different concentrations (w/v) of microgel dispersions before emulsification, samples just after emulsification and samples after 1 week of emulsification	134
Figure 5.9 Emulsions of hexadecane/water mixtures in presence of different concentrations of p(NIPAM- <i>co</i> -5% AA)- hexenol, samples after emulsification	135
Figure 5.10 Optical and fluorescent microscopy images of tricaprylin/water emulsion in the presence of 0.1, 0.2, 0.25 and 0.3% w/v of p(NIPAM- <i>co</i> -5% AA)- hexenol.	136
Figure 5.11 Optical and fluorescent microscopy images of hexadecane/water emulsion in presence of 0.2, 0.3, 0.4 and 0.45% w/v of p(NIPAM- <i>co</i> -5% AA)- hexenol	137
Figure 5.12 Representation of the molecular structure of microgellosomes	139
Figure 5.13 SEM image of microgellosomes formed by polymerizing p(NIPAM- <i>co</i> -5% AA)-hexenol	140
Figure 5.14 Optical microscopy image of microgellosomes (0.1 w/v) stabilized emulsion	140
List of tables	

LIST OF TABLES

Chapter One

Introduction

Table 1.1 Characterization methods for microgels	8
---	----------

Figure

Chapter Two

Deposition of fluorescent poly(*N-isopropylacrylamide-co-vinyl cinnamate*) particles on solid surfaces: quantitative analysis and the factors affecting it

Table 2.1 Expected and measured characteristics of solid surfaces before deposition of microgel particles (surface charge, relative hydrophobicity and surface roughness), and microgel particle mass deposited and % desorbed from slide surfaces at 25°C and 60°C	42
Table 2.2 Comparison between the surface roughness averages of glass, quartz, stainless steel, gold and Teflon coated with p(NIPAM- <i>co</i> -5% VC) microgel particles at 25°C and 60°C	50

Chapter Three

Design, synthesis and characterization of poly(*N-isopropylacrylamide-co-acrylic acid*)-ethylene diamine-rhodamine B particles

Table 3.1 Particle size and polydispersity index values of p(NIPAM- <i>co</i> -5% AA), p(NIPAM- <i>co</i> -5% AA)-EDA and p(NIPAM- <i>co</i> -5% AA)-EDA-RhB	62
Table 3.2 The fluorescence intensity of 0.2 µg/mL p(NIPAM- <i>co</i> -5% AA)-EDA, p(NIPAM- <i>co</i> -5% AA)-EDA-RhB and RhB excited at 540 nm at 25°C at pH 6.5	66
Table 3.3 FT-IR bands of p(NIPAM- <i>co</i> -5% AA) and p(NIPAM- <i>co</i> -5% AA)-EDA-RhB	72
Table 3.4 FT-IR bands of RhB	73

Chapter Four Design, synthesis, characterization and toxicity studies of poly(*N*-isopropylacrylamide-co-lucifer yellow) for drug delivery applications

Table 4.1 The design of plates A and B and the concentrations used for the toxicity testing of dextran, NIPAM monomer, p(NIPAM), p(NIPAM-co-5% LY) and poly(ethylenimine) (PEI)	
Table 4.2 FT-IR bands values of p(NIPAM) and p(NIPAM-co-5% LY)	96
Table 4.3 FT-IR bands values of LY	97
Table 4.4 LC ₅₀ of dextran, NIPAM monomer, p(NIPAM), p(NIPAM-co-5% LY) and PEI on HeLa and Vero cells	103

Chapter Five Synthesis, characterization and emulsification properties of poly(*N*-isopropylacrylamide-co-acrylic acid)-hexenol

Table 5.1 FT-IR bands of p(NIPAM-co-5% AA) and p(NIPAM-co-5% AA) hexenol	129
Table 5.2 FT-IR bands of 5 hexen-1-ol	130

ABBREVIATIONS

Abbreviations

Symbol	Description
AA	Acrylic acid
AFM	Atomic force microscopy
ATR	Attenuated total reflection
BA	<i>N,N'</i> -methylenebisacrylamide
BMA	Butyl methacrylate
CPS	Counts per second
D_h	Hydrodynamic diameter
DLS	Dynamic light scattering
DMAPAAm	<i>N,N'</i> -dimethylaminopropylacrylamide
DMEM	Dulbecco's Modified Eagle Medium
DMSO	Dimethyl sulphoxide
EDA	Ethylene diamine
EDC	1-ethyl-3-(3-dimethyl aminopropyl) carbodiimide
EDX	Energy dispersive X-ray spectroscopy
FBS	Fetal Bovine Serum
FITC	Fluorescein <i>is</i> o thiocyanate filter
FITC-BSA	Flourescein <i>is</i> o thiocyanate bovine serum albumin
FPBA	2-aminomethyl-5-fluorophenylboronic acid
GPC	Gel permeation chromatography
HeLa CCL2	Human cervical epithelial cells
Hex	Hexenol
HPLC	High performance liquid chromatography
HSDSC	High sensitivity differential scanning calorimetry
IR	Infrared spectroscopy
KPS	Potassium persulphate
kV	kilovolt
LY	Lucifer yellow
MEM	Minimum essential medium
MeOH	Methanol

Abbreviations

MES	4-Morpholineethanesulfonic acid monohydrate
MTT	(3-(4,5-Dimethylthiazol-2-yl)-2,5-diphenyltetrazolium bromide
NIPAM	<i>N</i> -isopropylacrylamide
NMR	Nuclear magnetic resonance
p(NIPAM)	Poly(<i>N</i> -isopropylacrylamide)
p(NIPAM-co-5% AA)	Poly(<i>N</i> -isopropylacrylamide-co-5% acrylic acid)
p(NIPAM-co-5% LY)	Poly(<i>N</i> -isopropylacrylamide-co-5% lucifer yellow)
p(NIPAM-co-5% VC)	Poly(<i>N</i> -isopropylacrylamide-co-5% vinyl cinnamate)
p(NIPAM-co-HDT)	Poly(<i>N</i> -isopropylacrylamide-co-hexadecanethiol)
PBS	Phosphate buffered saline
PCS	Photon correlation spectroscopy
PdI	Polydispersity index
PEI	Branched poly(ethylenimine)
p <i>K</i> _a	Acid dissociation constant
PSG	Penicillin-Streptomycin-Glutamine
PTFE	Poly(tetrafluoroethene)
PZC	Point of zero charge
RfD	Reference dose
RhB	Rhodamine B
SANS	Small-angle neutron scattering
SEM	Scanning electron microscope
SFEP	Surfactant-free emulsion polymerization
SLS	Static light scattering
VC	Vinyl cinnamate
Vero CCL-81	Normal kidney of <i>Cercopithecus aethiops</i>
VPTT	Volume phase transition temperature
w/v	Weight per volume
w/w	Weight per weight
λ	Wavelength

Abbreviations

λ_{ex}

Excitation wavelength

λ_{em}

Emission wavelength

CONFERENCES/SEMINARS AND PUBLICATIONS

CONFERENCES/SEMINARS

- Title:** Design, synthesis, characterization and suggested application of novel poly(*N*-isopropylacrylamide)-*co*-5% lucifer yellow particles
- Conference:** University of Greenwich – American Academy of Pharmaceutical Sciences Student Chapter Conference 16th -18th July, 2014.
- Type:** Poster Presentation
-
- Title:** Temperature/pH sensitive fluorescent nanogels for drug delivery applications
- Conference:** Third Euro-India International Conference on Nanomedicine and Tissue Engineering (ICNT 2013) Kottayam, Kerala, India, August 9th 11th, 2013.
- Type:** Oral Presentation (**Invited speaker**)
-
- Title:** Deposition of fluorescent NIPAM based nanoparticles on different solid surfaces; quantitative analysis and the factors affecting it
- Conference:** University of Greenwich- AAPS Student Chapter Conference, March 25th, 2013.
- Type:** Poster Presentation

Conferences/Seminars and publications

- Title:** pH induced flocculation of microgel particles
- Conference:** UK Polymer Colloids Forum, 14th UKPCF Annual Meeting, University of Hull
14th-16th of September 2009.
- Type:** Poster Presentation

Publications

- Title:** Characterization of thermo and pH responsive NIPAM based microgels and their membrane blocking potential
- Authors:** Reham Mohsen, George J. Vine, Natasa Majcen, Bruce D. Alexander, Martin J. Snowden
- Journal:** Colloids and Surfaces A: Physicochemical and Engineering Aspects, 2013, 428, 53-59.
-
- Title:** Deposition of fluorescent NIPAM-based nanoparticles on solid surfaces: quantitative analysis and the factors affecting it
- Authors:** Reham Mohsen, Joanna B. Thorne, Bruce D. Alexander and Martin J. Snowden
- Journal:** Colloids and Surfaces A: Physicochemical and Engineering Aspects, 2014, 457, 107-115.
-
- Title:** Design, synthesis, characterization and toxicity studies of poly(*N*isopropylacrylamide-*co*-lucifer yellow) particles for drug delivery applications
- Authors:** Reham Mohsen, Bruce D. Alexander, Simon C.W. Richardson, John C. Mitchell, George J. Vine, Ayman A. Diab and Martin J. Snowden
- Status:** To be submitted.
-
- Title:** Synthesis, characterization and emulsification properties of poly(*N*-isopropylacrylamide)-*co*-5% AA-hexenol
- Authors:** Reham Mohsen, Anupam Das, Bruce D. Alexander, Vesko Puavnov and Martin J. Snowden

Conferences/Seminars and publications

Status: Langmuir, 2015, to be submitted.

Title: Design, synthesis and characterization of fluorescent poly(*N*isopropylacrylamide)-*co*-acrylic acid-rhodamine B particles

Authors: Reham Mohsen, Blerina Shkodra, Bruce D. Alexander, John C. Mitchell and Martin J. Snowden

Status: Polymer, 2015, in preparation.

Chapter One Introduction

1.1 Microgels

A microgel is defined as “a cross linked latex particle which is swollen by a good solvent”. The term microgel was first introduced by Baker but microgels were first prepared by Staudinger and Husmann (1). Microgels are considered as a class of smart materials, as they are highly sensitive to the environmental changes around them, which cause them to dramatically change their physico-chemical properties (*e.g.* particle size). This is facilitated by the high surface-area-to-volume ratio of the microgels which make it easier for an environmental stimulus, such as the pH or temperature, to affect the particles. The high surface-area-to volume ratio also contributes to the biomedical and industrial importance of this class of smart materials (2).

Microgels have the same polymer chemistry as bulk gels, but their different physical molecular arrangement (discrete gel-like particles) causes some differences such as the bulk viscosity characteristics, the surface-area-to-volume ratios and the speed at which conformational changes occur. Microgels undergo conformational changes in seconds, while other kinds of gels like hydrogels may take hours or even days (2).

1.1.1 *N-isopropylacrylamide* (NIPAM)

There are many monomers used for the preparation of thermo-responsive microgels of which the most commonly used is NIPAM. The lower critical solution temperature (LCST) for linear poly(*N-isopropylacrylamide*) (p(NIPAM)) chains in water is 32°C; accordingly the polymer swells when below 32°C and de-swells when the temperature further increases (3). The structure of NIPAM (Figure 1.1) and its properties are similar to acrylamide (4). NIPAM has a hydrophilic amide group and a hydrophobic *isopropyl* group.

p(NIPAM) microgels were first prepared in 1986 by Pelton and Chibante (5), using a surfactant-free emulsion polymerization (SFEP) process by which they produced a monodisperse microgel which was found to have a thermo-reversible conformational transition in water at around 34°C.

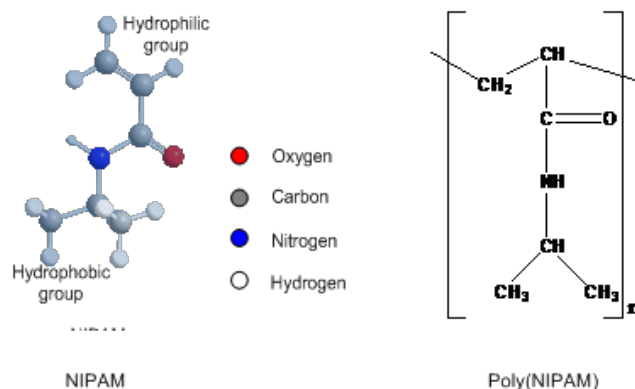


Figure 1.1 Structure of NIPAM monomer (left) and structure of the polymer (right) where “n” represents the number of monomer units

When NIPAM molecules are heated in presence of an initiator and a cross linker, they undergo cross-linking to give a temperature sensitive gel network which shrinks by expelling water within a narrow temperature range. The temperature at which the gel acquires the largest and sharpest swellability changes is called the volume phase transition temperature (VPTT). Even for a temperature sensitive microgel, the temperature is not the only factor that affects swellability; other factors include the type of microgel, the hydrophilicity of the particle, degree of cross-linking and monomer and/or co-monomer composition and concentration.

Being hydrophilic in nature, p(NIPAM) is completely soluble and swells in aqueous solvents when the temperature is below 34°C (VPTT), while above it, the polymer phase separates.

1.1.2 Types of microgels

Microgels can be composed of one monomer (in addition to the initiator and cross linker), and accordingly, it acquires the properties of this monomer only. p(NIPAM) is the most common homo-polymer microgel but other examples include *N*-ethylacrylamide (6) and *N*-ethylmethacrylamide (7).

Also, a small amount of a co-polymer can be incorporated in the microgel (1-5 % w/w of the main monomer), the resultant microgel is highly affected by the co-polymer properties. This makes it possible to control and alter the properties of microgels according to the properties of the co-monomer used. VPTT modifications of temperature-sensitive microgels can be achieved using co-monomers with different hydrophobicities (8-11).

Furthermore, microgels sensitive to more than one stimulus can be prepared using different co-polymers; *e.g.* the addition of a pH sensitive (ionisable) co-monomer to a temperature sensitive monomer, results in a polymer sensitive to both temperature and pH (12,13).

A p(NIPAM) microgel co-polymerized with acrylic acid displays volume change in response to both temperature and pH. When the pH is below the pK_a of acrylic acid, the microgel particles acquire a compact structure, while when the pH is above the pK_a of acrylic acid, the microgel particles swell (Figure 1.2).

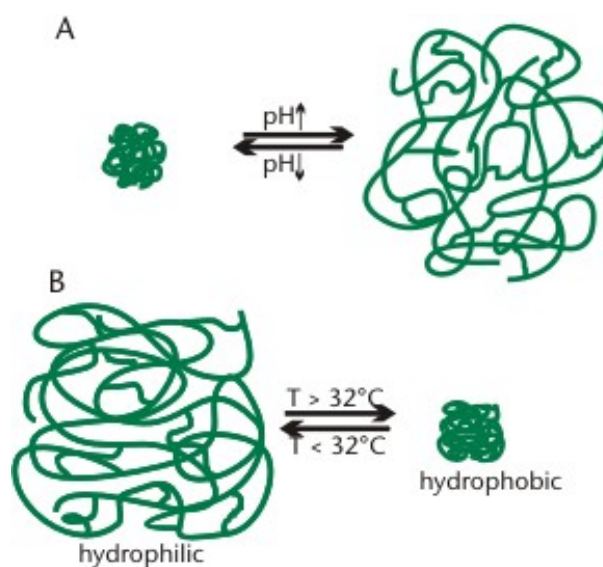


Figure 1.2 A schematic of the swelling-deswelling transition of a pH-responsive (a) and a temperature-responsive (b) microgel

1.1.3 Preparation of microgels

Several methods have been reported for the preparation of microgels, these include emulsion polymerization (10, 11), inverse emulsion polymerization (14), living free radical polymerization (15) and radiation methods (16, 17), of which the most widely used is the emulsion polymerization technique (18, 19). Emulsion polymerization can either be carried out using a surfactant (conventional emulsion polymerization, EP) or without surfactant (surfactant-free emulsion polymerization, SFEP), also called precipitation polymerization.

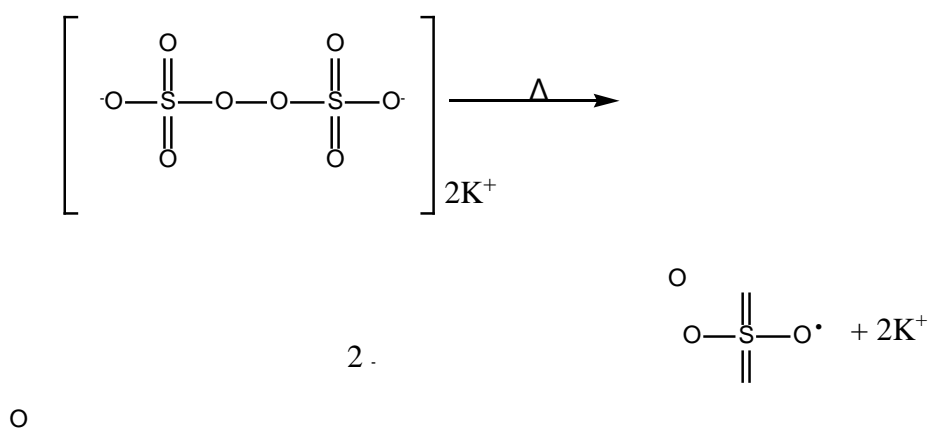
To prepare a microgel with very small particles (a particle diameter less than 150 nm), the conventional emulsion polymerization technique (EP) can be used; this is because the surfactant inhibits the particle growth. The disadvantage of this technique is that it is very hard to remove the remaining unreacted surfactant molecules.

For larger particle sizes (up to 1000 nm), SFEP is the method of choice (20). Conditions for applying this method include the use of continuous phase of a high dielectric constant (*e.g.* water) and the addition of ionic initiators (*e.g.* potassium persulphate $K_2S_2O_8$). The extensive use of SFEP is due to its advantages, of which the most important is avoiding the risk of surfactant contamination (the main disadvantage of the EP), this is because the polymerization reaction yields charged polymer chains that are surface active which stabilize the growing particles without the need to use surfactants. Also this method is characterized by a high product yield (around 95 %) of monodispersed particles that are regular in both size and composition. The main disadvantage of this method is that it produces dilute dispersions (low particle concentration).

1.1.3.1 The mechanism of surfactant free emulsion polymerization

1.1.3.1.1 Thermal decomposition of the initiator

When heated, the ionic initiator is thermally decomposed to form ionic water-soluble free radicals. Metal persulphates are of the most commonly used sources of free radicals in aqueous solutions (21). Potassium and ammonium salts for example are used to initiate polymerization in aqueous and emulsion systems. Equation 1.1 illustrates the thermal decomposition mechanism of persulphates.



Equation 1.1

1.1.3.1.2 Initiation

The ionic radicals react with the monomer molecules forming monomeric radicals. Equation 1.2 shows the reaction between the persulphate radical and the monomer M.



Equation 1.2

1.1.3.1.3 Propagation

Further reaction of the formed monomeric radicals with other monomer molecules leads to the formation of surface active oligomeric radicals. These are characterized by having a polar head and a non-polar tail as shown in Equation 1.3.



The solubilization of oligomeric radicals in water continues till the chain length exceeds the solubility limit of the solvent. The oligomer chains aggregate with each other and hence increase the surface charge and form small particles. The formed particles contain hydrophobic non-polar chains in the center and polar head groups to the outside. The polar heads on the particles surface mainly originate from the initiator and stabilize the dispersion by the electrostatic repulsion forces between the surface charged groups. The particles grow more and more due to the adsorption of further monomers or oligomers, causing particle swelling.

1.1.3.1.4 Termination

Reaction termination takes place when the monomers are totally depleted or when another free radical reacts with the growing particle and terminates the reaction. SFEP technique is characterized by short nucleation period (minutes) the production of monodispersed particles regular in both size and composition (18, 22). Figure 1.3 shows the mechanism of the synthesis of microgel particles using SFEP.

Synthesis

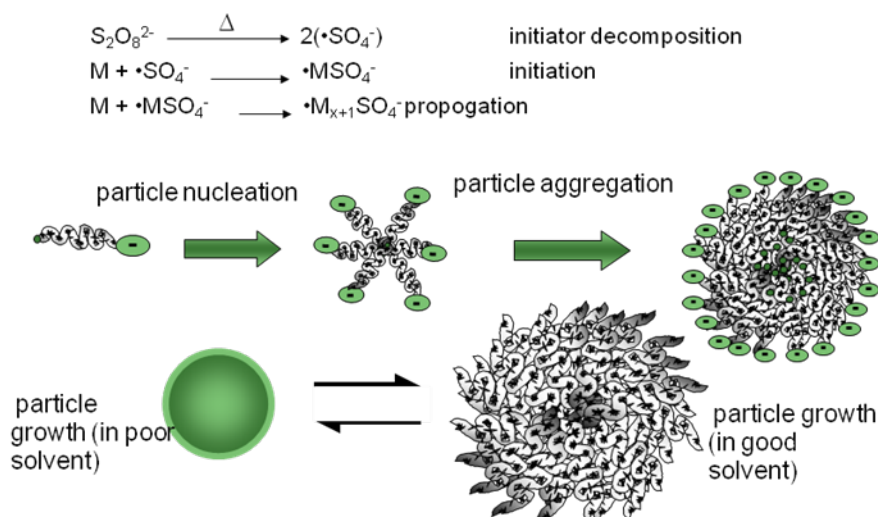


Figure 1.3 Mechanism for the preparation of microgel particles by SFEP where M represents a monomer (18)
1.1.4 Properties of microgels

1.1.4.1 Swelling behaviour of microgels

As swelling-deswelling is the most characteristic property of the microgels, it also tends to be the most important one (23). There are many factors that affect the swelling properties of microgels such as the cross-linker. Highly cross-linked microgels acquire a tighter and less swelled structure than the similar microgels with lower cross-linking ratio (the ratio of the moles of cross-linking agent to the moles of the polymer repeating units) (23). Furthermore, microgels with a high cross-linker concentration will undergo more rapid conformational changes because the polymer chains are close to each other, which will allow quicker collapse. Microgels with low cross-linker concentrations have properties similar to those of the high molecular weight polymers.

Another factor that affects the swelling of the microgels is the chemical structure of the polymer. In water or aqueous solvents, a polymer with more hydrophilic groups (such as p(NIPAM), Fig. 1.1) swells more than that with hydrophobic ones. On the other hand, microgels with hydrophobic groups (*e.g.* isopropyl methacrylate (24)) collapse in aqueous solvents and hence swell less than the microgels with hydrophilic ones (*e.g.* acrylic acid (1)).

1.1.4.1.1 The effect of temperature

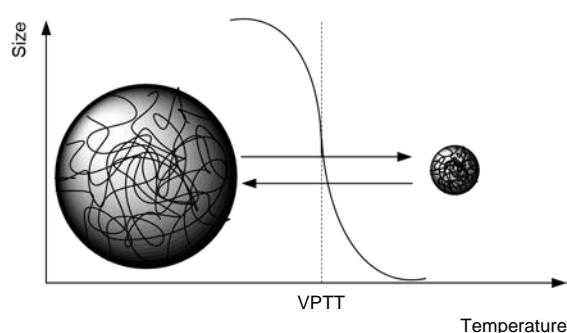


Figure 1.4 Schematic illustrating the conformational change at the VPTT for thermo-responsive microgels (3)

Microgels are temperature sensitive when the main monomer forming it exhibits temperature sensitive behavior in a specific solvent. The best known temperature-sensitive polymer is p(NIPAM) whose particles are sponge like. It swells and deswells according to temperature changes of the surrounding media. The temperature where the highest size change occurs (VPTT) of the microgel can be modulated by the addition of co-monomers of different

hydrophilic/hydrophobic properties. Accordingly, co-polymer microgels can acquire a range of VPTT values dependent on the type of co-monomer incorporated (10).

Below the VPTT, both the polymer-polymer and polymer-solvent interactions are weak, the interstitial spaces between the microgel particles are filled with water and the microgel particles are swollen {Pelton, 1986}. Above the VPTT, the polymer-polymer interactions become stronger than the polymer-solvent ones and so the polymer particles tend to collapse (Figure 1.4). When the temperature is increased, the polymer chains tend to interact with each other rather than with the solvent molecules and the hydrogen bonding between the polymer chains and the solvent molecules is reduced, this causes most of the solvent entrapped within the interstitial spaces of the polymer matrix to be expelled, forming hard sphere particles and the microgel tends to shrink. During this collapsed state, the particles are dispersed; this is due to the repulsion between the similar ionic charges on the particle surface caused by the ionic initiators. This process (deswelling) is reversible, so if the temperature goes back below the VPTT, the interactions between the polymer and the solvent improve and the microgel swells again {Pelton, 1986}.

1.1.4.1.2 The effect of pH

Microgels sensitive to both pH and temperature can be prepared by incorporating acidic or basic co-monomers into p(NIPAM) microgel matrix. An example of this is the p(NIPAM-co-acrylic acid) microgel (18). The pH conformational transition point depends upon the pK_a of the functional groups incorporated. At pH values below the pK_a of acrylic acid, the microgel particles are in a collapsed state but when the pH is more than the pK_a , the electrostatic repulsion forces between the ionized acrylic acid molecules within the polymer matrix cause the gel to acquire a more swollen configuration (Figure 1.5).

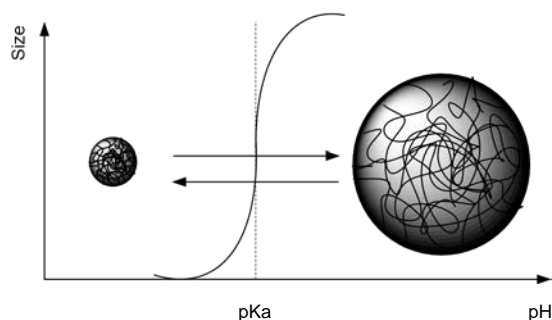


Figure 1.5 Schematic illustrating the conformational change at the pK_a of the monomer for pH-responsive microgels (25)

1.1.4.2 Electrophoretic mobility

The electrical properties of microgels are induced by the surface charge of the particle, which is caused by the initiator. The surface charge arises during the microgel synthesis, the formed oligomers have hydrophilic heads and hydrophobic tails $\bullet M_{x+1}SO_4^-$ (Figure 1.3). These oligomers then aggregate together forming micelles and since the solvent is water, the hydrophilic groups are on the surface (in contact with the solvent) while the hydrophobic ones are inside. The electrophoretic mobility of a microgel is temperature dependant. In the swollen state, a microgel particle has an electrophoretic mobility close to zero and increases by heating as the temperature reaches the VPTT (26).

1.1.5 Characterization of microgels

Several methods have been reported for the characterization of microgels (summarized in Table 1.1).

Table 1.1 Characterization methods of microgels (2)

TECHNIQUE	PARAMETER	REFERENCES
Dynamic light scattering (DLS)/Photon correlation spectroscopy (PCS)	Hydrodynamic diameter and polydispersity	(23, 27-30)
Static light scattering (SLS)	Particle molecular weight	(31, 32)
Gel permeation chromatography (GPC)	Molecular weight and polydispersity	(33)
Nuclear magnetic resonance (NMR)	Internal structure	(24, 35)
Transmission electron microscopy (TEM), Scanning electron microscopy (SEM)	Visual assessment of the particles, measuring of particles diameter	(14, 27, 30)
UV-vis spectroscopy	Determination of VPTT, monitoring stability/flocculation	(24, 35, 36)
Small-angle neutron scattering (SANS)	Particle composition	(3, 27, 30)
High sensitivity differential scanning calorimetry (HSDSC)	Thermodynamic properties, determination of VPTT	(37)

1.1.5.1 Dynamic light scattering

Dynamic light scattering (DLS) is widely used in the colloidal dispersion studies due to its ability to estimate the size, interactions and electrophoretic mobility of the particles (25).

When a beam of light is directed at a colloidal sample, some of the light is absorbed, while the rest either pass through the sample or is scattered by it. The light scattered by the colloidal microgel particles is the cause of the opaque, milky nature of these dispersions. When an incident beam of light hits the sample, it induces periodic oscillations in its electric field. These oscillations act as secondary sources for the emission of scattered light. The intensity of the scattered light increases by increasing the difference between the refractive index of the dispersed particles and that of the dispersion medium (25).

Dynamic light scattering is mainly used for measuring the hydrodynamic diameter of submicron particles such as microgels (24, 38). It is also used for monitoring the conformational behaviour of the microgel particles in different solvents as a function of temperature. DLS measures the Brownian motion of the particles in the dispersion and then relates it to the size of the particles. Brownian motion can be defined as “the random movement of particles due to the bombardment by the solvent molecules surrounding them.” For systems where the particles undergo Brownian motion, the intensity of the scattered light fluctuates when detected by a suitable optical arrangement. The rate of fluctuation of the intensity of the dispersed light depends upon the size of the particles. Using the rate of the fluctuation of the intensity of the dispersed light, the particle diffusion co-efficient can be calculated (40). Using the Stokes-Einstein equation, the particle diameter can be calculated using the diffusion coefficient of spherical particles. This can be achieved using dilute dispersions, where the interactions between the particles can be neglected (25). The relation between the diffusion coefficient of a suspended material and the frictional coefficient of its particles is given by Einstein’s law of diffusion:

$$Df = k_B T \quad \text{Equation 1.4}$$

Where; D is the diffusion co-efficient, f is the frictional co-efficient, k_B is Boltzmann’s constant and T is temperature.

The frictional coefficient of spherical particles is given by Stoke’s law of diffusion:

$$f = 6\pi\eta R_h \quad \text{Equation 1.5}$$

Where R_h is the hydrodynamic diameter of the particles and η is the solvent viscosity.

Combining the above two equations, allows the calculation of the hydrodynamic diameter of a particle from its diffusion coefficient (Stoke-Einstein equation):

$$R_h = \frac{k_B T}{3\pi\eta D} \quad \text{Equation 1.6}$$

In this case, the particle diameter is referred to as the hydrodynamic diameter due to its relation to the particle diffusion through a liquid (40).

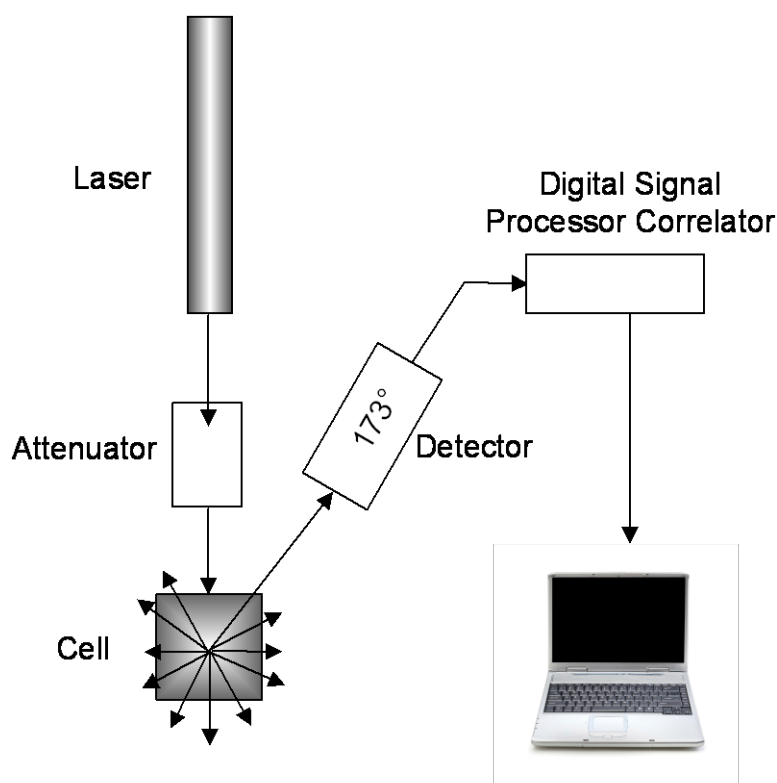


Figure 1.6 Optical arrangement of the Zetasizer for size measurements (25, 40)

Figure 1.6 illustrates the optical arrangement of the Zetasizer. The laser beam represents the light source, which illuminates the sample in the cell. In case of dilute dispersions such as microgels, some of the laser beam is scattered by the particles, while most of it passes through the sample. The scattered light is measured by the detector which is placed at 173° from the

laser beam, which passes straight through the sample. The detector is placed in this position to detect the backscattered light. The advantages of the detector can be summarized as follows: (1) it reduces the multiple scattering, since the laser beam is not required to pass through the whole sample and (2) using back-scattered detection will partially exclude the effect of large particles (such as dust), since the large particles generally scatter light in a forward direction (39). The function of the attenuator is to optimize the intensity of the light beam passing through the sample. It prevents the saturation of the detector by reducing the intensity of the laser beam passing through a strong scattering sample or increase it in case of a weakly scattering one. The attenuator can also change the position of the measurement point from the center of the cuvette in order to obtain optimum scattering. The scattering signal passes from the detector to a digital processing board called the correlator. This correlator determines the rate of change in intensity by comparing the scattering intensity at successive time intervals. The data then passes from the correlator to the computer where it is analyzed by the software to derive the hydrodynamic diameter (40).

1.1.6 Colloidal stability and interactions of microgels

To make good use of colloidal systems, such as microgels, it is very important to study the stability of these systems (1, 40). A colloidal system is said to be stable when the particles remain dispersed as single particles for a long period of time such as months or years (39). Stability can be achieved using the balance of attractive and repulsive forces between the colloidal particles.

Properties of the colloidal systems are determined by factors such as (41):

- Particle size
- Particle shape and flexibility
- Surface properties (including the surface charge density)
- Particle-particle interactions
- Particle-solvent interactions
- Temperature, pH and ionic strength of the particulate system.

Since the stability depends upon two kinds of interactions (particle-particle and particlesolvent interactions), the stability between particles of the same size differs from that between particles of different sizes in the same medium. While suspended, there are many factors that cause the particles to display random particle collisions; these factors include thermal, hydrodynamic, external forces such as shear, agitation, flow and intrinsic Brownian

motion. In the case of large particles, sedimentation can also be an effective factor (1). These collisions may cause the particles to be rebound or to aggregate, this aggregation may cause a permanent contact called coagulation or a temporary one called flocculation. Figure 1.7 shows the possible types of interactions in a colloidal dispersion.

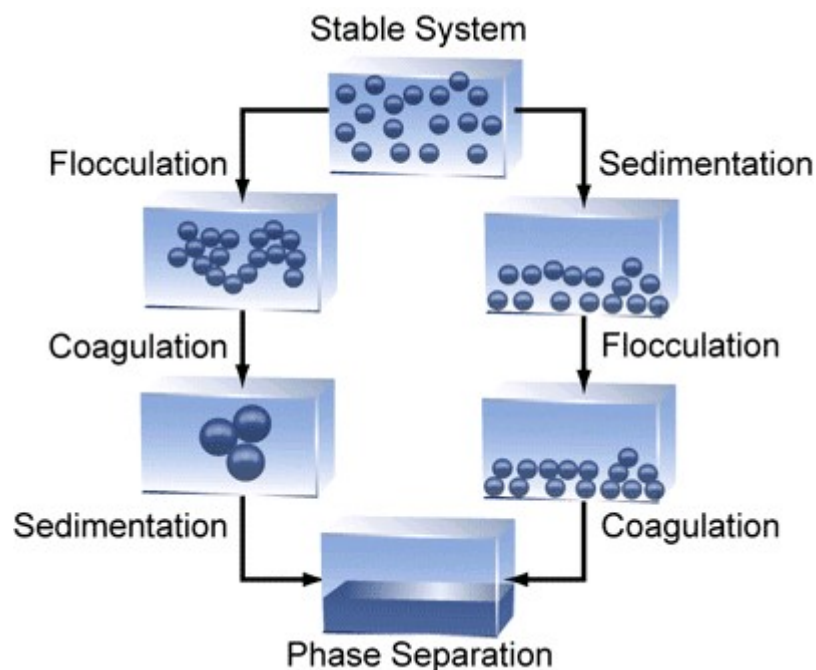


Figure 1.7 Types of possible emulsion interactions in a colloidal system (15)

If the aggregating system is made up of one type of particle, then the process is called homoaggregation, while in the case of different kinds of particles, it is heteroaggregation, heterocoagulation or heteroflocculation (2). Permanent irreversible particle contact is generally referred to as heterocoagulation. Temporary reversible particle associations are defined as heteroflocculation and heteroassociation, while the term heteroaggregation is generally applied for particle aggregation. Colloidal particles have different particle size, composition, shape, surface charge and surface potential (1). Particles with dissimilar surfaces are more likely to react with each other than those of the same type (42-45).

1.1.6.1 Electrical double layer

In aqueous colloidal dispersions, particles usually possess a surface charge. The origins of this charge include the ionization of surface charge groups, differential loss of ions and adsorption of charge species. The surface charge affects the distribution of nearby ions in a polar solution where ions of the same charge (co-ions) are repelled and those of opposite charge (counter-ions) are attracted to the surface. This leads to the formation of an electrical

double layer; Figure 1.8 shows the negatively charged particle surface is surrounded by positively charged counter ions.

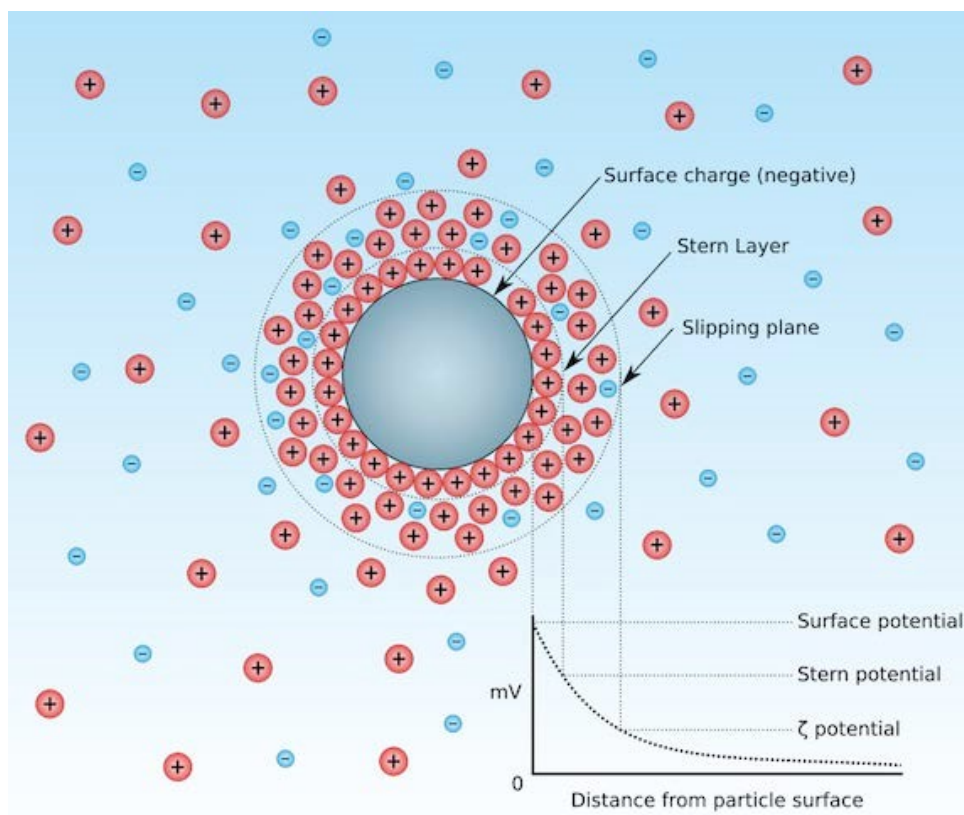


Figure 1.8 A schematic representing the electrical double layer

1.1.6.2 Origins of surface charge

Microgel particles suspended in an aqueous solution usually carry an electric charge. The surface charge arises from various sources that depend upon the dispersion media as well as the nature of the particle. When particles are dispersed in a liquid, the dissociation of the functional surface groups and/or adsorption of ions are the most important sources of surface charge. A net surface charge can be acquired by the unequal adsorption of oppositely charged ions (46).

1.1.6.3 Double layer interactions

In aqueous solution, ionized particles interact with each other by electrostatic forces. These interactions are affected by two main factors; oppositely charged ions are attracted to each other (at least loosely) and electrostatic forces are screened by ions in the bulk solution (46).

The electrical double layer consists of two main regions; an inner region where the ions are strongly bound (Stern layer) and an outer region where they are loosely attached (diffuse region). The diffuse layer is balanced by the electrostatic forces and the random thermal motion. The charge potential is maximized close to the particle surface and decays as the distance increases away from the particle surface till it reaches zero in the bulk solution. The bound and the diffuse layers are separated by a surface (slipping plane or surface of shear) where the particles and the solution move in opposite directions when an external field is applied. The electrostatic potential on that surface is called the *zeta* potential (46).

1.1.6.4 Stern potential

The Stern double layer model is usually used to describe the charge distribution. Electrokinetic measurements are used to estimate the Stern potential (Ψ_d). Electrical charges on the surface of the particles cause them to be affected by an applied electrical field; this is defined as electrokinetic effects. The electrokinetic behavior of a particle mainly depends on the potential at the slipping plane between the charged surface and the electrolyte solution. This potential is called the electrokinetic or *zeta* potential (ξ) (46).

1.1.6.5 Electrophoresis

The movement of a charged entity in a surrounding fluid with an electric field either causing or resulting from it is referred to as electrophoresis. When an electric field is applied across an electrolyte, charged particles suspended in the electrolyte are attracted towards the electrode of the opposite charge. The velocity of the particle movement depends upon the strength of the electric field, the dielectric constant, the viscosity of the medium and the *zeta* potential. The velocity of the particles in a unit field is called “electrophoretic mobility”. For hard particles where there is a well-defined boundary, the electrophoretic mobility may be translated into *zeta* potential. This however is not the case for microgels as they have a diffuse outer layer. The exact position of which is not well defined. The electrophoretic mobility of a particle can be related to its *zeta* potential using the Henry equation for conducting and non-conducting spheres (46):

$$U_E = \text{Equation 1.7} \frac{2\varepsilon \xi f(ka)}{3\eta}$$

Where U_E = electrophoretic mobility, ζ = *zeta* potential, ε = dielectric constant, η = viscosity and $f(ka)$ = Henry's function which describes the thickness of the double layer and the particle diameter.

Particles dispersed in non-polar media have a minimum $f(ka)$ of 1 while those dispersed in polar media have a maximum $f(ka)$ value of 1.5. This value is used in the Smoluchowski approximation (46):

$$U_E = \text{Equation 1.8} \quad \frac{2 \varepsilon \zeta}{3\eta}$$

So, for systems that fit the Smoluchowski model, the *zeta* potential can be directly calculated from the electrophoretic mobility. An example of such a system is dispersion of particles of particles size larger than 200 nm with an electrolyte concentration of 10^{-3} M NaCl (46).

1.1.6.6 DLVO theory

The acronym DLVO refers to the two names of the groups who developed this model. These are Derjaguin and Landau (47) in 1940 and Verwey and Overbeek (48) in 1948. The model describes the changes in potential energy resulting from colloidal forces when two spherical monodispersed particles approach each other. Colloidal dispersions are characterized by the tendency of their particles to aggregate. When particles are dispersed in a liquid, they undergo continuous collisions. The interaction between the particles during collisions determine the stability of the dispersion (47,48). Particle aggregation is mainly caused by the long range van der Waals attractive forces between particles. So, to sustain the dispersion stability, an equal long-range repulsive force (usually electrostatic) is required to counteract van der Waals attractive ones.

DLVO theory assumes the stability of a colloidal system is accounted for by the interaction between charged colloidal particles. It is used to calculate the sum of the total potential energy (V_T), this includes the van der Waals attractive potential (V_A) initiated when the particles approach each other and the repulsive electrostatic potential (V_R) (arising from the electrical double layer around the particle) which prevents particle aggregation (equation 1.13).

$$V_T = V_A + V_R$$

Equation 1.9

Dispersions that are mainly stabilized by electrostatic repulsion aggregate in the presence of an electrolyte due to the compression of the electrical double layer. This enables the particles to come in close contact with each other allowing van der Waals attractive forces (V_R) to predominate and induce aggregation. When $V_R > V_A$, the particles are stable, while when $V_R < V_A$, they tend to aggregate.

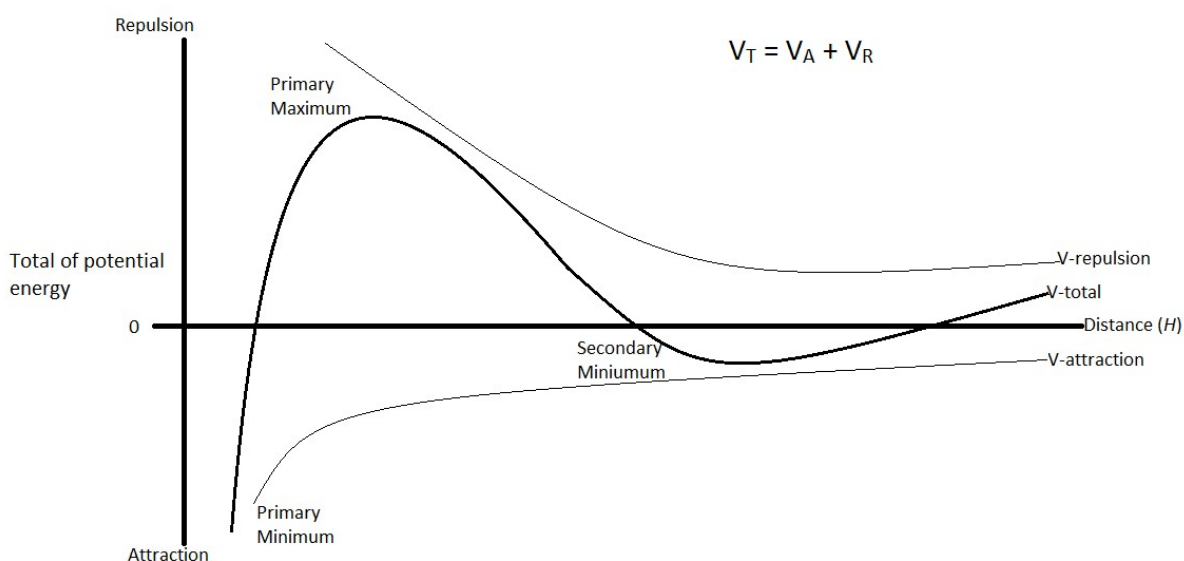


Figure 1.9 A schematic representing the DLVO potential energy diagram showing interaction curves; van der Waals attractive forces (V_A) and electrostatic repulsive forces (V_R) and the net total interactive forces (V_T) (47-49)

Figure 1.9 represents the interaction energy – distance curve which highly affects the colloid stability. When the distance between particles is large, the secondary minimum occurs where the net attractive forces dominate over the repulsive ones. The secondary minimum provides a metastable dispersed state. The primary minimum is the lowest energy state and it occurs when the particles are almost in contact.

When the distance between two particles is large (>100 nm), both the attractive van der Waals (V_A) and the repulsive electrostatic forces (V_R) have no influence on the particles. When the particles get closer, both V_A and V_R increase but V_A increase faster ($V_A > V_R$), so, it dominates leading to V_R forming a secondary minimum promoting aggregation. When the separating distance between the two particles further decreases, V_R dominates over V_A

preventing aggregation and leading V_T to form a primary maximum. This represents the energy barrier that must be overcome before the particles can aggregate (47). At very small separating distances, V_A dominates again leading to particle aggregation (in the primary minimum), aggregation that occurs in this stage is irreversible.

1.1.7 Fluorescent microgels

Many co-monomers have been incorporated into microgel particles to confer a new property to environmental responsive particles. Synthesis of coloured and/or fluorescent particles have been carried out recently and used for different applications.

Liu *et al.* have synthesized a NIPAM based smart microparticle incorporating picolinamine based acceptors (Cu^{2+} detector) and a fluorophore (dansylaminoethyl – acrylamide) for the selective determination of Cu^{2+} . This has provided a Cu^{2+} detection system that can be dispersed in water and also enhanced the detection sensitivity of Cu^{2+} . When the temperature is below the VPTT, the fluorescent microgel particles are swollen and can selectively bind to Cu^{2+} leading to the quenching of the particle fluorescence intensity. When the temperature increases above the VPTT, the detection limit of the particle highly improves (the particles can detect even lower amounts of Cu^{2+}). For example, for a particle concentration of 3×10^{-6} g/mL, the Cu^{2+} detection limit below the VPTT is 46 nmol while above the VPTT it decreases to 8 nmol (50).

In 2010, Chen-Yen Chen and Chao-Tsen Chen incorporated 3-hydroxyflavone (3-HF) in p(NIPAM) particles to produce fluorescent thermo-sensitive microgel particles. 3-HF is characterized by the display of a dual band emission band associated with normal excited state intramolecular charge transfer. 3HFs display a greenish emission in polar and aprotic solvents and a blue one in highly polar and protic solvents. Based upon this property, the new p(NIPAM-co-3HF) acquired/displayed a two-band fluorescence that changes around the VPTT. Below the VPTT, the particles are swollen in the surrounding aqueous media which acts as a highly polar and protic environment which leads to a blue fluorescent emission. When the temperature exceeds the VPTT, the particles shrink leading to a more hydrophobic environment giving rise to a greenish emission. The fluorescence shift is characterized by being sensitive and reversible. The authors suggested the use of the new particles as a thermometer especially because the sensing temperature range is in the range of 33-40°C

which makes it a very suitable candidate for the use in measurements of biological activity such as cell imaging (51).

Other trials to incorporate fluorophores in environmental responsive microgel particles include the incorporation of azo-dyes (52) and pyran based fluorophores (53). Suggested applications for such particles include sensors and dye-sensitized solar cells, respectively (53).

1.1.8 Applications of microgels

The properties of microgels can have many applications. Examples of the fields where microgels can be used include:

- ❖ Drug delivery systems (54-59)
- ❖ Cosmetic and pharmaceutical applications (10, 60, 61)
- ❖ Surface coating industry (3, 62)
- ❖ Printing industry (3)
- ❖ Biosciences application (8)
- ❖ Water purification (63)
- ❖ Oil recovery (64)
- ❖ Microgels in Biotechnology (65)
- ❖ Removal of water from biodiesel (66)
- ❖ Treatment of dentinal hypersensitivity (25)
- ❖ Templates for nano-particle synthesis (59)

1.1.8.1 Microgels as drug delivery systems

Site specific drug delivery mainly aims at delivery of the drug to a certain organ and/or specific tissues in the body; it may also be used to accurately control the release rate of the drug. The development of polymer and material science caused a great improvement in the drug delivery systems and thus serving the pharmaceutical aspects.

One of the main limitations of traditional drug delivery systems is the management of the system to release the required amount of the drug at a specific rate (67). The more the concepts of chronopharmacokinetics and the variations in the disease symptoms are understood, the more it becomes desirable to find an ideal drug delivery system that overcomes the disadvantages of the traditional ones. The assumed system should release a specific amount of the drug, in a specific site in the body at a specific rate. It is also suggested that the system releases the drug in response to the need of the body for the drug, for example, a drug delivery system that releases insulin according to the blood sugar level. The swelling properties of microgels enable them to play the role of a drug delivery system that can protect sensitive drugs and control the release of rapidly metabolized ones. Many scientists are currently testing the ability of microgels to play this role especially as oral or transdermal drug delivery systems.

1.1.8.1.1 Microgels and oral drug delivery

The ability of the microgel to change its conformation according to the surrounding environmental conditions can be used for oral drug delivery. Since stomach conditions are different from those outside the stomach, pH/temperature sensitive microgels were used for the delivery of peptide and protein drugs. The controlled delivery of insulin using (*N*isopropylacrylamide/butyl methacrylate/acrylic acid) co-polymer microgels was tested (66). Under environmental conditions similar to the stomach (pH 2, which is below the pK_a of acrylic acid), the microgel particles are collapsed and thus the drug cannot be released. Under environmental conditions similar to the gastrointestinal tract (pH 7.4, which is above the pK_a of acrylic acid), the microgel particles swell and start releasing the insulin slowly for eight hours.

1.1.8.1.2 Microgels as transdermal drug delivery systems

The ability of thermo-responsive microgels to play the role of a model transdermal drug delivery system was studied by Snowden *et al.* (69). The surfactant-free emulsion polymerization technique was used to synthesize a microgel based on a co-polymer of p(NIPAM-co-10 % butyl acrylate)

Inspite of the great progress in the field of drug delivery, protein macromolecules still rapidly degrade due to their sensitivity to the surrounding environmental conditions. This made the parenteral route the most convenient one for protein macromolecules. The entrapment of the biomacromolecules (as proteins) enables its administration as an injection. Different

materials are used as polymers and co-polymers, providing a wide range of hydrophilicity and hydrophobicity; examples of these are the poly(D, L lactidecoglycolide). Being “soft and rubbery” and with water content, microgels are like natural living tissues causing minimal irritation to the surrounding tissues; furthermore, microgels exhibit all the properties required for a drug delivery system such as environment responsiveness, injectability, degradability and biocompatibility (7).

1.2 Environmental responsive surfaces

1.2.1 Deposition of microgels on surfaces

Recently, environmental responsive surfaces have attracted the attention of many researchers due to their potential applications (53, 50-74). Researchers have deposited environmental responsive particles on different surfaces using different techniques, qualitatively tested their response to environmental conditions and studied the possible applications of the new surfaces (75-78). However, very few scientists have approached the quantitative analysis of the deposition of environmental responsive particles on surfaces (79). Determining the amount of particles deposited on surfaces is very important in order to determine the extent of response of the surface to environmental conditions and also for commercial considerations. To move the suggested application from the research phase to a practical application one requires a clear understanding of the amount of particles that can be deposited on each surface and the factors affecting deposition.

Burdokova *et al.* (80) have studied the p(NIPAM) induced hydrophilic/hydrophobic transition, the effect of p(NIPAM) on the surface charge of silica surfaces and the p(NIPAM) induced hydrophobic attraction and adhesion between silica surfaces using contact angle measurement, *zeta* potential measurements and atomic force spectroscopy, respectively. The contact angle measurement results showed that the presence of p(NIPAM) at silica glass surfaces causes the silica surfaces to become more hydrophobic. Increasing the molecular weight of the p(NIPAM) leads to a significant increase in the degree of hydrophobicity, regardless of the temperature. However, if the temperature is raised above the LCST, the increase in hydrophobicity is significantly greater than that at a lower temperature. The *zeta* potential measurements showed that at room temperature at pH 6, the silica surfaces carry a strong negative charge. However, the *zeta* potential decreases at 50°C. The results also showed that *zeta* potential significantly decreases by increasing the molecular weight of the polymer regardless of the temperature. The authors explained that the addition of a non-ionic

polymer onto the charged silica surface shifts the shear plane away from the surface of the particles leading to a decrease in the diffusion layer potential (*zeta* potential). The results also showed that p(NIPAM) adsorbs on a silica surface at low temperature (below the LCST) but to a much lesser extent than at a higher temperature. The atomic force microscopy (AFM) results showed net repulsive forces between silica surfaces both in the presence and absence of p(NIPAM); the surfaces with higher molecular weight p(NIPAM) showed longer range repulsion which was attributed to steric repulsion.

Studies revealed that p(NIPAM) can be highly useful in facilitating mineral aggregation and consolidation (80). During mineral flotation procedures, p(NIPAM) can serve as an effective flotation collector (these are reagents that render the surfaces more hydrophobic and thus enhance its attachment to air bubbles). At high temperature (above the LCST), when p(NIPAM) is adsorbed on the surface of the mineral particles, it increases its hydrophobicity.

Zavgorodnya and Serpe (79) also studied the deposition of microgels onto solid surfaces. They deposited p(NIPAM-*co*-acrylic acid) (AA) on glass substrates coated with polyelectrolyte multilayers with different layer thickness and surface charges at different pHs (below and above the pK_a of AA). These multilayers are composed of the polycation poly(allyl amine hydrochloride) (PAH) and the polyanion poly(sodium 4-styrenesulfonate) (PSS). During their study they used different techniques such as digital image correlation, microgel counting, SEM and AFM. They concluded that the charge of the particles is the most important factor affecting the number of particles deposited on the surface.

1.2.2 Applications of environmental responsive surfaces

1.2.2.1 Control of protein adhesion

The reaction of environmental responsive surfaces with proteins can be either specific or non-specific. Switching the adsorption of proteins on and off is desirable in both cases, each of which has its own application. The specific surface – protein interaction can be used to switch the adsorption/desorption of a specific protein on the environmental responsive surface and repel the other biological species available (73).

Examples of non-specific protein binding on smart surfaces include the work of Alexander *et al.* (72). They managed to switch the adsorption/desorption of fluorescein *isothiocyanate* labelled bovine serum albumin (FITC-BSA) on p(NIPAM-*co*-hexadecanethiol) micropatterned surfaces tuned by the VPTT of the microgel. Meanwhile, this behavior was

less pronounced after repeated heating/cooling cycles or prolonged incubation. Also, Uhlmann *et al.* (51) managed to coat silicon surfaces with a pH-thermo-responsive polymer coating of poly(2-vinyl pyridine) and p(NIPAM). They used this system to control the binding of BSA adsorption by changing the temperature from below to above the VPTT.

An example of the specific smart surface – protein interactions is the approach of Zhang *et al.* (81). They prepared a p(NIPAM) microgel with a metal chelate co-monomer *N*-(4-vinyl)-benzyl iminodiacetic acid. In the presence of Cu^{2+} ions, this co-monomer forms a coordination complex with the template protein. Accordingly, the addition or omission of Cu^{2+} ions can be used to switch the imprinted microgel-protein interactions.

1.3 Context

This work aims at designing new NIPAM based particles to be used in different applications. Four new particles have been designed, synthesized, characterized using different techniques and used for a relevant application. One of the applications investigated in this work is the quantitative use of fluorescent p(NIPAM-*co*-5% vinyl cinnamate) microgel particles to produce smart surfaces. For p(NIPAM-*co*-5% lucifer yellow), toxicity studies were conducted aiming at studying the possibility of using these fluorescent temperature/pH responsive particles in drug delivery applications. Finally, the ability of p(NIPAM-*co*-5% acrylic acid)-hexenol to act as a surfactant was tested using two different oils (tricaprylin and hexadecane). Also, in this work, various techniques have been used to attach different co-monomers to p(NIPAM) particles. These include direct polymerization, coupling reactions and esterification reaction.

1.4 References

1. Saunders B. R., Crowther H. M., Morris G. E., Mears S. J., Cosgrove T., Vincent B. Factors affecting the swelling of poly(*N*-isopropylacrylamide) microgel particles: fundamental and commercial implications. *Colloids and Surfaces A-Physicochemical and Engineering Aspects*. 1999;149(1-3):57-64.
2. Gracia L. H., Snowden M. J., Williams P. A. *Handbook of Industrial water soluble polymers*. Williams PA, Blackwell; 2007.
3. Crowther H. M., Saunders B. R., Mears S. J., Cosgrove T., Vincent B., King S. M., Yu G. E. Poly(NIPAM) microgel particle de-swelling: a light scattering and small-angle neutron scattering study. *Colloids and Surfaces A - Physicochemical and Engineering Aspects*. 1999;152:327-333.

4. Ali M. M., Aguirre S. D., Xu Y., Filipe C. D., Pelton R., Li Y. Detection of DNA using bioactive paper strips. *Chemical Communications*. 2009;6640-6642.
5. Pelton R. H., Chibante P. Preparation of Aqueous Lattices with N-Isopropylacrylamide. *Colloids and Surfaces*. 1986; 20:247-56.
6. Lowe J. S., Chowdhry B. Z., Parsonage J. R., Snowden M. J. The preparation and physico-chemical properties of poly(N-ethylacrylamide) microgels. *Polymer*. 1998;39:1207-1212.
7. Hazot P., Delair T., Pichot C., Chapel J. P., Elaissari A. Poly(N-ethylmethacrylamide) thermally-sensitive microgel latexes: effect of the nature of the crosslinker on the polymerization kinetics and physicochemical properties. *Comptes Rendus Chimie*. 2003;6:1417-24.
8. Eke I., Elmas B., Tuncel M., Tuncel A. A new, highly stable cationicthermosensitive microgel: Uniform *isopropylacrylamide-dimethylaminopropylmethacrylamide* copolymer particles. *Colloids and Surfaces A-Physicochemical and Engineering Aspects*. 2006;279(1-3):247-253.
9. Kagawa G. B., Carey M. J., Such C., Saunders B. R. A new family of waterswellable microgel particles. *Journal of Colloid and Interface Science*. 2003;257:392-397.
10. Chen K., Ku Y., Lee C., Lin H., Lin F., Chen T. Immobilization of chitosan gel with cross-linking reagent on PNIPAAm gel/PP nonwoven composites surface. *Materials Science & Engineering C-Biomimetic and Supramolecular Systems*. 2005;25472-478.
11. Yildiz B., Isik B., Kis M. Synthesis and characterization of thermoresponsive *isopropylacrylamide-acrylamide* hydrogels. *European Polymer Journal*. 2002;38:1343-1347.
12. Christensen M. L., Keiding K. Study of the compositional heterogeneity in poly(*Nisopropylacrylamide-acrylic acid*) microgels by potentiometric titration experiments. *Colloids and Surfaces A-Physicochemical and Engineering Aspects*. 2005;252:61-69.
13. Kim H. I., Park S. J., Kim S. I., Kim N. G., Kim S. J. Electroactive polymer hydrogels composed of polyacrylic acid and poly(vinyl sulfonic acid) copolymer for application of biomaterial. *Synthetic Metals*. 2005;155:674-676.
14. Kaneda I., Sogabe A., Nakajima H. Water-swallowable polyelectrolyte microgels polymerized in an inverse microemulsion using a nonionic surfactant. *Journal of Colloid and Interface Science*. 2004;275:450-457.
15. http://malverninstruments.co.kr/LabEng/industry/colloids/colloids_stability.htm. Accessed on 24th of November, 2011.
16. Rosiak J. M. Radiation formation of hydrogels for drug-delivery. *Journal of Controlled Release*. 1994;31:9-19.

17. Ulanski P., Kadlubowski S., Rosiak J. M. Synthesis of poly(acrylic acid) nanogels by preparative pulse radiolysis. *Radiation Physics and Chemistry*. 2002;63:533-537.
18. Saunders B. R., Vincent B. Microgel particles as model colloids: theory, properties and applications. *Advances in Colloid and Interface Science*. 1999;80:1-25.
19. Murray M. J., Snowden M. J. The preparation, characterization and applications of colloidal microgels. *Advances in Colloid and Interface Science*. 1995;54:73-91.
20. Snowden M. J., Vincent B. The temperature-controlled flocculation of cross-linked latex-particles. *Chemical Communications*. 1992:1103-1105.
21. Price G., Clifton A. Sonochemical acceleration of persulfate decomposition. *Polymer*. 1996;37:3971-3973.
22. Goodwin J. W., Ottewill R. H., Pelton R., Vianello G., Yates D. E. Control of particle-size in formation of polymer lattices. *British Polymer Journal*. 1978;10:173-180.
23. Benee L. S. Smart Materials: polymeric microgels, their preparation, properties and application. PhD thesis, University of Greenwich; 2002.
24. Ma X., Xi J., Huang X., Zhao M., Tang X. Novel hydrophobically modified temperature-sensitive microgels with tunable volume-phase transition temperature. *Materials Letters*. 2004;58:3400-3404.
25. Majcen N. The development of novel smart wound dressings based on colloidal microgels and cotton fabric. PhD thesis, University of Greenwich; 2008.
26. Nur H. Colloidal microgels; synthesis, characterization and applications. PhD thesis, University of Greenwich; 2009.
27. Kratz K. Hellweg T., Eimer W. Structural changes in PNIPAM microgel particles as seen by SANS, DLS, and EM techniques. *Polymer*. 2001;42:6631-6639.
28. Lopez V. C., Hadgraft J., Snowden M. J. The use of colloidal microgels as a (trans)dermal drug delivery system. *International Journal of Pharmaceutics*. 2005;292:137147.
29. Snowden M. J., Chowdhry B. Z., Vincent B., Morris G. E. Colloidal copolymer microgels of *N-isopropylacrylamide* and acrylic acid: pH, ionic strength and temperature effects. *Journal of Chemical Society, Faraday Transactions*. 1996;92:5013-5016.
30. Hatto N., Cosgrove T., Snowden M. J. Novel microgel-particle colloids: the detailed characterisation of the layer structure and chain topology of silica: poly(NIPAM) core-shell particles. *Polymer*. 2000;41:7133-7137.
31. Narumi A. Kaga H., Miura Y., Satoh T., Kaneko N., Kakuchi T. Synthesis of polystyrene microgel with glucose as hydrophilic segment via controlled free-radical polymerization. *Polymer*. 2006;47:2269-2273.

32. Zimm B. H. Apparatus and methods for measurements and interpretation of angular variation of light scattering: preliminary results on polystyrene solutions. *Journal of Chemical Physics*. 1948;16:1099-1117.
33. Kim K. S., Cho S. H., Shin J. S. Preparation and characterization of monodisperse polyacrylamide microgels. *Polymer*. 1995;27:508.
34. Sierra-Martin B., Romro-Cano M. S., Cosgrove T., Vincent B., Fernandez-Barbero A. Solvent relaxation of swelling PNIPAM microgels by NMR. *Colloids and Surfaces A - Physicochemical and Engineering Aspects*. 2005;270-271:296-300.
35. Cao Z., Liu W., Gao P., Yao K., Li H., Wang G. Toward an understanding of thermoresponsive transition behavior of hydrophobically modified *N-isopropylacrylamide* copolymer solution. *Polymer*. 2005;46:5268-5277.
36. Erbil C. Sezai Saraç A. Description of the turbidity measurements near the phase transition temperature of poly(*N-isopropyl acrylamide*) copolymers: the effect of pH, concentration, hydrophilic and hydrophobic content on the turbidity. *European Polymer Journal*. 2002;38:1305-1310.
37. Woodward N. C., Chowdhry B. Z., Snowden M. J., Leharne S. A., Griffiths P. C., Winnington A. L. Calorimetric investigation of the influence of cross-linker concentration on the volume phase transition of poly(*N-isopropylacrylamide*) colloidal microgels. *Langmuir*. 2003;19:3202-3211.
38. Kratz K. Hellweg T., Eimer W. Structural changes in PNIPAM microgel particles as seen by SANS, DLS, and EM techniques. *Polymer*. 2001;42:6631-6639.
39. Malvern Instruments. Dynamic light scattering: An introduction in 30 minutes. www.malvern.com.2006. Accessed on 1st of December, 2011.
40. Gracia L. H., Chowdhry B. Z., Snowden M. J. Stabilization of Colloids by Polymers. *Encyclopedia of surface and colloid science*. 2006:5775.
41. Shaw D. J. *Colloid and surface chemistry*. Fourth edition ed.: Elsevier Science; Oxford; 1992.
42. Vincent B., Young C. A., Tadros T. F. Equilibrium aspects of hetero-flocculation in mixed sterically-stabilized dispersions. *Faraday Disc.Chem.Soc.*1978;74:337-47.
43. Wang G., Nicholson P. S. Heterocoagulation in ionically stabilized mixed-oxide colloidal dispersions in ethanol. *Journal of the American Ceramic Society*. 2001;84:1250-6.
44. Kim A. Y., Berg J. C. Fractal heteroaggregation of oppositely charged colloids. *Journal of Colloid and Interface Science*. 2000;229:607-14.

45. Kim A. Y., Hauch K. D., Berg J. C., Martin J. E., Anderson R. A. Linear chains and chain-like fractals from electrostatic heteroaggregation. *Journal of Colloid and Interface Science*. 2003;260:149-59.
46. Pinkrah V. T. The synthesis and physico-chemical characterization of novel microgel particles. PhD thesis, University of Greenwich; 2004.
47. Derjaguin B.V., Landau L. Theory of the stability of strongly charged lyophobic sols and the adhesion of strongly charged particles in solutions of electrolytes. *Acta Physicochim*. 1941;14:633-62.
48. Verwey E.J., Overbeek J.Th. Theory of the stability of lyophobic colloids, the interaction of sol particles having an electric double layer. Elsevier; Amsterdam; 1948.
49. Thorne J. B. Controlling the interfacial behaviour of colloidal microgel systems. PhD thesis, University of Greenwich; 2012.
50. Yin J., Guan X., Wang D., Liu S. Y. Metal-Chelating and Dansyl-Labeled Poly(*N*-isopropylacrylamide) Microgels as Fluorescent Cu²⁺ Sensors with Thermo-Enhanced Detection Sensitivity. *Langmuir*. 2009;25:11367–74.
- Burkert S., Bittrich E., Kuntzsch M., Muller M., Eichhorn K. J., Bellmann C., Uhlmann P., Stamm M. Protein Resistance of PNIPAAm Brushes: Application to Switchable Protein Adsorption. *Langmuir*. 2010;26:1786–95.
52. Lee E. M., Gwon S. Y., Ji B. C., Kim S. H. Temperature and Acid/base-driven Dual Switching of Poly(*N*-isopropylacrylamide) Hydrogel with Azo Dye. *Fibers and Polymers*. 2011;12:142-4.
53. Kim S. H. Hwang I. J., Gwon S. Y., Son Y. A. The thermoresponsive behaviour of a poly(*N*-isopropylacrylamide) hydrogel with a D-p-A type pyran-based fluorescent dye. *Dyes and Pigments*. 2010;87:84-8.
54. Gref R., Amiel C., Molinard K., Daoud-Mahammed S., Sebille B., Gillet B., Beloeil J. C., Ringard C., Rosilio V., Poupert J., Couvreur P. New self-assembled nanogels based on host-guest interactions: Characterization and drug loading. *Journal of Controlled Release*. 2006;111:316-24.
55. Lin S. Y., Chen K. S., Liang R. C. Design and evaluation of drug-loaded wound dressing having thermo responsive, adhesive, absorptive and easy peeling properties. *Biomaterials*. 2001;22:2999-3004.
56. Shin Y, Chang J. H., Liu J., Williford R., Shin Y. K., Exarhos G. J. Hybrid nanogels for sustainable positive thermosensitive drug release. *Journal of Controlled Release*. 2001;73:1-6.
57. Soppimath K. S., Kulkarni A. R., Aminabhavi T. M. Chemically modified polyacrylamide-g-guar gum-based crosslinked anionic microgels as pH-sensitive

- drug delivery systems: preparation and characterization. *Journal of Controlled Release*. 2001;75:331-45.
58. Vihola H., Laukkanen A., Hirvonen J., Tenhu H. Binding and release of drugs into and from thermosensitive poly(*N*-vinyl caprolactam) nanoparticles. *European Journal of Pharmaceutical Sciences*. 2002;16:69-74.
 59. Zhang X. Z., Lewis P. J., Chu C. C. Fabrication and characterization of a smart drug delivery system: microsphere in hydrogel. *Biomaterials*. 2005;26:3299-309.
 60. Kaneda I., Sogabe A. Rheological properties of water swellable microgel polymerized in a confined space. *Colloids and Surfaces A-Physicochemical and Engineering Aspects*. 2005;270:163-70.
 61. Lin F. H., Tsai J. C., Chen T. M., Chen K. S., Yang J. M., Kang P. L., Wu T. H. Fabrication and evaluation of auto-stripped tri-layer wound dressing for extensive burn injury. *Materials Chemistry and Physics*. 2007;102:152-8.
 62. Pelton R. Temperature-sensitive aqueous microgels. *Advances in Colloid and Interface Science*. 2000;85:1-33.
 63. Morris G. E., Vincent B., Snowden M. J. Adsorption of lead ions onto *N*isopropylacrylamide and acrylic acid copolymer microgels. *Journal of Colloid and Interface Science*. 1997;190:198-205.
 64. Snowden M. J., Vincent B. inventor. A novel method for the enhanced oil recovery. 1996b. Patent, application number GB 2262117A.
 65. Shiroya T., Tamura N., Yasui M., Fujimoto K., Kawaguchi H. Enzyme immobilization on thermosensitive hydrogel microspheres. *Colloids and Surfaces BBiointerfaces*. 1995;4:267-74.
 66. Nur H., Snowden M. J., Cornelius V. J. Mitchell J. C., Harvey P. J., Benez L. S. Colloidal microgel in removal of water from biodiesel. *Colloids and Surfaces APhysicochemical and Engineering Aspects*. 2009;335:133-7.
 67. Pinkrah V. T., Beezer A. E., Chowdhry B. Z., Gracia L. H., Cornelius V. J., Mitchell J. C., Castro-Lopez V., Snowden M. J. Swelling of cationic polyelectrolyte colloidal microgels: Thermodynamic considerations. *Colloids and Surfaces APhysicochemical and Engineering Aspects*. 2005;262:76-80.
 68. Ramkissoon-Ganorkar C., Liu F., Baudys M., Kim S. W. Modulating insulin release profile from pH thermosensitive polymeric beads through polymer molecular weight. *Journal of Controlled Release*. 1999;59:287-98.
 69. Castro Lopez V., Hadgraft J., Snowden M. J. The use of colloidal microgels as a (trans)dermal drug delivery system. *International Journal of Pharmaceutics*. 2005;292:137-47.

70. Kanazawa H., Nishikawa M., Mizutani A., Sakamoto C., Morita-Murase Y., Nagata Y., Kikuchi A., Okano T. Aqueous chromatographic system for separation of biomolecules using thermoresponsive polymer modified stationary phase. *Journal of Chromatography A*. 2008;1191:157-61.
71. Ayano E., Nambu K., Sakamoto C., Kanazawa H., Kikuchi A., Okano T. Aqueous chromatography system using pH- and temperature-responsive stationary phase with ionexchange groups. *Journal of Chromatography A*. 2006;1119:58-65.
72. Alarcon C. D., Farhan T., Osborne V. L., Huck W. T., Alexander C. Bioadhesion at micro-patterned stimuli-responsive polymer brushes. *Journal of Materials Chemistry*. 2005;15:2089-94.
73. Wischerhoff E., Badi N., Laschewsky A., Lutz J. F. Smart polymer surfaces: concepts and applications in biosciences. *Advanced Polymer Science*. 2011;240:1-33.
74. Sakamoto C., Okada Y., Kanazawa H., Ayano E., Nishimura T., Andob M, Kikuchi A., Okano T. Temperature- and pH-responsive aminopropyl-silica ion-exchange columns grafted with copolymers of *N-isopropylacrylamide*. *Journal of Chromatography A*. 2004;1030:247-53.
75. Kvítek O., Bot M., Svorčík V. Gold nanoparticles grafting on glass surface. *Applied Surface Science*. 2012;258:8991-5.
76. Guilherme M. R., De Moura M. R., Radovanovic E., Geuskens G., Rubira A. F., Muniz E. C. Novel thermo-responsive membranes composed of interpenetrated polymer networks of alginate-Ca²⁺ and poly(*N-isopropylacrylamide*). *Polymer*. 2005;46:2668-74.
77. Da Silva R. M., Mano J. F., Reis R. L. Smart thermoresponsive coatings and surfaces for tissue engineering: switching cell-material boundaries. *Trends in Biotechnology*. 2007;25:578-83.
78. Nerapusri V., Keddie J. L., Vincent B., Bushnak I. A. Swelling and Deswelling of Adsorbed Microgel Monolayers Triggered by Changes in Temperature, pH, and Electrolyte Concentration. *Langmuir*. 2006;22:5036-41.
79. Zavgorodnya O., Serpe M. J. Assembly of poly(*N-isopropylacrylamide*)-*co*-acrylic acid microgel thin films on polyelectrolyte multilayers: Effects of polyelectrolyte layer thickness, surface charge, and microgel solution pH. *Colloid and Polymer Sci*. 2011;289:591-602.
80. Burdukova E., Li H., Ishida N., O'Shea J. P., Franks G. V. Temperature controlled surface hydrophobicity and interaction forces induced by poly(*N-isopropylacrylamide*). *Journal of Colloid and Interface Science*. 2010;342:586-92.
81. Qin L., He X. W., Zhang W., Li W. Y., Zhang Y. K. Macroporous Thermosensitive Imprinted Hydrogel for Recognition of Protein by Metal Coordinate Interaction. *Analytical Chemistry*. 2009;81:7206-16.

Chapter Two Deposition of fluorescent poly(*N*-isopropylacrylamide-co-vinyl cinnamate) particles on solid surfaces: quantitative analysis and the factors affecting it

2.1 Introduction

The deposition of environmentally responsive colloidal microgel particles on surfaces has been carried out to produce environmentally responsive surfaces. The latter can be used in many applications such as the control of cell and protein adhesion, (1-4) and bioseparation (5, 6). For example, the reaction of stimuli-responsive surfaces with proteins can be either specific or non-specific, each of which has its own application. In the case of specific stimuli-responsive surfaces, the interactions of proteins with the surface can be controlled in order to switch the adsorption/desorption of a specific protein onto/from the surface and repel the other biological species available (7). Alarcón *et al.* (1) managed to switch the adsorption/desorption of fluorescein *isothiocyanate*-labelled bovine serum albumin (FITCBSA) on poly(*N*-isopropylacrylamide-co-hexadecanethiol) (p(NIPAM-co-HDT)) micropatterned surfaces, which was controlled by the volume phase transition temperature (VPTT) of the microgel particles. This behaviour was less pronounced after repeated heating/cooling cycles or prolonged incubation. Burkert *et al.* (2) coated silicon surfaces with a pH-thermo-responsive polymer layer of poly(2-vinyl pyridine) and p(NIPAM). This system was used to control the binding of BSA adsorption by changing the temperature from below to above the VPTT. Qin *et al.* (3) prepared p(NIPAM) microgel particles with a metal chelate co-monomer *N*-(4-vinyl)-benzyl iminodiacetic acid. In the presence of Cu²⁺ ions, this co-monomer forms a co-ordination complex with the template protein. Accordingly, the addition or omission of Cu²⁺ ions can be used to switch the imprinted particle-protein interactions.

In eukaryotic cell culture, some cells can be grown in free suspension while most cells derived from solid tissues need to be cultured on a solid surface. To lift the cells off the surface, common protocols include the use of digestive enzymes such as trypsin but as a consequence it is impossible to harvest completely intact cells. Using a stimuli-responsive surface for cell culture solves this problem. Changing environmental conditions (*e.g.* temperature) at the surface changes its physicochemical properties such as surface charge and hydrophilicity; this can be used to automatically switch the cell adhesion at the surface

on and off. Different physicochemical triggers were used to control cell adhesion, including electrochemistry, light and temperature (7).

Edahiro *et al.* used a photo- and thermo-responsive surface (cell culture substrate) modified with a polymerizable spiropyran derivative and a copolymer of NIPAM to switch the adhesion of Chinese hamster ovary cells on and off (8). At 37°C, when the surface was irradiated with UV light ($\lambda=365$ nm), the spiropyran was isomerized to a zwitterionic merocyanine form, which caused the cells to adhere to the surface. Reversing the isomerization by irradiating the surface with visible light ($\lambda=400$ nm) and washing the surface with cold water caused the cells to be lifted off. Further experiments proved the viability of the cells after the UV and visible light irradiation.

Other researchers have used exclusively thermo-responsive polymers such as p(NIPAM) to coat surfaces for different applications (4). At 37°C cells tend to adhere more to hydrophobic surfaces than to hydrophilic ones. Accordingly, using the latter will provide easier removal of the cells from the surface (7).

One application of thermo-responsive polymer coatings is the separation of biomolecules. For example, silica beads modified with temperature-sensitive p(NIPAM) were used as a stationary phase for HPLC for the temperature-modulated separation of steroids and peptides.

The Okano group (5) has made progress in designing new stationary phases. In 2006, they developed a new HPLC method for the analysis of non-steroidal anti-inflammatory drugs such as ibuprofen and ketoprofen (6). They designed a new temperature/pH sensitive stationary phase by modifying aminopropyl silica beads with a NIPAM-based microgel particles with two incorporated co-monomers: butyl methacrylate (BMA) and *N,N*-dimethylaminopropylacrylamide (DMAPAAm). Changing the temperature and pH caused the surface of the modified stationary phase to switch between hydrophilic/hydrophobic and charged/uncharged forms. Temperature changes can also cause the ion exchange groups to be exposed on the surface or hidden. This highly affects the retention time of the analytes. The authors suggest the new method will be suitable for the separation of charged biomolecules such as proteins, DNA and peptides, and they refer to this technique as “temperature-responsive chromatography.”

The work reported herein aims to determine the quantity of microgel particles deposited on different surfaces under specified conditions and to discuss the factors affecting it (substrate surface charge, surface roughness, hydrophilicity/hydrophobicity and the temperature at which the deposition/desorption processes take place). This is important to move the applications of stimuli responsive surfaces from the research phase to the practical application one with special consideration to the commercial factors associated with this process. To determine the amount of microgel particles deposited on a surface, a simple dip-coating technique was used, where the solid surface was dipped into a microgel dispersion of known loading, then left for three hours before the concentration of the supernatant was measured to infer the number of microgel particles deposited on the surface. A new fluorescent-labelled microgel particle (poly(*N*-isopropylacrylamide-co-5% vinyl cinnamate) was synthesized and fluorescence spectroscopy was used to determine the concentration of the microgel particles in the dispersions before and after solid dipping. This increases the sensitivity and reliability of the quantitation of deposited particles.

2.1.1 Vinyl cinnamate

Vinyl cinnamate (Figure 2.1) is a fluorescent molecule that is partially miscible in water and is believed to possess nematocidal activity (9). It was reported that cinnamates are photo-responsive and photo-cross-linkable and are therefore used in microelectronics (10).

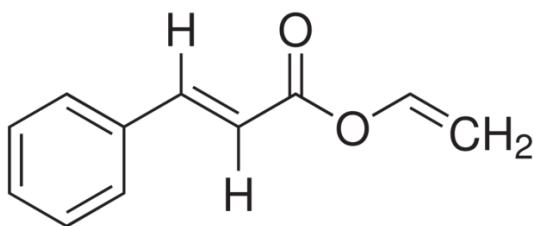


Figure 2.1 Molecular structure of vinyl cinnamate

2.1. Materials and methods

2.2.1 Microgel synthesis

In a 1 L reaction vessel, 1.84 mmol of the initiator 2,2-azobis(2-methylpropionamide) was dissolved in 800 mL of distilled water. A three-necked lid was clamped to the reaction vessel, which was then heated to 70°C with continuous stirring. The monomer (41.97 mmol NIPAM), co-monomer (1.43 mmol vinyl cinnamate, VC) and cross linker (3.24 mmol *N,N'*-methylenebisacrylamide) were stirred in distilled water (200 ml) then transferred into the reaction vessel containing the initiator and continuously stirred at 70°C for six hours under an inert atmosphere of nitrogen. When the reaction was complete, the microgel dispersion was allowed to cool to room temperature. Given the photosensitivity of VC, all the glassware used was wrapped in aluminium foil to protect the reaction from light and avoid the dimerization of VC molecules, which may have interfered with the polymerization reaction. The microgel dispersion was dialyzed in fresh de-ionized water changed daily for a week, centrifuged to decrease the water content and then the pellet was freeze dried. The resulting novel poly(NIPAM-co-5% vinyl cinnamate) microgel particles are herein referred to as p(NIPAM-co-5% VC).

A 100% p(NIPAM) dispersion was also prepared using the same method (without incorporation of the VC co-monomer), so that the characteristics of the novel p(NIPAM-co-5% VC) co-polymer particles could be compared with those of a standard, well characterized system.

2.2.2 Microgel characterization

2.2.2.1 Dynamic light scattering

Dynamic light scattering (DLS) measurements were carried out using a Malvern Zetasizer Nano ZS and a quartz cuvette with two polished windows (Starna Type 1). All samples were diluted with deionized water (1 mL of dialysed microgel dispersion was diluted with 2 mL of water) before measurements. The hydrodynamic diameter of the particles was measured in response to temperature change from 15 to 60°C). The temperature of the dispersion was controlled by a Peltier thermocouple. Data were collected every 1°C and the samples were equilibrated for 2 min before each data collection point. Three measurements, each consisting of 13 subruns, were taken at each temperature to obtain an average hydrodynamic diameter. The pH of the samples was adjusted to pH 3 or 10 using diluted HCl and NaOH to test for the effect of changing pH upon the size of the particles.

2.2.2.2 Fluorescence spectroscopy

A Horiba Jobin Yvon Fluoromax 4 spectrofluorometer was used for fluorescence experiments to determine the mass of microgel particles either deposited, or subsequently desorbed from, each surface. Firstly, a calibration curve was obtained using a known concentration of p(NIPAM-co-5% VC) dispersion that was prepared by re-dispersing freeze dried particles in water then underwent serial dilution. All samples were excited at 300 nm and the full emission spectra (315-540 nm) were recorded with bandwidth of 5 nm at 25°C. A 10 mm path length quartz cuvette with four polished windows (Starna Type 3) was used for all the measurements.

2.2.3 Slide surface treatments

2.2.3.1 Glass and quartz

Glass microscope slides were supplied by Sail Brand (75 x 25 mm, 1-1.2 mm thick). Quartz microscope slides (75 x 25 mm) were supplied by GPE Scientific Limited. To study the effect of surface treatment on the mass of microgel particles adsorbed on the surface, two types of glass surface were tested. The acid pre-treated glass and quartz slides were prepared in the same way: they were thoroughly washed with de-ionized water, sonicated in MeOH:HCl (1:1) (pH 0.12) for 30 min, thoroughly washed with de-ionized water, sonicated in 2 M H₂SO₄ for 30 min then finally rinsed with de-ionized water and stored in MeOH. The base pre-treated glass slides were thoroughly washed with de-ionized water, sonicated in MeOH:NaOH (1:1) (pH 11) for 30 min, rinsed with deionised water and stored in MeOH. Prior to use, all the slides were thoroughly washed with water and dried under N₂.

2.2.3.2 Stainless steel

Stainless steel slides were supplied by Reco Engineering Components Limited (75 x 25 mm, 1.2 mm thick). The slides were physically cleaned with wire wool, sonicated in 1.5% NaOH (pH 11) for an hour and then dried in oven at 50°C for an hour before use.

2.2.3.3 Gold

Clean microscope glass slides were coated with gold obtained from Agar Scientific by sputter coating from an Edwards 150B sputter coater. Both sides of the glass slides were coated before being kept in a clean container and used without any further treatment.

2.2.3.4 Teflon

A PTFE plastic sheet stock was supplied by RS Company and laser cut into slides (75 x 25 mm). The slides were thoroughly washed and sonicated for an hour in fresh soapy water (Teepol multipurpose detergent), then stored in fresh soapy water. Prior to use, slides were thoroughly washed with de-ionized water and dried under N₂.

2.2.4 Surface deposition/desorption of microgel particles

Dip coating was used to deposit microgel particles onto the different slide surfaces. The solid slides were dipped into Petri dishes containing 20 mL of a 2% w/v dispersion of p(NIPAM-co-5% VC). For each type of solid surface, three samples were coated (deposited) at 25°C and three at 60°C. Control experiments (of microgel dispersion alone, with no dipping of slides) were conducted in parallel to account for the adsorption of microgel particles on Petri dishes.

The slides were left covered in the Petri dishes for 3 hours. The slides were then removed from the residual microgel dispersions, which were then analysed using fluorescence spectroscopy (Section 2.5.1).

For desorption experiments, the solid slides previously used in the deposition experiments (Section 2.4.1) were dipped in Petri dishes containing 20 mL of deionized water and left for 3 hours. Again for each type of solid surface, three samples were desorbed at 25°C and three were desorbed at 60°C. Parallel control experiments were carried out to account for the deposition of microgel particles on Petri dishes. The residual microgel dispersions were then analysed using fluorescence spectroscopy (Section 2.5.1).

2.2.5 Surface characterization

2.2.5.1 Fluorescence spectroscopy

For the fluorescence measurements in all the deposition experiments, as well as the glass, quartz and stainless steel desorption experiments, the residual microgel dispersions remaining after deposition/desorption were firstly stirred then diluted by a factor of 1/4000. For the gold and Teflon desorption experiment fluorescent measurements, the residual microgel dispersions remaining after desorption were stirred but used undiluted. Measurements were carried out the same way as section 2.2.2.

The concentration of microgel particles (w/v) in the residual dispersions was calculated from the fluorescence intensity measurements using the calibration curve (Figure 2.4), then the mass of microgel particles in each residual dispersion was determined. The mass of microgel particles deposited was calculated by subtracting the mass of microgel particles in the residual dispersion from that in the control (2 % w/v microgel dispersion in a Petri dish that is treated the same as the sample).

2.2.5.2 Atomic force microscopy (AFM)

A Nanosurf easyscan 2 AFM was used to analyse both bare surfaces and surfaces with deposited microgel particles. Tapping mode was used using Tap190Al-G tips supplied by Budget Sensors. The image size per run was 10 μm by 10 μm at a resolution of 1024 lines, each containing 1024 points. The time per line was 1.5 s. Three sites per slide and three slides of each sample were tested to look at the uniformity of results.

2.2.5.3 Energy dispersive X-ray spectroscopy (EDX)

A Hitachi SU8030 FEG-SEM with a Thermo-Noran NSS system 7 EDX was used to determine the elemental composition of the bare solid surfaces before the deposition of the microgel particles.

2.3 Results and discussion

Cinnamic acid derivatives are widely used as fluorescent probes (11). They also possess some biological activity including an anti-tumor effect (11, 12). In this work, VC was used as a co-monomer to synthesize fluorescent colloidal microgel particles. The presence of a pendant vinyl group in the molecular structure of VC makes it readily polymerizable.

2.3.1 Characterization of p(NIPAM-co-5% VC) microgel particles

2.3.1.1 Size and VPTT

Figure 2.2 shows the change in particle size of p(NIPAM-co-5% VC) in response to temperature change. The initial particle diameter (below the VPTT) is approximately 280 nm and shrinks to 160 nm upon increasing the temperature above the VPTT. This is significantly smaller than 100% p(NIPAM) (synthesized in the same way) with a typical initial particle size of 550 nm (13) that shrinks to 290 nm above the VPTT. The incorporation of a hydrophobic co-monomer such as VC decreases the extent of water incorporation in the particle in comparison to 100% p(NIPAM), leading to a smaller particle size.

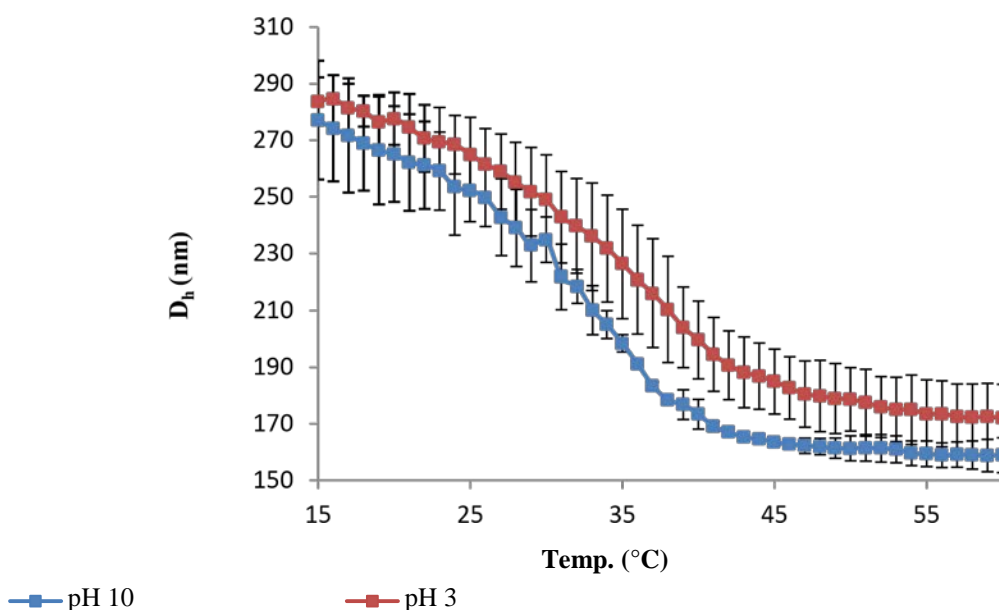


Figure 2.10 over a temperature range of 15-60°C 2 The effect of temperature (heating) on the particle size of p(NIPAM-co-5% VC) at pH 3 and

Figure 2.2 also indicated that the VPTT of the p(NIPAM-co-5% VC) particles is around 33°C, very similar to the VPTT of 34°C reported for the p(NIPAM) microgel particles (11). Together, these results confirm that incorporation of VC did not lead to a loss of thermosensitivity of the microgel particles but did influence (reduce) the particle size and extent of de-swelling.

Figure 2.2 also shows no significant difference between the particle size at pH 3 and 10. This is because the VC molecule does not include ionizable groups that would be affected by the change in pH. The minimal difference observed between the two pH values can be attributed to the cationic initiator groups on the particle surface.

2.3.1.2 Fluorescence spectroscopy

In order to confirm whether the VC co-monomer had been incorporated into the microgel particle structures, the emission spectra of 100% p(NIPAM) was compared with that of p(NIPAM-co-5% VC) when excited at the same wavelength (300 nm) (Figure 2.3). There is a clear shift in the emission band when comparing the two spectra. Furthermore, the p(NIPAM-co-5% VC) has the same reported λ_{em} as that of VC (350 nm) (14), which also

supports the conclusion that VC was incorporated into the new particles. In order to determine the concentration (w/v) of dispersions containing an unknown quantity of p(NIPAM-co-5% VC), a calibration curve at 25°C was prepared (Figure 2.4).

Figure 2.5 compares the response of 50 µg/mL p(NIPAM-co-5% VC) and 100% p(NIPAM) to changing temperature (heating-cooling) using fluorescence spectroscopy. When the temperature increases, the temperature-sensitive microgel particles shrink. This increases the local density of the incorporated VC fluorophores within the particle, leading to an increase in the overall fluorescence intensity of the microgel dispersion. The figure also shows that the VPTT p(NIPAM) is around 35°C while that of p(NIPAM-co-5% VC) is around 30°C. This is close to the VPTT shown by the DLS data in figure 2.2.

Figure 2.5 shows that the fluorescence intensity of p(NIPAM-co-5% VC) is almost five times greater than that of 100% p(NIPAM) considering that both dispersions are of the same concentration. Therefore, addition of a VC fluorophore co-monomer provides a sensitive method (at a concentration of 50µg/mL) for the quantitative analysis of the concentration (w/v) of microgel dispersions.

2.3.2 Characterization of solid surfaces

2.3.2.1 Energy dispersive X-ray spectroscopy

Figure 2.6 shows the EDX spectra and element composition of stainless steel, quartz, glass and Teflon samples used in this work as detected by EDX. The data show that the main component of stainless steel is iron followed by a considerable amount of chromium. This agrees with the results of Tanaka *et al.* (15). The stainless steel slides also contain nickel and traces of manganese. Unlike glass, quartz samples are purely composed of SiO₂. EDX results show that the glass surface include sodium, calcium and traces of magnesium, aluminium, potassium and sulphur.

The table also shows that the main constituents of Teflon used in this work are carbon and fluorine without any other impurities. This is to be predicted given that the Teflon molecular structure is CF₂-CF₂ (16).

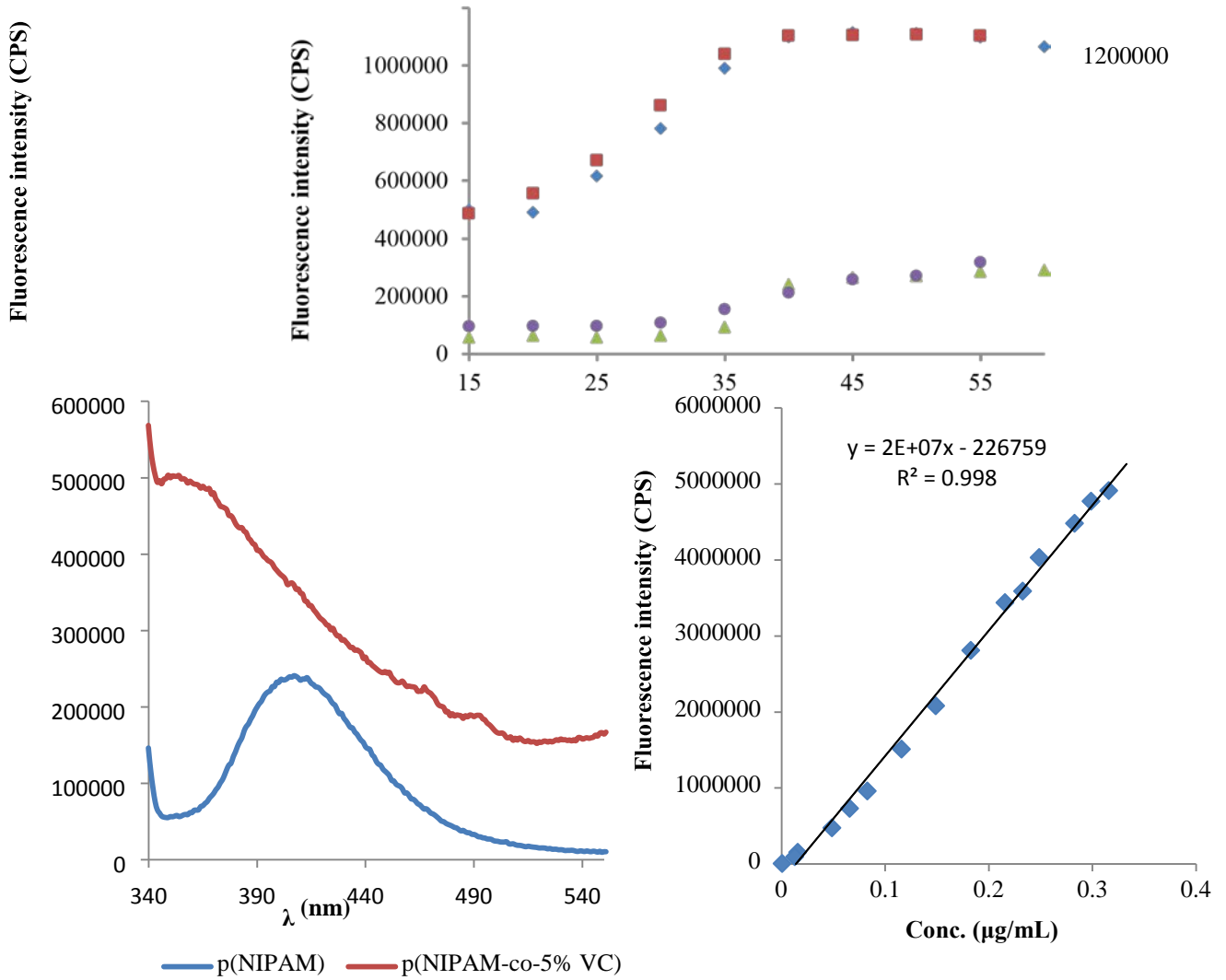


Figure 2.3 Comparison between the emission spectra of 50 µg/mL of 100 % p(NIPAM) and 5% VC in water, excited at 300 nm at 25°C

Figure 2.4 Calibration curve of p(NIPAM-co-5% VC) in water at 25°C, excited at 300 nm and emitted at 350 nm

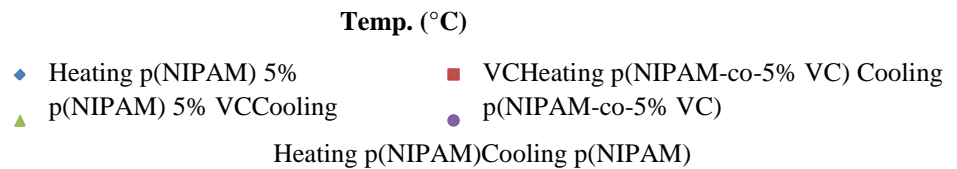
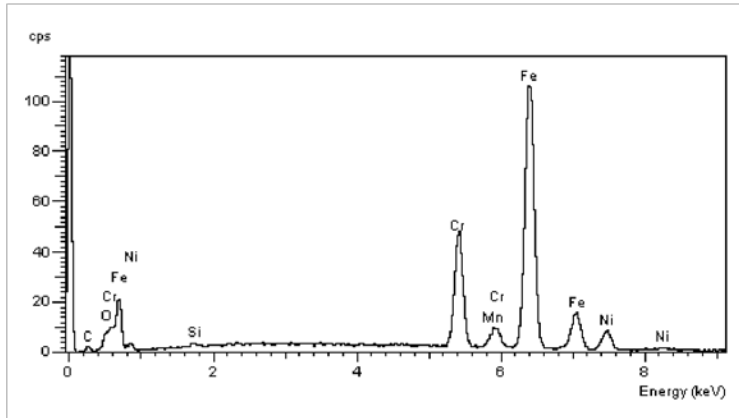


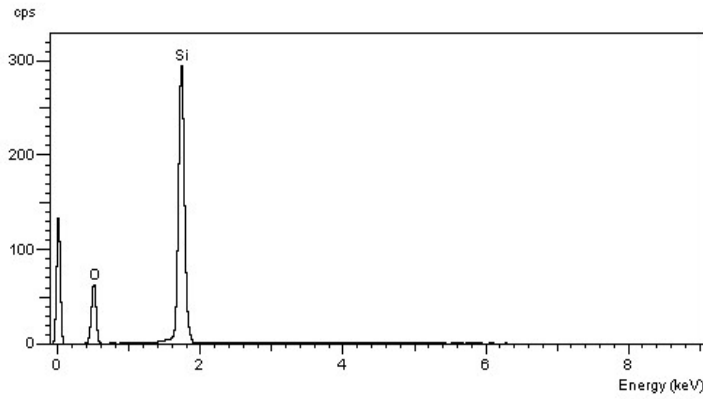
Figure 2.5 Fluorescence intensity of 50 µg/mL 100% p(NIPAM) and p(NIPAM-co-5% VC) in water in response to heating/cooling from 15-60°C, excited at 300 nm and emitted at 350 nm

Stainless

Mn 1.7



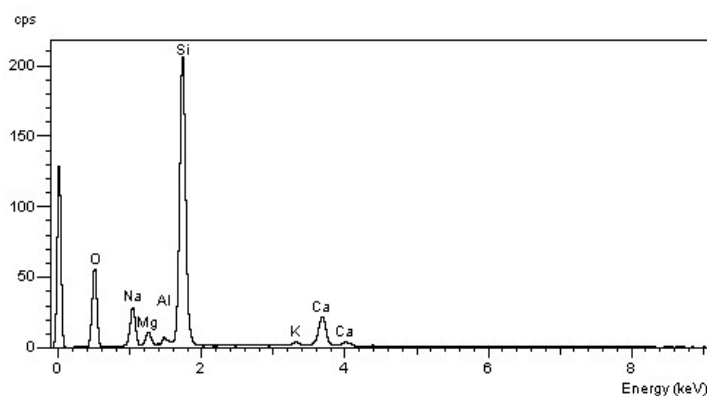
Element	Element %
Fe	72.0
Cr	18.57.7
Ni	steel



Element	Element %
Si	46.7
O	53.3

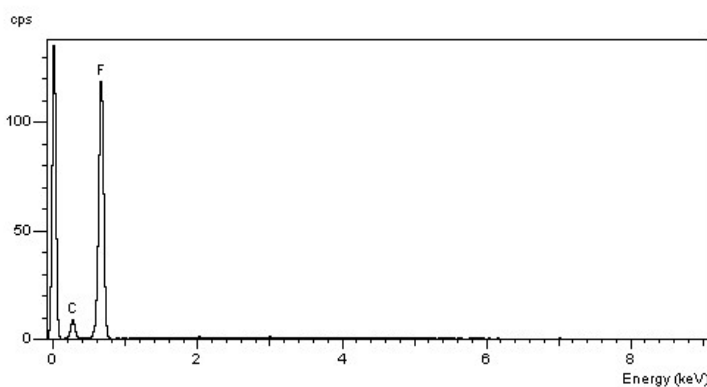
Quartz

Glass



Element	Element %
Na	10.1
Mg	2.7
Al	0.8
Si	33.80.1
K	0.5
Ca	5.1

Teflon



Element	Element %
C	20.3
F	79.7

Figure

2.6 Energy-dispersive x-ray analysis (EDX) of stainless steel, quartz, glass and Teflon

stainless steel, quartz, glass and Teflon

2.3.3 Factors affecting the mass of p(NIPAM-co-5% VC) deposited on different surfaces

Table 2.1 shows the mass of microgel particles adsorbed on each surface based on fluorescence spectroscopy measurements. At 25°C (lower than the VPTT of p(NIPAM-co5% VC), Figure 2.2). Stainless steel adsorbed the highest mass of microgel followed by glass pre-treated with base, glass pre-treated with acid, quartz, gold then teflon. The mass of particles deposited on steel was about five times that deposited on glass, ten times that deposited on quartz, fifty of gold and three hundred and sixty that on Teflon. Not only did steel have a large mass of microgel particles deposited on its surface but also a low desorption percentage and therefore the highest affinity towards the microgel particles.

At 60°C (above the VPTT of p(NIPAM-co-5% VC)) the mass of particles deposited on all surfaces was increased and, apart from base pre-treated glass, the percentage desorption decreased. The factors affecting the net mass of microgel particles deposited on or desorbed from the different surfaces will be discussed in detail below.

2.3.3.1 Effect of surface charge

For any given solid surface, usually there are functional groups expressed on the surface. The extent of ionization of these groups can be altered by changing the pH of the surrounding environment. This can be used to control the adsorption/desorption onto/from a solid surface. Therefore slide surface charge can be described by the point of zero charge (PZC). This is the pH where the net charge on the surface is zero (17).

Stainless steel

Takehara and Fukuzaki (18) reported the importance of stainless steel treatment on controlling its surface charge. They compared the surface charge of non-treated and acid-treated stainless steel and claimed that the surface charge is affected by the protonation ($M-OH_2^+$) and deprotonation ($M-O^-$) of the surface hydroxyl groups. Accordingly, acid treated stainless steel exhibited a protonated positive charge.

Table 2.1 Expected and measured characteristics of solid surfaces before deposition of microgel particles (surface charge, relative hydrophobicity and surface roughness), and microgel particle mass deposited and % desorbed from slide surfaces at 25°C and 60°C

Slide surface	Expected slide surface charge ¹	Contact angle with water and hydrophobicity/hydrophilicity	Measured average surface roughness S_a (nm)	25°C		60°C	
				Net mass microgel particles deposited (mg/m ²)	% Desorption	Net mass microgel particles deposited (mg/m ²)	% Desorption
Stainless steel	Negative	70-75° (21) Hydrophobic	89.60	21.64 (3.87)	6.30	25.84 (1.10)	4.20
Gold	Negative	56-66° (21, 22) Hydrophobic	7.07	0.43 (0.02)	41.00	5.32 (2.88)	6.60
Quartz	Slightly negative	22° (23) Hydrophilic	0.37	1.99 (1.60)	55.70	2.91 (2.22)	39.00
Base pre-treated glass	Negative	<10° (23) Hydrophilic	0.02	4.83 (1.38)	0.06	8.94 (0.80)	19.00

¹ Expected slide surface charge at pH of deposition microgel dispersion (pH 6.7) ²

Standard deviations presented in brackets

p(NIPAM-co-5% VC)

Chapter Two

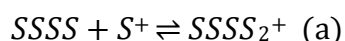
Acid pre-treated glass	Slightly negative		0.02	3.71 (0.85)	2.87	4.55 (1.89)	0.20
Telfon	Neutral	102° (23) Hydrophobic	103.7	0.06 (0.03)	90.00	2.13 (1.15)	34.00

Tanaka *et al.* (15) studied the concentration of hydroxyl groups on stainless steel surfaces and determined the PZC. The EDX data (Table 2.1) show a similarity between the composition of stainless steel used in this work and that used by Tanaka, who found untreated stainless steel to have a PZC of 5.6. Accordingly, it was claimed that the surface charge of stainless steel in a solution of pH 11 (far above the PZC) is negative.

In this work, stainless steel samples were sonicated in NaOH (pH 11) to expose the surfaces to a pH far above the PZC to ensure that the surface charge of the slides was negative prior to immersion in the microgel dispersion. Also, knowing that the pH of the microgel dispersion used for adsorption experiments carried out in this work is 6.7 (still above the PZC of stainless steel), it can be concluded that the surface charge of stainless steel immersed in the microgel dispersion remains negative. The negatively charged stainless steel surface electrostatically attracts the positively charged microgel particles (which are cationic due to the initiator used during the particle synthesis). This increases the mass of microgel particles deposited on the surface as well as decreases the percentage desorption and hence stainless steel showed a high net deposited mass of microgel particles (Table 2.1).

Glass and quartz

When immersed in a liquid, the surface charge of glass depends on its chemical composition and the pH of the solution. This can either cause the association or dissociation of protons to/from the oxide surface leading to positive or negative surface charge, respectively (Equations 2.1a and b) (19, 20).



Equation 2.1



The point of zero charge of glass is pH 3.5, while that of silica is pH 2.8 (24). In this work, glass slides pre-treated with acid and base were used, whilst quartz samples were treated with acid.

For the base pre-treated glass samples, the pH of the solution used for sonication was much higher than the PZC of glass. So, the glass slide surface charge at this point was considered

to be strongly negative. When immersed in the microgel dispersion with a pH above the PZC, the glass surface charge is still expected to be strongly negative.

For the acid pre-treated samples (glass and quartz), the pH of the solutions used for treatment was much lower than the PZC of both glass and quartz, so the surface charge of the treated sample surfaces was considered to be positive, with SiOH_2^+ groups dominant on the surface prior to immersion in the microgel dispersion. When immersed in the microgel dispersion with pH (6.7) above the PZC of both glass and quartz, surfaces are expected acquire a low magnitude of negative charge. In comparison to the base pretreated glass samples, both glass and quartz pre-treated with acid are expected to have relatively fewer negative charges on their surface.

Table 2.1 shows that the mass of microgel particles deposited on glass samples pre-treated with a base (highly negatively charged) was more than that deposited on those pre-treated with acid (with relatively less negative surface charge than the base treated slides). Also, the percentage of desorption of particles from base-treated glass samples was much less than that of the acid-treated ones at 25°C. This is attributed to the strong electrostatic attraction between the highly negatively charged surface (base pre-treated samples) and the positively charged particles; these forces are much less for the acid pre-treated slides and hence the much higher percentage desorption. This indicates that the effect of substrate surface charge on the mass of deposited particles is pronounced.

At 60°C, the same pattern of results is observed except that the percentage desorption of particles from the base treated glass is higher than that desorbed from the acid treated one (Table 2.1). This could be due to increased repulsion forces between the positively charged particles (which have an increase in surface charge density when the temperature exceeds the VPTT) (25).

Gold

Barten *et al.* (26) studied the deposition of linear positively charged poly(2-vinyl pyridine) (PVP⁺) on a gold electrode. Knowing that the PZC of gold is 4.9 (26), they studied the effect of changing the pH in the range of 3.5 to 6 (it is claimed that the surface charge of gold is constant above pH 6) (26). A slight increase in the adsorbed amount of PVP⁺ upon increasing the pH of the solution was reported. This can be attributed to the increase of the electrostatic

attraction forces between the negatively charged surface (gold in pH above 4.9) and the positively charged PVP⁺.

In this work, gold-coated glass was immersed in a microgel dispersion of pH 6.7. Being above the PZC of gold (4.9) (26), the surface was then expected to be negatively charged. This suggests the presence of electrostatic attraction forces between the negatively charged substrate surface and the positively charged particles which is expected to result in a high net deposition mass of microgel particles. However, Table 2.1 shows that the mass of microgel particles deposited on gold substrate surfaces is the second lowest deposited mass when compared to the other surfaces. This can be attributed to the magnitude of negative charge on each substrate surface.

Teflon

The molecular structure of Teflon is a polymer of tetrafluoroethene. The absence of ionisable groups in the polymer suggests that the surface is neutral. Also, the CF₃ backbone minimizes the Van der Waals interaction forces between Teflon surfaces and anything that comes in contact with them. For these reasons, Teflon surfaces are said to have low surface energy and hence used as non-stick materials. So, the effect of the substrate surface charge is expected to be eliminated in this case. This is reflected by the fact that the mass of microgel particles deposited on Teflon was observed to be the least compared to the other substrates.

The expected surface charge of each surface and their relative hydrophobicities are summarized in Table 2.1. An electrostatic attraction force is generated between the negatively charged surfaces (stainless steel, base pre-treated glass, acid pre-treated glass, quartz and gold) and the positively charged microgel particles. For the acid pre-treated glass and quartz samples, the electrostatic attraction force between the surface and the particle is expected to be less than that between the base pre-treated glass sample and the particle. On the other hand, Teflon is neutral and thus there is no electrostatic force in this case.

Table 2.1 shows that the highest mass of deposited particles and the lowest desorption percentages were observed for stainless steel, base pre-treated glass, acid pre-treated glass, quartz and gold (negatively charged surfaces), while the neutral surface (Teflon) had the lowest deposition mass and the highest desorption percentage. Accordingly, the data suggest that the surface charge affects the mass of microgel particles adsorbed on/desorbed from

surfaces. The magnitude of the slide surface charge is also thought to be a significant factor affecting the adsorption/desorption of microgel particles on/from different negative surfaces. It was not possible to measure this within the scope of this study, however, as per discussed, an estimate of the relative surface charge could be inferred (*e.g.* acid pre-treated glass was less negatively charged than the base pre-treated one).

For the same surface (glass), increasing the negative surface charge on the glass slide by treating it with a base rather an acid increases the electrostatic attraction force between the negative glass surface and the positive microgel particle which increases the mass of deposited microgel particles (Table 2.1).

At 60°C, the ranking of different solid surfaces considering the adsorption/desorption of microgel particles on/from the surface is similar to that at 25°C. The minor changes observed (for example, at 25°C the mass of microgel particles adsorbed on acid pre-treated glass is more than that adsorbed on quartz while at 60°C, the opposite is observed) are thought to be due to the increased particle surface charge at 60°C (above the VPTT) which increases the electrostatic repulsion between particles. Also, the difference between the magnitude of surface charge of the different solid slide substrates will be an important factor.

2.3.3.2 Effect of surface roughness

Surface roughness (S_a) is a description of the “irregularity” of a surface (27). Figure 2.7 and Table 2.1 provide AFM topography images of each surface and the roughness average (S_a) of different surfaces before the deposition of microgel particles. These can be determined from line profiles across a section of surface (Equation 2.2).

$$S_a = \frac{1}{L} \int_0^L |z(x) - z_0| dx \quad \text{Equation 2.2}$$

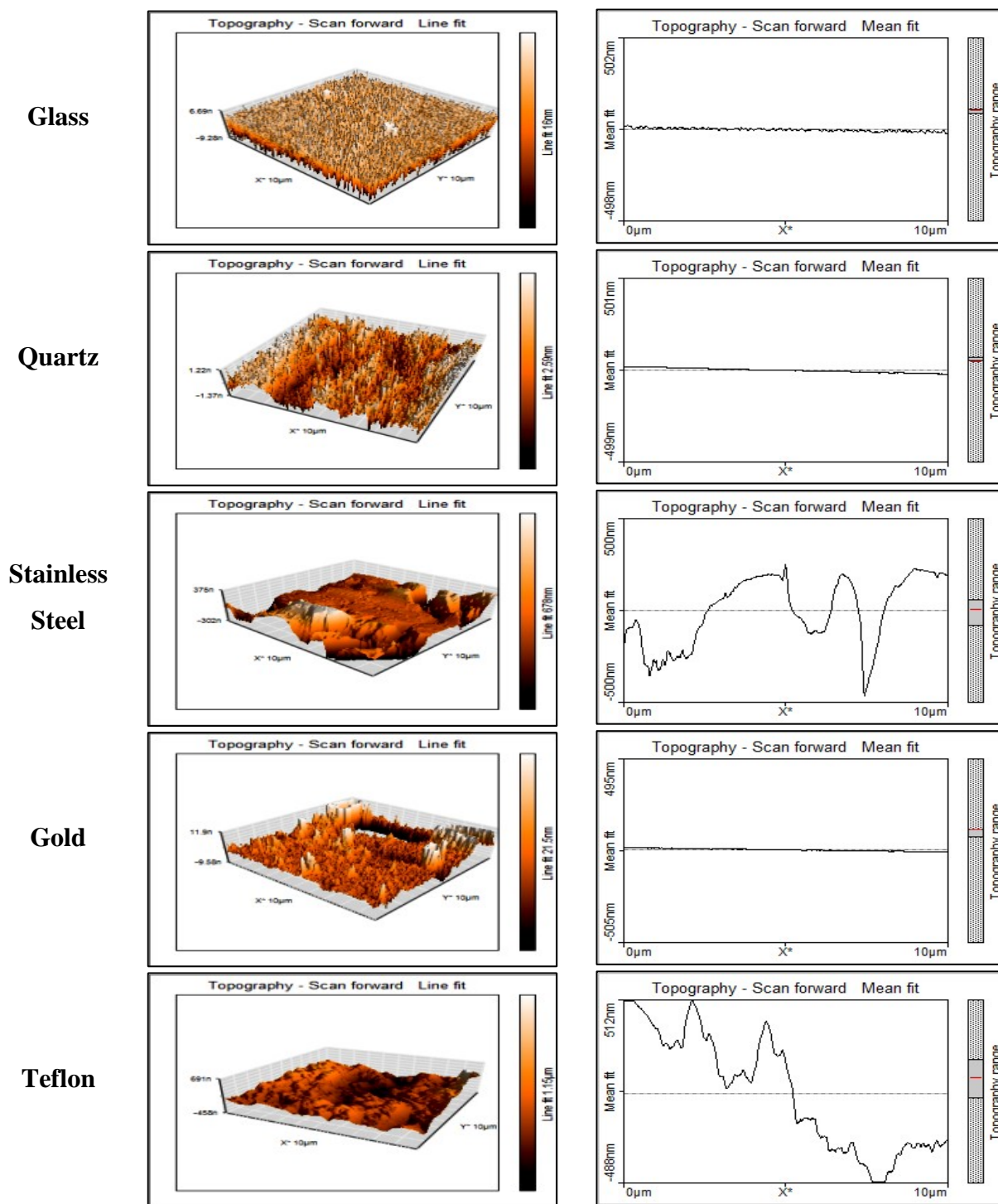


Figure 2.7 AFM topography and line profile for glass, quartz, stainless steel, gold and Teflon before deposition of microgel particles

Where L is the evaluation length, z is the height and x is the distance along measurement (roughness profile). S_a is the area between the roughness profile and its mean line (Equation 2.2) (27). The higher the S_a value, the deeper and/or wider are the pores on the sample

surface. These pores can trap microgel particles inside and increase the surface area where the particles can be adsorbed. The S_a values of the solid surfaces before the deposition of microgel particles (Table 2.1) show that Teflon has the highest surface roughness used in this work, followed by stainless steel, gold, quartz and glass, respectively. Comparing the surface roughness data (Table 2.1 and Figure 2.7) to that of deposition (Table 2.1), one can conclude that the degree of irregularity of the surface does not affect the mass of microgel particles deposited on/desorbed from it. For example, at 25°C, Teflon had the highest S_a and yet it had the lowest adsorption and the highest desorption percentage, whilst stainless steel had the second highest S_a , the highest deposition but one of the lowest desorption values. On the other hand, correlating the effect of surface roughness with that of surface charge, it is clear that for negatively charged surfaces (stainless steel, gold, quartz and base-treated glass), the one that possesses a significantly higher S_a (stainless steel) showed higher adsorption and lower desorption than the rest. For the latter three negatively charged surfaces where there was not much difference in S_a , the magnitude of surface charge is thought to be the main reason why the mass of microgel particles adsorbed on/desorbed from the surface varied. Hence, it can be concluded that the surface roughness can be considered as a secondary effect that boosts that of surface charge. The combination of both (surface charge and roughness) strongly influences the extent of adsorption and desorption on/from the surface. Comparing the mass of the net adsorbed particles on the stainless steel and base-treated glass samples (Table 2.1) supports this explanation. Both samples acquire a negative surface charge, yet the adsorption of the positive microgel particles on the stainless steel surface is 4.5 times more than that on glass. This is thought to be due to the fact that the average surface roughness of stainless steel is significantly higher than that of glass (Table 2.1 and Figure 2.7).

2.3.3.3 Effect of hydrophilicity/hydrophobicity

A comparison of the hydrophilicity/hydrophobicity of all surfaces (Table 2.1) suggests that this factor has a minimal effect on the amount of particles deposited on/desorbed from different surfaces. The surface with the highest adsorption and lowest desorption percentage (stainless steel) and that with the lowest adsorption and highest desorption (Teflon) are both thought to be hydrophobic (21, 23). Also, the difference between the mass of particles deposited on hydrophilic surfaces is significant. This suggests that the effect of hydrophilicity/hydrophobicity is of less importance than that of substrate surface charge and

surface roughness. However, further studies with more systematic comparison characters may help elucidate influence of relative hydrophilicity in more details.

2.3.3.4 Effect of temperature

The deposition/desorption data provided in Table 2.1 shows that the mass of microgel particles deposited on all surfaces at 60°C was higher than that at 25°C. Also, the percentage desorption decreased with temperature (except for base pre-treated glass), leading to an increased net mass of deposition. When the temperature increases above the VPTT (32°C), the particles deswell (Figure 2.5). This means that the surface charge density on the particle increases which increases the electrostatic attraction between the positively charged microgel particles and the negatively charged surfaces. Also, the number of de-swollen particles that fit in the pores of solid surfaces will be more than that of the swollen ones. AFM images (Figure 2.8) show that increasing the temperature above the VPTT affects the packing of the particles. In case of base pre-treated glass, the percentage of desorbed microgel particles is more than that at 25°C. The suggested reason for this is the increased electrostatic repulsion between the positive microgel particles when the temperature exceeds the VPTT (32°C).

Table 2.2 shows the S_a of adsorbed particles on different surfaces at 25 and 60°C. Despite the fact that the mass of microgel particles deposited at 60°C is higher than that deposited at 25°C (Table 2.2), the S_a (representing the roughness of the deposited layer) is generally (except for stainless steel and Teflon) smaller at 60°C than at 25°C. This is due to the regular dense packing of particles at 60°C while at 25°C this is not always the case (Figure 2.8). In case of stainless steel and Teflon, the S_a at 60°C is bigger than that at 25°C. This is thought to be caused by the increased electrostatic repulsion force between the positive microgel particles (due to increased surface charge density above the VPTT).

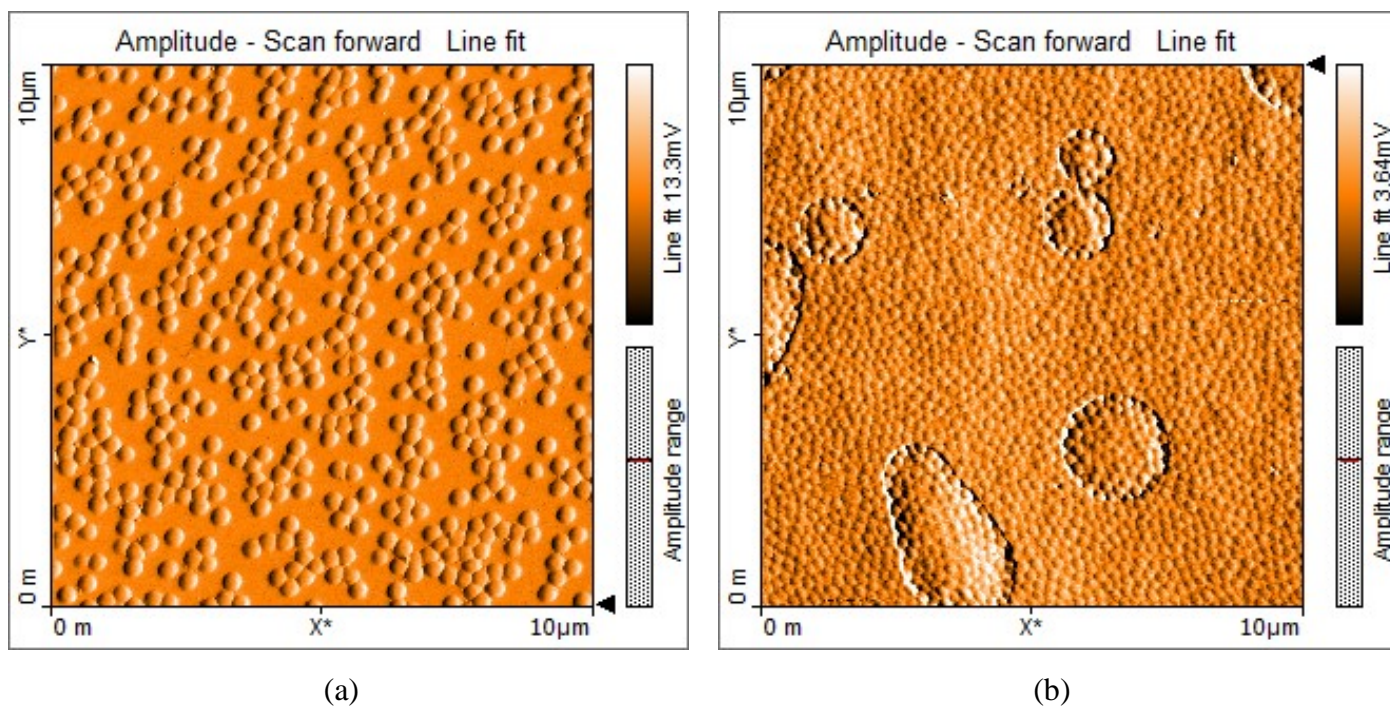


Figure 2. 8 AFM images of p(NIPAM-co-5% VC) particles deposited on glass (a) at 25°C and (b) at 60°C

Table 2.2 Comparison between the surface roughness averages of stainless steel, gold, quartz, glass and Teflon coated with p(NIPAM-co-5% VC) microgel particles at 25°C and 60°C

	S_a at 25°C (nm)	S_a at 60°C (nm)
Stainless steel	65	77
Gold	10	9
Quartz	25	10
Glass pre-treated with base	17	9
Glass pre-treated with acid	18	10
Teflon	19	43

2.4 Conclusions

A novel fluorescent temperature sensitive microgel particle (p(NIPAM-co-5% VC)) was synthesized and characterized. It was then used to develop a novel sensitive method (using fluorescence spectroscopy) to quantify the mass of microgel particles deposited on different solid surfaces per unit area and the factors affecting it. The mass of microgel particles deposited on/desorbed from different surfaces is affected by different factors, the most important of which is the surface charge followed by the surface roughness of the solid surface. The effect of temperature has also proved to be significant since it alters the physico-chemical properties of the microgel particles and hence alters its interaction with the solid surface. On the other hand, the effect of hydrophilicity/hydrophobicity of the solid surface was shown to be of less importance than the previously tested factors.

2.5 References

1. Alarco C. D., Farhan T., Osborne V. L., Huck W. T., Alexander C. Bioadhesion at micro-patterned stimuli-responsive polymer brushes. *Journal of Materials Chemistry*. 2005;15:2089–94.
2. Burkert S., Bittrich E., Kuntzsch M., Muller M., Eichhorn K. J., Bellmann C., Uhlmann P., Stamm M. Protein Resistance of PNIPAAm Brushes: Application to Switchable Protein Adsorption. *Langmuir*. 2010;26:1786–95.
3. Qin L., He X. W., Zhang W., Li W. Y., Zhang Y. K. Macroporous thermosensitive imprinted hydrogel for recognition of protein by metal coordinate interaction. *Analytical Chemistry*. 2009;81:7206–16.
4. Nagase K., Kobayashi J., Okano T. Temperature-responsive intelligent interfaces for biomolecular separation and cell sheet engineering. *Journal of the Royal Society Interface*. 2009;6:S293–S309.
5. Kanazawa H., Nishikawa M., Mizutani A., Sakamoto C., Morita-Murase Y., Nagata Y., Kikuchi A., Okano T. Aqueous chromatographic system for separation of biomolecules using thermoresponsive polymer modified stationary phase. *Journal of Chromatography A*. 2008;1191:157-61.
6. Ayano E., Nambu K., Sakamoto C., Kanazawa H., Kikuchi A., Okano T. Aqueous chromatography system using pH- and temperature-responsive stationary phase with ionexchange groups. *Journal of Chromatography A*. 2006;1119:58-65.
7. Wischerhoff E., Badi N., Laschewsky A., Lutz J. F. Smart polymer surfaces: concepts and applications in biosciences. *Advanced Polymer Science*. 2011;240:1-33.

8. Edahiro J., Sumaru K., Tada Y., Ohi K., Takagi T., Kameda M., Shinbo T., Kanamori T., Yoshimi Y. In situ control of cell adhesion using photoresponsive culture surface. *Biomacromolecules*. 2005; 6:970-4.
9. Kong J. O., Lee S. M., Moon Y. S., Lee S. G., Ahn Y. J. Nematicidal Activity of Cassia and Cinnamon Oil Compounds and Related Compounds toward *Bursaphelenchus xylophilus* (Nematoda: Parasitaphelenchidae). *Journal of Nematology*. 2007;39:31-6.
10. Assaid I., Bosc D., Hardy I. Improvements of the Poly(vinyl cinnamate) Photoresponse in Order to Induce High Refractive Index Variations. *The Journal of Physical Chemistry*. 2004;108:2801-6.
11. Singh T. S., Mitra S. Interaction of cinnamic acid derivatives with serum albumins: A fluorescence spectroscopic study. *Spectrochimica Acta Part A: Molecular and Biomolecular Spectroscopy*. 2011;78:942-8.
12. Min J., Meng-Xia X., Dong Z., Yuan L., Xiao-Yu L., Xing C. Spectroscopic studies on the interaction of cinnamic acid and its hydroxyl derivatives with human serum albumin. *Journal of Molecular Structure*. 2004;692:71-80.
13. Mohsen R., Vine G. J., Majcen N., Alexander B. D., Snowden M. J. Characterization of thermo and pH responsive NIPAM based microgels and their membrane blocking potential. *Colloids and Surfaces A: Physicochemical and Engineering Aspects*. 2013;428:53-9.
14. Torres J. M. Designing dual thermoresponsive & photoresponsive materials for biomedical applications. MSc. thesis, McMaster University; 2011.
15. Tanaka Y., Saito H., Tsutsumi Y., Doi H., Imai H., Hanawa T. Active Hydroxyl Groups on Surface Oxide Film of Titanium, 316L Stainless Steel, and Cobalt-ChromiumMolybdenum Alloy and Its Effect on the Immobilization of Poly(Ethylene Glycol). *Materials Transactions*. 2008;49:805-11.
16. Teng H. Overview of the Development of the Fluoropolymer Industry. *Applied Sciences*. 2012;2:496-512.
17. Appel C., Ma L. Q., Rhue R. D., Kennelley E. Point of zero charge determination in soils and minerals via traditional methods and detection of electroacoustic mobility. *Geoderma*. 2003;113:77- 93.
18. Takehara A., Fukuzaki S. Effect of the Surface Charge of Stainless Steel on Adsorption Behavior of Pectin. *Biocontrol Science*. 2002;7:9-15.
19. Sabia R., Ukrainczyk L. Surface chemistry of SiO₂ and TiO₂±SiO₂ glasses as determined by titration of soot particles. *Journal of Non-Crystalline Solids*. 2000;277:1-9.

20. Behrens S. H., Grier D. G. The Charge of Glass and Silica Surfaces. Online report, Department of Physics, James Franck Institute, and Institute for Biophysical Dynamics, The University of Chicago. 2008. <http://physics.nyu.edu/grierlab/charge6c/charge6c.pdf>. Accessed on 15th of February, 2012.
21. Arkles B. Hydrophobicity, Hydrophilicity and Silanes. Online report, Paint & Coatings Industry magazine. 2006. <http://www.gelest.com/goods/pdf/Library/advances/HydrophobicityHydrophilicityandSilanes.pdf>. Accessed on 10th of March, 2012.
22. Osborne K. L. Temperature-Dependence of the Contact Angle of Water on Graphite, Silicon, and Gold. MSc. thesis, Worcester Polytechnic Institute; 2009.
23. Sumner A. L., Menke E. J., Dubowski Y., Newberg J. T., Penner R. M., Hemminger J. C., Wingen L. M., Brauners T., Finlayson-Pitts B. J. The nature of water on surfaces of laboratory systems and implications for heterogeneous chemistry in the troposphere. *Physical Chemistry Chemical Physics*. 2004;6:604–613.
24. Churchill H., Teng H., Hazen R. M. Correlation of pH-dependent surface interaction forces to amino acid adsorption: implications for the origin of life. *American Mineralogist*. 2004;89:1048–55.
25. Thorne J. B., Vine G. J., Snowden M. J. Microgel applications and commercial considerations. *Colloid and Polymer Science*. 2011: 289:629-646.
26. Barten D., Kleijn J. M., Stuart M. A. Adsorption of a linear polyelectrolyte on a gold electrode. *Physical Chemistry Chemical Physics*. 2003;5:4258–64.
27. Amaral R., Chong L. H. Surface Roughness. Online report, 2002. <http://citeseerx.ist.psu.edu/viewdoc/download?doi=10.1.1.198.163&rep=rep1&type=pdf>. Accessed on the 7th of November 2013.

Chapter Three Design, synthesis and characterization of fluorescent poly(*N*-isopropylacrylamide-*co*acrylic acid)-ethylene diamine-rhodamine B particles

3.1 Introduction

Microgels can be functionalized with markers or labeling agents to aid targeted delivery and diagnosis (1-5). In previous research, microgels have been coupled to inorganic particles and dyes to synthesize magnetic-responsive and photosensitive drug delivery systems respectively (7). They have also been designed to respond to various external stimuli such as pH, ionic strength and electric current (8). Owing to their water-swollen polymeric structure and their controllable rheology, microgels have been employed as tissue-engineering scaffolds (9), as artificial muscle materials (10), as mechanical supporting gels in degenerated intervertebral discs (11) and for vocal fold regeneration (12).

In this work, p(NIPAM-*co*-5% acrylic acid) (p(NIPAM-*co*-5% AA)) particles were coupled to rhodamine B (RhB) using ethylene diamine (EDA) as a linker molecule between them. The objective of this work was to produce a fluorescent temperature and pH responsive particle that can be useful in different applications such as diagnostics. Also, the ability to incorporate fluorescent molecules with different molecular structures and to produce mono-dispersed particles was tested.

3.1.1 Rhodamine B (RhB)

Rhodamine B is a fluorescent molecule used as a labelling agent. Its IUPAC name is [9-(2carboxyphenyl)-6-diethylamino-3-xanthenylidene]-diethylammonium chloride. It has the advantages of a long wavelength of the spectroscopic signal of absorption and emission (which makes it easy to separate from biomolecules which mostly have short excitation and emission wavelengths (13)), high fluorescence quantum yield (that increases by increasing the hydrophobicity of its environment) and high photo-stability (14). Rhodamine B (RhB) is also used as a fluorescence standard (in the Parker and Rees method) to determine the absolute fluorescence quantum yield of other molecules (15). The quantum yield of rhodamine B is in the range of 0.45 to 0.5 (15).

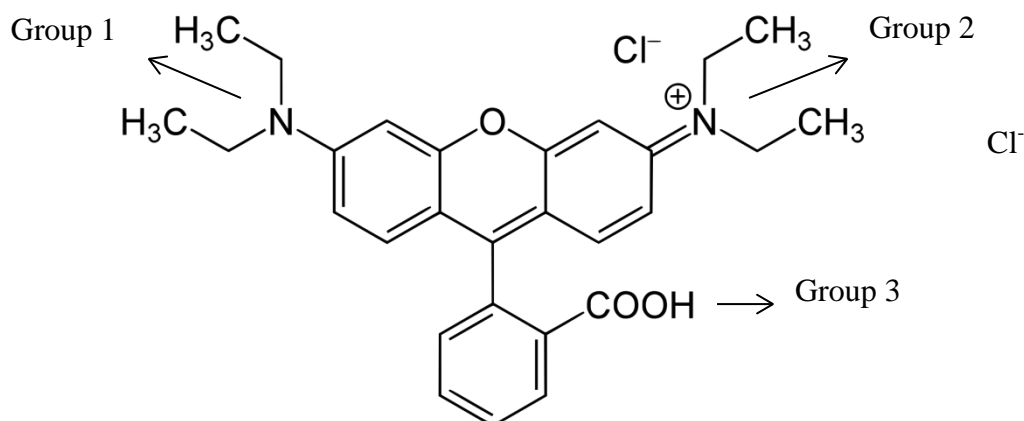


Figure 3.1 The molecular structure of rhodamine B

The molecular structure of rhodamine B is shown in Figure 3.1. The molecular structure is characterized by three ionizable groups, two of which are cationic (dimethyl amino groups) and one is anionic (carboxylic acid group).

The acid dissociation constant (pK_a) of RhB was calculated using ACD labs (6). RhB was found to have two close pK_a values, these are: $pH 3 \pm 0.9$ and $pH 3.8 \pm 0.8$ (6). The concentration of each protonation state of the RhB molecule versus pH as well as its two pK_a values are represented in Figure 3.2 (6). At pH 2, the three ionizable groups are protonated (6). When the pH increases above the pK_a , the COOH group (group 3) is deprotonated into COO^- as well as one of the cationic groups (group 1). Group 2 (N^+) carries a positive charge at all pH values (6). The positive charges on the cationic dimethyl amino groups (groups 1 and 2) are stabilized by the resonance effect of the aromatic rings attached to it (16).

This work aims at coupling the COOH group (group 3) of RhB to the NH_2 group of EDA and thus groups 1 and 2 are the only ionizable groups remaining after conjugation.

3.2 Materials and methods

3.2.1 Materials

N-isopropylacrylamide (NIPAM) (Wako), acrylic acid, *N,N'*-methylenebisacrylamide 99%, potassium persulfate, ethylenediamine (EDA), *N*-hydroxysuccinimide 98%, *N*-(3dimethylaminopropyl)-*N'*-ethylcarbodiimide hydrochloride, rhodamine B,

(4morpholineethanesulfonic acid monohydrate) 99.5% (MES) and sodium chloride were purchased from Sigma Aldrich UK and used without further purification.

3.2.2 Methods

3.2.2.1 Synthesis

For preparation of fluorescent microgels, three synthetic steps were performed: (i) synthesis of p(NIPAM-*co*-5% AA) microgels (ii) coupling of COOH groups in (NIPAM-*co*-5% AA) to EDA and (iii) coupling of microgels-EDA to rhodamine B fluorescent dye.

3.2.2.2 Synthesis of p(NIPAM-*co*-5% AA) (w/v)

p(NIPAM-*co*-5% AA) microgel particles were prepared using surfactant-free emulsion polymerization technique. In a 1 L reaction vessel, 0.5 g of potassium persulfate (initiator) was dissolved in 800 mL of deionized water. A three-necked lid was clamped to the reaction vessel, which was then heated to 70°C with continuous stirring. The monomer (4.75 g NIPAM), co-monomer (0.25 g acrylic acid) and cross linker (0.5g of *N,N'*-methylenebisacrylamide) were dissolved in 200 mL of deionized water then transferred in the reaction vessel containing the initiator. The reaction was then left to proceed for six hours under an inert atmosphere of nitrogen. After the reaction was terminated, the microgel particles were dialyzed in deionized water to remove unreacted species from the dispersion. The dialysis was undertaken in 7 cycles, changing the water every 24 hours.

3.2.2.3 Microgel-EDA coupling

Coupling of p(NIPAM-*co*-5% AA) to EDA was achieved via carbodiimide chemistry. The microgel particles (0.80 g p(NIPAM-*co*-5% AA)) was dispersed in 100 mL MES (0.1 M, pH 5.5). In another beaker, 0.24 g of EDA was dissolved in 5 mL MES (0.1 M, pH 5.5). EDA was then added drop-wise to the p(NIPAM-*co*-5% AA) dispersion and stirred. N-hydroxysuccinimide (0.86 g) and *N*-(3-dimethylaminopropyl)-*N'*-ethylcarbodiimide hydrochloride (0.76 g) were added into the reaction beaker and the reaction was left stirring at 300 rpm for 4 hours. Following the synthesis, p(NIPAM-*co*-AA)-EDA was dialyzed in deionized water for 7 cycles and then lyophilized.

3.2.2.4 Microgel-EDA-rhodamine B coupling

The EDA-containing microgels were further coupled to rhodamine B (RhB). Rhodamine B contains carboxylic acid groups which facilitate conjugation to the amine groups of EDA

via carbodiimide chemistry. Microgel-EDA particles (0.5 g) were dispersed in 80 mL MES (0.1 M, pH 5.5) in a beaker. In a separate beaker, a solution of RhB (0.3698 g) was dissolved in 5 mL MES. The RhB was added drop-wise to the microgel dispersion before *N*-hydroxysuccinimide (0.5424 g) and *N*-(3-dimethylaminopropyl)-*N*'-ethylcarbodiimide hydrochloride (0.4789 g) solid powders were added. The reaction proceeded for 4 hours at room temperature, stirring at 300 rpm. The new particles were dialyzed in fresh deionized water which was changed daily for 7 days.

3.2.2.5 Characterization of microgel particles

Microgel particles were characterized using several techniques to study the physicochemical properties of the novel particles. Dynamic light scattering was used to determine the particle size and the electrophoretic mobility of microgel particles. The turbidity of the particles was analyzed by UV spectroscopy. Infrared spectroscopy was used to determine the functional groups in each of the steps during the particle synthesis. Fluorescence spectroscopy and fluorescence microscopy were used to confirm the fluorescence of the novel RhB containing particles as well as visualize them and confirm the ability to trace them. Scanning electron microscope (SEM) was used to generate high-resolution images of the morphology of the particles.

3.2.2.5.1 Dynamic light scattering

Dynamic light scattering (DLS) measurements were carried out using a Malvern Zetasizer Nano ZS. All experiments were repeated 3 times, the figures shown were plot using the average of the experiments while the error bars represent the calculated the standard deviations.

The hydrodynamic diameter of the particles was measured in response to temperature in the 15 to 60°C range. All samples were diluted with deionized water (1 mL of dialyzed microgel dispersion was diluted with 2 mL of water) before measurements. A quartz cuvette with two polished windows (Starna Type 1) was used for all the measurements and the temperature of the dispersion was controlled by a Peltier thermocouple. Data were collected every 1°C and the samples were equilibrated for 2 min before each data collection point. Three measurements, each consisting of 13 subruns, were taken at each temperature to obtain an average hydrodynamic diameter. Experiments were also conducted where the pH of the

samples was adjusted to different pH values using HCl and NaOH to test for the effect of changing pH upon the size of the particles.

To measure the electrophoretic mobility of p(NIPAM-*co*-5% AA)-EDA and p(NIPAM-*co*5% AA)-EDA-RhB, samples were diluted (1 mL of dialyzed microgel dispersion was diluted with 2 mL of NaCl solution) to reach a salt concentration of 1×10^{-4} M NaCl. The electrophoretic mobility was measured in response to temperature change (heating) across the range of 15-60°C every 1°C with 2 minutes equilibration time using a disposable folded capillary cell.

3.2.2.5.2 Fluorescence spectroscopy

The fluorescence emission spectra of microgels and RhB were determined using a FluoroMax-4 Spectrofluorometer from Horiba Jobin Yvon. All samples were excited at 430 nm and the full emission spectra (450–1050 nm) were recorded with bandwidth of 5 nm at 25°C. A 10 mm path length quartz cuvette with four polished windows (Starna Type 3) was used for all the measurements.

3.2.2.5.3 Infrared spectroscopy

A Shimadzu IR-Prestige 21 Fourier-transform infrared spectrophotometer FT-IR was used to carry out the IR experiment in this work. Microgel dispersions were dialyzed and freeze-dried then the solid samples were used for IR experiments using attenuated total reflection (ATR) with a diamond crystal.

3.2.2.5.4 Microscopy

3.2.2.5.4.1 Scanning electron microscopy

A Hitachi SU8030 cold cathode field-emission gun scanning electron microscope operating with an accelerating voltage of 30 kV was used to obtain images of the novel particles using a transmission detector. To prepare the samples, 1 μ L of each of p(NIPAM-*co*-5% AA), p(NIPAM-*co*-5% AA)-EDA, p(NIPAM-*co*-5% AA)-EDA-RhB was tipped onto a separate carbon coated copper TEM grid. Samples (on the grid) were then left to dry in air, placed on the sample holder, then introduced in the vacuum chamber of the SEM.

3.2.2.5.4.2 Fluorescence microscopy

A Nikon Eclipse 90i microscope, fitted with a fluorescein isothiocyanate filter (FITC) and a Nikon Digital Sight DS-U3 camera were used to take fluorescent images of the particles.

Plan Fluor x100 oil Ph3 DLL lens was used with working distance of 0.16 mm. The numerical aperture of the objective was 1.3, refractive index 1.5 and exposure time 3 s. The sample was placed on a microscopic slide, left to dry in air and then immersion oil was added on it.

3.3 Results and discussion

The advantages of environmental-responsive microgels include the flexibility of the synthesis strategies used to produce them and the ability to incorporate co-monomers with different structures and of different chemical classes. Different synthesis strategies have been used by different researchers to synthesize NIPAM based particles with different comonomers. An important factor that affects the synthesis protocol is the molecular structure of the co-monomer. Most of the co-monomers that incorporate a pendant vinyl group can undergo direct polymerization synthesis where the co-monomer can be directly added to the synthesis reaction vessel. For co-monomers with no vinyl group but their structure possesses amino (NH₂) or carboxylic (COOH) groups, coupling chemistry can be used to attach these groups to relevant groups in the particle (acidic or basic groups, respectively). For example, to attach a co-monomer with a NH₂ group, a p(NIPAM-*co*acrylic acid) particle can be synthesized and then the COOH of acrylic acid can be coupled to the NH₂ of the pendant molecule (attachment). In this work, the pendant molecule used (rhodamine B) includes a COOH group in its molecular structure (Figure 3.1). Accordingly, a three-steps-synthesis method was designed as previously discussed in the methods section.

Figure 3.2 represents the suggested molecular structure of p(NIPAM-*co*-5% AA)-EDARhB. The surface of the particle carries SO₄⁻ from the anionic initiator (potassium persulfate) used during the synthesis of p(NIPAM-*co*-5%AA) in step 1. Some of the COOH acid groups (from the co-monomer acrylic acid) are expected to be conjugated to NH₂ of EDA (in step 2) while some are expected to be free.

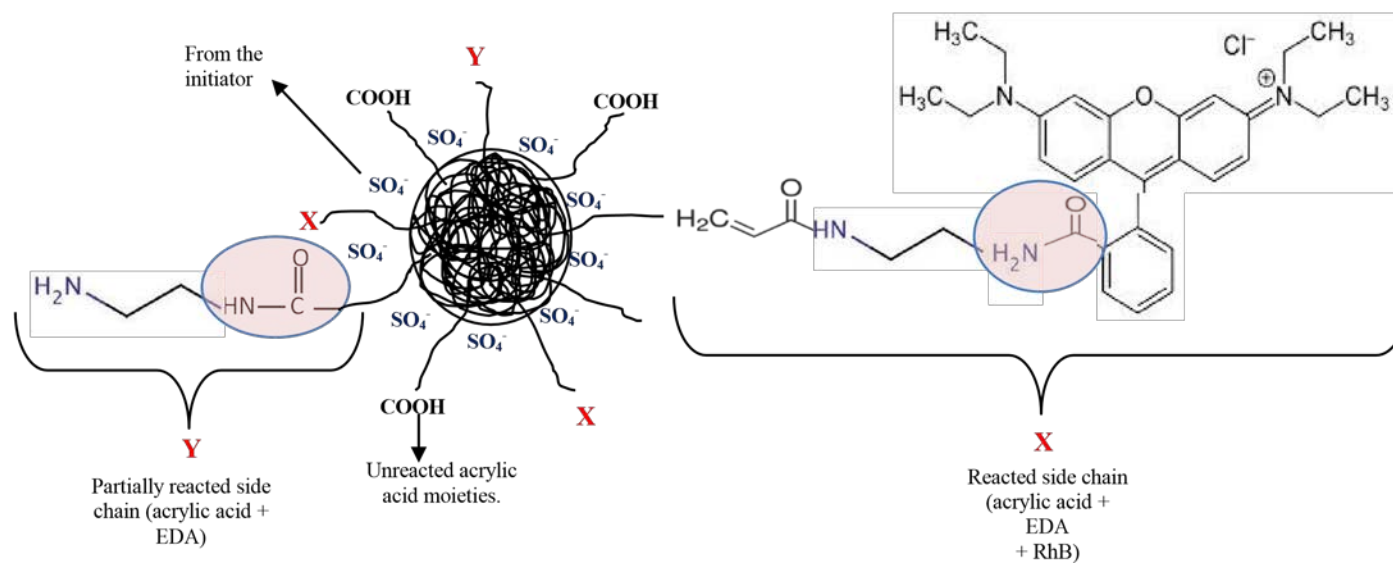


Figure 3.2 The suggested molecular structure of p(NIPAM-co-5% AA)-EDA-RhB

Similarly, some of the NH₂ of the EDA are expected to be conjugated with the COOH of RhB while some others are expected to be unattached. Accordingly, two chains are expected to be conjugated to the particle; these are COOH-EDA-RhB and COOH-EDA. Charged species on the particle surface are expected to be: SO₄⁻, COOH of AA, NH₂ of EDA and N⁺ of RhB.

3.3.1. Particle size analysis

3.3.1.1 Effect of temperature

Figure 3.3 shows the change in particle size of p(NIPAM-*co*-5% AA), p(NIPAM-*co*5% AA)-EDA and p(NIPAM-*co*-5% AA)-EDA-RhB. The figure shows that the three different particles mentioned above maintain the thermo-sensitivity where the particle size changes when the temperature exceeds the VPTT (35°C). The initial particle size of p(NIPAM-*co*-5% AA) at 15°C is around 500 nm which is similar to the previously reported particle size previously mentioned in literature (17). Increasing the temperature above the volume phase transition temperature (VPTT) (35°C), the particles deswell and the particle size decreases to be 250 nm. Table 3.1 shows that the PdI value (polydispersity index = standard deviation/mean size) of p(NIPAM-*co*5% AA) at both 15°C and 60°C is 0.04. Having a PdI value very close to zero indicates the mono-dispersity of the particles. This means that all the particles are of the same size. This is because the AA molecule incorporates a vinyl group and is directly co-polymerized with the p(NIPAM) particles during the synthesis.

Conjugating the COOH groups of p(NIPAM-*co*-5% AA) with the amino group of hydrophilic ethylenediamine (EDA) causes the particle size to increase. At 15°C, the particle size of p(NIPAM-*co*-5% AA)-EDA is 1150 nm which is almost double that of p(NIPAM-*co*-5% AA) at the same temperature. p(NIPAM) particles are characterized by a hydrophobic core and a hydrophilic shell (18), accordingly, when conjugated with a hydrophilic co-monomer, it tends to be located in the particle shell (surface). Hydrogen bonding between the hydrophilic EDA on the particle surface and the water molecules in the dispersion is created. This leads to an increase in the particle size as shown in Figure 3.3.

A change in the behavior of p(NIPAM-co-5% AA)-EDA particles is observed at 38°C which is slightly higher than the equivalent temperature (VPTT) of p(NIPAM-co-5% AA) (35°C). This is due to the increased hydrogen bonding between the particles and the water molecules (18) (due to incorporating a hydrophilic co-monomer). At 15°C, p(NIPAM-co-5% AA)-EDA particles show a PDI of 0.02 which means that they are all of the same size (all swollen due to the EDA).

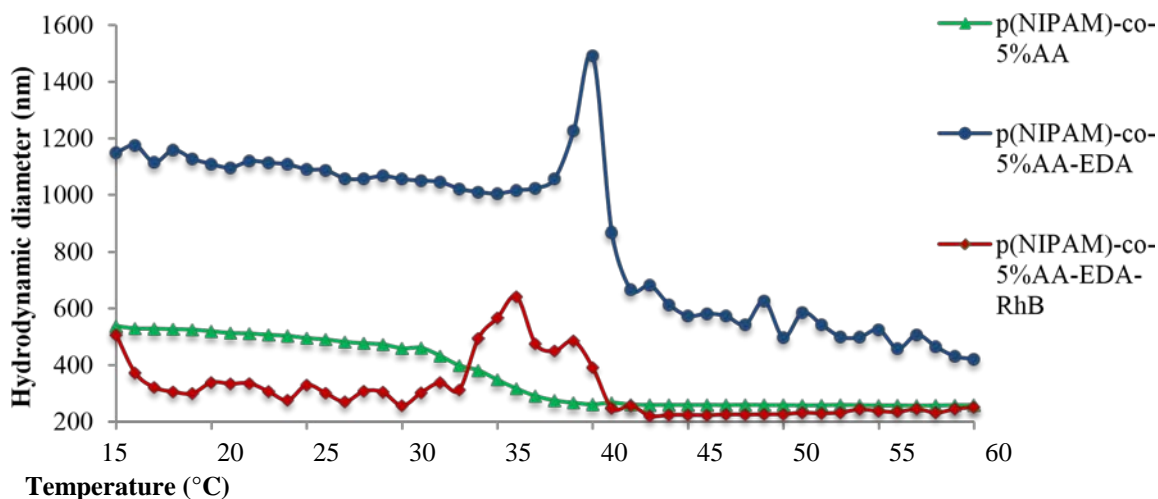


Figure 3.3 The effect of temperature on the particle size of p(NIPAM-co-5% AA)-EDA and p(NIPAM-co-5% AA)-EDA-RhB at pH 11.5

Table 3.1 Particle size and polydispersity index values of p(NIPAM-co-5% AA)-EDA-RhB (standard deviations are presented between brackets)

	15°C		60°C	
	D _h (nm)	PDI	D _h (nm)	PDI
p(NIPAM-co-5% AA)	510 (±19)	0.04	230 (±4)	0.04
p(NIPAM-co-5% AA)-EDA	1150 (±77)	0.02	420 (±3)	0.6
p(NIPAM-co-5% AA)-EDARhB	507 (±44)	0.65	250 (±20)	0.8

When the temperature is above the VPTT, the particles show a higher PDI value (0.16) indicating some variance between the sizes of different particles. Flocculation of some of the particles can also be a possible cause of higher PDI values at temperatures higher than the VPTT.

Further conjugating the NH₂ group of EDA with the COOH group of RhB results in a smaller particle size than that of p(NIPAM-co-5% AA)-EDA (Figure 3.3). A hydrophobic co-monomer tends to be located in the hydrophobic core of the particle; accordingly, the conjugated hairs tend to be directed towards the core of the particle rather than the surface, leading to a smaller particle size. It may also be possible that the attachment of the bulky RhB molecules in the particle causes steric hindrance between the COO⁻ from the AA and accordingly decreases the electrostatic repulsion forces on the particle and decreases its size.

In case of p(NIPAM-co-5% AA)-EDA-RhB, the change in the behavior of the particles is observed at a temperature around 33°C (Figure 3.3). The incorporation of a hydrophobic co-monomer, limits the hydrogen bonding between the particle and the water molecules and hence lower the temperature where the change in behavior is observed (18). Table 3.1 shows that the PdI of p(NIPAM-co-5% AA)-EDA-RhB at 15°C (below the VPTT) is 0.65. This shows that the particles of the same dispersion acquire different sizes. This can be attributed to an uneven conjugation of RhB with the NH₂ of the different particles in the dispersion. At 60°C (above the VPTT), the PdI decreases to 0.25 showing more mono-dispersity between the particles. It is thought that lower PdI values can be obtained by adjusting the conjugation reaction conditions such as the concentrations of the reactants (p(NIPAM-co-5% AA)-EDA and the RhB). Despite repeating the size measurements for the three particles several times, the overall dataset remain the same. It would appear to be unreliable (for p(NIPAM-co-5% AA)-EDA and p(NIPAM-co-5% AA)-EDA-RhB) and therefore these particles were not used for further study (use in an application).

3.3.1.2 Effect of pH

The data shown in Figure 3.3 and Table 3.1 were measured at pH 11.5. Lowering the pH of p(NIPAM-co-5% AA)-EDA-RhB dispersions to pH values of 6 and 2, results in particle aggregation. EDA has two dissociation constant values (pH 7.56 and pH 10.71) (19) due to the presence of two amino groups in its molecular structure. In this work, one of the amino groups of EDA is coupled to the COO⁻ of AA while the other one is pendant (in case of p(NIPAM-co-5% AA)-EDA-RhB, some of the second amino groups is coupled to the COO⁻ of RhB while some others are pendant).

Accordingly, the pK_a of the pendant EDA molecules is expected to be 10.7. At lower pH values (below the pK_a of EDA, the amino groups of NH_2 are protonated to (NH_3^+) . On the other hand, the surface of the particles is negative due to the anionic initiator (potassium persulfate) and the COO^- of acrylic acid (in case of pH 6) with pK_a of 4.2 (17). This creates *intra* and *inter*-particle electrostatic attraction forces that result in particle aggregation. At higher pH values (pH 11.5), the NH_2 groups of EDA are deprotonated, the RhB molecule (with pK_a values of 3 ± 0.9 and $pH 3.8 \pm 0.8$) carries a weak positive charge (due to the distribution effect caused by the resonance in the aromatic rings (Figure 3.1)) on one of the dimethyl amino groups and the $COOH$ of AA is deprotonated into COO^- . Accordingly, the dominating charge is negative which initiates *inter* and *intra*-particle electrostatic repulsion forces and hence maintains the stability of the dispersion.

3.3.2 Electrophoretic mobility

Both particles (p(NIPAM-co-5% AA)-EDA and p(NIPAM-co-5% AA)-EDA-RhB) carry negative charges due to SO_4^- from the initiator and the free $COOH$ from the acrylic acid. The free NH_2 from the EDA is expected to remain deprotonated at pH 11.5 (above the pK_a of EDA). In case of p(NIPAM-co-5% AA)-EDA-RhB particles, the positive charge of the RhB molecule due to the dimethyl amino group is stabilized by the resonance of the aromatic rings attached as well as the alkaline pH in the media. This suggests that the effect of the positive charge on the RhB will be minimal (16).

Figure 3.4 shows the effect of temperature on the electrophoretic mobility of p(NIPAM-co-5% AA)-EDA and p(NIPAM-co-5% AA)-EDA-RhB. The figure shows that both particles are negatively charged. At $15^\circ C$, the electrophoretic mobility of p(NIPAM-co-5% AA)-EDA-RhB ($-2 \mu mcm/Vs$) is higher than that of p(NIPAM-co-5% AA)-EDA ($-1 \mu mcm/Vs$) indicating less positive charges and hence more net negative charges on the particles. This agrees with the particle size data in Figure 3.3. At $15^\circ C$, the particle size of p(NIPAM-co-5% AA)-EDA is 1150 nm, while that of p(NIPAM-co-5% AA)-EDA-RhB at the same temperature is around 500 nm. This means that the size of p(NIPAM-co-5% AA)-EDA particle is more than twice that of p(NIPAM-co-5% AA)-EDA-RhB. This leads to a lower surface charge density on the bigger particle (p(NIPAM-co-5% AA)-EDA) than that on the smaller one (p(NIPAM-co-5% AA)-

EDA-RhB) and hence lower electrophoretic mobility. Another possible reason, is the fact that the larger particles move slower than the smaller ones. So, the movement of p(NIPAM-co-5% AA)-EDA towards the electrode is slower than that of p(NIPAM-co-5% AA)-EDA-RhB and accordingly shows lower electrophoretic mobility. A combination of both reasons is suggested to cause p(NIPAM-co-5% AA)-EDA-RhB to be higher than p(NIPAM-co-5% AA)-EDA.

For p(NIPAM-co-5% AA)-EDA, increasing the temperature to above 35°C, the particles deswell leading to increased surface charge density. Accordingly, an increase in the electrophoretic mobility is observed (Figure 3.4). In case of p(NIPAM-co-5% AA)-EDA-RhB, a different behavior is observed. Increasing the temperature to above 33°C (the temperature where the behavior of the particles starts to change according to the particle size data (Figure 3.3), little effect on the electrophoretic mobility was observed (Figure 3.4). A suggested explanation to this behavior is the steric hindrance effect of the long hairy chain (AA-EDA-RhB). When the particle deswells, the hairy chains collapse masking some of the charges on the particle surface which leads to a lower electrophoretic mobility.

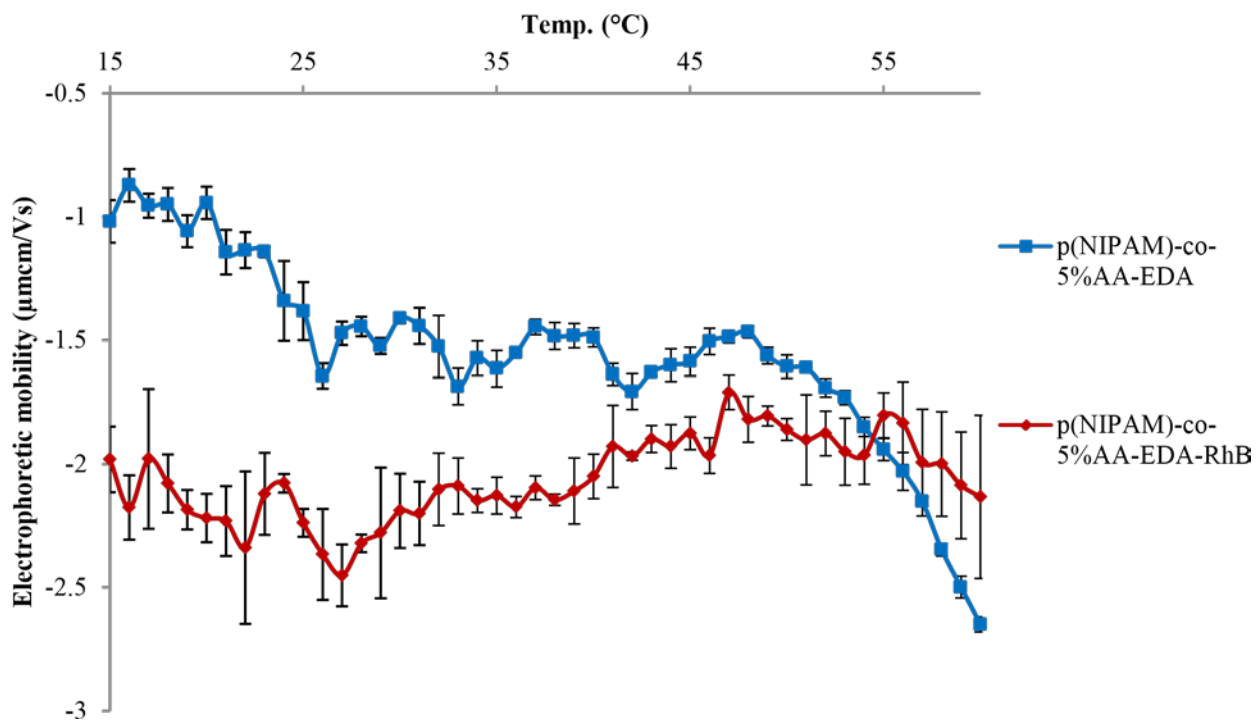


Figure 3.4 The effect of temperature on the electrophoretic mobility of p(NIPAM-co-5% AA)-EDA and p(NIPAM-co-5% AA)-EDA-RhB at pH 11.5

3.3.3 Fluorescence spectroscopy

3.3.3.1 Effect of addition of rhodamine B

Figure 3.5 compares the fluorescence spectra of p(NIPAM-co-5% AA)-EDA, p(NIPAM-co-5% AA)-EDA-RhB and RhB excited at 540 nm at 25°C at pH 6.5 (above the pK_a of RhB). At this diluted concentration (0.2 $\mu\text{g/mL}$), the particles do not aggregate at pH 6.5 as in the higher concentration (0.16 mg/mL) used for the dynamic light scattering measurements. The figure shows that p(NIPAM-co-5% AA)EDA does not show any fluorescence. It also shows that the maximum emission wavelength of p(NIPAM-co-5% AA)-EDA-RhB is the same as that of RhB (630 nm). The fluorescence intensity of RhB is a lot higher than that of p(NIPAM-co-5% AA)EDA-RhB (although both are prepared to be of the same theoretical concentration of the particles). This is because the added amount of rhodamine B during the conjugation to p(NIPAM-co-5% AA)-EDA particles is not all actually conjugated to the particles. Accordingly, the theoretical concentration of the fluorophore (RhB) attached to the p(NIPAM-co-5% AA)-EDA does not equal its actual concentration in dispersion.

Table 3.2 The fluorescence intensity of 0.2 $\mu\text{g/mL}$ p(NIPAM-co-5% AA)-EDA, p(NIPAM-co-5% AA)-EDA-RhB and RhB excited at 540 nm at 25°C at pH 6.5

	Emission fluorescence intensity at 630 nm (CPS)
p(NIPAM-co-5% AA)-EDA	13950
p(NIPAM-co-5% AA)-EDA-RhB	1159290
RhB	16272240

Table 3.2 shows the emission fluorescence intensity of 0.2 $\mu\text{g/mL}$ p(NIPAM-co-5% AA)-EDA, p(NIPAM-co-5% AA)-EDA-RhB and RhB excited at 540 nm. The fluorescence intensity of p(NIPAM-co-5% AA)-EDA is mainly attributed to the light scattering of the particles (20). The fluorescence of p(NIPAM-co-5% AA)-EDA-RhB is attributed to both the light scattering of the particles plus the fluorescence of the RhB molecules. Accordingly, subtracting the value of the fluorescence intensity of p(NIPAM-co-5% AA)-EDA from that of p(NIPAM-co-5% AA)-EDA-RhB will yield the actual fluorescence of p(NIPAM-co-5% AA)-EDA-RhB without turbidity effect (1145340 CPS). Comparing this value to that of RhB alone (of the same concentration)

suggests that the fluorescence intensity of p(NIPAM-co-5% AA)EDA-RhB is equivalent to approximately 7% of that of RhB solution at the same concentration (in other words equivalent to 0.014 $\mu\text{g/mL}$ of RhB). Knowing that during the coupling reaction of RhB to the p(NIPAM-co-5% AA)-EDA particles, the concentration of RhB added was 4.35 $\mu\text{g/mL}$, it can be concluded that 0.32 % of the added RhB was actually coupled to the particles. This calculation is only an estimate of the percentage incorporation of RhB in the particles. Other factors might affect the fluorescence of RhB when incorporated in a different environment (the particles) such as fluorescence quenching from hydrochloric acid and sodium hydroxide for pH adjustments or any unreacted species in the dispersion used.

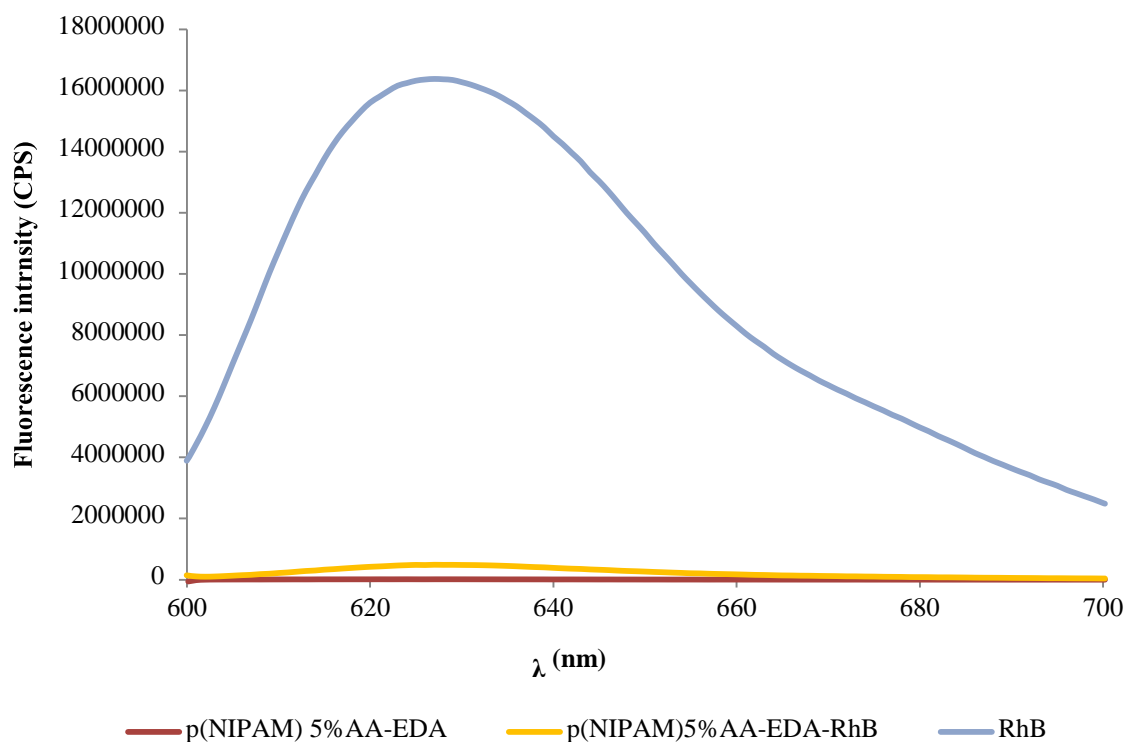


Figure 3.5 The fluorescence spectra of 0.2 $\mu\text{g/mL}$ p(NIPAM-co-5% AA)-EDA, p(NIPAM-co-5% AA)-EDA-RhB and RhB excited at 540 nm at 25°C at pH 6.5

3.3.3.2 Effect of temperature

The effect of temperature on the fluorescence intensity of p(NIPAM-co-5% AA)EDA-RhB and RhB at pH 2, 6.5 and 11.5 is shown in Figure 3.6. The figure shows that for both p(NIPAM-co-5% AA)-EDA-RhB and RhB (at different pH values), increasing the temperature did not cause a change in the emission wavelength (630 nm) of the

dispersion/solution, respectively. On the other hand, a consistent decrease in the fluorescence intensity was observed by increasing the temperature. A possible explanation to this is that when the temperature increases, it causes the particles to deswell and the hairs to collapse on the particle surface; this might have a quenching effect on the fluorescence of RhB. An exception for the noticed temperature effect is the fluorescence intensity of p(NIPAM-co-5% AA)-EDA-RhB at pH 11.5 where the fluorescence intensity at 45°C is higher than that at 35°C.

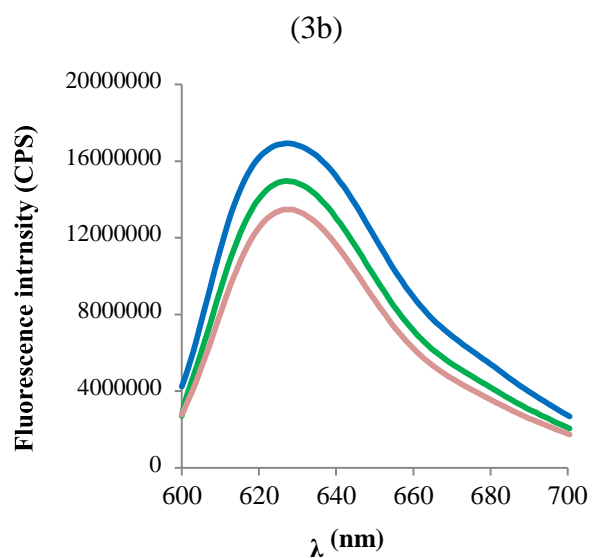
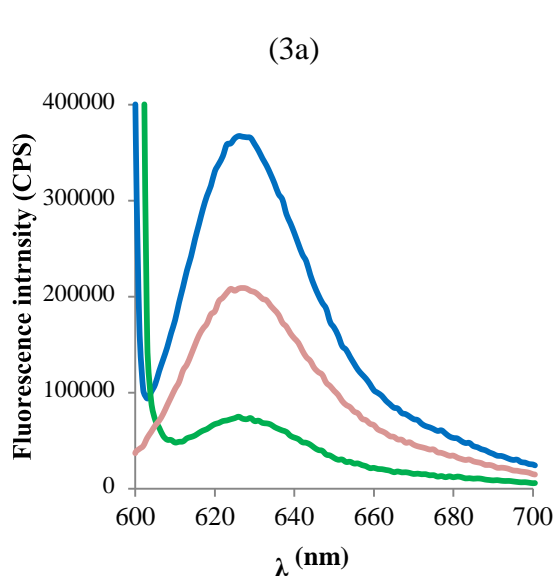
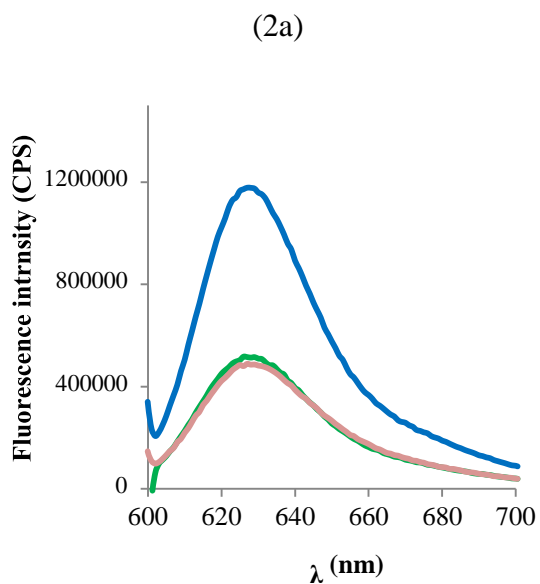
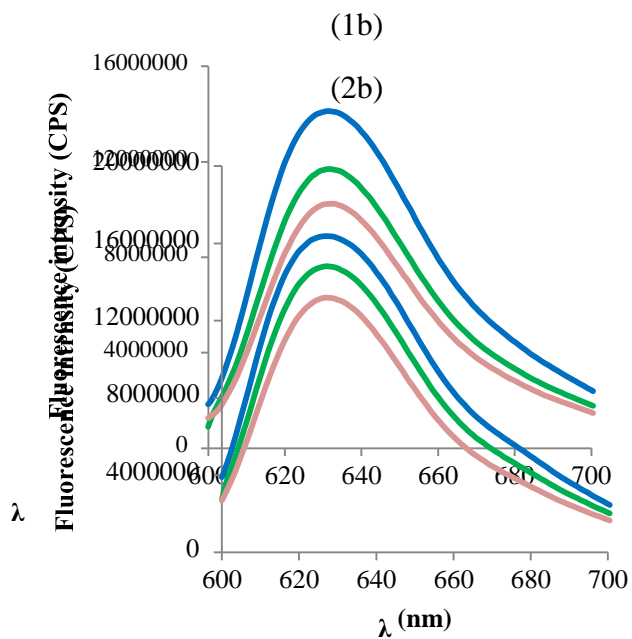
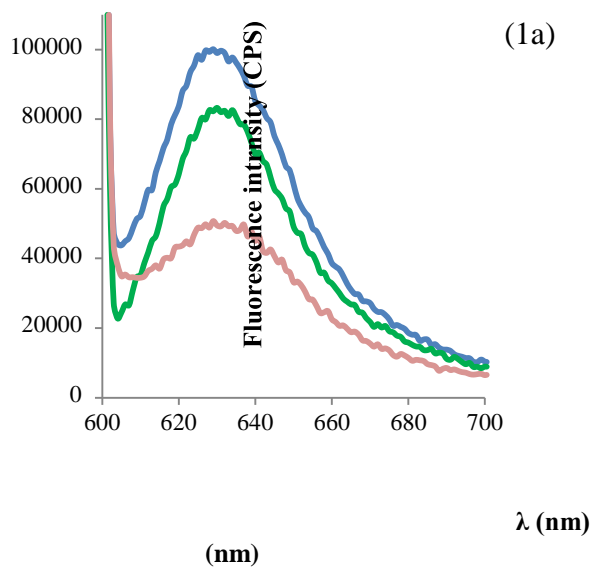


Figure 3.6 Fluorescence emission spectra of 0.2 $\mu\text{g/mL}$ p(NIPAM-co-5% AA)-EDA-RhB at (1a) pH 2 (2a) pH 6.5 and (3a) pH 11.5 and 0.2 $\mu\text{g/mL}$ RhB excited at 540 nm at (1b) pH 2 (2b) pH 6.5 and (3b) 11.5 at 25°C (blue), 35°C (green) and 45°C (red)

3.3.3.3 Effect of pH

The acid dissociation constant (pK_a) and the different protonation states of RhB was calculated using ACD/I-Lab (6). The effect of pH on the fluorescence of RhB and p(NIPAM)5% AA-EDA-RhB is shown in Figures 3.7 and 3.8, respectively.

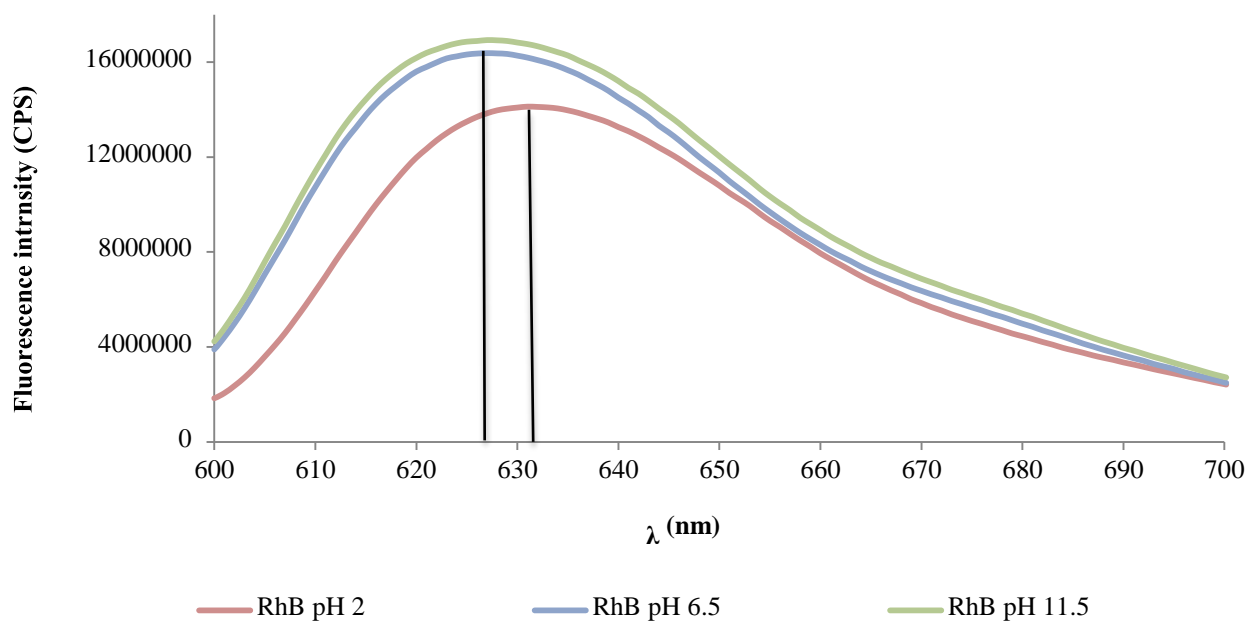
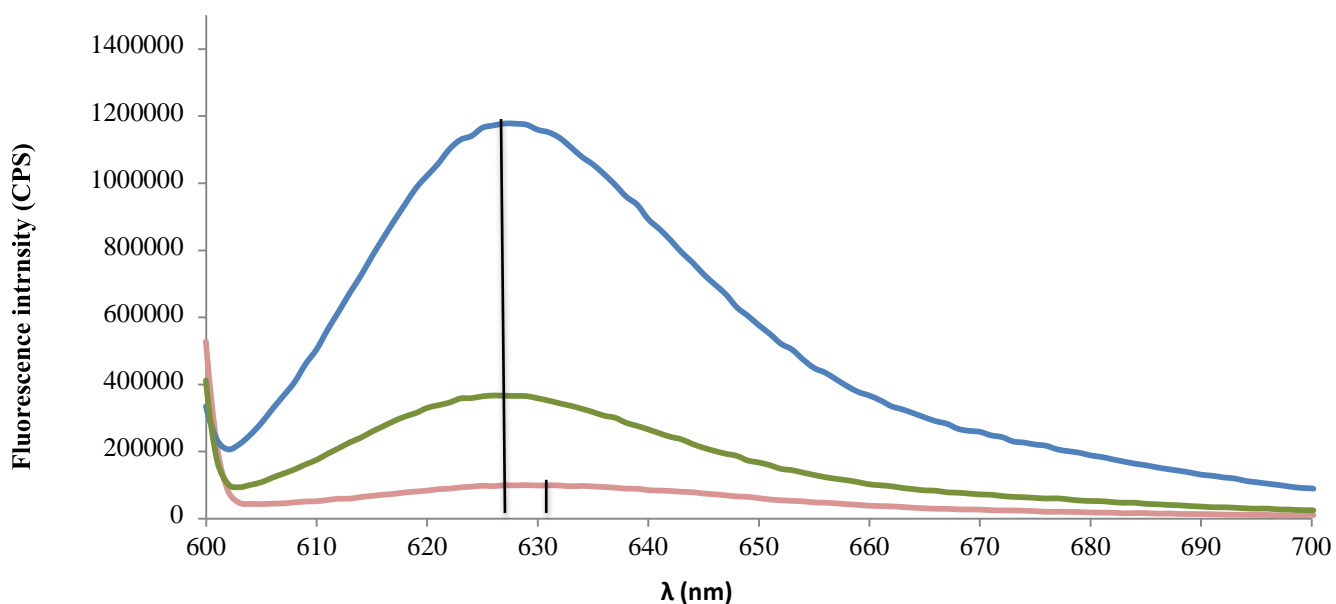


Figure 3.7 Fluorescence of 0.2 $\mu\text{g/mL}$ RhB excited at 540 nm at 25°C at pH 2.5, 6.5 and 11.5



p(NIPAM)5%AA-EDA-RhB pH 2.5 — p(NIPAM)5%AA-EDA-RhB pH 6.8
 p(NIPAM)5%AA-EDA-RhB pH 11.5 —

Figure 3.8 Fluorescence of 0.2 $\mu\text{g/mL}$ p(NIPAM-co-5% AA)-EDA-RhB excited at 540 nm at 25°C at pH 2.5, 6.5 and 11.5

For RhB (Figure 3.7), at pH 2, a maximum emission band (λ_{em}) is shown at 632 nm (21). When the pH increases to 6.5 and 11.5, a blue shift was observed where the λ_{em} is around 625 nm. This agrees with the findings of Jorge *et al.* (21) who observed a shift in the emission band of RhB impregnated into silica when the pH is increased from 2 to 7. They suggest that RhB is stable in acidic media while increasing the pH causes a change in the physical and spectroscopic properties of rhodamine B. The pK_a of RhB is 3.7, at pH between pH 4 and 8, it is said to be zwitterionic (22). When the pH exceeds 3.8, the carboxylic groups are deprotonated which creates electrostatic attraction forces between the COO^- and the N^+ on the xanthene groups leading to aggregation of RhB monomers forming dimers (22). It is also observed that the fluorescence intensity decreases by decreasing the pH. This agrees with the findings of Fikry *et al.* (23) who reported that decreasing the pH of RhB dissolved in polar solvents causes a decrease in its fluorescence intensity. The suggested explanation to this is that the RhB molecule exists in different molecular structures (cationic, zwitterionic, quinonic and lactonic) which can change by the change in pH and hence affect the fluorescence intensity. Another possible explanation for the decrease in fluorescence intensity by lowering the pH can be the use of hydrochloric acid to adjust the pH of the samples. Chloride ions are known to have quenching effects on many fluorescent molecules, one of which is rhodamine B (24, 25).

For p(NIPAM-co-5% AA)-EDA-RhB, similar results were obtained. At pH 2, the λ_{em} is 632 nm and by increasing the pH to 6.5 and 11.5, a blue shift is observed where the λ_{em} becomes 627 nm. This can be mainly attributed to the RhB properties as discussed above. Also, the change in the particle size and charge by changing the pH of the surrounding environment can affect the fluorescence intensity.

3.3.4 Infrared spectroscopy

Table 3.3 list the infrared (IR) bands of p(NIPAM-co-5% AA), p(NIPAM-co-5% AA)-EDA and p(NIPAM-co-5% AA)-EDA-RhB while Table 3.4 list the IR bands of RhB. The spectra of p(NIPAM-co-5% AA), p(NIPAM-co-5% AA)-EDA, p(NIPAM-co-5% AA)-EDA-RhB and RhB. The spectra of the three particles compare to those previously reported for p(NIPAM-co-5% AA) (26-29). Figure 3.9 shows that the spectra of the three particles (mentioned above) are very similar. Areas where possible difference can be detected, (*e.g.* shift in some peaks) are highlighted. The amount of EDA and RhB attached to the particles is too small to be detected by IR, hence the resemblance of the spectra. The IR bands and spectrum of RhB shown in Table 3.4 and Figure 3.9 agree with reported literature (30-32).

Table 3.3 FT-IR bands of p(NIPAM-co-5% AA) and p(NIPAM-co-5% AA)-EDA-RhB

Band number	Wavenumber (cm)	Assignment
1	3250	N-H stretching (26, 29, 33)
2	2964	-CH ₃ asymmetric stretching (26, 33)
3	1620	C=O (amide I bond stretching) (26-29, 33)
4	1523	N-H (amide II bond stretching) (28, 29, 33)
5	1448	-CH ₃ asymmetric deformation (33)
6	1363	-CH ₂ symmetric deformation (29, 33)
7	1166	C-N bending (26)

-1

Table 3.4 FT-IR bands of RhB

Peak number	Wavenumber (cm)	Assignment
1	3354	-OH stretching (33)
2	2978	CH ₂ and CH ₃ antisymmetric and symmetric stretching (30, 33)
3	1996	Substituted benzene rings (overtone and combination bands) (33)
4	1703	C=O stretching (30, 33)
5	1643	C-N stretching (30)
6	1581	Aromatic ring vibrations (stretching) (30, 34)
7	1548	
8	1463	
9	1408	OH in carboxylic acids in plane OH bending (33)
10	1332	Aryl bond vibrations (in-plane deformation) (30, 34)
11	1273	C-N stretching in aromatic amines (33)
12	1247	C-C-N bending in amines (33)
13	754	CH ₂ in hydrocarbons (rocking)
14	709	CH (out of plane deformation) in <i>o</i> substituted benzenes (33)
15	680	O-C=O in carboxylic acids (bending) (33)

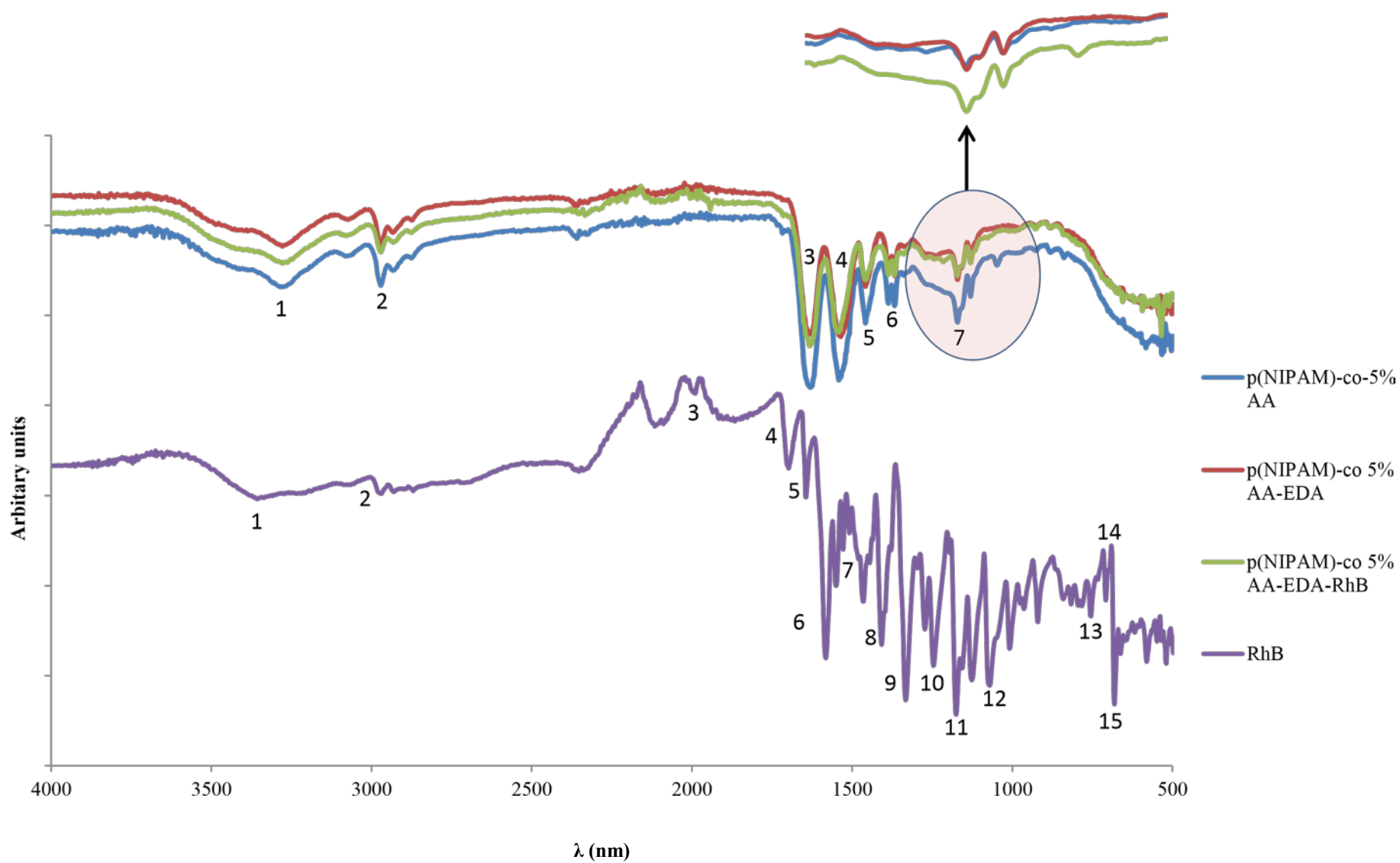


Figure 3.9 FT-IR spectra of p(NIPAM-co-5% AA)-EDA-RhB, p(NIPAM-co-5% AA)-EDA, p(NIPAM-co-5% AA) and RhB

3.3.5 Fluorescence microscopy

Figure 3.10 shows the fluorescence microscopy images of p(NIPAM-co-5% AA)EDA-RhB. The figure shows that the particles are spherical in shape and fluorescent. The figure also shows that some particles are more fluorescent than the others. This indicates the uneven distribution of the fluorophore (RhB) among the particles. This agrees with the high PDI value obtained by the DLS experiments (Table 3.1). The figure suggests that the fluorophore is located in the core of the particles. This agrees with the theory that suggests that the NIPAM based particles acquire a core/shell structure where the core is hydrophobic and the shell is hydrophilic (7).

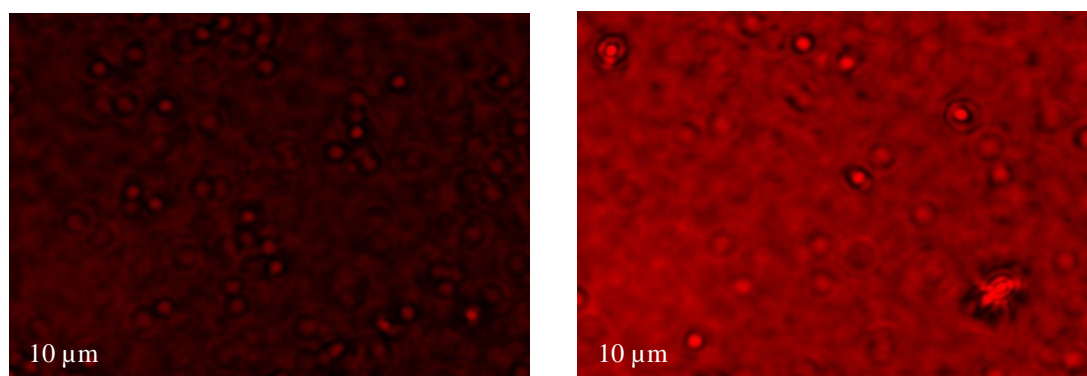


Figure 3.10 Fluorescence microscopy images of p(NIPAM-co-5% AA)-EDA-RhB at 25°C

3.3.6 Scanning electron microscopy

Figure 3.11 a, b and c shows the Scanning electron microscopy (SEM) images of p(NIPAM-co-5% AA), p(NIPAM-co-5% AA)-EDA and p(NIPAM-co-5% AA)-EDA-RhB, respectively at 25°C. The figure (3.12 a) shows that the p(NIPAM-co-5% AA) particles are spherical and the average particle size is 300 nm. The conjugation of EDA chains to the particles caused the hairy layer to be extended. Figure 3.11 b shows that p(NIPAM-co-5% AA)-EDA particles exhibit longer hairy chains which are not shown in p(NIPAM-co-5% AA) (Figure 3.11 a). After further conjugation of RhB to the particles, the particles still exhibit a spherical shape with a diameter of 270 nm.

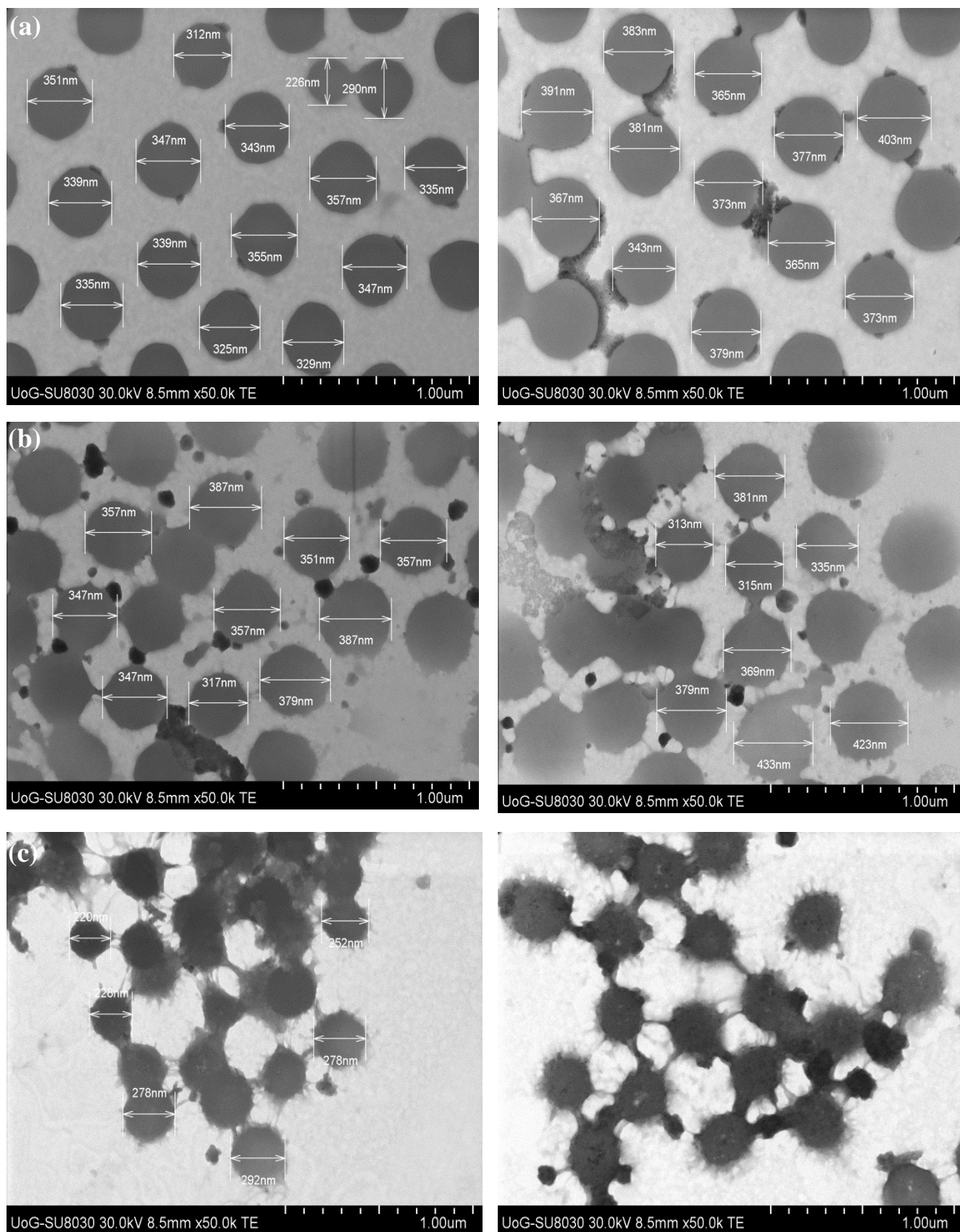


Figure 3.11 SEM images of (a) p(NIPAM-co-5% AA), (b) p(NIPAM-co-5% AA)-EDA and (c) p(NIPAMco-5% AA)-EDA-RhB at 25°C

The particle sizes shown in Figure 3.11 for the three different particles all compare to those shown by the DLS (Figure 3.3) considering that the particles are deswollen (STEM sample was dry). Figure 3.11 c shows that the p(NIPAM-co-5% AA)-EDARhB particles have longer hairs than those of p(NIPAM-co-5% AA)-EDA. This can be attributed to the attachment of two conjugates (EDA and RhB). In some cases, the hairs of the particles are long enough to form bridges between the particles.

3.4 Conclusions and future work

3.4.1 Conclusions

A fluorescent temperature-sensitive NIPAM based was synthesized using a three-step procedure. Step one was the synthesis of p(NIPAM-co-5% AA) particles while steps two and three were the conjugation of EDA and RhB, respectively. The new particle has more than one ionized chemical group on its surface, some of which are anionic (such as COOH from the AA and SO_4^- from the initiator) and others are cationic such as NH_2^{3+} from the EDA. The initial particle size of p(NIPAM-co-5% AA)-EDA-RhB at 15°C at pH 11.5 is 500 nm and decreases to about 250 nm when the temperature exceeds the VPTT (33°C). The particles are most stable at pH 11.5, at lower pH values; the particles show a high poly dispersity index indicating that the particles do not acquire the same size. The particles are negatively charged with an initial electrophoretic mobility at 15°C equal to $-2 \mu\text{mcm/Vs}$. Calculations of the fluorescence intensity of p(NIPAM-co-5% AA)-EDA-RhB and RhB at the same concentration estimates that about 7% of the RhB added to the conjugation reaction is actually conjugated. Temperature and pH showed an effect on the fluorescence of the particles. Increasing the temperature caused a decrease in the fluorescence intensity. The increase in pH has been shown to cause a blue shift of the emission spectra. At pH 2 (below the $\text{p}K_a$ of RhB), the emission wavelength (λ_{em}) was 632 nm. When the pH increases to above the $\text{p}K_a$, the λ_{em} shifts to 627 nm. Fluorescence microscopy pictures show that the particles are spherical and suggest that the fluorophore (RhB) is located in the core of the particle. The pictures obtained by TEM also show that the particles are spherical. The pictures also show some bridging between the particles which can be attributed to the long hairy chains conjugated to the particles.

3.4.2 Future work

Future work will include trials to obtain lower PDI values which contribute to more mono-dispersed particles. This can be achieved by changing and optimizing the percentages of conjugates used (EDA and RhB). Also suggested applications for the new particle will be tested. These will include the use of an emulsifier (considering the bridges between the particles shown by TEM images).

3.5 References

1. Pinkrah V. T., Beezer A. E., Chowdhry B. Z., Gracia L. H., Cornelius V. J., Mitchell J. C., Castro-Lopez V., Snowden M. J. Swelling of cationic polyelectrolyte colloidal microgels: Thermodynamic considerations. *Colloids and Surfaces A Physicochemical and Engineering Aspects*. 2005;262:76-80.
2. Ramkissoon-Ganorkar C., Liu F., Baudys M., Kim S. W. Modulating insulin release profile from pH thermosensitive polymeric beads through polymer molecular weight. *Journal of Controlled Release*. 1999;59:287-98.
3. Castro Lopez V., Hadgraft J., Snowden M. J. The use of colloidal microgels as a (trans)dermal drug delivery system. *International Journal of Pharmaceutics*. 2005;292:137-47.
4. Wu W., Chen S., Hu Y., Zhou S. A Fluorescent Responsive Hybrid Nanogel for Closed-Loop Control of Glucose. *Journal of Diabetes Science and Technology*. 2012;6:892-901.
5. Ravaine V., Ancla C., Catargi B. Chemically controlled closed-loop insulin delivery. *Journal of Controlled Release*. 2008;132:2-11.
6. <https://ilab.acdlabs.com/iLab2/.1994> - accessed on the 26th of September, 2014.
7. Wong J. E., Gaharwar A. K., Müller-Schulte D., Bahadur D., Richtering W. Dual-stimuli responsive PNIPAM microgel achieved via layer-by-layer assembly: Magnetic and thermoresponsive. *Journal of Colloid and Interface Science*. 2008;324:47-54.
8. Schmaljohann D. Thermo- and pH-responsive polymers in drug delivery. *Advanced Drug Delivery Reviews*. 2006;58:1655-70.
9. Zhu J., Marchant R. E. Design properties of hydrogel tissue-engineering scaffolds. *NIH Public Access*. 2011;8:607-26.
10. Moschou E. A., Madou M. J., Bachas L. G., Daunert S. Voltage-switchable artificial muscles actuating at near neutral pH. *Sensors and Actuators B*. 2006;115:379-83.

11. Lally S., Mackenzie P., LeMaitre C. L., Freemont T. J., Saunders B. R. Microgel particles containing methacrylic acid: pH-triggered swelling behaviour and potential for biomaterial application. *Journal of Colloid and Interface Science*. 2007;316:367–75.
12. Jia X., Yeo Y., Clifton R. J., Jiao T., Kohane D. S., Kobler J. B., Zeitels S. M., Langer R. Hyaluronic Acid-Based Microgels and Microgel Networks for Vocal Fold Regeneration. *Biomacromolecules*. 2006;7:3336–44.
13. Maeda H., Maeda T., Mizuno K., Fujimoto K., Shimizu H., Inouye M. Alkynylpyrenes as Improved Pyrene-Based Biomolecular Probes with the Advantages of High Fluorescence Quantum Yields and Long Absorption/Emission Wavelengths. *Chem. Eur. J.*, 2006; 12: 824 – 31.
14. Shiraishi Y., Miyamoto R., Zhang X., Hirai T. Rhodamine-Based Fluorescent Thermometer Exhibiting Selective Emission Enhancement at a Specific Temperature Range. *Organic Letters*. 2007;9:3921-4.
15. Karstens T., Kobs K. Rhodamine B and Rhodamine 101 as Reference Substances for Fluorescence Quantum Yield Measurements. *The Journal of Physical Chemistry*. 1980;84:1871-2.
16. Carey F. A., Sundberg R. J. *Advanced Organic Chemistry. Part A: Structure and Mechanisms*. Fifth edition. 2008, New York: Springer.
17. Mohsen R. Vine G. J., Majcen N., Alexander B. D., Snowden M. J. Characterization of thermo and pH responsive NIPAM based microgels and their membrane blocking potential. *Colloids and Surfaces A: Physicochemical and Engineering Aspects*. 2013;428:53-9.
18. Thorne J. B. Controlling the interfacial behaviour of colloidal microgel systems. PhD thesis , University of Greenwich; 2012.
19. UNEP publications. Ethylenediamine. SIDS initial assessment report. Washington, DC: United States Environmental Protection Agency; 2001.
20. Tsuji S., Kawaguchi H. Colored Thin Films Prepared from Hydrogel Microspheres. *Langmuir*, 2005; 21: 8439-42.
21. Jorge J., Castro G. R., Martines M. A. Comparison among Different pH Values of Rhodamine B Solution Impregnated into Mesoporous Silica. *The Electronic Journal of Chemistry*. 2013;5.
22. Zamouche M., Hamdaoui O. Sorption of Rhodamine B by cedar cone: effect of pH and ionic strength. *Energy Procedia*. 2012;18:1228 – 39.

23. Fikry M., Omar M. M., Ismail L. Z., Effect of Host Medium on the Fluorescence Emission Intensity of Rhodamine B in Liquid and Solid Phase. *J Fluoresc*, 2009; 19: 741–46.
24. Jiang Z. L., Zhang B. M., Liang A. H. A new sensitive and selective fluorescence method for determination of chlorine dioxide in water using rhodamine S. *Talanta*, 2005; 66: 783–88.
25. Geddes C. D. Optical thin film polymeric sensors for the determination of aqueous chloride, bromide and iodide ions at high pH, based on the quenching of fluorescence of two acridinium dyes. *Dyes and Pigments*, 2000. 45: 243-251.
26. Farooqi Z. H., Khan H. U., Shah S. M., Siddiq M. Stability of poly(Nisopropylacrylamide-*co*-acrylic acid) polymer microgels under various conditions of temperature, pH and salt concentration. *Arabian Journal of Chemistry*. 2013, In press.
27. Chen H., Fang Y. Synthesis and characterization of temperature and pH responsive Poly(N-isopropylacrylamide) copolymer. China: MOE Key Laboratory of Food Colloids and Biotechnology, School of Chemical & Material Engineering, Jiangnan University.
28. Luo Q., Guan Y., Zhang Y., Siddiq M. Lead-Sensitive PNIPAM Microgels Modified with Crown Ether Groups. *Journal of Polymer Science: Part A: Polymer Chemistry*. 2010;48:4120–7.
29. Hu X., Hao X., Wu Y., Zhang J., Zhang X., Wang P. C., Zou G. and Liang X. J. Multifunctional hybrid silica nanoparticles for controlled doxorubicin loading and release with thermal and pH dual response. *Journal of Materials Chemistry B*. 2013;1:1109.
30. Jing-yi L., Wan-hong M., Peng-xiang L., Jin-cai Z. Detection of intermediates in the TiO₂-assisted photodegradation of Rhodamine B under visible light irradiation. *Journal of Environmental Sciences*. 2007;19:892–6.
31. Ma Y., Jin X., Zhou M., Zhang Z., Teng X., Chen H. Chemiluminescence behavior based on oxidation reaction of rhodamine B with cerium(IV) in sulfuric acid medium. *Analytica Chimica Acta*. 2003;489:173–81.
32. Zhang R., Hummelgard M., Lv G., Olin H. Real time monitoring of the drug release of rhodamine B on graphene oxide. *Carbon*. 2011;49:1126-32.
33. Lambert J. B., Shurvell H. F., Lightner D., Cooks R. G. Introduction to organic spectroscopy. Verbit L. New York/London: Macmillan Publishing Company/Collier Macmillan publishers; 1987.

34. Renjith R., Mary Y., Panicker C. Y., Varghese H. T., Pakosińska-Parys M., Alsenoy C. V., Al-Saadi A. A. Spectroscopic (FT-IR, FT-Raman) investigations and quantum chemical calculations of 1,7,8,9-tetrachloro-10,10-dimethoxy-4-{3-(4-(3-methoxyphenyl)piperazin-1-yl)propyl}-4-azatricyclo (5.2.1.0^{2,6})dec-8-ene-3,5-dione. *Spectrochimica Acta Part A: Molecular and Biomolecular Spectroscopy*, 2014; 129: 438–50.

Chapter Four

Design, synthesis, characterization and toxicity studies of poly(*N*isopropylacrylamide-co-lucifer yellow) for drug delivery applications

4.1 Introduction

Poly(*N*-isopropylacrylamide) (p(NIPAM)) particles are characterized by their ability to change their conformation and physico-chemical properties (such as particle size and surface charge density) according to the change in the surrounding environment such as temperature, pH and ionic strength (1-3). This is thought to be a property that can be used in different applications such as drug delivery (5). The fact that the volume phase transition temperature (VPTT) of NIPAM based microgel particles (35°C) (1) is very close to the human body temperature (37°C) makes them a good choice for biomedical applications. As an example of suggested drug delivery applications based on temperature trigger, the particles are swollen at room temperature (around 25°C which is below the VPTT), so, if they incorporate a drug in its matrix, when administered in the human body

VPTT, it will deswell and release the drug. Many researchers suggested drug delivery (68), diagnostics (9) and protein binding (10-12) applications of NIPAM-based microgel particles. The incorporation of a fluorescent dye such as lucifer yellow (LY) to p(NIPAM) particles adds a new function (colour and fluorescence) that makes it traceable. This can suggest new applications especially in the field of diagnosis of different diseases either *in vivo* or *in vitro*. Combining the previously suggested drug delivery applications of microgels (6-8) to its ability to being traced in the human body can be a promising system for combined diagnosis and delivery of drugs to suitable environments (13, 14).

In this chapter, a novel microgel particle, p(NIPAM-co-5% LY), is synthesized and characterized using DLS (particle size and electrophoretic mobility), infrared spectroscopy, scanning electron microscopy and fluorescence microscopy. Being a candidate for biomedical applications, the toxicity was tested using two cell lines: kidney cells (Vero) and breast cancer cells (HeLa).

4.1.1 Lucifer yellow VS

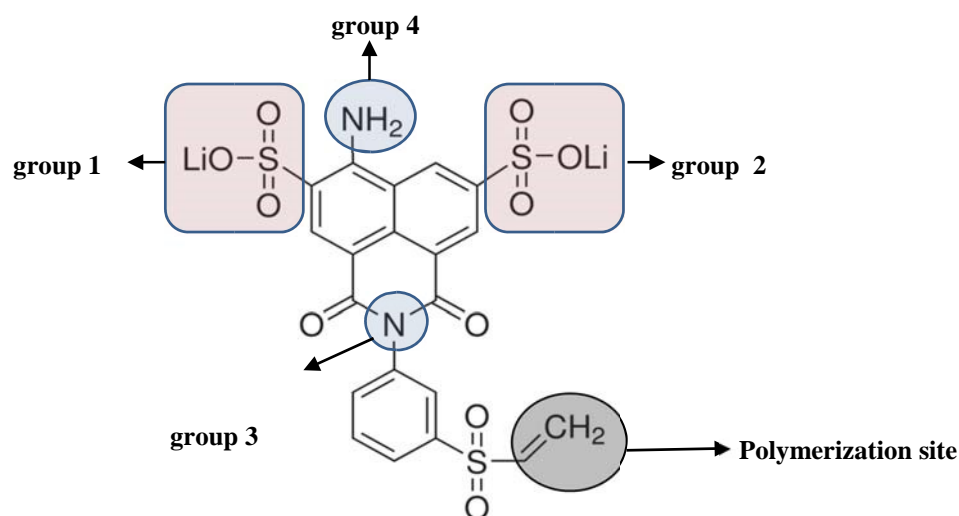


Figure 4.1 Molecular structure of lucifer yellow VS dilithium salt (4)

Lucifer yellow VS dilithium is a water soluble fluorescent dye of molecular weight 550.39 g/mol (15). The presence of 3 benzene rings, gives it a hydrophobic character. It has two excitation wavelengths (280 and 430 nm) and an emission wavelength of 540 nm (16). Lucifer yellow is used for different biomedical applications including marking cells, neurons, albumin, cholesterol, phospholipids, collagenase, polynucleotides, progesterone derivatives, testosterone, estriol (15), and tracers of cell-cell fusion (17). It also selectively binds to copper (18) which can be used in industrial and environmental applications.

The logarithm of acid dissociation constant (pK_a) of LY was calculated using the online database ACD/labs (19). The presence of more than one ionisable group in the molecular structure of LY (Figure 4.1) results in more than one pK_a , these are; -2.2 (± 0.6), -0.7 (± 0.5), 1.4 (± 0.8) and 5.7 (± 0.8)

From polymerization point of view, lucifer yellow VS dilithium salt is a perfect choice. This is due to the presence of a pendant vinyl group (coloured in grey) (Figure 4.1) which makes it readily polymerizable with other monomers under suitable conditions. This is important for synthesizing monodispersed particles with the similar electrophoretic mobilities. On the other hand, a disadvantage of using lucifer yellow is its relatively low molar extinction coefficient (ϵ) of $12000 \text{ M}^{-1} \text{ cm}^{-1}$ (16, 21, 22) when compared to other fluorophores such as fluorescein *isothiocyanate* (FITC) with a molar extinction co-efficient of $75000 \text{ M}^{-1} \text{ cm}^{-1}$

¹ (23), Texas red ($\epsilon = 85000 \text{ M}^{-1} \text{ cm}^{-1}$) (24) and tetramethyl rhodamine *isothiocyanate* (TRITC) with an ϵ of $100000 \text{ M}^{-1} \text{ cm}^{-1}$ (23). It is also characterized by a relatively low quantum yield (21%) (25) compared to other fluorophores such as rhodamine 6G (95%), fluorescein (95%) and quinine sulphate (58%) (26).

4.2 Materials and methods

4.2.1 Materials

N-isopropylacrylamide (NIPAM) 97% (Aldrich), lucifer yellow (LY) (Aldrich), *N,N*'methylenebisacrylamide 99% (Aldrich), potassium persulphate 98% (BDH Laboratory Suppliers), branched poly(ethylenimine) (PEI) of molecular weight 25 kD (Cat. 18197-8) (Aldrich) were obtained from commercial suppliers and used without further purification. Vero CCL-81 (normal kidney of *Cercopithecus aethiops*) and HeLa CCL2 (human cervical epithelial cells) from ATCC company. Media were purchased from Gibco life technologies. For Vero cells, Dulbecco's Modified Eagle Medium (DMEM) was used while for HeLa cells, Minimum Essential Medium (MEM) was used. PenicillinStreptomycin-Glutamine (PSG) (100x) and fetal Bovine Serum (FBS) were purchased from Gibco Life Technologies. (3-(4,5-Dimethylthiazol-2-yl)-2,5-diphenyltetrazolium bromide (MTT) was purchased from Sigma Aldrich UK.

4.2.2 Methods

4.2.2.1 Synthesis of p(NIPAM-co-5% LY) (w/v)

In a 1 L reaction vessel, 0.5 g of the initiator (potassium per sulphate) was dissolved in 800 mL of distilled water. A three-necked lid was clamped to the reaction vessel, which was then heated to 70°C with continuous stirring. Monomer (4.75 g NIPAM), co-monomer (0.25 g lucifer yellow (LY)) and cross linker (0.5 g *N,N*'-methylenebisacrylamide) were stirred in distilled water (200 mL) and transferred into the reaction vessel containing the initiator and continuously stirred at 70°C for six hours under an inert atmosphere of nitrogen. When the reaction was complete, the microgel dispersion was allowed to cool to room temperature. The microgel was dialyzed in fresh de-ionised water for a week (changed daily), centrifuged and the pellet was freeze dried.

4.2.2.2 Dynamic light scattering

Dynamic light scattering (DLS) measurements were carried out using a Malvern Zetasizer Nano ZS. The hydrodynamic diameter of the particles was measured in response to temperature in the 15 to 60°C range. All samples were diluted with deionized water (1 mL of dialysed microgel dispersion was diluted with 2 mL of water) before measurements. A quartz cuvette with two polished windows (Starna Type 1) was used for all the measurements and the temperature of the dispersion was controlled by a Peltier thermocouple. Data for p(NIPAM-co-5% LY) measurements were collected every 1°C and the samples were equilibrated for 2 min before each data collection point. Three measurements, each consisting of 13 subruns, were taken at each temperature to obtain an average hydrodynamic diameter. Experiments were also conducted where the pH of the samples was adjusted to different pH values using HCl and NaOH to test for the effect of changing pH upon the size of the particles.

The electrophoretic mobility of p(NIPAM-co-5% LY) in a salt concentration of 1×10^{-4} M NaCl was measured in response to temperature change across the range of 15-60°C using a disposable folded capillary cell.

4.2.2.3 Fluorescence spectroscopy

A Horiba Jobin Yvon Fluoromax 4 spectrofluorometer was used for fluorescence experiments. All samples were excited at 430 nm and the full emission spectra (450–1050 nm) were recorded with bandwidth of 5 nm at 25°C. A 10 mm path length quartz cuvette with four polished windows (Starna Type 3) was used for all the measurements.

4.2.2.4 Infrared spectroscopy

A Thermo Nicolet Nexus Fourier transform infrared spectrophotometer (FT-IR) was used to carry out the IR experiment in this work. Microgel dispersions were dialysed and freeze-dried then the solid samples (powder) were used for IR experiments using attenuated total reflection (ATR) ZnSe crystal.

4.2.2.5 Microscopy

4.2.2.5.1 Scanning electron microscopy

A Hitachi SU8030 cold cathode filled emission gun scanning electron microscope was used with an accelerating voltage of 5.0 kV to obtain images of the novel particles.

4.2.2.5.2 Fluorescence microscopy

A Nikon Eclipse 90i microscope, fitted with a fluorescein *isothiocyanate* filter (FITC) and a Nikon digital sight DS-U3 camera were used to take fluorescent images of the particles.

Plan Fluor 100x oil Ph3 DLL lens was used with working distance of 0.16 mm. The numerical aperture of the images was 1.3, refractive index 1.5 and the exposure time was 3 seconds. The sample was placed on a microscopic slide, left to dry in air and then immersion oil was added on it.

4.2.2.6 Toxicity studies

4.2.2.6.1 Sterilization:

All the pipetting tips, phosphate buffered saline (PBS), glassware, magnetic stirrers, spatulas used in this experiment were sterilized used an Astell autoclave at 121°C for 85 minutes.

4.2.2.6.2 Preparation of media

To prepare a complete media, 50 mL PSG (100x) and 5 mL Fetal Bovine Serum (FBS) were added (without any dilution) to a 500 mL media bottle (either DMEM or MEM).

Media were kept in the fridge at 4°C.

4.2.2.6.3 Cell sub-culturing

In a clean and sterile class II laminar flow hood, the media in the flask were removed using a disposable sterile 10 mL serological pipette (Fisher brand). The flask was then washed with 10 mL of sterilized phosphate buffered saline (PBS) 3 times (using a new serological pipette each time). Trypsin EDTA (0.5 mL) was added and spread among the flask which is then placed in an incubator (Thermo Scientific HERACELL 150i CO₂ incubator) at 37°C and 5% CO₂ v/v for 5-7 minutes after which the viability of cells was checked under a microscope (Nikon Japan with a x10 ELWD lens with working distance 2.62–1.8 mm). After that, 10 mL of fresh media (MEM for HeLa and DMEM for Vero cells) were added to the flask and well mixed with the cells, and then 9 mL of the media (now mixed with wells) were removed and put in an Eppendorf tube to be used for the seeding step. Fresh media (9 mL) were then added to the flask, mixed then put in the incubator. Cells were split twice weekly.

4.2.2.6.4 Cell seeding

Cell count (using a haemocytometer) of the cell suspension from the splitting step (9 mL removed after using trypsin) was carried out. Accordingly, a cell suspension of a concentration (1×10^4 cell/mL) was prepared. In a 96-well plate (excluding the peripheral cells, these are columns 1 and 12 and rows A and H (Figure 4.2)), 100 μ L of the freshly prepared cell suspension were placed in each well. The plate was then put in the incubator for 24 hours.

4.2.2.6.5 Sample preparation

In an autoclaved beaker, the sample (either dextran, NIPAM monomer, p(NIPAM), p(NIPAM-co-5% LY) or PEI) is weighed. Sterile fresh media (MEM for HeLa and DMEM for Vero cells) was added and left stirring for an hour. In a sterile class II laminar flow hood, the sample dispersion/solution was filtered using a single use filter unit with a pore size of 2 μ m (Minisart® Sartorius stedium biotech). A serial dilution was then prepared and used for cell dosing.

4.2.2.6.6 Cell dosing

The previously seeded 96-well plates are placed in a clean and sterile fume cupboard, the 100 μ L of media (in each well) are removed using sterile pipette tips. The first two columns are used as control wells (100 μ L of fresh media is put in each well) while the rest of the columns is used for the different concentrations of the sample. In each well, 100 μ L of the pre-prepared sample-media suspension is accurately put using a sterile pipette tip. For each sample, two plates are set up; Figure 4.2 shows the design of each plate while Table 4.1 shows the concentrations used in each one. For each cell line (HeLa and Vero), a whole plate was set up to be a control one. Plates are placed in the incubator for 72 hours after which the MTT assay is carried out.

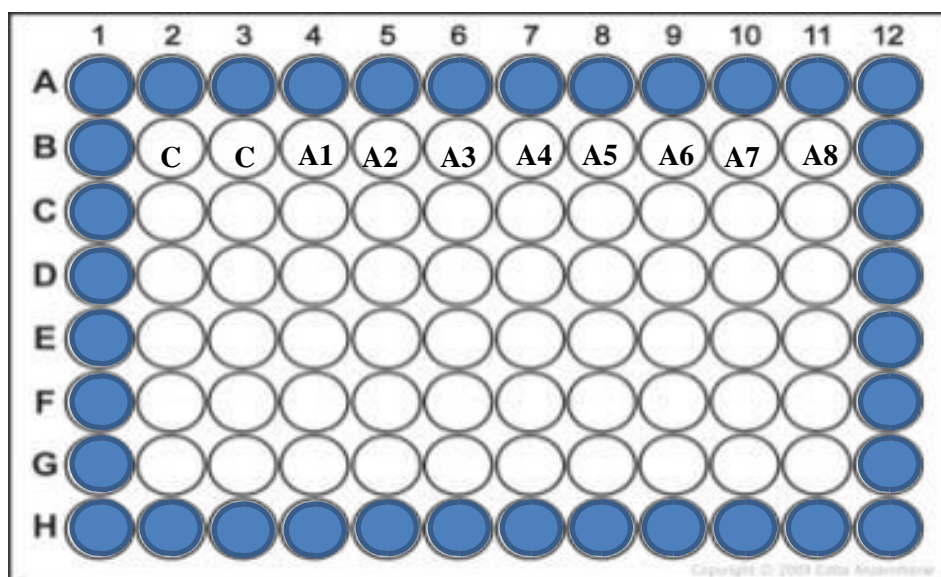


Figure 4.2 Structure and organisation of the 96-well plates used for toxicity studies. Blue cells were kept empty. The concentrations of the columns are shown in Table 4.1

4.2.2.6.7 MTT assay

For the preparation of MTT solution, 250 mg of MTT reagent were dissolved in PBS and sterilized at 121°C for 85 minutes. In each well, 10 μ L of pre-prepared of MTT solution was added. Plates were then placed in the incubator and left for 4 hours.

Table 4.1 The design of plates A and B and the concentrations used for the toxicity testing of dextran, NIPAM monomer, p(NIPAM), p(NIPAM-co-5% LY) and poly(ethylenimine) (PEI)

Conc.	C	C	A1	A2	A3	A4	A5	A6	A7	A8
Plate A										
mg/mL	Control	Control	3	1	0.7	0.3	0.1	0.07	0.03	0.01
Plate B										
μ g/mL	Control	Control	7	3	1	0.7	0.3	0.1	0.07	0.03

The media was then removed (this includes 100 μ L sample in media and 10 μ L MTT) and 100 μ L of dimethyl sulphoxide (DMSO) are added in each well and plates are left in the incubator for 30 minutes. The absorbance at 540 nm of the DMSO in each well is then determined using a Thermo Electron Corporation Multiskan Ascent plate reader.

4.2.2.6.8 Growth curves

Cells were seeded at a concentration of 1×10^4 cell/mL (as explained above) in a 96 well plate. Every day (for 10 days), MTT assay was carried out (as explained above) on one column of the plate.

4.3. Results and discussion

4.3.1 Particle size

4.3.1.1 Effect of temperature

Figure 4.3 shows the response of p(NIPAM-co-5% LY) to the change in temperature across a temperature range of 15-60°C both during heating and cooling. The initial particle size at 15°C at pH 7 is 250 nm which is considerably smaller than that of 100% p(NIPAM) with an initial particle size of 550 nm (1, 27). The incorporation of a hydrophobic comonomer such as lucifer yellow (28) decreases the critical chain length for micellisation of the growing oligomeric chains. This gives rise to a greater number of particle nuclei, so, smaller particle. The incorporation of LY also decreases the extent of hydrogen bonding between the particle and water (solvent) compared to 100% p(NIPAM), so, less water will be incorporated in the particle leading to a smaller particle size (29). It also changes the reaction conditions such as the rate of the reaction, solubility of the monomer and comonomer and the extent of reaction before termination (30). The DLS data suggest that LY was successfully incorporated in the new particle. The figure also shows that the novel fluorescent microgel particle maintains the reversible temperature responsive behaviour of p(NIPAM) with a VPTT of 32°C which is slightly less than that of 100% p(NIPAM) (35°C) (1). The polydispersity index (PDI) value (Figure 4.3), which is close to zero (0.04), suggests that the majority of the particles in the dispersion acquire an even size.

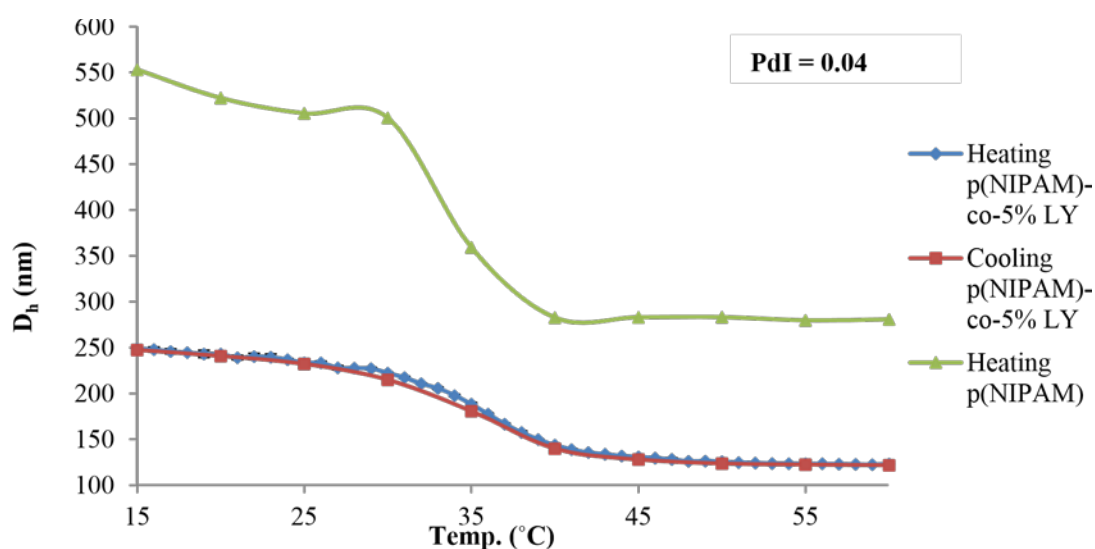


Figure 4.3 The effect of temperature on the particle size of p(NIPAM-co-5% LY) at pH 7 across temperature range (15-60°C)

4.3.1.2 Effect of pH

The effect of pH on the hydrodynamic diameter of p(NIPAM-co-5% LY) is shown in Figure 4.4. The figure shows an increase in the particle size by increasing the pH at the same temperature (25°C). At pH (0.5-3), the particle diameter was 190 nm and increased by 20% to reach 230 nm at pH (5-10). At pH 11, the particle further swells by 9% to reach 248 nm. The change in particle size is thought to be mainly attributed to the change of the protonation state of the co-monomer lucifer yellow by the change in pH (Figure 4.2). Several pH sensitive NIPAM based particles (with different co-monomers such as acrylic acid) have been studied (1). At pH lower than the pK_a of the co-monomer, the anionic groups are protonated, accordingly, they are not charged and hence the electrostatic repulsion force is minimal. When the pH increases above the pK_a of the co-monomer, the anionic co-monomer groups are deprotonated, creating more surface charge on the particle, leading to more electrostatic repulsion forces and hence the increase in the particle size.

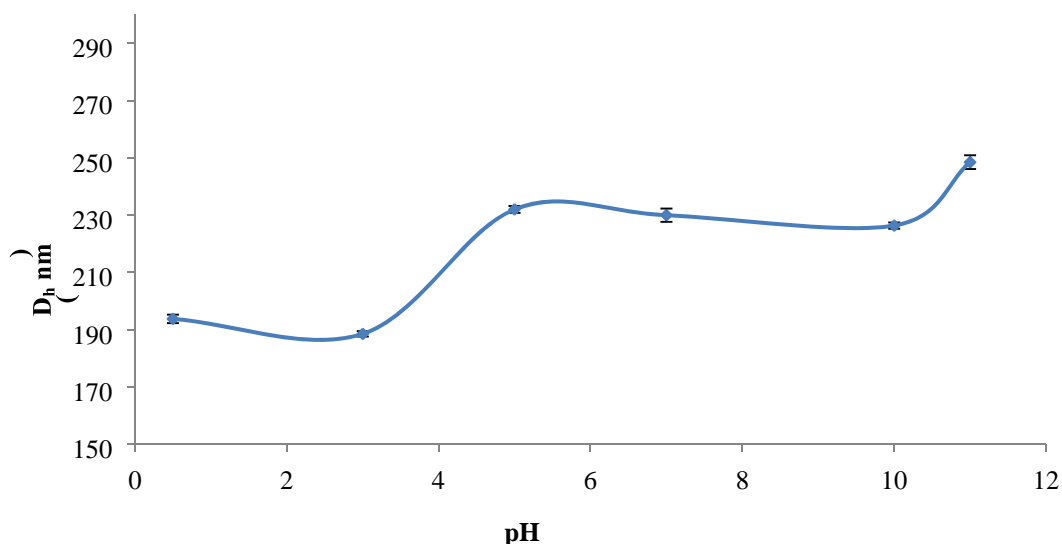


Figure 4.4 The effect of pH on the hydrodynamic diameter of p(NIPAM-co-5% LY) at 25°C

Lucifer yellow VS shows two positive pK_a values (1.4 (0.8) and 5.7 (0.9)) (20). Figure 4.4 shows the change in the hydrodynamic diameter of p(NIPAM-co-5% LY) according to the change of pH. The first positive pK_a of LY (1.4) (caused by the deprotonation of the nitrogen of the piperidine ring) (20) shows a minimal effect on the particle size (Figure 4.4). Comparing the particle size at pH 0.5 to that at pH 3 shows minimal change in the particle size at the two cases. An increase in the particle size around the pH of 5 which is in the range of the second positive pK_a of LY (caused by the deprotonation of the amino group (Figures 4.1 and 4.2) (20) is observed. The figure shows 23 % increase in particle size by increasing the pH from 3 to 5.

At pH below 5.7 (± 0.9), p(NIPAM-co-5% LY) can be considered as a zwitterionic particle. The negative surface charge on p(NIPAM-co-5% LY) particles is caused by the SO_4^- groups from the anionic initiator used during the particle synthesis ($K_2S_2O_8$) and the fluorescent dye (lucifer yellow) with sulphonate groups (Figure 4.1). Having two negative pK_a values, the sulphonate groups of lucifer yellow are deprotonated when the pH is above zero (Figure 4.2) (20). At pH below 1.4, the nitrogen group of the piperidine ring and the amino group of the aniline are both protonated creating positive charge that masks some of the negative charge created by the initiator and the sulphonate groups of LY. At $1.4 < \text{pH} < 5.7$, the nitrogen of the piperidine is deprotonated, but the tertiary amine group of the aniline is protonated and thus charged, so, positive charge caused by the protonated amino group can still mask some of the negative charges. When the pH exceeds 5.7 (± 0.9), both groups

(nitrogen of piperidine and amino of aniline) are deprotonated and thus no positive charges are created. At this point, the negative surface charge on p(NIPAM-co-5% LY) is maximal and not masked by positive charges (the particle is not zwitterionic anymore and tends to only carry negative charges on its surface. This increases the electrostatic repulsion within the particle and hence increases the particle size (Figure 4.4).

It is worth mentioning that the magnitude of change in the particle diameter of p(NIPAM-co-5% LY) at different pH values is less than that of previously known temperature/pH responsive particles such as p(NIPAM-co-5% AA) (1). The initial particle diameter of p(NIPAM-co-5% AA) at 15°C at pH 3 is 290 nm while at pH 6 (at the same temperature) is 550 nm (1). This shows a 90% increase in the particle size by changing the pH of the particle dispersion. In the case of p(NIPAM-co-5% LY), the particles only show a 32% increase in diameter when the pH is changed from 0.5 to 11.

The magnitude of particle size change in response to pH change can be increased by incorporating another co-monomer. This has been carried out by many researchers such as the incorporation of AA (1), *N-t*-butylacrylamide (31). The suggested result then is the synthesis of a fluorescent temperature/pH sensitive particle with a higher magnitude of pH sensitivity.

4.3.2 Electrophoretic mobility

4.3.2.1 Effect of temperature

Figure 4.5 compares between the electrophoretic mobility of p(NIPAM) and p(NIPAM-co-5% LY). p(NIPAM) has a negative surface charge due to the anionic initiator used during synthesis while p(NIPAM-co-5% LY) has a negative surface charge due to both the initiator and the anionic co-monomer (LY) (32). The figure shows that at 15°C the electrophoretic mobility of p(NIPAM-co-5% LY) ($-0.32 \mu\text{mcm/Vs}$) is higher than that of p(NIPAM) ($-0.17 \mu\text{mcm/Vs}$). This can be attributed to two main reasons; first, the presence of a higher surface charge density on p(NIPAM-co-5% LY) particles due to the addition of an anionic co-monomer (lucifer yellow) (32) beside the anionic initiator used during the synthesis.

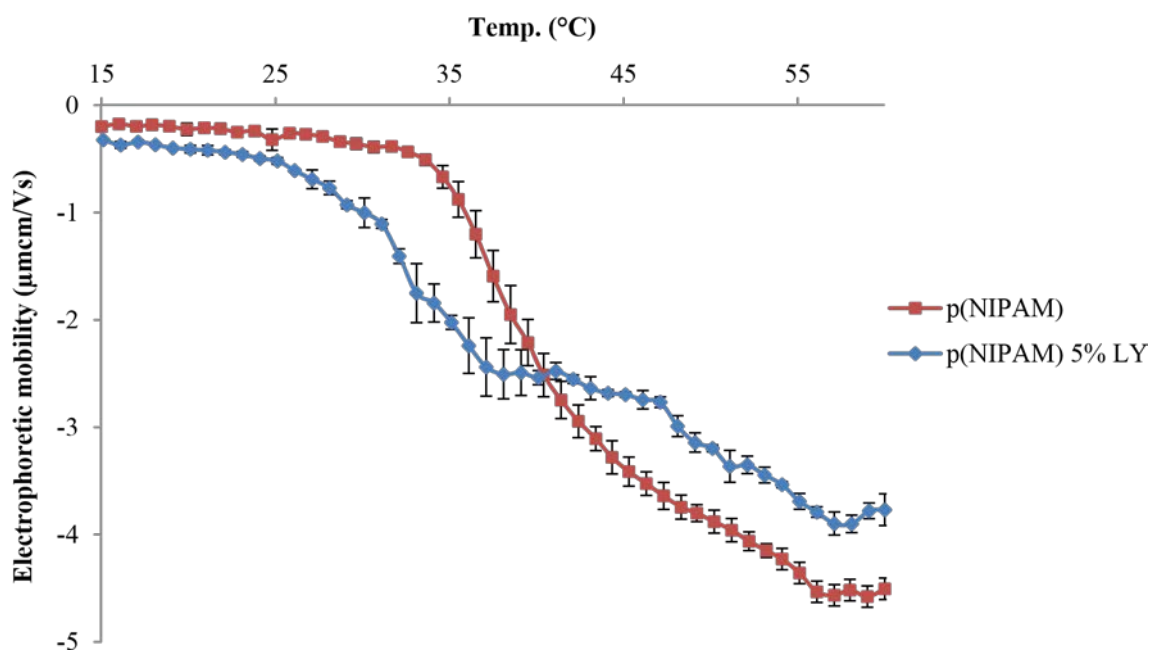


Figure 4.5 The effect of temperature (heating) across a range (15-60°C) on the electrophoretic mobility of p(NIPAM-co-5% LY) and p(NIPAM) in 10^{-4} M NaCl at pH 7

Second, is that the particle size of p(NIPAM-co-5% LY) is smaller than that of p(NIPAM) which causes the particles to move faster. When the temperature exceeds the VPTT, the particle deswells which results in a higher surface charge density (29) and leads to a higher electrophoretic mobility. It is also worth mentioning that the data in Figure 4.5, p(NIPAM-co-5% LY) shows a lower VPTT (32°C) than that of p(NIPAM) (35°C). This agrees with the results previously shown by the particle size measurements and is attributed to the incorporation of the hydrophobic co-monomer LY.

4.3.2.2 Effect of pH

The effect of pH on the electrophoretic mobility of p(NIPAM-co-5% LY) in 1×10^{-4} M NaCl at 25°C is shown in Figure 4.6. As discussed above (point 3.1.1.2), the electrophoretic mobility increases around the pK_a of LY (5.7 (0.9)) due to the deprotonation of the amino group of the aniline (20) (Figure 4.1) that causes an increase of the net negative charge on the particle surface.

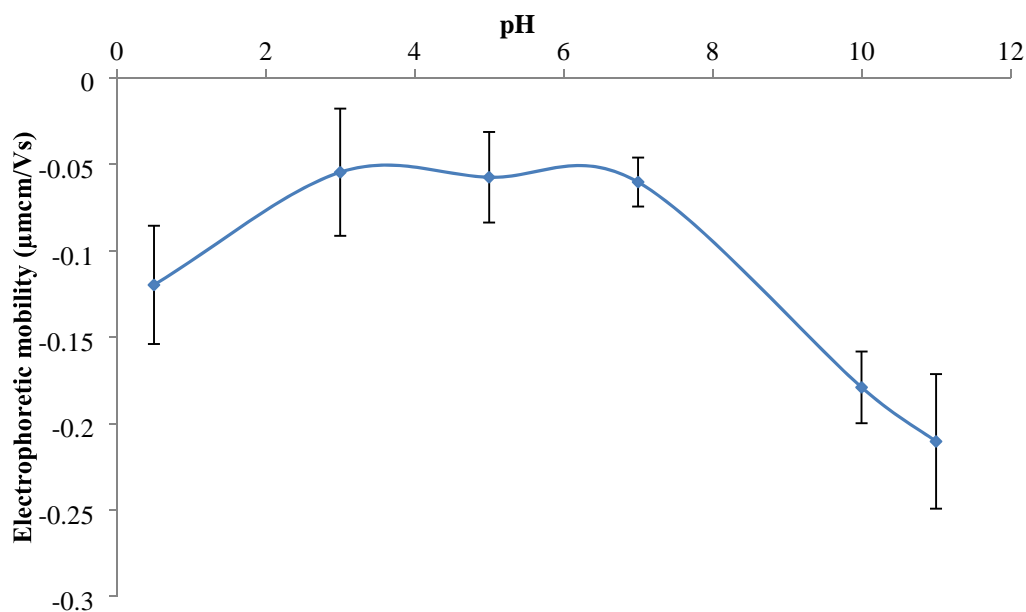


Figure 4.6 The effect of pH on the electrophoretic mobility of p(NIPAM-co-5% LY) in 1×10^{-4} M NaCl at 25°C

4.3.3 Fluorescence spectroscopy

The fluorescence spectra of 0.01 μg/mL LY, 0.2 μg/mL p(NIPAM) and 0.2 μg/mL p(NIPAM-co-5% LY) excited at 430 nm at 25°C and 45°C at pH 3 and 7 are shown in Figures 4.8 and 4.9.

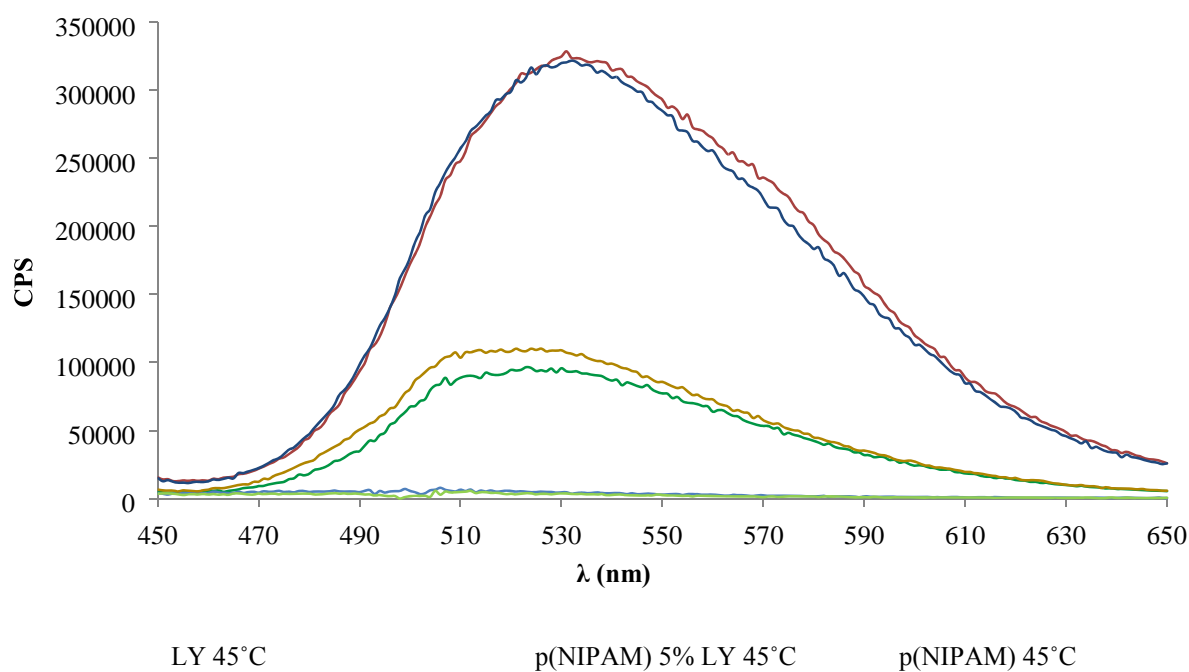
4.3.3.1 Effect of addition of lucifer yellow

The concentration of LY used for the fluorescence spectra in Figures 4.8 and 4.9 (0.01 μg/mL) is the theoretical concentration of LY incorporated in 0.2 μg/mL p(NIPAM-co-5% LY) (5%), in other words, it is the concentration of LY added during the synthesis of p(NIPAM-co-5% LY), and was selected to give a qualitative comparison of the emission spectrum intensity. However, the fluorescence intensity of LY is significantly higher than that of p(NIPAM-co-5% LY) which suggests that either not all the LY added during the synthesis reaction is incorporated in the new particle, or the quantum yield of LY was quenched by the p(NIPAM) particles, or other environmental conditions such as solvent polarity (17).

The second suggestion is supported by Furstenberg *et al.* (17) who studied the excited state dynamics of lucifer yellow and concluded that LY is an environment sensitive probe whose

fluorescence dynamics change in the presence of proteins and by changing the solvent. They also concluded that the fluorescence of LY is quenched by amino acids. Given the fact that both proteins and polymer particles are considered as large complex molecules/particles, it is a possibility that polymer particles might have similar quenching effect on the fluorescence of LY.

p(NIPAM) does not show an emission peak in a similar region or of a similar intensity to that of LY and p(NIPAM-co-5% LY). On the other hand, it shows some fluorescence intensity (of much lower magnitude than p(NIPAM-co-5% LY) which is thought to be due to light scattering) (33). This is a common characteristic of colloidal dispersions that is related to particle size. The turbidity of colloidal dispersions is due to the intense light scattering by its particles. The size and shape of the scattering particles are the main factors affecting the intensity of the scattered light. If a colloidal microgel sample is placed in a UV spectrophotometer and a beam of light is passed through it, a fraction of the light will be scattered as it passes through the sample. While measuring fluorescence of p(NIPAM) and p(NIPAM-co-5% LY), the scattered light from the particles can partially interfere with the fluorescence emission.



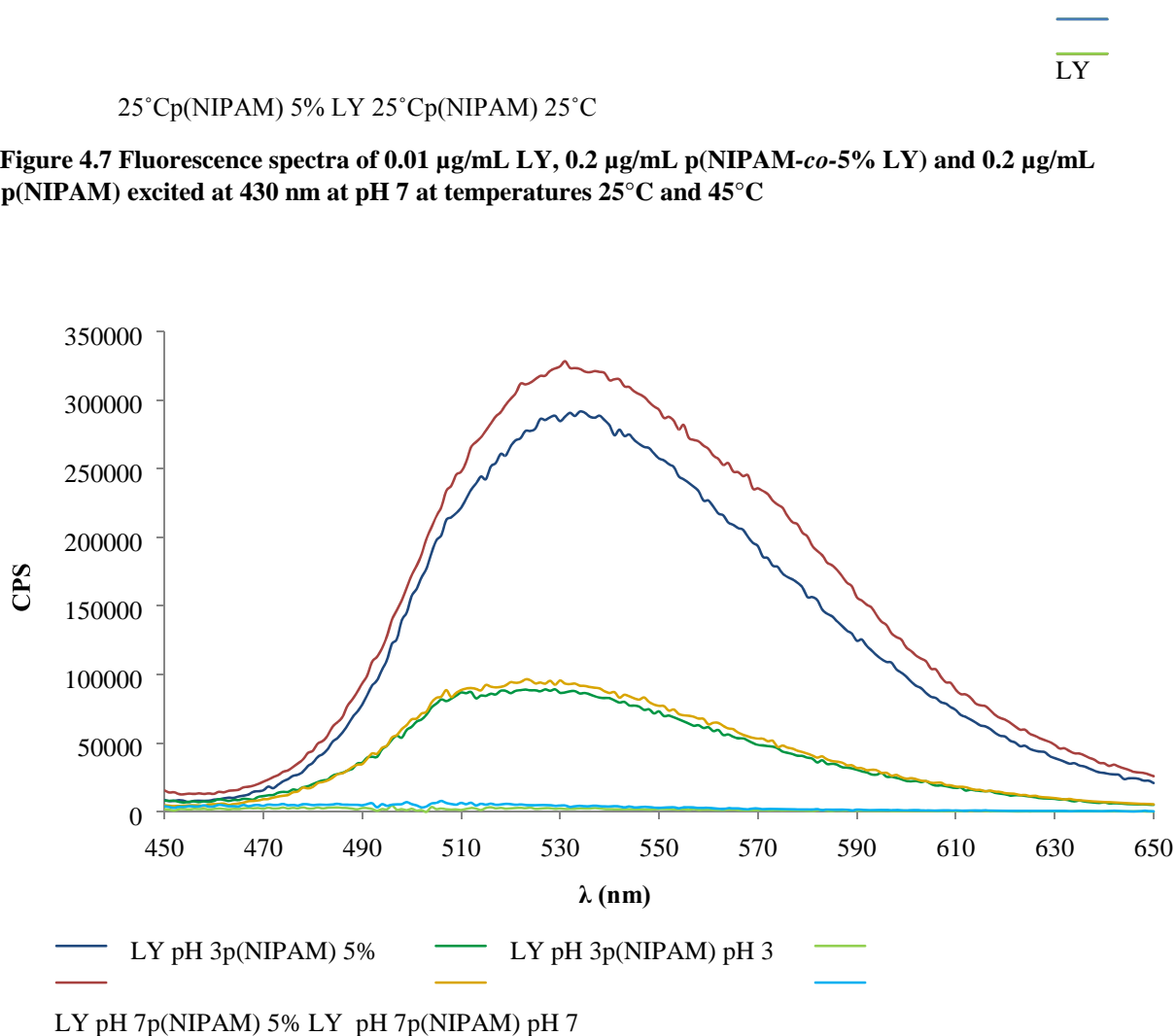


Figure 4.8 Fluorescence spectra of 0.01 $\mu\text{g/mL}$ LY, 0.2 $\mu\text{g/mL}$ p(NIPAM-co-5% LY) and 0.2 $\mu\text{g/mL}$ p(NIPAM) excited at 430 nm at 25°C at pH 3 and 7

4.3.3.2 Effect of temperature

The effect of temperature on the fluorescence of LY, p(NIPAM-co-5% LY) and p(NIPAM) can be compared using Figure 4.7. In 1852, Sir G. G. Stokes observed that fluorescence emission generally occurs at lower energies and longer wavelengths than that of absorption (34). In the case of LY, the emission peak at the same pH (pH 7) and different temperatures (25°C and 45°C) show similar λ_{max} , peak shape and intensity. This indicates that the effect of internal conversion (due to temperature change) on Stokes shift is minimal. In terms of fluorescence intensity, no significant difference between the fluorescence at temperatures of 25°C and 45°C is shown (Figure 4.7). The percentage change between both temperatures is 4% at pH 3 and 1.6% at pH 7.

In the case of p(NIPAM-co-5% LY), the emission peaks at 25°C and 45°C (both at pH 7) show similar λ_{\max} and peak shape. On the other hand, a change in the fluorescence intensity is observed by changing the temperature (Figure 4.7). The percentage change in the fluorescence intensity was 11.7% at pH 3 (3 times higher than that of LY) (data not shown) and 14.6% at pH 7 (9 times higher than that of LY). This can be attributed to different factors such as the change in particle size by changing the temperature from below to above the VPTT (Figure 4.3) which changes the fluorophore density and accordingly the fluorescence intensity. It is worth mentioning that the particle size of p(NIPAM-co-5% LY) decrease by 43% when the temperature increases from 25°C to 45°C at pH 3 and 7. The change in temperature can also cause a change in the quantum yield of fluorescence due to change in solvent properties such as solvent polarity (17, 35). For p(NIPAM), the particles deswell when the temperature exceeds the VPTT (35°C), thus at 45°C, they acquire a de-swollen configuration and the dispersion is more turbid. This boosts the light scattering effect which is shown here as higher fluorescence intensity.

4.3.3.3 Effect of pH

Lucifer yellow is a pH insensitive fluorescent probe (36). This agrees with the results shown in Figure 4.8 where the emission peaks of LY at same temperature (25°C) and different pH values (3 and 7) are similar (same λ_{em}). The same result is also shown for p(NIPAM-co-5% LY).

The fluorescence intensity of LY is affected by the change in pH (Figure 4.8). This can be due to different factors that affect the quantum yield of the fluorophore Lucifer yellow.

These include the change of the polarity of the surrounding polymer (p(NIPAM)) and its electrophoretic mobility which affects the polarity of the solvent (17). Changing the solvent polarity highly affects the fluorescence lifetime which in return affects the quantum yield (17, 37, 38). In the case of p(NIPAM-co-5% LY), no change in the fluorescence intensity is observed. This is can be attributed to the incorporation of a small percentage of LY in the particles. Accordingly, the effect of pH on the fluorescence of the particles is not pronounced.

4.3.4 Infrared spectroscopy

Figure 4.9 shows the FT-IR spectra of p(NIPAM), p(NIPAM-co-5% LY) and LY in the mid IR region (3800-1200 cm^{-1}) while Figure 4.10 shows the spectra in the range 1300-750 cm^{-1} .

The spectrum of p(NIPAM) is comparable to those in the literature (39, 40). Table 4.2 lists the main bands of p(NIPAM) and p(NIPAM-co-5% LY) and their assignments while Table 4.3 list the bands of LY and their assignments.

Table 4.2 FT-IR bands values of p(NIPAM) and p(NIPAM-co-5% LY)

	Wavenumber (cm ⁻¹)	Assignment (41)
a	3292	secondary amide N-H stretching
b	3065	Amide B stretching
c	2970	-CH ₃ asymmetric stretching
d	2929	-CH ₂ asymmetric stretching
e	2874	-CH ₃ symmetric stretching
f	1650	amide I band stretching
g	1550	amide II band stretching
h	1469	-CH ₃ asymmetric deformation
i	1387	-CH ₃ symmetric deformation
j	1368	-CH ₂ symmetric
k	1173	-CH ₃ skeletal
l	1132	-CH ₃ rocking

Table 4.3 FT-IR bands values of LY

	Wavenumber (cm ⁻¹)	Assignment (41)
1	3450	-NH ₂ primary amide stretching
2	3065	C-H stretching
3	1700	overtone and combination bands
4	1650	NH ₂ primary amide deformation
5	1585	Aromatic ring (stretching)
6	1519	
7	1477	
8	1430	
9	1190	S=O stretching
10	1140	SO ₂ symmetrical in sulfones stretching
11	1050	SO ₃ H in sulfonic acids stretching
12	1026	
13	1000	CH=CH ₂ in vinyl compounds out of plane

14	976	
15	890	aromatic C-C (stretching)
16	802	R-NH ₂ in primary amines NH ₂ wag
17	770	<i>m</i> -disubstituted benzene (CH out of plane)

The IR spectrum of p(NIPAM-co-5% LY) is comparable to that of p(NIPAM) (Figures 4.10 and 4.11). On the other hand, the incorporation of lucifer yellow is indicated by the band at 1054 cm⁻¹ for LY and 1046 for p(NIPAM-co-5% LY) (indicating the sulphoxides in lucifer yellow). At 994 cm⁻¹, p(NIPAM) show a small band indicating vinyl group (41) (also present in LY at 1000 cm⁻¹), the absence of this group in the p(NIPAM-co-5% LY) spectrum suggest the absence of free vinyl groups since they were polymerized during the synthesis of the microgel. It is also worth mentioning that none of the spectra of p(NIPAM), p(NIPAM-co-5% LY) and LY show the C=C (of the vinyl group) stretch band in the range of 1690 - 1670 cm⁻¹ (Tables 4.2 and 4.3 and Figure 4.9) (41). This can be attributed to the presence of the strong amide band at 1650 cm⁻¹ and in case of LY the overtone and combination bands at 1700 (Table 4.3 and Figure 4.9). The presence of these bands in a close range to that of C=C stretch band might have shifted or masked it.

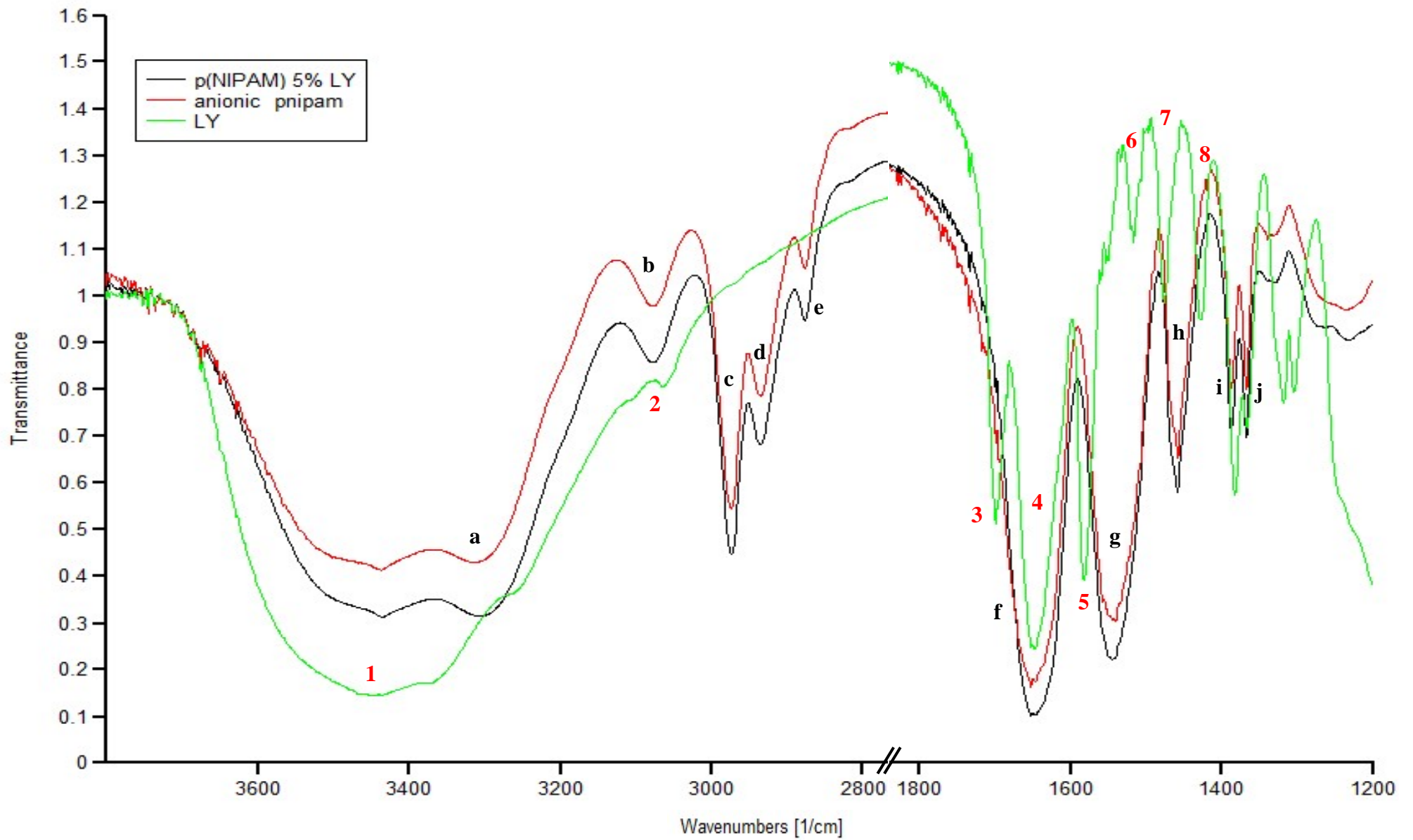


Figure 4.9 FT-IR spectra of p(NIPAM) (red), p(NIPAM-co-5% LY) (black) and LY (green) in the region (3800-1400 cm^{-1})

98

p(NIPAM-co-5% LY)

Chapter Four

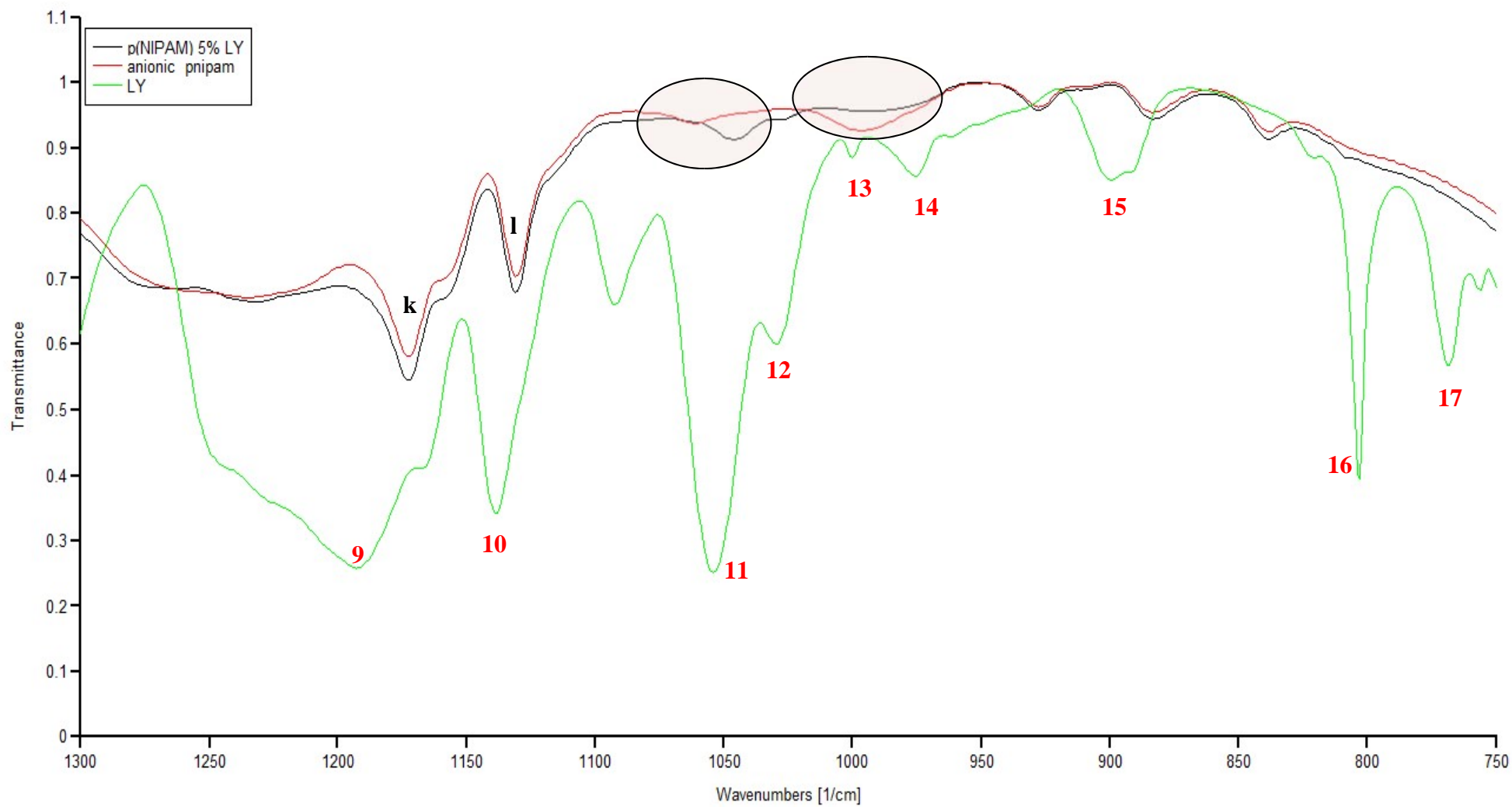


Figure 4.10 FT-IR spectra of p(NIPAM) (red), p(NIPAM-co-5% LY) (black) and LY (green) in the region (1300-750 cm⁻¹)

4.3.5 Microscopy

The novel microgel particles were examined using SEM (Figure 4.11) and fluorescence microscopy (Figure 4.12). Figure 4.11 show that the particles are spherical, monodispersed and their average size is 120 nm which is comparable to that shown by DLS at deswollen state (Figure 4.3). In few occasions, the dehydration of the sample causes some of the particles to be associated (Figure 4.11). The fluorescence microscopy (Figure 4.12) also confirms the results of SEM where the particles are shown to be spherical, roughly of the same size and fluorescent. Figure 4.12 supports the suggestion that LY is incorporated in the novel p(NIPAM-co-5% LY) microgel particles and that they are fluorescent. Accordingly, it can be suggested that these particles can be traced in the human body (given their fluorescence) which can serve as a diagnostic tool. Researches have tried incorporating fluorescent dyes into microgels (42, 43), on the other hand, there are no upto-date data showing fluorescence microscopy images of fluorescent microgels.

4.3.5.1 Scanning electron microscopy

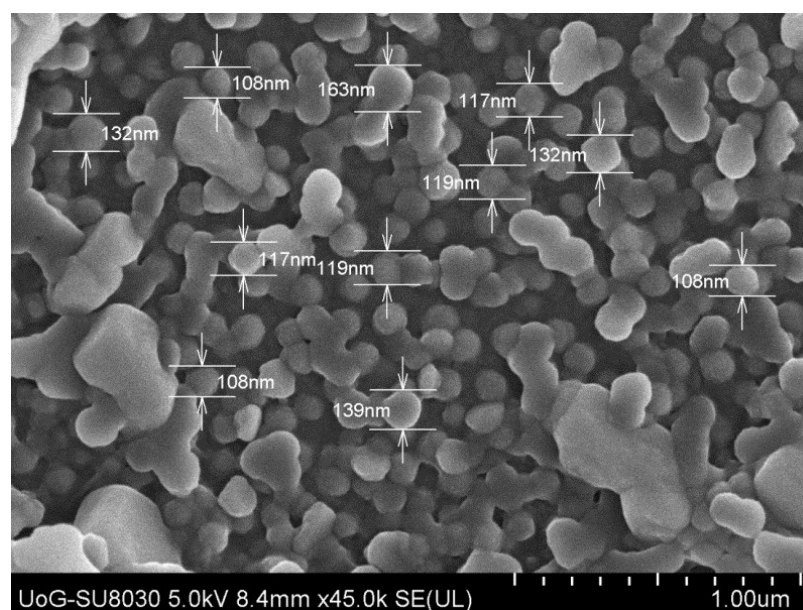


Figure 4.11 SEM pictures of p(NIPAM-co-5% LY) at pH 3 (x 45,000)

4.3.5.2 Fluorescence microscopy

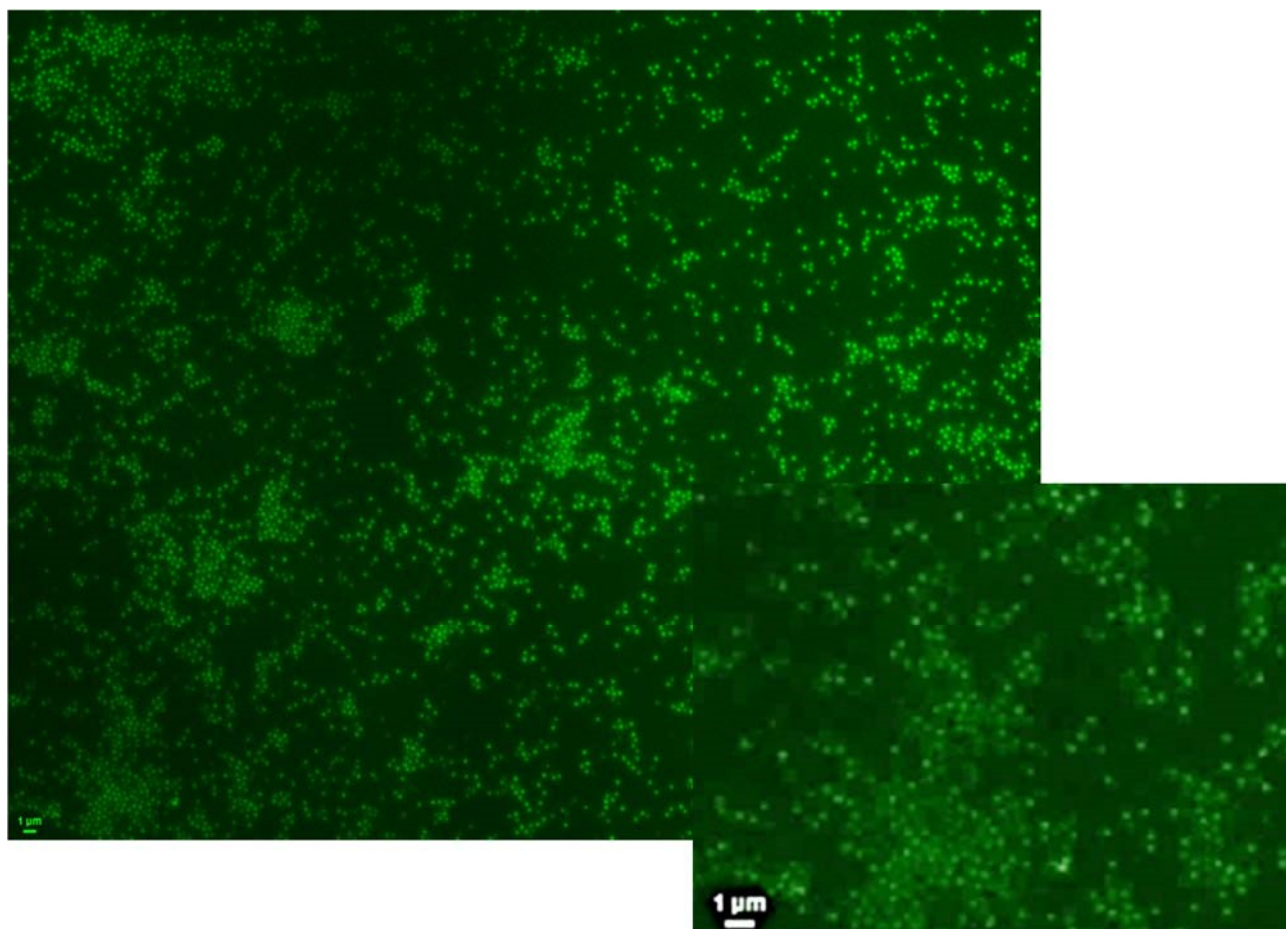


Figure 4.12 Fluorescence microscopy pictures of 2 $\mu\text{g/mL}$ p(NIPAM-co-5% LY) (x 100)

4.3.6 Toxicity studies

p(NIPAM) based microgels have been studied for a number of years (44-48). Many applications have been suggested for this polymer due to its ability to change its physicochemical properties according to the change in environmental conditions (1, 2). Considering that the VPTT of p(NIPAM) particles is 33-35°C (1) which is very close to the human body temperature, many researchers investigated the possible use of p(NIPAM) microgel particles in drug delivery (7, 49-51), delivery of stem cells (52) and other biomedical applications such as tissue engineering (27), biomedical implants (53), treatment of dentinal hypersensitivity (1) and wound dressings (54, 55). A very important point to consider in this case is the toxicity of NIPAM based microgels; on the other hand, not many data are available in this context in literature up to date.

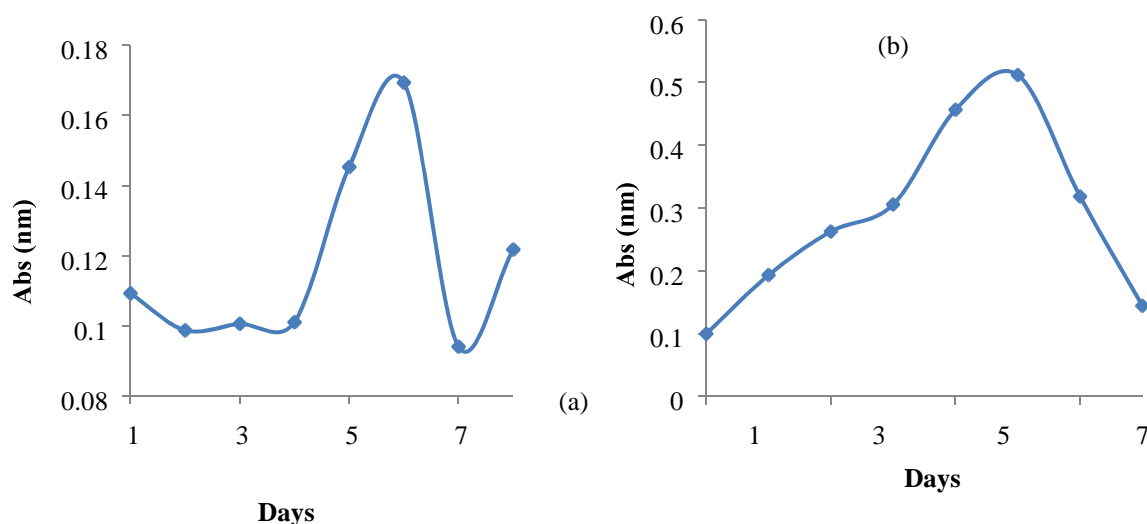
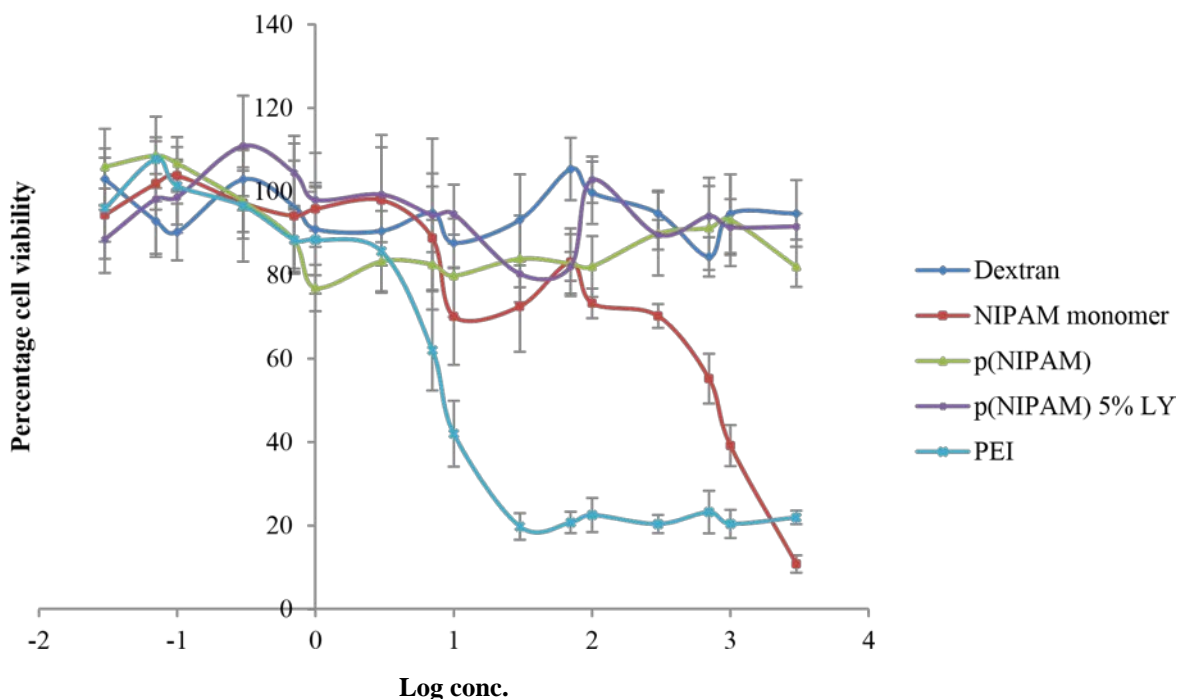


Figure 4.13 Growth curves of (a) HeLa cells and (b) Vero cells

The growth curve of both HeLa and Vero cells are shown in Figure 4.13. Both curves are comparable to those reported in literature (56, 57). The growth of both cells passes through different phases. Phase 1 is the lag phase when the cells do not divide but adapt to the culture conditions. The seeding density and the kind of cell line define the length of this phase. Phase 2 is the lag phase when the cells proliferate actively and the cell density exponentially increases. The cell proliferation kinetics varies from one cell line to another. Phase 3 is the plateau or stationary phase when the cell proliferation slows down and the cells are susceptible to injury. Phase 4 and the last is the decline phase when cell death dominates and the number of viable cells decreases dramatically (58).



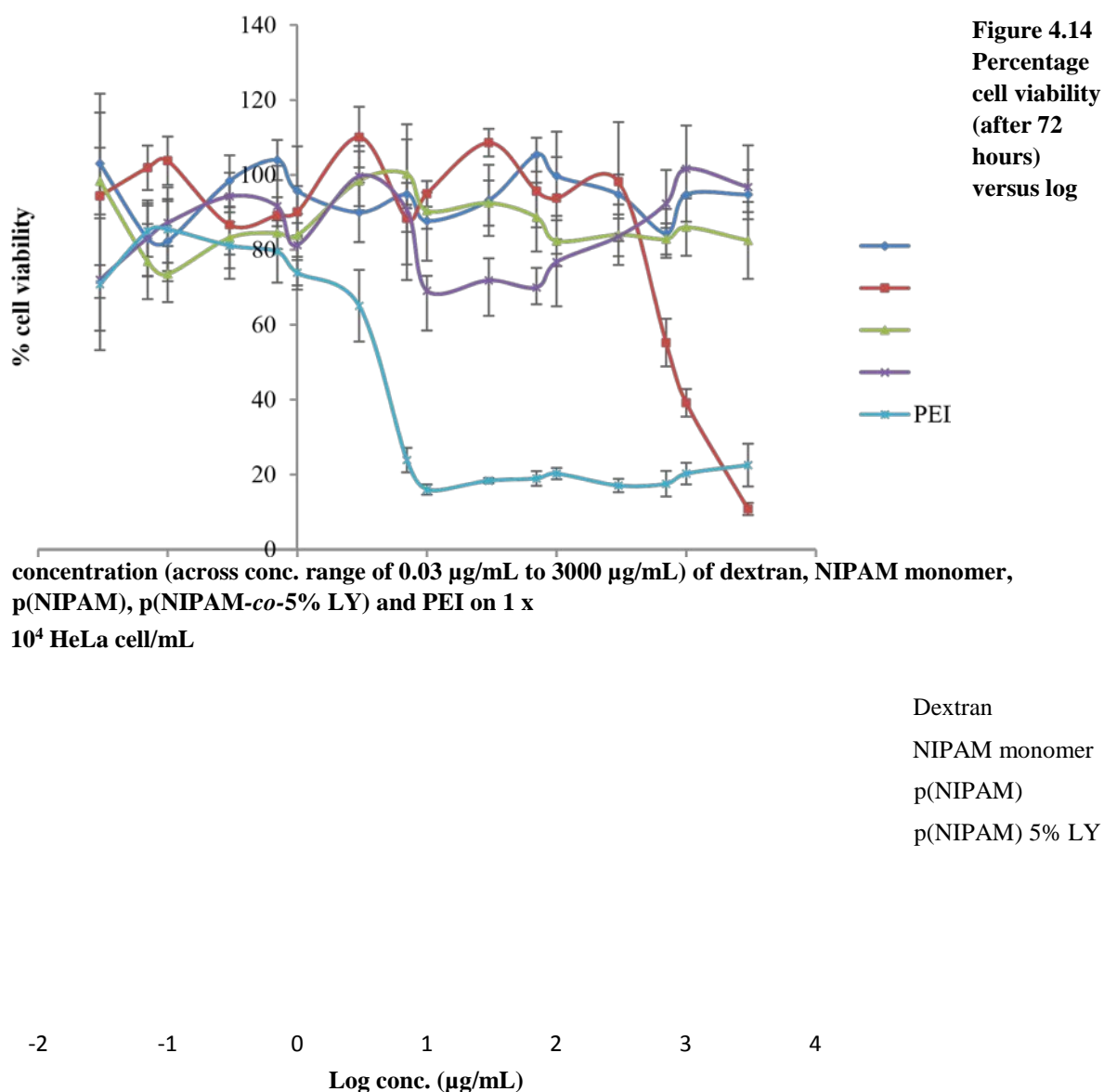


Figure 4.15 percentage cell viability (after 72 hours) versus log concentration (across conc. range of 0.03 µg/mL to 3000 µg/mL) of dextran, NIPAM monomer, p(NIPAM), p(NIPAM-co-5% LY) and PEI on 1 x 10⁴ Vero cell/mL

Table 4.4 LC₅₀ of dextran, NIPAM monomer, p(NIPAM), p(NIPAM-co-5% LY) and PEI on HeLa and Vero cells (std error values are presented in brackets)

	LC ₅₀ on HeLa cells (µg/mL)	LC ₅₀ on Vero cells (µg/mL)
Dextran	≥ 3000	
NIPAM monomer	700 (6)	700 (6)

p(NIPAM)	≥ 3000	
p(NIPAM) 5% LY	≥ 3000	
PEI	0.7 (0.2)	3 (0.9)

In 2010, Naha *et al.*, (59) studied the cyto- and geno-toxicity of p(NIPAM) particles (within a concentration range of 25-1000 mg/L) on two different mammalian cell lines, SW480 (colon) and HaCaT (dermal cell line). The viability of cells (both cell lines) after 24, 48, 72 and 96 hours were shown to be 100%. Also, the geno- and eco-toxicity (60) data confirmed the results of the cytotoxicity suggesting that p(NIPAM) particles have an excellent bioavailability profile *in vitro*. Naha *et al.* (59) have further studied p(NIPAM) based microgel particles inside cells and concluded that the particles enter the cells and are localized in the lysosomes.

The cytotoxicity and uptake of p(NIPAM) based microgel particles with incorporated hyperbranched polyglycerol (HPG) was investigated by Cuggino *et al.*, (61). The cytotoxic effect of p(NIPAM-co-HPG) particles on epithelial human lung cancer cell line A549, human hematopoietic cells U-937, and human epidermoid carcinoma cells A431. Results suggest that doses above 0.5 mg/mL are required to cause adverse effects on the cells. It is also worth mentioning that the particles could penetrate the cell membrane of lung cancer cells A549 incubated at 37°C and were distributed in the perinuclear region (61).

Herein, the effect of dextran, NIPAM monomer, p(NIPAM), p(NIPAM-co-5% LY) and PEI on the cell viability of both HeLa and Vero cell lines is reported. HeLa cells are human epithelial cells of a strain maintained in tissue culture since 1951 and used in research, especially in virology. The original cells were provided by cervical carcinoma of *Henrietta Lacks* (62). Vero cells are taken from the kidneys of the African green monkey, *Cercopithecus aethiops sabaeus*, and used to grow certain viruses for vaccine production (63).

Figure 4.14 shows the effect of different concentrations (concentration range between 0.03 µg/mL to 3 mg/mL) of dextran, NIPAM monomer, p(NIPAM), p(NIPAM) 5% LY and PEI on the cell viability of HeLa cells. The figure shows that the effect of dextran (used as a negative control) on the cell viability was minimal as the cells showed over 90% viability

across the whole range of concentrations. On the other hand, PEI (used a positive control) shows cell viability above 80 % at concentrations less than 0.003 mg/mL. When the concentration further increases, the cell viability significantly decreases till it reaches 20% at a concentration of 0.03 mg/mL. In spite of its reported toxicity (64, 65), PEI is widely researched as one of the main non-viral vectors for gene therapy (66). These results are comparable to those of Zhizhong *et al.* (67) who studied the cytotoxicity of linear 25 kD PEI (known to be less toxic than branched PEI (64, 66, 68)) on OS-RC-2 cell line and reported that cell viability under 30 µg/mL of 25 kD PEI was 50%. For 2 kD PEI, half of the cells were viable when the concentration was 200-300 µg/mL. Similar results were also shown by Thomas *et al.* (69) who reported that less than 50 % of COS-7 cells were viable when the concentration of 25 kD PEI was more than 20 µg/mL while less than 5 % of the cells were viable when its concentration was above 35 µg/mL.

Despite its reported cytotoxicity (64, 66-70), the use of PEI has been studied for biological applications such as gene delivery (65, 67, 71, 72), nucleic acid delivery (68, 69, 73-75), drug delivery (70), cosmetics (76) and tissue engineering (77). In 2012, Wegmann *et al.* (78) claimed that PEI is a potent mucosal adjuvant for human use and suggested that further investigation for improvement of potency and safety of PEI as an adjuvant suggests promising results. Many attempts to decrease the cytotoxicity of PEI by conjugation with other molecules have been varied out. These aim at turning PEI into a bioequivalent delivery system (67-69, 74, 75). Similarly, it can be suggested that the conjugation of acrylamide and its derivative NIPAM into p(NIPAM) based particles can yield particles with significantly lower toxicity. It is also worth mentioning that PEI is currently commercially available (in the form of PEI-HCl) in a drug in the German market known as 'Epi pak' used for mouth disorders (79).

The main challenge for the use of NIPAM based particles as drug delivery systems is its toxicity. The fact that the main monomer NIPAM includes acrylamide group which is known for its toxicity (80), suggests that the polymerized particle and/or its metabolic products (such as NIPAM monomer and/or acrylamide) might acquire the same properties. Accordingly, the toxicity of the novel particle p(NIPAM-co-5% LY), p(NIPAM) and the monomer was tested. In Figure 4.14 p(NIPAM) shows cell viability over 80 % up to a concentration 3 mg/mL while NIPAM monomer showed a high cell viability (over 80 %) for concentration equal to, or less than, 0.3 mg/mL. Above this concentration, NIPAM

monomer shows considerably less viability until it reaches 10 % at a dosing concentration of 3 mg/mL.

For the novel p(NIPAM-co-5% LY) particles, the results show that the cell viability is around 80% or higher up to 3 mg/mL. This suggests that p(NIPAM-co-5% LY) is suitable for medical and/or pharmaceutical use when used within the specified concentrations. Similar results for the effect of the same concentrations of dextran, NIPAM monomer, p(NIPAM), p(NIPAM-co-5% LY) and PEI on the cell viability of Vero cells. Figure 4.15 shows that dextran showed cell viability over 80% across all the dosing concentrations. PEI showed cell viability over 80% at concentrations equal to, or less than, 0.001 mg/mL. Increasing the dosing concentration decreased the cell viability till it reached 15 % at 0.01 mg/mL. NIPAM monomer showed high cell viability (between 80 and 100%) at concentrations equal to, or less than, 0.3 mg/mL. Both p(NIPAM) and p(NIPAM) 5% LY showed cell viability around 80% or more for all the dosing concentrations used.

Comparing the cytotoxicity (for both HeLa and Vero cells) of p(NIPAM) 5% LY and p(NIPAM) to that of PEI shows that the former particles show a safer toxicity profile. While a concentration of (0.7 μ g/mL for HeLa and 3 μ g/mL for Vero) of PEI killed half of the cells (Table 4.4), 3 mg/mL of the NIPAM based particles kept more than 80 % of the cells alive (Figures 4.15 and 4.16). Furthermore, NIPAM monomer which is expected to be one of the metabolic products of p(NIPAM) based particles has an LC₅₀ of 700 μ g/mL (for both HeLa and Vero cells) which is considerably higher than that of PEI. Thus, the results show that p(NIPAM) based particles as well as NIPAM monomer (at the specified concentrations) have a safer toxicity profile when compared to PEI. Considering the ongoing research and use of PEI in biological and pharmaceutical applications (previously discussed) and the properties of p(NIPAM) based particles such as temperature, pH, ionic strength responsiveness, it is suggested that further research of the toxicity of p(NIPAM) based particles as well as modification of the particles can yield very useful and promising systems for biological and pharmaceutical applications such as drug delivery, gene therapy and treatment of dentinal hypersensitivity.

The biocompatibility of p(NIPAM), p(NIPAM-co-AA) and p(NIPAM-co-BA) with skin has been studied by Abu Samah *et al.* (81). The effects of the three particles on the expression of cyclooxygenase-2 (COX-2) was determined using western blotting which showed that the particles have penetrated the skin and the keratinocytes of the vital epidermis. p(NIPAM-

co-BA) showed 67% higher COX-2 expression than the control group which indicates a pro-inflammatory response. For p(NIPAM-co-AA), no significant modulation in the expression of COX-2 was shown, indicating the compatibility of the particles with skin. Comparable results were obtained for microgel particles loaded with citric acid solution. Accordingly, the authors support the use of the multiresponsive p(NIPAM-co-AA) as a triggered or controlled topical drug delivery system.

For *in vivo* testing, Aslam *et al.* (82) tested the effect of different concentrations (0, 0.2, 0.4, 0.6, 0.8 and 1 mg/mL) of 150 nm p(NIPAM) on Swiss Albino mice (*Mus musculus*). Oral p(NIPAM) dispersions (with the previously mentioned concentrations) were given to the mice daily for 30 days. The results suggest that lower doses (0.2 mg/mL) had no lethal effect on the mice. Increasing the dose of p(NIPAM) (0.4, 0.6 and 0.8 mg/mL), half the mice died in 20-25 days. For 1 mg/mL p(NIPAM) dispersions, half the mice died in 28 days. The authors suggest that p(NIPAM) is tolerable at low doses, on the other hand, the accumulation of high doses of the particles (by daily administration of 1 mg/mL/kg) has a lethal effect in an average of 18 days.

In 1981, Tanii *et al.* claimed that the metabolic product of NIPAM is acrylamide (83), accordingly, it is very important to consider its toxicity while studying the toxicity of NIPAM based particles. Many researchers have claimed that acrylamide is toxic (84), some mention its neurotoxicity (84), others mention its genotoxicity (84) as well as other serious effects such as testicular degeneration, necrosis of the liver, congestion of the lungs. Acrylamides are formed when some foods including certain nutrients are cooked at certain temperatures during grilling, frying and baking (79, 85). A review studying the dose-response relationship of acrylamide was carried out by Shipp *et al.* (85), the study states that the reference dose (RfD) (safe dose) of acrylamide is 0.83 $\mu\text{g}/\text{kg}/\text{day}$ (considering reproductive effects and genotoxicity) and 1.2 $\mu\text{g}/\text{kg}/\text{day}$ (considering neurotoxicity). The review also claims that most of the reports of acrylamide toxicity did not consider very important factors such as the smoking state of the patients which is extremely important (85). Considering the RfD mentioned by Shipp *et al.* (85), an adult of average weight 70 kg can safely have 58 $\mu\text{g}/\text{day}$ of acrylamide.

In 1992, an occupational safety and health guideline for acrylamide was produced by the US Department of health and human services and the US Department of Labor (84). The

toxicology results in this report states that the lethal dose 50 (LD₅₀) (the dose that kills half of the animals) of orally administered acrylamide in rabbits is 150 - 180 mg/kg while for dermally applied acrylamide it is 2250 mg/kg. In rats, the report states that the LD₅₀ was 565 mg/kg and 490 mg/kg for males and females, respectively (84). Only when continuously exposed to an acrylamide dose of 1 mg/kg/day did cats, rats and monkeys develop neuropathies (84). In theory, if we apply this to humans, an adult human being of average weight 70 kg needs to orally administer 70 mg/day to develop neuropathy.

An example of polyacrylamide containing drug that have been available in the German market for years is a drug commercially known as 'Geliperm' gel and wound dressing (86) for the treatment of wounds. The active ingredient of this drug is poly(acrylamide-*N,N'*methylenediacrylamide) (79). The drug is produced by two companies; Geistlich Pharma and Yamanouchi Pharma GmbH (86). In spite of being an acrylamide polymer, the drug has been used in the European market for years which suggests no major problems were reported concerning its toxicity. In 1988, the U.S. Naval research office in London mentioned Geliperm as one of the drugs commonly used in treatment of wounds (87). In 2006, the medical uses of Geliperm were further extended to be used as a hydrogel wound dressing for protecting the eyes of anaesthetized patients during surgery and in the intensive care unit (88). It was also used as a sterile, solid gel interface between ultrasound probe and skin for producing ultrasound images (88). Such an example, suggests that the medical and pharmaceutical use of p(NIPAM) particles can be applicable if well studied and applied.

Very important questions arise on this occasion. If used as a drug delivery system, how much acrylamide would the metabolism of p(NIPAM) based particles yield? How much p(NIPAM) based particles would be required for drug delivery? Does p(NIPAM) metabolism yield any other metabolites? Can the metabolic pathways of p(NIPAM) be altered? Would the route of administration of p(NIPAM) particles highly affect the toxicity profile? Would the synthesis method of p(NIPAM) particles make much difference in its toxicity? Does anionic p(NIPAM) have a different toxicity than cationic one? Considering late cases of cancer or other serious diseases, is there a study that compares the advantages and the disadvantages of using p(NIPAM) particles as a delivery system (in case of late stages of fatal diseases such as cancer)? Some of these questions are being addressed (59, 81, 89). Yet, a lot more research is needed to find out if p(NIPAM) based particles can be a promising non-toxic drug delivery system, some of which will be targeted in the future

research plan. This will include more *in vitro* toxicity studies with different environmental conditions, more animal testing with different doses to define a dose response curve of p(NIPAM) and its metabolites. According to the results obtained, the decision will be made whether or not proceed to human testing.

Most of the drugs currently available in the market can cause different kind of toxicities and can even be lethal if administered at the wrong dose. It is worth mentioning at this point, that p(NIPAM) based particles (if pharmaceutically used) are intended to be used as a drug delivery system and not a drug, this might be important while calculating the required dose.

4.4 Conclusions and future work

4.4.1 Conclusions

A novel fluorescent negatively charged temperature/pH-sensitive particle (p(NIPAM-co5% LY)) was successfully synthesized and characterized using different techniques. At pH 7 and 15°C (the particle is swollen), the particle size is 250 nm. When the temperature exceeds the VPTT (35°C) the particle de-swells to reach 130 nm. These particle sizes are approximately half that of p(NIPAM) at similar conditions. The PDI and the intensity peaks of the novel microgel dispersion indicate a uniform particle size across the dispersion. The particle shows pH sensitivity where the particle size increases around pH 5 which is the calculated pK_a of LY. The fluorescence emission intensity is affected by the change in temperature. Increasing the temperature causes an increase in the fluorescence emission intensity. The microscopy experiments show that the particles are spherical, monodispersed and fluorescent.

This study only provides initial evidence of the biocompatibility of NIPAM based particles and its metabolite at the specified concentrations. However, it can be concluded that NIPAM monomer is more toxic than both p(NIPAM) and p(NIPAM-co-5% LY). The two microgel particles show cell viability over 80% (for both cell lines HeLa and Vero) up to a concentration of 3 mg/mL while NIPAM monomer show cell viability over 80% equal to or less than 0.3 mg/mL. At concentration of 3 mg/mL, NIPAM monomer shows 10% cell viability. These data add to the few existing reports on the toxicity of NIPAM based particles and provide some encouragement around their biocompatibility and possible use for drug delivery applications.

4.4.2 Future work

Further improvement of p(NIPAM-co-5% LY) particle will be carried out to support its suggested use as a combined diagnostic and drug delivery system that specifically targets cancer cells. This will include the incorporation of other co-monomers to improve the pH sensitivity of the particle. To further improve the tracing and diagnostic abilities of the particle, the incorporation of other fluorescent molecules that can change the colour of their fluorescence by the change in pH can be investigated. Also, the incorporation of comonomers with specific groups that bind with specific receptors of the cell membrane of cancer cells will be carried out.

To determine if p(NIPAM) based particles are biocompatible, more studies considering all the factors that can affect toxicity should be conducted. These studies will investigate the pharmacology and pharmaco-kintetics of p(NIPAM) based particles. These studies are not only required to further investigate the *in vitro* toxicity on different cell lines but also test the *in vivo* toxicity (animal and human testing), determine the metabolic products of NIPAM based microgel particles and study their effect on the human body. Based upon these studies, it is to be decided whether or not these particles shall be used in medical and pharmaceutical applications such as drug, gene and nucleic acid delivery. Future experiments will also include the localization of p(NIPAM-co-5% LY) inside cells to understand its behaviour *in vivo*. The uptake and release of different drugs from p(NIPAM-co-5% LY) and the factors affecting them will also be investigated.

4.5 References

1. Mohsen R., Vine G. J., Majcen N., Alexander B. D., Snowden M. J. Characterization of thermo and pH responsive NIPAM based microgels and their membrane blocking potential. *Colloids and Surfaces A: Physicochemical and Engineering Aspects*. 2013;428:53-9.
2. Saunders B. R., Laajam N., Daly E., Teow S., Hu X., Stepto R. Microgels: From responsive polymer colloids to biomaterials. *Advances in Colloid and Interface Science*. 2009;147-48:251-62.
3. Ma X., Tang X. Flocculation behavior of temperature-sensitive poly(*N*-isopropylacrylamide) microgels containing polar side chains with -OH groups. *Journal of Colloid and Interface Science*. 2006;299:217-24.
4. ACD/Labs Lucifer yellow VS. 2010 file:///C:/Users/user/Downloads/pka%20(2).pdf. Accessed on the 14th of November, 2014.

5. Sigma. Lucifer yellow vs.
<http://www.sigmaaldrich.com/catalog/product/aldrich/862053?lang=en®ion=GB>.
Accessed on the 16th of April, 2013.
6. Thorne J. B., Vine G. J., Snowden M. J. Microgel applications and commercial considerations. *Colloid Polym Sci.* 2011;289:625-46.
7. Pinkrah V. T., Beezer A. E., Chowdhry B. Z., Gracia L. H., Cornelius V. J., Mitchell J. C., Castro-Lopez V., Snowden M. J. Swelling of cationic polyelectrolyte colloidal microgels: Thermodynamic considerations. *Colloids and Surfaces APhysicochemical and Engineering Aspects.* 2005;262:76-80.
8. Ramkisson-Ganorkar C., Liu F., Baudys M., Kim S. W. Modulating insulin release profile from pH thermosensitive polymeric beads through polymer molecular weight. *Journal of Controlled Release.* 1999;59:287-98.
9. Castro Lopez V., Hadgraft J., Snowden M. J. The use of colloidal microgels as a (trans)dermal drug delivery system. *International Journal of Pharmaceutics.* 2005;292:137-47.
10. Pelton R. Temperature-sensitive aqueous microgels. *Advances in Colloid and Interface Science.* 2000;85:1-33.
11. Yasui M., Shiroya T., Fujimoto K., Kawaguchi H. Activity of enzymes immobilized on microspheres with thermosensitive hairs. *Colloids and Surfaces B: Biointerfaces.* 1997;8:311-9.
12. Kondo A., Oku S., Higashitani K. Adsorption of gamma-globulin, a model protein for antibody on colloidal particles. *Biotechnology and Bioengineering.* 1991;37:537-43.
13. Kitano H., Nakamura K., Hirai Y., Kaku T., Ise N. Restricted diffusion effect on the binding of proteins to porous polymer resins as studied by repetitive injection method. *Biotechnology and Bioengineering.* 1988;31:547-52.
14. Weitai Wu, Shoumin Chen, Yumei Hu, Shuiqin Zhou. A Fluorescent Responsive Hybrid Nanogel for Closed-Loop Control of Glucose. *Journal of Diabetes Science and Technology.* 2012;6:892-901.
15. Ravaine V., Ancla C., Catargi B. Chemically controlled closed-loop insulin delivery. *Journal of Controlled Release.* 2008;132:2-11.
16. Sabnis R. W. *Handbook of biological dyes and stains. Synthesis and industrial applications.* New-Jersey: Wiley; 2010.

17. Sigma. Product information. Saint Lois - USA: https://www.sigmaaldrich.com/content/dam/sigmaaldrich/docs/Sigma/Product_Information_Sheet/2/10259pis.pdf. Accessed on 10th of April, 2013.
18. Urstenberg A., Vauthey E. Excited-state dynamics of the fluorescent probe Lucifer Yellow in liquid solutions and in heterogeneous media. *Photochemical & Photobiological Sciences*. 2005;4:260-67.
19. Mayr T. Optical sensors for determination of heavy metal ions: Universitat Regensburg; 2002.
20. ACD/Labs. 2010 <https://ilab.acdlabs.com/iLab2/>. Accessed on the 14th of November, 2014.
21. Heller M. J., Jablonski E. J. Fluorescent stokes shift probes for polynucleotide hybridization assays. Patent. 1990, application number CA 523997.
22. Buetow D. E., Cameron I. T., Padilla G. M., Zimmerman A. M., Stevens J. K., Mills L. R., Trogadis J. E. Three-Dimensional Confocal Microscopy: Volume Investigation of Biological Specimens. Editors: Stevens J., Mills L. and Trugadis J. California: Academic Press; 1994.
23. Thermo Scientific. FITC and TRITC. Rockford: Thermo Scientific. Report No.: 46424 46425 46112. http://tools.lifetechnologies.com/content/sfs/manuals/MAN0011646_FITC_TRITC_UG.pdf
24. Thermo Scientific. Texas Red Sulfonyl Chloride. Rockford: Thermo Scientific Report No.: 46115. <http://www.funakoshi.co.jp/data/datasheet/PCC/46115.pdf>.
25. Lucifer Yellow CH Dilitium salt. <http://www.fluorophores.tugraz.at/substance/30>. Accessed on 12th of February, 2015.
26. Fluorescence Quantum Yield Standards. 1984 http://www.iss.com/resources/reference/data_tables/FL_QuantumYieldStandards.html. Accessed on 5th of June, 2014.
27. Stephan D., Sbai O., Wen J., Couraud P. O., Putterman C., Khrestchatisky M., Desplat-Jégo S. TWEAK/Fn14 pathway modulates properties of a human microvascular endothelial cell model of blood brain barrier. *Journal of Neuroinflammation* 2013;10.
28. Thorne J. B. Controlling the interfacial behaviour of colloidal microgel systems. PhD thesis, University of Greenwich; 2012.
29. Elaissari A. Colloidal Biomolecules, Biomaterials, and Biomedical Applications. Surfactant Science. Lyon - France: CRC Press; 2003.

30. Alarcon C. D., Twaites B., Cunliffe D., Smith J. R., Alexander C. Grafted thermo- and pH responsive co-polymers: Surface-properties and bacterial adsorption. *International Journal of Pharmaceutics*. 2005;295:77-91.
31. Ballatori N., Hager D. N., Nundy S., Miller D. S., Boyer J. L. Carrier-mediated uptake of lucifer yellow in skate and rat hepatocytes: a fluid-phase marker revisited. *Gastrointest Liver Physiol*. 1999;40:G896–G904.
32. Tsuji S., Kawaguchi K. Colored Thin Films Prepared from Hydrogel Microspheres. *Langmuir*. 2005;21:8439-42.
33. Lakowicz J. R. Principles of Fluorescence Spectroscopy. Baltimore - USA: Springer; 2007.
34. Herron J. N., Jiskoot W., Crommelin D. J. Physical methods to characterize pharmaceutical proteins. New York and London: Plenum Press; 1995.
35. Steinberg T. H., Newman A. S., Swanson J. A., Silverstein S. C. Macrophages Possess Probenecid-inhibitible Organic Anion Transporters that Remove Fluorescent Dyes from the Cytoplasmic Matrix. *The Journal of Cell Biology*. 1987;105:2695-702.
36. Pant S., Tripathi H. B. , Pant D. D. Solvent polarity and viscosity effect on the fluorescence spectrum and excited state lifetime of quinine dication. *Journal of Photochemistry and Photobiology A: Chemistry*. 1995;85:33–8.
37. Baruah M., Qin W., Flors C., Hofkens J., Valle R. A., Beljonne D., Van der Auweraer M., Borggraeve W. M., Boens N. Solvent and pH Dependent Fluorescent Properties of a Dimethylaminostyryl Borondipyrromethene Dye in Solution. *J Phys Chem A*. 2006;110:5998-6009.
38. Sun B., Lin Y., Wu P. Structure Analysis of Poly(*N*-isopropylacrylamide) Using Near-Infrared Spectroscopy and Generalized Two-Dimensional Correlation Infrared Spectroscopy. *Applied Spectroscopy*. 2007;61:765-71.
39. Li D., Zhang X., Yao J., Simon G. P., Wang H. Stimuli-Responsive Polymer Hydrogels as a New Class of Draw Agent for Forward Osmosis Desalination. *Chemical Communications*. 2011.
40. Lambert J. B., Shurvell H. F., Lightner D. and Cooks R. G. Introduction to organic spectroscopy. Editor: Verbit L. New York/London: Collier Macmillan publishers; 1987.
41. Zenkl G., Klimant I. Fluorescent acrylamide nanoparticles for boronic acid sugar sensing - from probes to sensors. *Microchim Acta*. 2009;166:123-31.

42. Yin J., Guan X., Wang D., Liu S. Metal-Chelating and Dansyl-Labeled Poly(*N*isopropylacrylamide) Microgels as Fluorescent Cu²⁺ Sensors with Thermo-Enhanced Detection Sensitivity. *Langmuir*. 2009;25:11367–74.
43. Saunders B. R., Crowther H. M., Morris G. E., Mears S. J., Cosgrove T., Vincent B. Factors affecting the swelling of poly(*N*-isopropylacrylamide) microgel particles: fundamental and commercial implications. *Colloids and Surfaces A- Physicochemical and Engineering Aspects*. 1999;149:57-64.
44. Gracia L. H., Snowden M. J. *Handbook of Industrial water soluble polymers*. editor: Williams P.. Blackwell publishing; 2007.
45. Crowther H. M., Saunders B. R., Mears S. J., Cosgrove T., Vincent B., King S. M., Yu G. E. Poly(NIPAM) microgel particle deswelling: a light scattering and small-angle neutron scattering study. *Colloids and Surfaces A: Physicochemical and Engineering Aspects*. 1999;152:327-33.
46. Ali M. M., Aguirre S. D., Yaqin X., Filipe C. D., Pelton R., Li Y. Detection of DNA using bioactive paper strips. *Chemical Communications*. 2009;43:6640-2.
47. Pelton R. H., Chibante P. Preparation of aqueous lattices with *N*isopropylacrylamide. *Colloids and Surfaces*. 1986;20:247-56.
48. Hazot P., Delair T., Pichot C., Chapel J. P., Elaissari A. Poly(*N*-ethylmethacrylamide) thermally-sensitive microgel latexes: Effect of the nature of the crosslinker on the polymerization kinetics and physicochemical properties. *Comptes Rendus Chimie*. 2003;6:1417-24.
49. Oh J. K., Drumright R., Siegwart D. J., Matyjaszewski K. The development of microgels/nanogels for drug delivery applications. *Prog Polym Sci*. 2008;33:448–77.
50. Kurdi M., Chidiac R., Hoemann C., Zouein F., Zgheib C., Booz G. W. Hydrogels as a Platform for Stem Cell Delivery to the Heart. *Wiley Periodicals*. 2010;16:132-5.
51. Bridges A. W., Singh N., Burns K. L., Babensee J. E., Lyon L.A., Garcia A. J. Reduced acute inflammatory responses to microgel conformal coatings. *Biomaterials*. 2008;29:4605–15.
52. Lin S. Y., Chen K. S., Liang R. C. Design and evaluation of drug-loaded wound dressing having thermo responsive, adhesive, absorptive and easy peeling properties. *Biomaterials*. 2001;22:2999-3004.
53. Lin F. H., Tsai J. C., Chen T. M., Chen K. S., Yang J. M., Kang P. L., Wu T. H. Fabrication and evaluation of auto-stripped tri-layer wound dressing for extensive burn injury. *Materials Chemistry and Physics*. 2007;102:152-8.

54. Percell Biolytica. Growth of HeLa Cells. Online report. Åstorp, Sweden. Application Note 116.
55. Percell Biolytica. Growth of Vero and GMK Cells. Online report. Åstorp, Sweden. Application Note 115.
56. Sigma Aldrich (Cook Book Sept 2010 Volume 12 FTiCCLH-nE. Cell Types and Culture Characteristics. 2010; Available from: <http://www.sigmaaldrich.com/technicaldocuments/protocols/biology/cell-types-culture.html>. Accessed on the 11th of June, 2014.
57. Naha P. C., Bhattacharya K., Tenuta T., Dawson K. A., Lynch I., Gracia A, Lyng F. M., Byrne H. J. Intracellular localisation, geno- and cytotoxic response of poly*N*isopropylacrylamide (PNIPAM) nanoparticles to human keratinocyte (HaCaT) and colon cells (SW 480). *Toxicology Letters*. 2010;198:134-43.
58. Naha P., Casey A., Tenuta T., Lynch I., Dawson K. A., Byrne H. J., Davoren M. Preparation, characterization and ecotoxicological evaluation of four environmentally relevant species of *N*-isopropylacrylamide and *N*-isopropylacrylamide-co-*N*-tertbutylacrylamide copolymer nanoparticles. Dublin Institute of Technology, Articles Radiation and Environmental Science Centre. 2009; 92:146-54.
59. Cuggino J. C., Alvarez C. I., Strumia M. C., Welker P., Licha K., Steinhilber D., Mutihac R. C., Calderón M. Thermosensitive nanogels based in dendritic polyglycerol and *N*-isopropylacrylamide. *Soft Matter*. 2011;7:11259-66.
60. Gold M. A Conspiracy of Cells: One woman's Immortal Legacy-And the Medical Scandal It Caused. New York - United States of America: SUNY Press; 1986.
61. Voevodin A. F., Marx P. A. Simian Virology. New Delhi - India: John Wiley & Sons; 2009.
62. Kafil V., Omidi Y. Cytotoxic Impacts of Linear and Branched Polyethylenimine Nanostructures in A431 Cells. *BioImpacts*. 2011;1:23-30.
63. Florea B. I, Meaney C., Junginger H. E., Borchard G. Transfection Efficiency and Toxicity of Polyethylenimine in Differentiated Calu-3 and Nondifferentiated COS-1 Cell Cultures. *AAPS PharmSci*. 2002;4:1-11.
64. Okon E. U., Hammed G., Abu El Wafa P., Abraham O., Case N., Henry E. In-vitro cytotoxicity of Polyethyleneimine on HeLa and Vero Cells. *International Journal of Innovation and Applied Studies*. 2014;5:192-9.
65. Xu Z., Shen G., Xia X., Zhao X., Zhang P., Wu H., Guo Q., Qian Z., Wei Y., Liang S. Comparisons of three polyethyleneimine-derived nanoparticles as a gene therapy delivery system for renal cell carcinoma. *Journal of Translational Medicine*. 2011;9(46).

66. Dahai J. Application of polymers in nucleic acid delivery. PhD thesis, University of Iowa; 2011.
67. Thomas M., Ge Q., Lu J. J., Chen J., Klibanov A. M. Cross-linked Small Polyethylenimines: While Still Nontoxic, Deliver DNA Efficiently to Mammalian Cells in Vitro and in Vivo. *Pharmaceutical Research*. 2005;22:373 - 80.
68. Bauer J. A., Rao W., Smith D. J. Evaluation of linear polyethyleneimine/nitric oxide adduct on wound repair: therapy versus toxicity. *Wound Repair and Regeneration*. 1998;6:569-77.
69. Wang X., Zhou L., Ma Y., Li X., Gu H. Control of Aggregate Size of Polyethyleneimine-Coated Magnetic Nanoparticles for Magnetofection. *Nano Res*. 2009;2:365-72.
70. Sharma A., Tandon A., Tovey J. C., Gupta R., Robertson J. D., Fortune J. A., Klibanov A. M., Cowden J. W., Rieger F. G., Mohan R. R. Polyethyleneimine-conjugated gold nanoparticles: Gene transfer potential and low toxicity in the cornea. *Nanomedicine*. 2011;7:505–13.
71. Lee M. Apoptosis Induced by Polyethyleneimine/DNA Complex in Polymer Mediated Gene Delivery. *Bull Korean Chem Soc*. 2007;28:95-8.
72. Han S. E., Kang H., Shim G. Y., Kim S. J., Choi H. G., Kim J., Hahn S. K., Oh Y. K. Cationic derivatives of biocompatible hyaluronic acids for delivery of siRNA and antisense oligonucleotides. *Journal of Drug Targeting*. 2009;17:123–32.
73. Huang Y. P., Lin I. J., Chen C. C., Hsu Y. C., Chang C. C., Lee M. J. Delivery of small interfering RNAs in human cervical cancer cells by polyethyleneimine-functionalized carbon nanotubes. *Nanoscale Research Letters*. 2013;8:267-78.
74. Inventor: Gordon Trent Hewitt, Upper Montclair, N.J., assignor to ColgatePalmolive Company, New York, NY., Polyethyleneimine Shampoo Compositions. United States of America. 1973.
75. Khanam N., Mikoryak C., Draper R. K., Balkus K. J. Electrospun linear polyethyleneimine scaffolds for cell growth. *Acta Biomaterialia*. 2007;3:1050-59.
76. Wegmann F., Gartlan K. H., Harandi A. M., Brinckmann S. A., Coccia M., Hillson W. R., Kok W. L., Cole S., Ho L. P., Lambe T., Puthia M., Svanborg C., Scherer E. M., Krashias G., Williams A., Blattman J. N., Greenberg P. D., Flavell R., Moghaddam A. E., Sheppard N. C., Sattentau Q. J. Polyethyleneimine is a potent mucosal adjuvant for glycoproteins with innate and adaptive immune activating properties. *Nat Biotechnol*. 2012;30:883–8.
77. Martindale: The Complete Drug Reference London: Sweetman SC

(Ed),Pharmaceutical Press; 1933-2005.

78. U.S. Department of Health and Human Services. Toxicological profile for acrylamide. Atlanta, Georgia: U.S. Department of Health and Human Services - Public Health Service - Agency for Toxic Substances and Disease Registry; 2012.
79. Abu Samah N. H., Heard C. M. The effects of topically applied polyNIPAM-based nanogels and their monomers on skin cyclooxygenase expression, ex vivo. *Nanotoxicology*. 2014;8:100-6.
80. Aslam I., Verma R. K., Roy R., Roy S. P. Synthesis of polymeric nanoparticle “pnipam” poly (*N-isopropylacrylamide*) and their toxicity assay on Swiss albino mice *Mus musculus*. *Indian Journal of Fundamental and Applied Life Sciences*. 2013;3:116-9.
81. Tanii H., Hashimoto K. Studies on in vitro metabolism of acrylamide and related compounds. *Archives of Toxicology* 1981;48:157-66.
82. US Department of health and human services, US Department of Labor. Occupational safety and health guideline for acrylamide: US Department of health and human services - National institute for occupational safety and health - Division of standards development and technology transfer, US Department of Labor - Occupational Safety and health administration.1992.
83. Shipp A., Lawrence G., Gentry R., McDonald T., Bartow H., Bounds J., Macdonald N., Clewell H., Allen B., Landingham C. V. Acrylamide: Review of Toxicity Data and Dose-Response Analyses for Cancer and Noncancer Effects. *Critical Reviews in Toxicology*. 2006;36:481–608.
84. European Society of Clinical Pharmacy. Euroepan Drug Index. Fourth ed. Editors: Muller N., Dessing R. Parallelboulevard - The Netherlands: Amsterdam Medical Press B.V.; 1997.
85. Zomzely-Neurath C. E. Biotechnology Conference: Drug Delivery and Drug Targeting Systems. London: U.S. Office of Naval Research Branch Office, London; 1988. Report No.: 8-007-C.
86. Lynch M. Ultrasound guided central venous catheter placement using Geliperm. *Anaesthesia* 2006;61:505-17.
87. Al-Haydari M. D. Immune Response to Synthesized Pnipam-Based Graft Hydrogels Containing Chitosan and Hyaluronic Acid. MSc. thesis, McMaster University; 2010.

Chapter Five Synthesis, characterization and emulsification properties of poly(*N*-isopropylacrylamide-co-acrylic acid)-hexenol

5.1 Introduction

Emulsions can be defined as “an opaque, heterogeneous system of two immiscible liquid phases, where one of the phases is dispersed in the other as drops of microscopic or colloidal size” (1). A surfactant is a substance which lowers the surface tension of the medium in which it is dissolved and/or the interfacial tension with other phases and accordingly is positively adsorbed at the interface between two phases (2). Colloidal particles are able to act similar to surfactants by being held at liquid-liquid interfaces without aggregating. Emulsions that are stabilized by particles are called “Pickering emulsions”. The surfactant effect of colloidal particles is achieved by one of two mechanisms; first is that the colloidal particles (acting as a surfactant) provide steric hindrance to droplet-droplet coalescence (of the liquid) and the second is that the particles change the rheological properties of the emulsion at the interface (3). In Pickering emulsions, the particles irreversibly adsorb at the oil-water interface. Accordingly, the desorption of these particles requires high energy (much higher than that required for the desorption of conventional emulsifiers). Different studies have investigated the emulsion stabilizing effects of microgel particles (3-9) where some of them were water-in-oil emulsions (9) and others were oil-in-water (8). Using environmentally responsive particles can make it possible to control the stability of Pickering emulsions (6, 10, 11).

Different factors are thought to affect the ability of microgel particles to act as a surfactant. For example, when the particles are more hydrophobic they can spread more into the oil phase and thus lower the interfacial tension between the two phases. Also, the wettability of the particles that enable them to hold the aqueous phase (5, 7) is an important factor. Other factors include the surface charge of the particles and the interaction between them (5).

The advantages of Pickering emulsions over conventional ones include their ability to reduce tissue irritation and that their viscosity can be easily changed by changing the nature and content of the solid material (6) as well as the environmental conditions around them (12). In their review about microgel particles at the liquid-liquid interface, Li *et al.*

(5) suggested that microgel stabilized systems are more stable than surfactant stabilized ones. On the other hand, some challenges still face the use of microgel particles as emulsion stabilizers (5). These include the synthetic approach where most of the particles prepared by

precipitation polymerization are inhomogeneous. This affects the physical properties of the particles such as the particle surface charge, elasticity and swelling which highly affects the behaviour of the particle at the interface. Also, the protrusion of the particles in the oil phase is limited and the mechanism of adsorption of the microgel particles and their molecular arrangement at the oil-water interface is poorly understood.

The novel particles synthesized in this work address the challenges pointed out by Ngai *et al.* (5) who suggest that the synthetic approach to microgels has a big influence on their physical properties. Microgels prepared using precipitation polymerization are often characterized by inhomogeneous spatial distribution of the different functional groups used during synthesis. This causes a lack of control of the behaviour of the particles in terms of the swelling time, charge distribution and particle elasticity (5). The synthetic approach used in this work (surfactant free emulsion polymerization (SFEP) technique followed by carbodiimide coupling) yielded mono-dispersed particles as proven by the DLS and SEM data (Figures 5.2 and 5.7 respectively). The advantages of SFEP are its high product yield (around 95%) of monodispersed particles and the regularity in both size and composition of the resultant particles. This is achieved without the need to use surfactants which are not easily removed after the synthesis.

The NIPAM monomer has a hydrophobic group (*isopropyl*) and a hydrophilic one (*amide*). During the microgel synthesis, the monomer molecules are arranged so that the hydrophobic groups are at the centre and the hydrophilic ones are at the periphery. Accordingly, p(NIPAM) particles are characterized by having a hydrophobic core and a hydrophilic shell (13). Increasing the number of hydrophobic groups used in a microgel would allow the particles to penetrate more in the hydrophobic phase while increasing the number of hydrophilic groups would allow the particles to penetrate into the aqueous one. This is supposed to play an important role in lowering the interfacial tension between the two phases and thus allow them to act as an emulsifying agent. In this work, hexenol which has a hydrophobic hydrocarbon chain, is attached to p(NIPAM-co-5% acrylic acid).

This approach suggests an improvement in the second challenge mentioned by Ngai *et al.* (5) who claim that the microgel particles appear to be flattened at the interface and protruded only a little into the oil phase. Moreover, the presence of a pendant vinyl group at the end of the hexenol chain makes it possible to further polymerize the particles to form

bigger structures referred to in this work as “microgellosomes”. These are new structures that are suggested to act as emulsifying agents as well as delivery vehicles.

5.2 Materials and methods:

5.2.1 Materials

For the particle synthesis: *N*-isopropylacrylamide (NIPAM) 97% (Aldrich), *N,N*'methylenebisacrylamide 99% (Aldrich), potassium persulphate 98% (BDH Laboratory Suppliers), 5-hexen-1-ol (Aldrich), *N*-(3-dimethylaminopropyl)-*N*'-ethylcarbodiimide hydrochloride (EDC) and *N*-hydroxysuccinimide (NHS) were obtained from commercial suppliers and used without further purification. For the emulsification: glyceryl trioctanoate (tricaprylin), hexadecane and rhodamine 6G were all purchased from SigmaAldrich, UK. A solution of rhodamine 6G was prepared by dissolving the dye at a concentration of 1×10^{-3} mol/L in an ultra-pure Milli-Q water.

5.2.2 Methods

5.2.2.1 Synthesis of p(NIPAM-co-5% AA)-hexenol

Step 1: Synthesis of p(NIPAM-co-5% AA) (w/v)

In a 1 L reaction vessel, 0.5 g of potassium persulphate was dissolved in 800 mL of distilled water. A three-necked lid was clamped to the reaction vessel, which was then heated to 70°C with continuous stirring. 4.75 g NIPAM, 0.25 g acrylic acid (AA) and 0.5 g *N,N*'-methylenebisacrylamide were stirred in distilled water (200 ml) and transferred into the reaction vessel containing the initiator (potassium persulphate) and continuously stirred at 70°C for six hours under an inert atmosphere of nitrogen. When the reaction was complete, the microgel dispersion was allowed to cool to room temperature. The microgel was dialyzed in fresh de-ionized water for a week (changed daily), centrifuged to decrease the water content then freeze dried.

Step 2: Esterification of p(NIPAM-co-5% AA) with 5-hexen-1-ol

The carboxylic acid of AA is coupled with the hydroxyl of 5-hexen-1-ol using *N*-(3dimethylaminopropyl)-*N*'-ethylcarbodiimide hydrochloride (EDC) and

N-hydroxysuccinimide. In beaker A, 0.4 g of p(NIPAM-co-5% AA) were dissolved in preprepared 100 mL of MES buffer prepared from 0.1 M 2-(*N*-Morpholino) ethanesulfonic acid hydrate, 4-morpholineethanesulfonic acid (MES) adjusted at pH 5.5. In beaker B, 0.005 g of 5-hexen-1-ol were dissolved in *isopropanol*. The contents of beaker B were added to beaker A, then 0.4 g of *N*-hydroxysulfosuccinimide sodium salt (NHS) and 0.4 g of *N*-(3-dimethylaminopropyl)-*N'*-ethylcarbodiimide hydrochloride (EDC) were added and were all left stirring overnight at 300 rpm then dialysed for a week in fresh de-ionized water which was changed daily.

5.2.2.2 Dynamic light scattering

Dynamic light scattering (DLS) measurements were carried out for p(NIPAM-co-5% AA)hex using a Malvern Zetasizer Nano ZS. In addition, the pH of different samples was adjusted to different pH values using HCl and NaOH to test for the effect of changing pH upon the size and electrophoretic mobility of the particles.

The hydrodynamic diameter of the particles was measured in response to temperature change from 15 to 60°C). Samples were diluted with deionized water (1 mL of dialysed microgel dispersion was diluted with 2 mL of water) before measurements. A quartz cuvette with two polished windows (Starna Type 1) was used for all the measurements and the temperature of the dispersion was controlled by a Peltier thermocouple. Data were collected every 1°C and the samples were equilibrated for 2 minutes before each data collection point. Three measurements, each consisting of 13 subruns, were taken at each temperature to obtain an average and standard deviation of the hydrodynamic diameter. The data presented are the average of the three measurements and the error bars are the standard deviation data.

Samples (p(NIPAM-co-5% AA)-hexenol) were diluted with sodium chloride (NaCl) solutions (1 mL of dialysed particle dispersion was diluted with 2 mL of NaCl solution) to reach a concentration of 1×10^{-4} M NaCl before measurements. The electrophoretic mobility of p(NIPAM-co-5% AA)-hexenol was then measured in response to temperature change across the range of 15-60°C using a disposable folded capillary cell.

5.2.2.3 Infrared spectroscopy

A Shimadzu Fourier transform infrared (FT-IR) spectrophotometer with a KBr beam splitter and diamond attenuated total reflection (ATR) crystal was used to carry out the IR experiment in this work. Sixty-four scans for each sample were carried out. Microgel

dispersions were dialysed and freeze-dried then the solid samples were used for IR experiments. To record the spectrum of hexenol, liquid hexenol was used as purchased from the commercial supplier (Sigma Aldrich) without any further modification.

5.2.2.4 Scanning electron microscopy

A Hitachi SU8030 cold cathode filled emission gun scanning electron microscope was used to obtain micrographs of p(NIPAM-*co*-5% AA)-hex particles. The accelerating voltage used was 30 kV, the magnification was $\times 25000$ and $\times 35000$ and the working distance was 8.4 mm.

5.2.2.5 Emulsification

The emulsions were prepared by mixing glyceryl trioctanoate (tricaprylin) with (0-0.3 wt %) p(NIPAM-*co*-5% AA)-hexenol suspended in ultra-pure Milli-Q water. The pH was adjusted to 1.8 using HCl then all the components were mixed using an Ultra Turrax T25 basic dispersing instrument at 16000 rpm for 5 minutes. The above procedure was repeated using hexadecane as an oil phase at concentrations from 0-0.45 wt%.

5.2.2.6 Synthesis of microgelsomes

Emulsions were prepared by mixing hexadecane with p(NIPAM-*co*-5% AA)-hexenol (4% v/v and 8.6% v/v, respectively in relation to the final emulsion volume) in Milli-Q water. The pH was adjusted to 1.8 using HCl and then mixed using an Ultra Turrax T25 basic at 16000 rpm for 5 minutes at 55-60°C. An initiator (potassium persulphate) with concentration of 2.5 % w/v (in respect to the total emulsion volume) was dissolved in the water phase before the homogenization.

The emulsion was then transferred to a 3-necked round-bottom flask equipped with a magnetic stirrer and a condenser, and was kept under nitrogen gas atmosphere for at least 15 minutes. The flask was then immersed in hot oil bath to maintain the temperature at 75°C and the reaction was continued for 6 hours.

5.2.2.7 Optical microscopy

The mixtures before and after the emulsification reaction were observed using an optical microscope (Olympus DP70).

5.2.2.8 Fluorescence microscopy

The bright field and fluorescence images of the emulsions were captured using a BX-51 fluorescence microscope equipped with a DP70 digital camera. The different objectives used were 4x, 20x and 50x. The Hg-arc lamp, housed in a U-RFL-T power supply was used as an excitation light source for fluorescence microscopy. All filters and equipment above were manufactured by Olympus, Japan. Fluorescein diacetate treated samples required a MWIBA2 filter set ($\lambda_{\text{excitation}} = 460\text{-}490$ nm, $\lambda_{\text{emission}} = 510\text{-}550$ nm). Image analysis software package Image Pro Plus 6 was used to capture and process the microscope images from the DP70 digital camera.

5.2.2.9 Scanning electron microscopy

After emulsification, the reaction mixture was centrifuged at 1400 rpm for 15 minutes in an Eppendorf mini spin plus in acetone to get rid of the oil in the samples. The aliquot was air dried, crushed using a spatula and observed under a Hitachi TM 3000 bench top scanning electron microscope operating in transmission mode with an accelerating voltage of 30 kV. The samples were fixed on aluminium SEM stubs 15 mm x 6 mm mounted with carbon tabs 12 mm diameter all purchased from Agar Scientific, UK.

5.3. Results and discussion

The suggested structure of p(NIPAM-co-5% AA)-hexenol particles is shown in Figure 5.1. The novel particles are expected to maintain the matrix structure of p(NIPAM). Several charged groups affect the surface charge on the particle, these are; the SO_4^- arising from the initiator used during the synthesis of p(NIPAM-co-5% AA) and the unreacted carboxylic acid groups of acrylic acid. The figure also shows the expected presence of long hairy structures formed by the esterification of the carboxylic acid (arising from acrylic acid) with the hydroxyl group of 5-hexen-1-ol. These end with a vinyl group that will be further used to polymerize particles together.

The use of 1-ethyl-3-(3-dimethyl aminopropyl) carbodiimide (EDC) as a coupling agent between the carboxylic acid groups and amines to form amide groups (14, 15) or alcohols to form corresponding esters (16-18) has been previously reported. This is due to its ability to activate COOH groups which allow reactions involving nucleophilic attacks (19). It is sometimes used in combination of *N*-hydroxysuccinimide (NHS) which helps activating the COOH groups leading to

more efficient cross-linking reactions (19). One of the advantages of using this technique is that the unreacted starting materials are water soluble and can be easily removed after the reaction (19).

Using EDC/NHS coupling methods made it possible to design particles with different attached side chains with specific properties. Wu *et al.* have used EDC to catalyse the coupling of the carboxylic acid of acrylic acid units in p(NIPAM-co-AA) particles to 2-aminomethyl-5-fluorophenylboronic acid (FPBA) which is a glucose recognition moiety to yield a microgel capable of sensing the glucose concentration in blood and releasing insulin accordingly (20). Other studies have used EDC catalysis to couple carboxylic acid containing microgels with antibodies and DNA (21), graphene (22), 3-aminophenylboronic acid (APBA) (23), amine functionalized poly ethylene glycols (24), adipic acid dihydrozide (15).

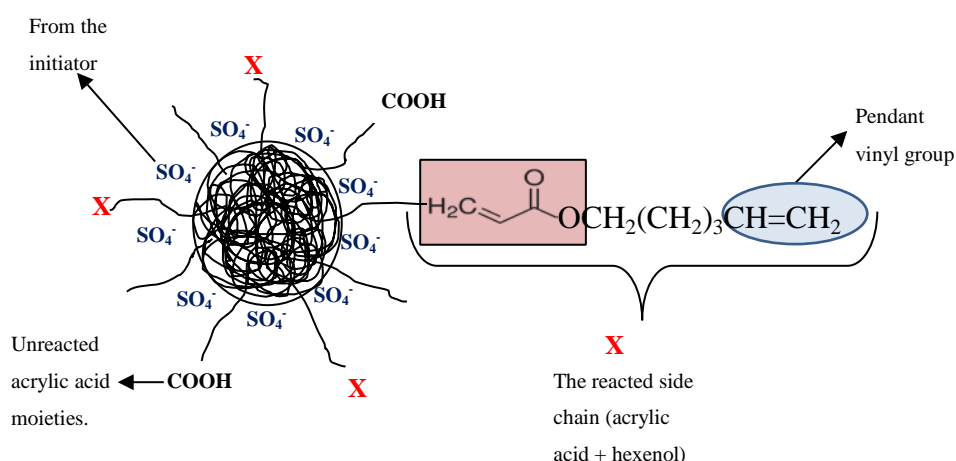


Figure 5.1 The suggested structure of p(NIPAM-co-5% AA)-hexenol

5.3.1 Characterization of p(NIPAM-co-5% AA)-hexenol particle

5.3.1.1 Particle size

5.3.1.1.1 Effect of temperature

Figure 5.2 shows that the initial hydrodynamic diameter of p(NIPAM-co-5% AA)-hexenol is approximately 680 nm. This size is larger than that of p(NIPAM-co-5% AA) (550 nm) (12) due to the incorporation of a hydrophilic group (carboxylic acid group from acrylic acid). Also, the attachment of hexenol to the AA extends the hairy layer of the particle (Figure 5.1) and accordingly, the particle size. When the temperature exceeds the VPTT (35°C), the particles deswell and at 45°C, the size is approximately 280 nm. This confirms that the particles still show temperature responsiveness even after the attachment of the side chain.

The change in particle size is reversible; when the heated sample is cooled, the particle swells again (data not shown) and the particle size at 15°C is comparable to the initial value (before heating).

The uniformity of the particles can be determined using the Poly Dispersity Index (PdI). This is a dimensionless parameter that represents the size distribution at every measurement. PdI is scaled such that values close to zero are thought to be highly monodispersed. Meanwhile, values greater than 0.7 indicate that the sample has a very broad size distribution and is probably not suitable for the dynamic light scattering (DLS) technique. The PdI of all the measurements of p(NIPAM-co-5% AA)-hexenol is 0.05-0.2 (across the temperature range studied) which suggests a mono-dispersed particle size distribution.

5.3.1.1.2 Effect of pH

The presence of unreacted carboxylic acid groups in the structure of p(NIPAM-co-5% AA)-hexenol suggests that it is pH sensitive. When the pH is below the pK_a of AA (4.7) (12), the COOH groups of AA are protonated and accordingly neutral (does not add surface charge to the particle). When the pH exceeds the pK_a of AA, the COOH groups are deprotonated into COO^- which increases the repulsion forces between the negatively charged groups on the particle leading to a larger particle size (Figure 5.3). Accordingly, Figure 5.3 shows that the major change in the particle size takes place around pH 5. This behaviour compares to that of p(NIPAM-co-5% AA) (33).

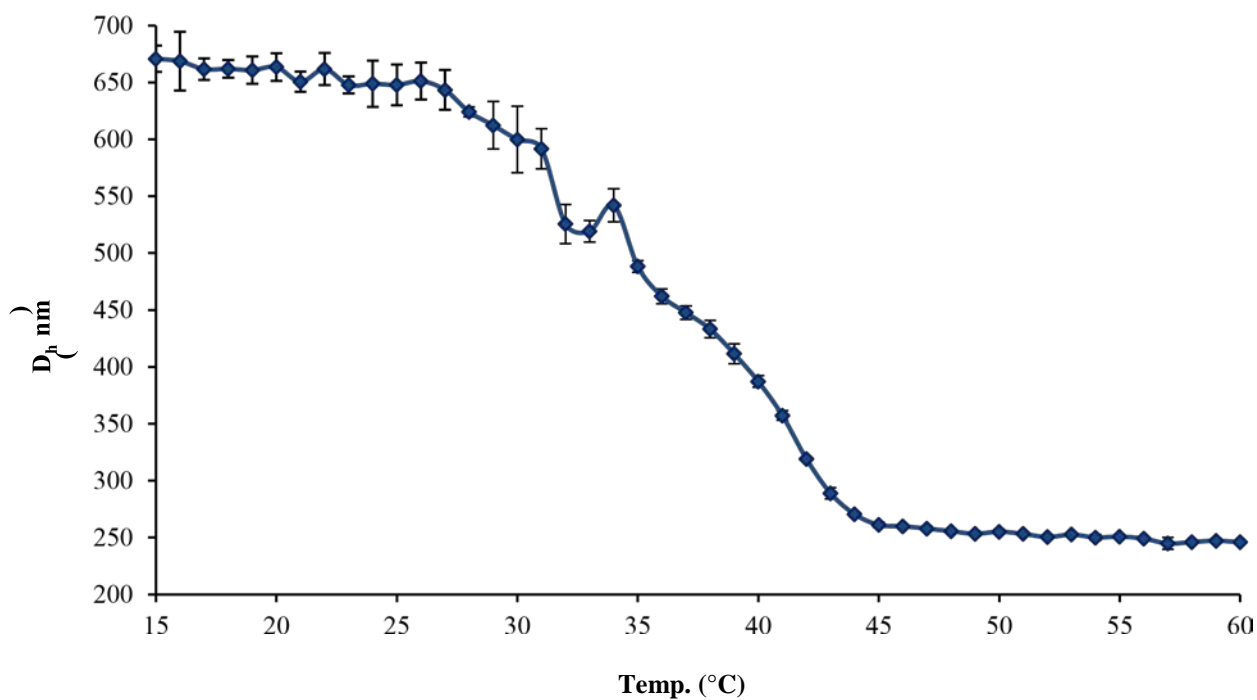


Figure 5.2 The hydrodynamic diameter of p(NIPAM-co-5% AA)-hexenol at pH 7 in response to increasing the temperature (15-60°C)

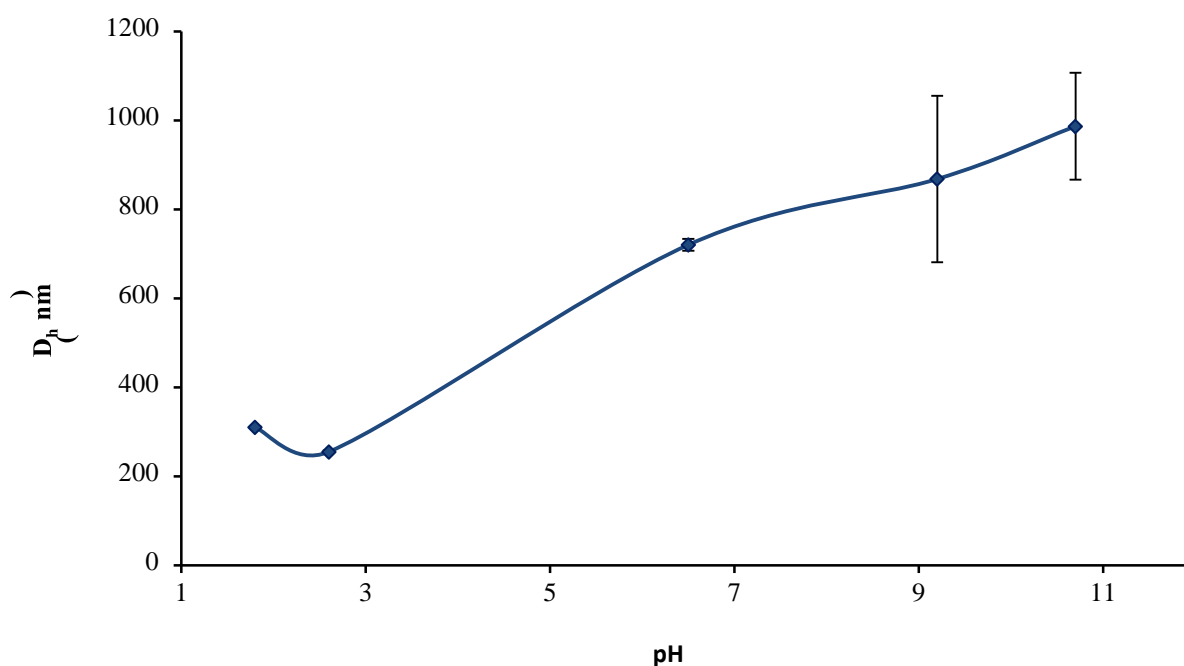


Figure 5.3 The hydrodynamic diameter of p(NIPAM-co-5% AA)-hexenol at 25°C in response to pH change

5.3.1.2 Electrophoretic mobility

5.3.1.2.1 Effect of temperature

The negative charges on the surface of the novel particles originate from the unreacted carboxylic groups (from the AA) that are ionized into COO^- and also because of the SO_4^-

from the initiator. Figure 5.4 shows that the initial electrophoretic mobility of p(NIPAM-co-5% AA)-hexenol at 15°C is $-1.78 \mu\text{mcm/Vs}$. Increasing the temperature causes the particle to deswell and hence increase the surface charge density and the electrophoretic mobility. The electrophoretic mobility goes down to $-2.8 \mu\text{mcm/Vs}$ at 45°C. Cooling the heated dispersion to 15°C, the electrophoretic mobility increases to $-1.68 \mu\text{mcm/Vs}$ (comparable to the initial value). This shows that the effect of temperature on the mobility is reversible.

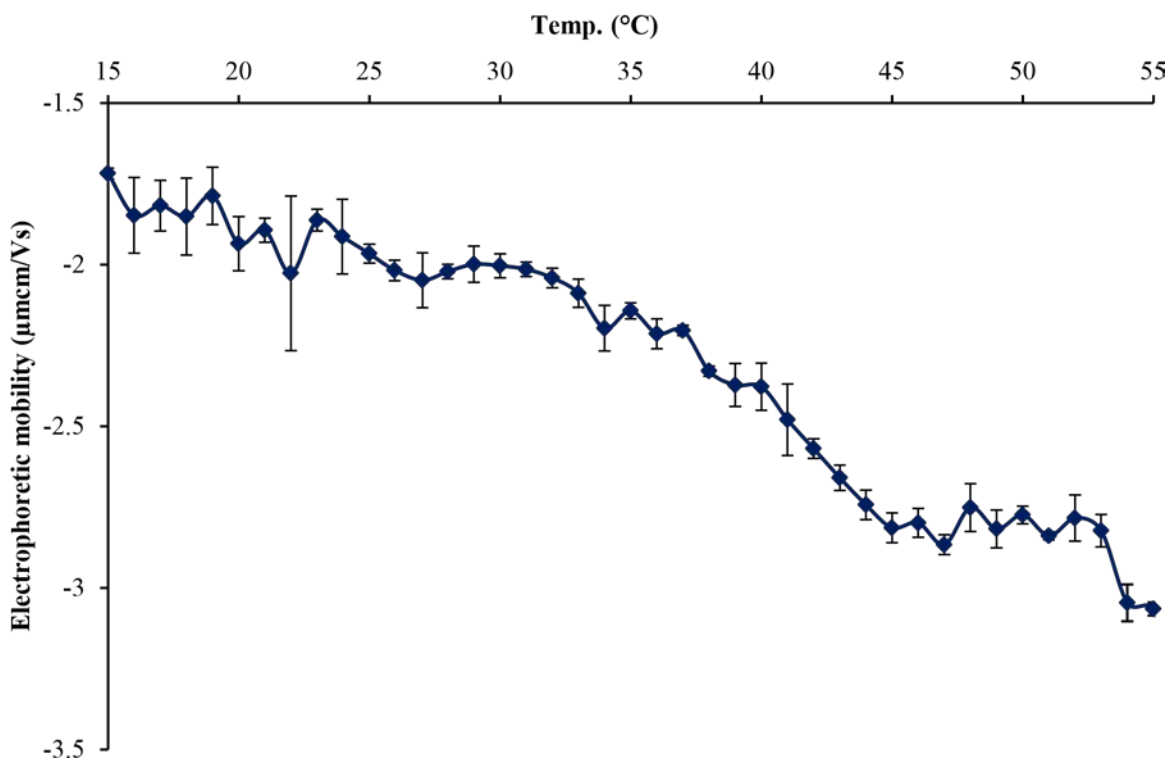


Figure 5.4 The electrophoretic mobility of p(NIPAM-co-5% AA)-hexenol in response to temperature change (15-55°C) at pH 7

5.3.1.2.2 Effect of pH

The effect of changing pH on the electrophoretic mobility of p(NIPAM-co-5% AA)-hexenol particles is shown in Figure 5.5. As previously explained, increasing the pH above the pK_a of acrylic acid (4.7) causes the COOH groups to deprotonate into COO^- and thus highly increasing the particle surface charge and its electrophoretic mobility. The data in Figure 5.5

compare to the size ones in Figure 5.3. The major change in the electrophoretic mobility is seen around pH 5 which is close to the pK_a of AA.

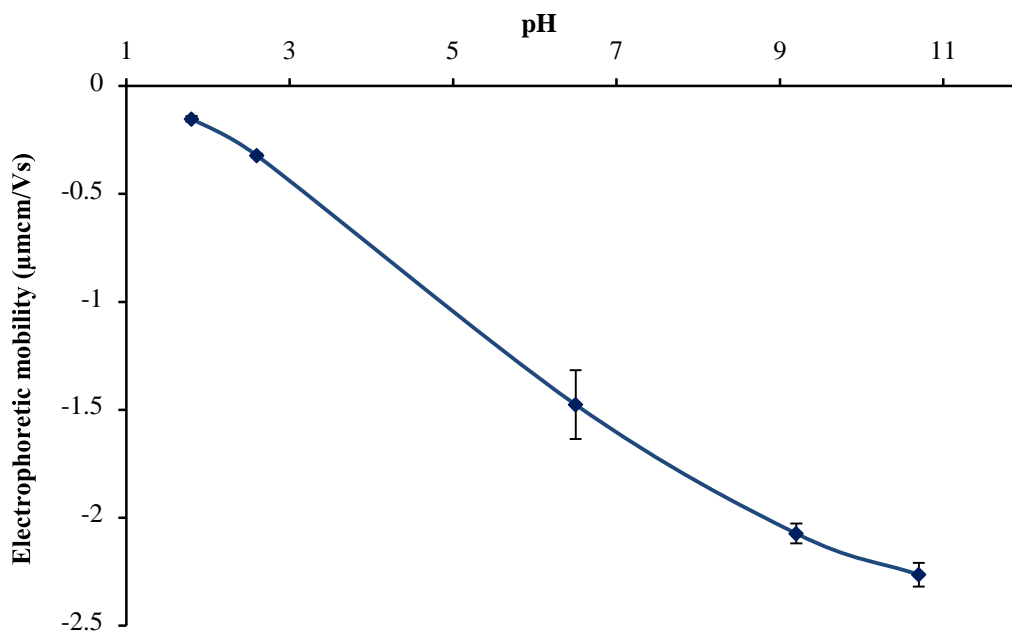


Figure 5.5 The electrophoretic mobility of p(NIPAM-co-5% AA)-hexenol at 25°C in response to pH change

5.3.1.3 Infrared spectroscopy

Tables 5.1 and 5.2 as well as Figure 5.6 show the FT-IR spectra of p(NIPAM-co-5% AA), p(NIPAM-co-5% AA)-hexenol and 5-hexen-1-ol respectively. The spectra of p(NIPAM-co-5% AA) compares well with the literature (25-28) and so does hexenol (29). The spectrum of p(NIPAM-co-5% AA)-hexenol show similarity to that of p(NIPAM-co-5% AA) (Table 5.1 and Figure 5.6). Areas that show shifts in the band or new bands are coloured in grey (Figure 5.6). These are the areas between 1200 cm^{-1} and 1100 cm^{-1} and is between 630 cm^{-1} and 450 cm^{-1} . The spectrum of p(NIPAM-co-5% AA)-hexenol shows an extra band that is not shown in p(NIPAM-co-5% AA), this is at 1200 cm^{-1} (Table 5.1 and Figure 5.6). This band is thought to signify an ester linkage (30) referring to the esterification of the COOH of acrylic acid and the OH of hexenol. This suggests the attachment of the hexenol to the particle.

Table 5.1 FT-IR bands of p(NIPAM-co-5% AA) and p(NIPAM-co-5% AA) hexenol

Peak number	Wavenumber (cm ⁻¹) (p(NIPAM-co-5% AA))	Wavenumber (cm ⁻¹) (p(NIPAM-co-5% AA)-hex)	Assignment	References
1	3271	3263	N-H stretch	(25, 28, 30)
2	2960	2954	-CH ₃ asymmetric and symmetric stretch	(25, 30)
3	2908	2899		
4	1622	1625	C=O stretch (amide I bond)	(25-28, 30)
5	1525	1537	N-H deformation (amide II bond)	(27, 28, 30)
6	1448	1454	-CH ₃ asymmetric deformation	(30)
7	1375	1375	-CH ₂ symmetric deformation	(28, 30)
8	1363	1361		
9	-	1200	C-O-C anti-sym stretch (ester)	(30)
10	1163	-	C-C-N bending in amines	(25)
11	-	1145	C-O-C anti-sym stretch (ester)	(30)
12	-	623	O-C-O bending in esters	(30)
13	-	615		
14	-	545	=CH ₂ in vinyl compounds	(30)

Table 5.2 FT-IR bands of 5-hexen-1-ol

	Wavenumber (cm)	Assignment (30)
1	3305	OH stretch in alcohols
2	3070	=CH stretch in aromatic and unsaturated hydrocarbons

3	2926	CH ₃ and CH ₂ (sym and asym stretch) in aliphatic compounds
4	2856	
5	1639	C=C stretch in alkenes
6	1452	C-OH in-plane bend
7	1433	
8	1411	
9	1249	
10	1055	CH ₂ - O-H stretch in primary alcohols (C-O)
11	1031	
12	991	CH=CH ₂ out of plane wag in vinyl compounds
13	906	
14	817	CH=CH ₂ out of plane wag
15	729	(CH ₂) _n rocking in hydrocarbons
16	628	C-OH bending in alcohols
17	549	CH=CH ₂ twisting in vinyl compounds

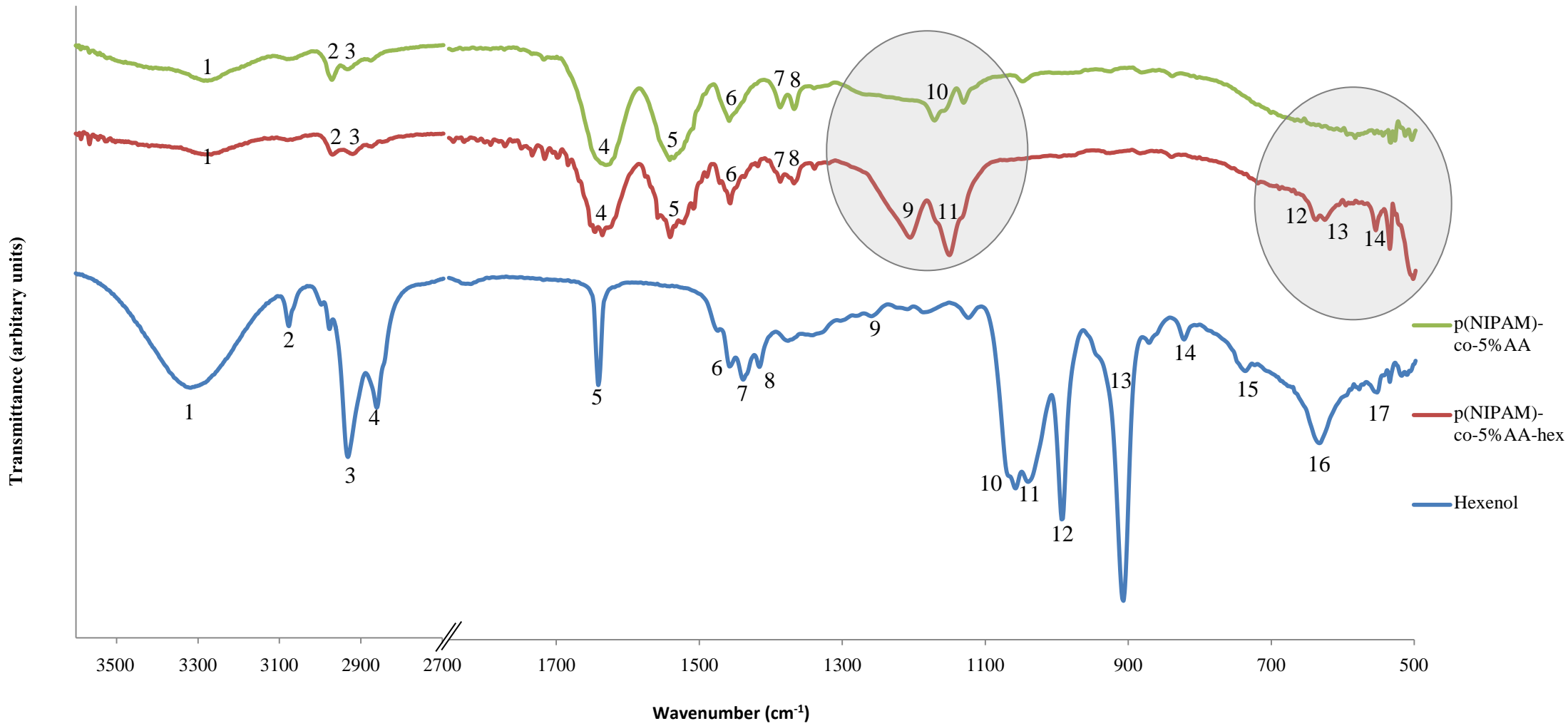


Figure 5.6 The FT-IR spectra of **p(NIPAM-co-5% AA)-hexenol** and **p(NIPAM-co-5% AA)** and **5-hexen-1-ol**

5.3.1.4 Scanning electron microscopy

Figure 5.7 show the SEM pictures of p(NIPAM-co-5% AA)-hexenol. The Figures show that the particles are spherical in shape and monodispersed. The particle size shown in Figure 5.7 b compares to that shown by the DLS results (Figure 5.2).

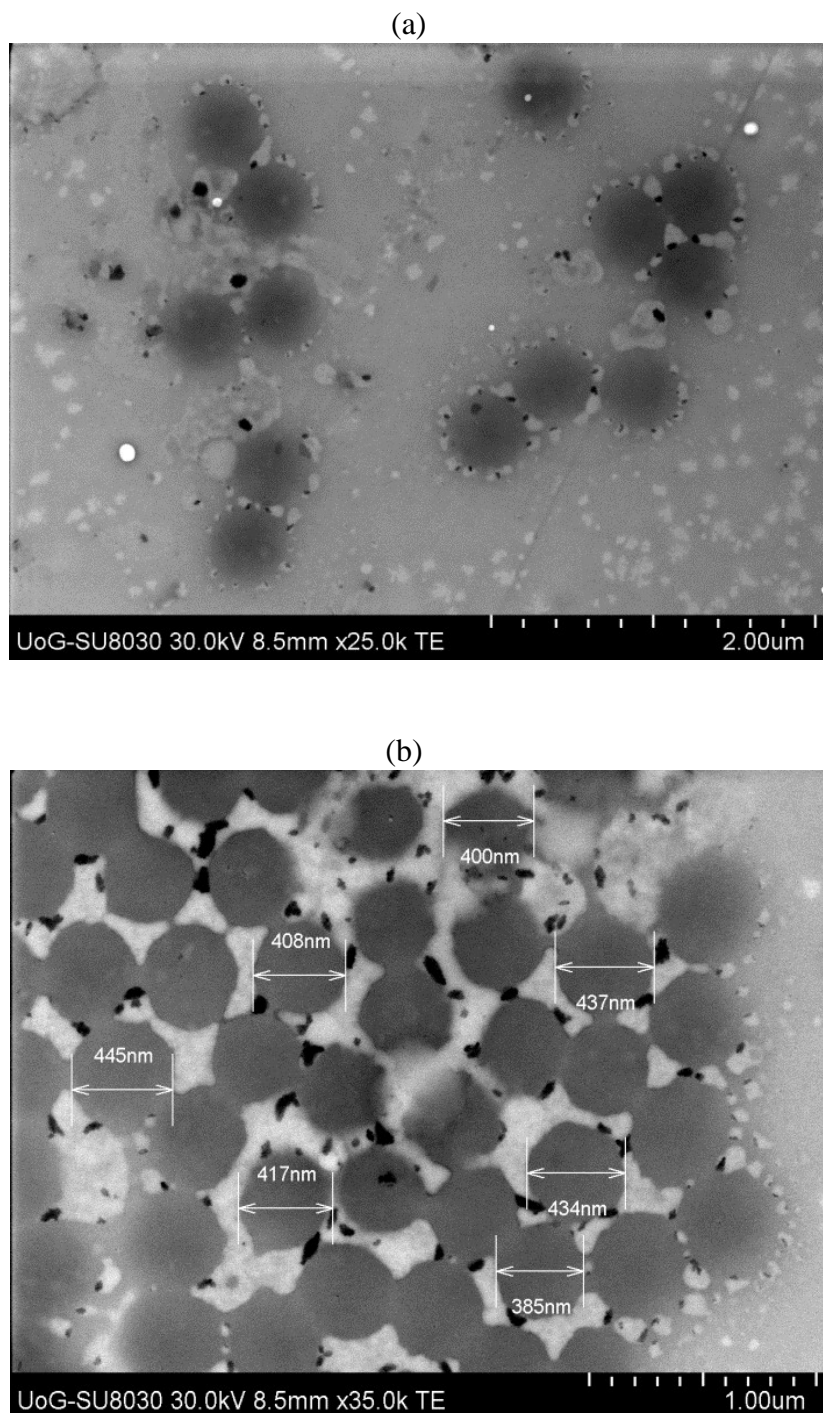


Figure 5.7 SEM pictures of p(NIPAM-co-5% AA)-hexenol at 25°C with a magnification of (a) x25,000 and (b) x35,000

5.3.2 Characterization of the emulsion stabilized by p(NIPAM-co-5% AA)-hexenol particles

The effect of microgel particles as an emulsifying agent was tested using two oils (tricaprylin and hexadecane). These oils were chosen because their density was close to that of water where the density of water, tricaprylin and hexadecane are 0.99 g/mL, 0.95 g/mL and 0.77 g/mL, respectively (31, 32). In both cases (using the two different oils), the use of the microgel with a suitable concentration showed a significant effect on the emulsion stabilization (Figures 5.8 and 5.9). Furthermore, the effect was shown to be consistent for a week (Figures 5.8 and 5.9). At low microgel concentrations, it is clear that there are two different phases (oily and aqueous) and an opaque top layer was observed due to the creaming of the droplets. Increasing the microgel concentration caused a significant decrease in the rate of creaming (Figures 5.8 and 5.9). Also, the number of emulsion droplets increased with the increase in microgel concentration (as shown in Figures 5.10 and 5.11) hence it can be concluded that the microgel was successfully adsorbed at the oil water interface and caused the emulsion to be more stable.

The comparison between Figures 5.8 and 5.9 show that there is a difference in the emulsifying properties of the particles for tricaprylin-in-water (Figure 5.8) and hexadecane-in-water (Figure 5.9) emulsions. In the case of tricaprylin-in-water (Figure 5.8) emulsions, a concentration of 0.3% (w/v) completely emulsifies the two phases. For the hexadecane-in-water emulsion (Figure 5.9), the same concentration (0.3% w/v) shows two distinct layers of liquid. Increasing the concentration of the particles to 0.45% (w/v) shows a more homogenous phase than that at particle concentrations below 0.45% w/v. The difference in the emulsification effect of the particles in the two different emulsions (at particle concentrations of 0.3% w/v) can be attributed to the difference in the physical and chemical properties of the two oils (tricaprylin and hexadecane). The difference in the densities of both oils is an important factor. The density of tricaprylin (0.95 g/mL) is close to that of water (0.99 g/mL) while hexadecane shows a lower density (0.77 g/mL) (31, 32).

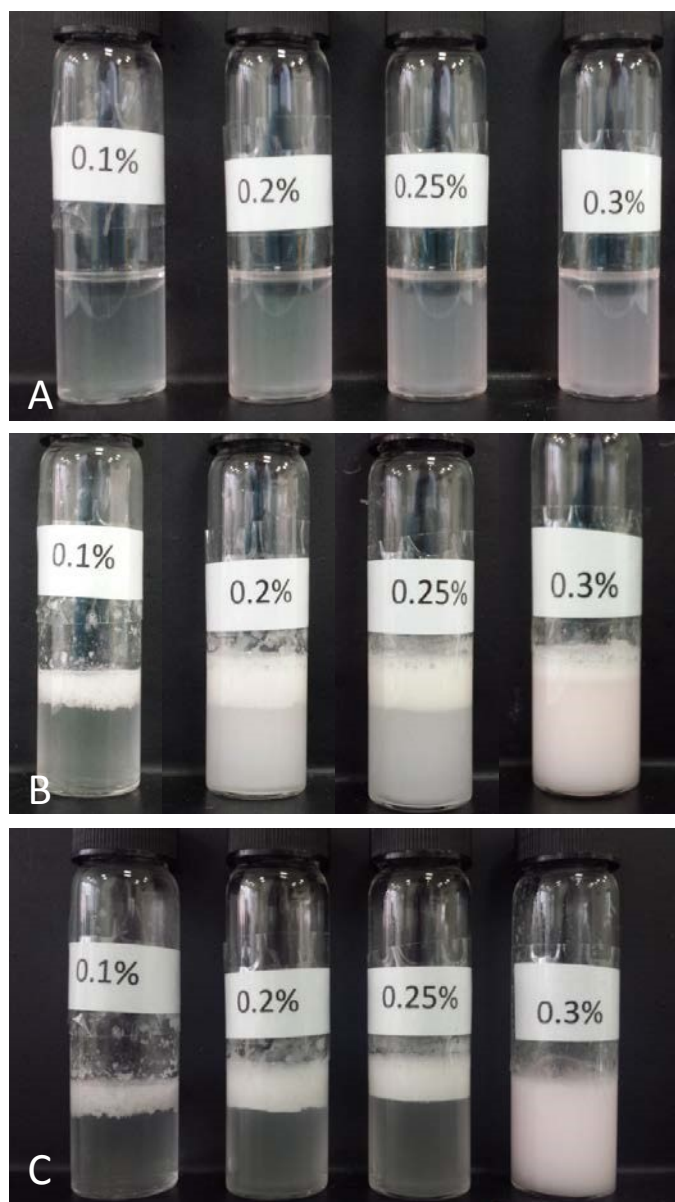


Figure 5.8 Emulsions of tricaprylin/water mixtures in the presence of different concentrations of p(NIPAM-co-5% AA)-hexenol (a) Different concentrations (w/v) of microgel dispersions before emulsification (b) Samples just after emulsification (c) Samples after 1 week of emulsification

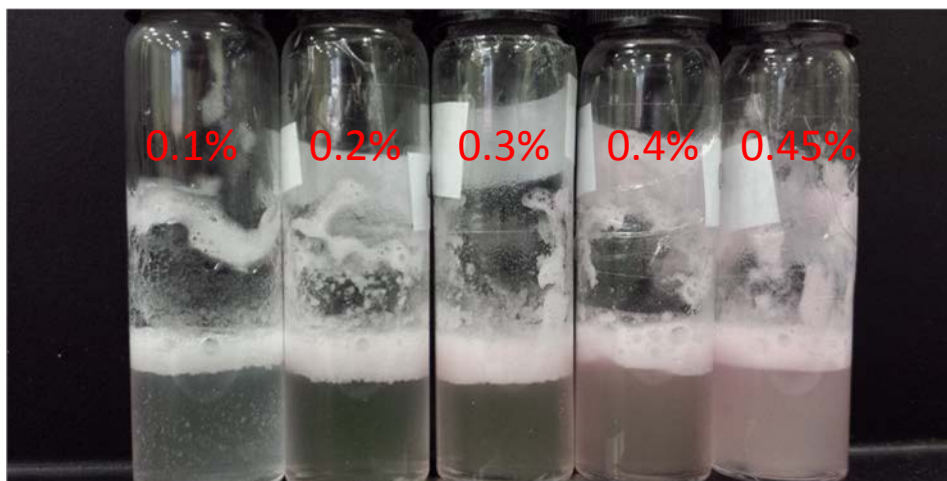


Figure 5.9 Emulsions of hexadecane/water mixtures in the presence of different concentrations of p(NIPAM-co-5% AA)-hexenol, samples after emulsification

Also, the molecular structures of the two oils may be an important factor. The molecular structure of tricaprylin has three ester groups (six oxygen atoms) and a branched hydrocarbon chain. This suggests an increase in the ability of the oil to protrude in the aqueous phase. In the case of hexadecane, the molecular structure only consists of a hydrocarbon chain which suggests less protrusion in the aqueous phase than tricaprylin.

The microscopy images of both tricaprylin-in-water and hexadecane-in-water emulsions (Figures 5.10 and 5.11, respectively) show some differences between the two emulsions. At the same particle concentration, the tricaprylin-in-water emulsion (Figure 5.10) has more droplets than the hexadecane-in-water and of smaller size. This difference in behaviour is attributed to the difference of the densities of the two oils in comparison to water.

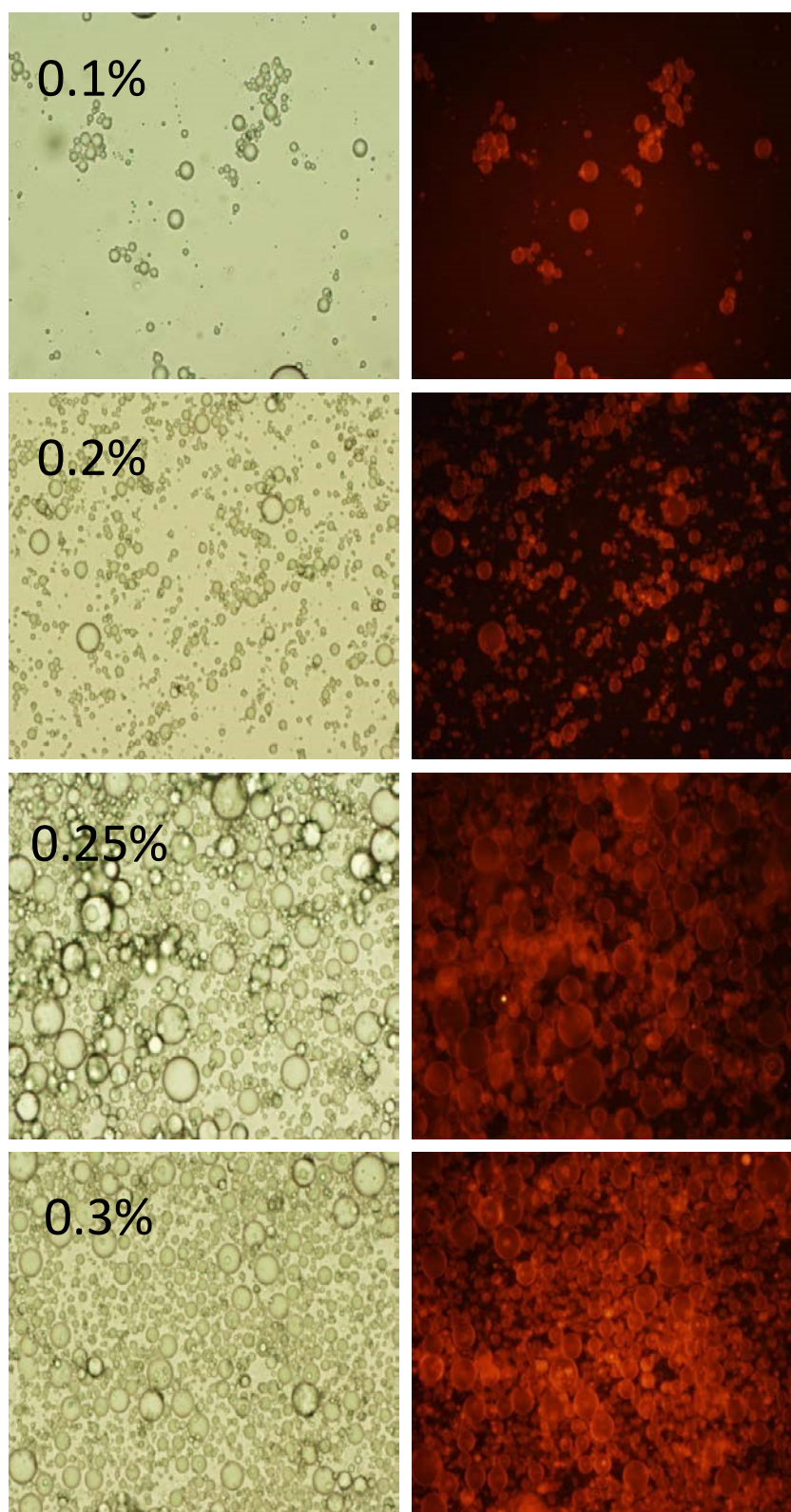


Figure 5.10 Optical (left) and fluorescent (right) microscopy images of tricaprylin/water emulsion in presence of 0.1, 0.2, 0.25 and 0.3% w/v of p(NIPAM -co-5% AA)-hexenol. All scale bars are 100 μm in size

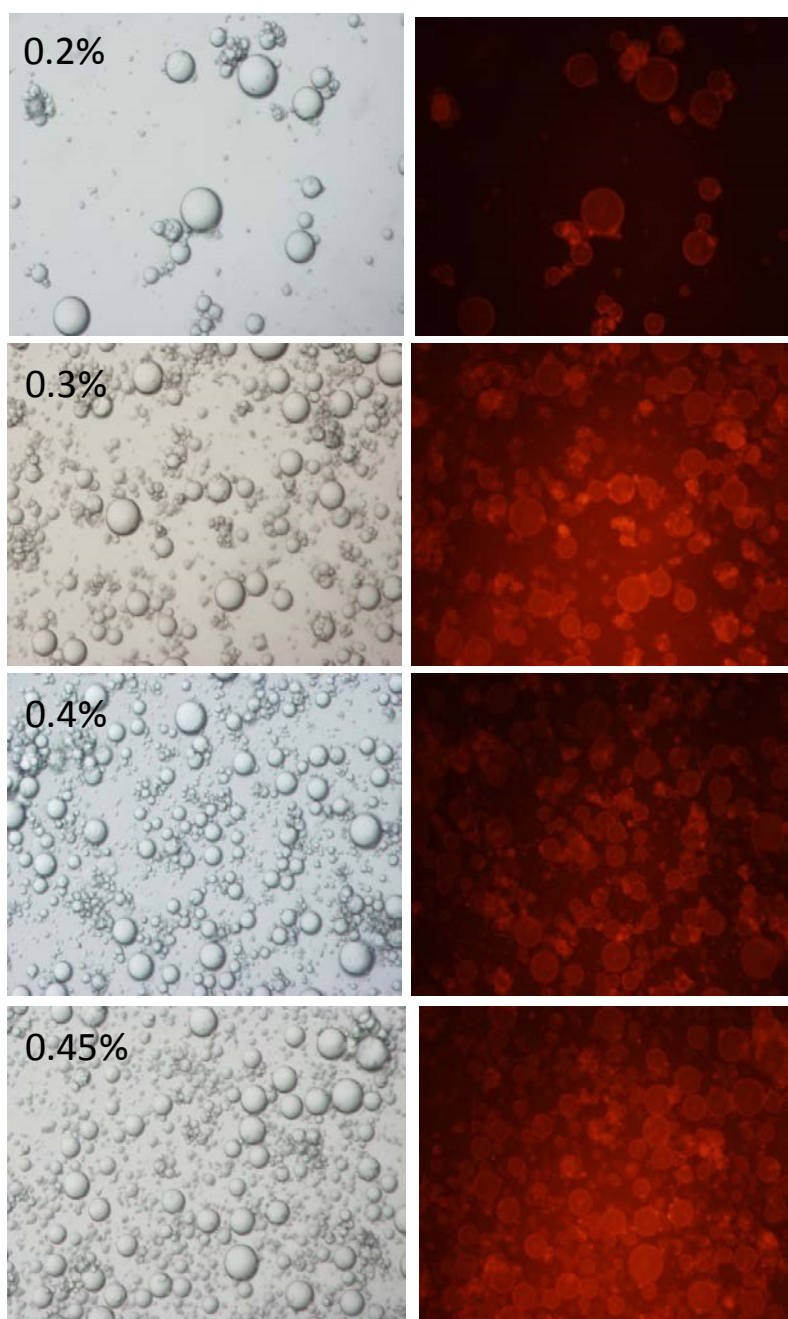


Figure 5.11 Optical (left) and fluorescent (right) microscopy images of hexadecane/water emulsion in sizepresence of 0.2, 0.3, 0.4 and 0.45% w/v of p(NIPAM -co-5% AA)-hexenol. All scale bars are 100 μm in

5.3.3 Microgelloosomes

The presence of a pendant vinyl group at the side chain of p(NIPAM-co-5% AA)-hexenol particles made it possible to further crosslink the particles to form bigger structures referred

to as microgellosomes. Figure 5.12 shows a representation of the suggested molecular structure of microgellosomes. The size and morphology of the particles are important factors that affect the stabilization of Pickering emulsions (33). Microgellosomes can be synthesized in situ at the interface of oil and water and thus entrap the oil droplets inside its hollow matrix and stabilize the emulsion. Since the building blocks of these microstructures are p(NIPAM-*co*-5% AA)-hexenol particles, it is thought that the emulsions stabilized by microgellosomes can be switched on/off by changing the environmental conditions such as temperature and pH of the emulsion. These microstructures can be used in surfactant-free formulations in cosmetics and personal care products. Other possible uses can include drug delivery and industrial applications.

5.3.3.1 Characterization of microgellosomes

The SEM imaging of microgellosomes (Figure 5.13) shows that they are hollow structures, 15 – 20 μm in size. This compares with an original microgel size of 670 nm. The implication therefore is that each microgellosome consists of 20 – 30 microgel particles. Also, there are some smaller particles in the background, these can be smaller microgellosomes or some unreacted singlet particles. The image in Figure 5.13 is consistent with what might be expected from a “gel globule” formed as a result of an addition reaction between the pendant vinyl groups as proposed in Figure 5.12.

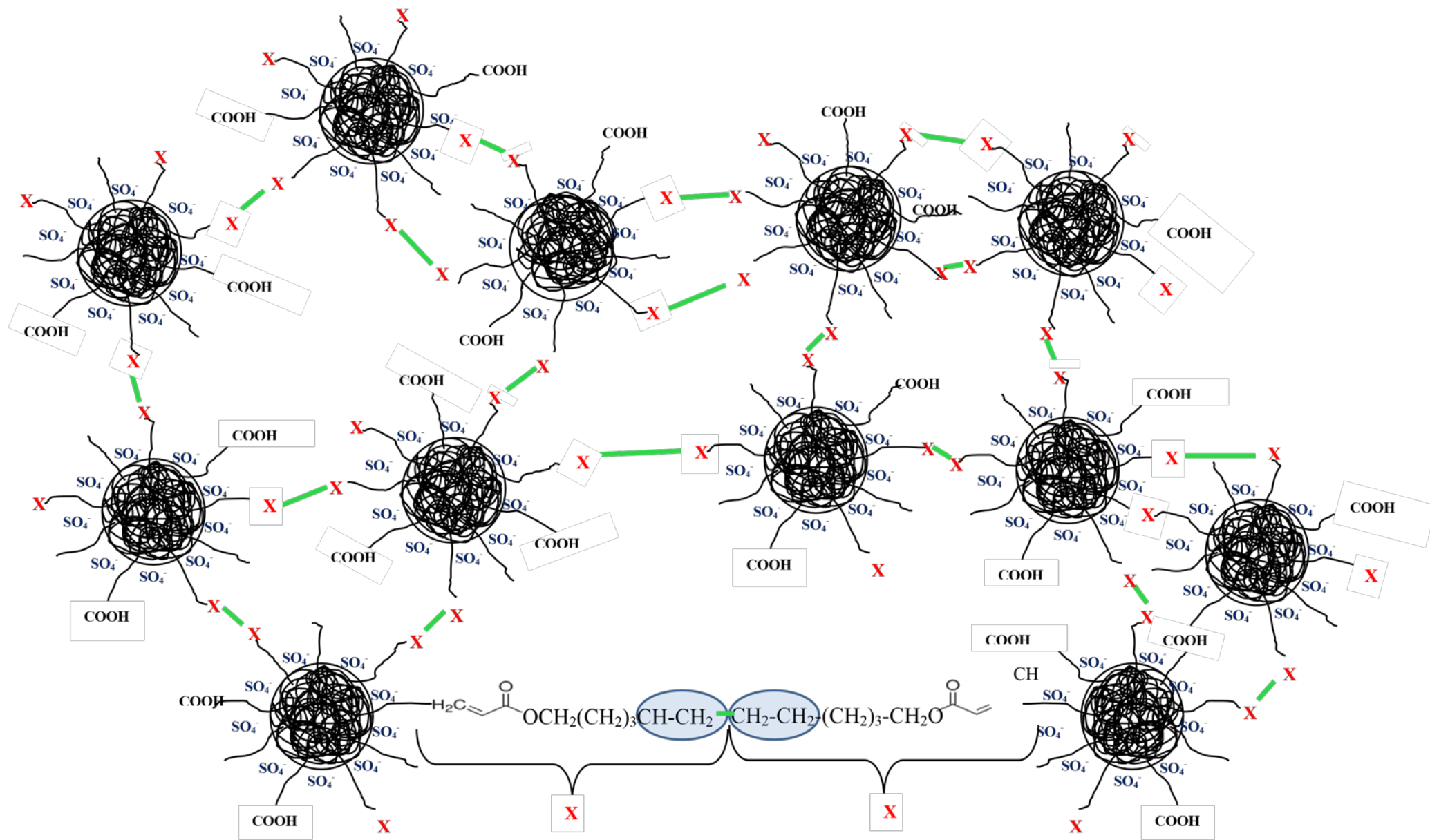


Figure 5.12 Representation of the molecular structure of microgelsomes

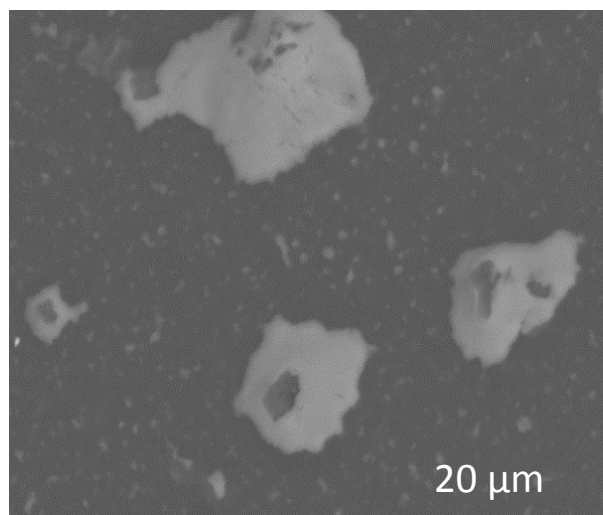


Figure 5.13 SEM image of microgellosomes formed by polymerizing p(NIPAM-co-5% AA)-hexenol

5.3.4 Characterization of emulsions stabilized by microgellosomes

The microgellosomes were used to stabilize a hexadecane-in-water emulsion. Figure 5.14 shows the formation of large droplets with average size of 20-30 μm. Both larger and smaller species (microgellosomes and/or particles) shown in Figure 5.13 may well be making a contribution towards the formation of emulsion droplets shown in Figure 5.14. It is not suggested that one species is more important than the other.

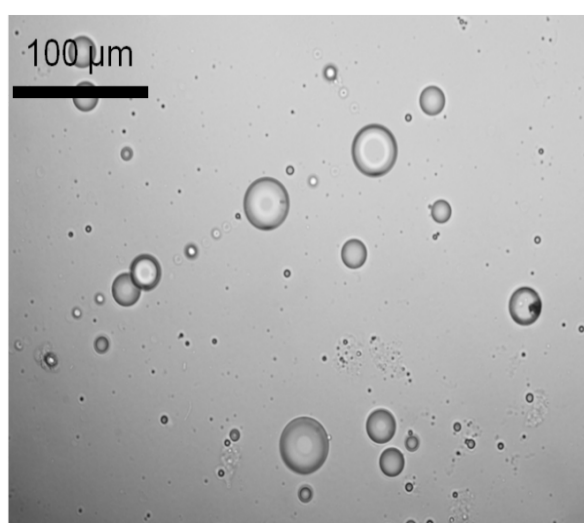


Figure 5.14 Optical microscopy image of microgellosomes (0.1 w/v) stabilized emulsion

5.4 Conclusions and future work

5.4.1 Conclusions

A novel particle p(NIPAM-*co*-5% AA)-hexenol was synthesized, characterized and tested for its ability to stabilize emulsions (using two different oils). The new particles are spherical in shape, negatively charged and show a larger size than p (NIPAM-*co*-5% AA). Furthermore, they still show temperature/pH sensitivity and mono-dispersity. The IR spectroscopy experiments suggest the chemical attachment of hexenol to the particles.

Oil-in-water emulsions (hexadecane or tricaprylin in water) could be stabilized by addition of p(NIPAM-*co*-5% AA)-hexenol. The stability of the emulsions increased with increasing the concentration of the microgel. The emulsions were stabilized by the formation of a layer of microgel at the oil-water interface. The emulsions were poly-dispersed, though droplet size of the dispersed phase was found to decrease with the increase in microgel concentration and the number of droplets increased with the increase in the concentration of the microgel. For the tricaprylin-in-water emulsion, a concentration of 0.3% w/v of the novel microgel particles managed to stabilize the emulsion for a week. In case of the hexadecane emulsion in water, 0.45% w/v microgel particles could show an increase in the emulsion stability and a decrease in the creaming. Higher concentrations are thought to further improve the emulsion stability.

The novel (p(NIPAM-*co*-5% AA)-hexenol) particles with a pendant vinyl group were also further polymerized in the oil-water interface of emulsion droplets to synthesize a new structure referred to as “microgelloosomes”. The SEM images of washed polymerized particles showed hollow capsules, which is typical for polymers produced for the interface of emulsion droplets. Since the novel particles have a hairy structure and their size is influenced by the temperature and pH change, we expect that the microgel capsules produced will inherit these properties and have a semi-permeable membrane. These enhanced properties would allow such particles to be used as pH and heat-responsive drug carriers.

5.4.2 Future work

Further research is required to tune the ability of the novel microgel particles and microgelloosomes to turn the emulsifying properties on and off in response to environmental triggers such as temperature and pH. More oils and concentrations can also be tried to

optimize the amounts and concentrations needed to obtain a stable emulsion. These concentrations are expected to vary according to the type and concentration of the oil used.

Also, further tests to investigate the potential applications of microgellosomes will be conducted. These include testing the encapsulation, loading and release capabilities of them (the microgellosomes). The ability of microgellosomes to deliver a loaded drug to a specific site will also be tested. This can be applied to the release of drug molecules in specific sites in the body.

5.5 References

1. Thorne J. B., Vine G. J., Snowden M. J. Microgel applications and commercial considerations. *Colloid and Polymer Science*. 2011;289:625-46.
2. International Union of Pure and Applied Chemistry. *Compendium of Chemical Terminology - Gold Book*. 2014.
3. Ngai T., Auweter H., Behrens S. H. Environmental Responsiveness of Microgel Particles and Particle-Stabilized Emulsions. *Macromolecules*. 2006;39:8171-7.
4. Attaa A. M., Dyab A. K., Allohedan H. A. A novel route to prepare highly surface active nanogel particles based on nonaqueous emulsion polymerization. *Polymers for Advanced Technologies*. 2013;24:986-96.
5. Li Z., Ngai T. Microgel particles at the fluid–fluid interfaces. *Nanoscale*. 2013;5:1399.
6. Zoppe J. O., Venditti R. A., Rojas O. J. Pickering emulsions stabilized by cellulose nanocrystals grafted with thermo-responsive polymer brushes. *Journal of Colloid and Interface Science*. 2012;369:202-9.
7. Tsuji S., Kawaguchi H. Thermosensitive Pickering Emulsion Stabilized by Poly(*N*isopropylacrylamide)-Carrying Particles. *Langmuir*. 2008;24:3300-5.
8. Chevalier Y., Bolzinger A. M. Emulsions stabilized with solid nanoparticles: Pickering emulsions. *Colloids and Surfaces A: Physicochemical and Engineering Aspects*. 2013;439:23-34.
9. Destribats M., Lapeyre M., Sellier V., Leal-Calderon E., Schmitt F., Ravaine V. Water-in-Oil Emulsions Stabilized by Water-Dispersible Poly(*N*-isopropylacrylamide) Microgels: Understanding Anti-Finkle Behavior. *Langmuir*. 2011;27:14096-107.

10. Destribats M., Wolfs M., Pinaud M., Lapeyre F., Sellier V., Schmitt E., Ravaine V. Pickering Emulsions Stabilized by Soft Microgels: Influence of the Emulsification Process on Particle Interfacial Organization and Emulsion Properties. *Langmuir*. 2013;29:1236774.
11. Destribats M., Lapeyre M., Wolfs V., Sellier M., Leal-Calderon E., Ravaine F., Schmitt V., Ravaine V. Soft microgels as Pickering emulsion stabilisers: role of particle deformability. *Soft Matter*. 2011;7:7689-98.
12. Mohsen R. Vine G. J., Majcen N., Alexander B. D., Snowden M. J. Characterization of thermo and pH responsive NIPAM based microgels and their membrane blocking potential. *Colloids and Surfaces A: Physicochemical and Engineering Aspects*. 2013;428:53-9.
13. Pelton R. Temperature-sensitive aqueous microgels. *Advances in Colloid and Interface Science*. 2000;85:1-33.
14. Vashist S. K. Comparison of 1-Ethyl-3-(3-Dimethylaminopropyl) Carbodiimide Based Strategies to Crosslink Antibodies on Amine-Functionalized Platforms for Immunodiagnostic Applications. *Diagnostics*. 2012;2:23-33.
15. Huang G. Synthesis and Study of Crystalline Hydrogels, Guided by a Phase Diagram. PhD thesis, University of North Texas; 2004.
16. Kammili V. R., Reddy G. M., Mukkanti K. Oxidation of alcohol to carboxylic acid under mild acidic condition and followed by synthesis of ester analogues of Corey's lactone. *Der Pharma Chemica*. 2011;3:141-5.
17. Soto-Castro D., Cruz-Morales J. A., Apan M. T., Guadarrama P. Synthesis of NonCytotoxic Poly(Ester-Amine) Dendrimers as Potential Solubility Enhancers for Drugs: Methotrexate as a Case Study. *Molecules*. 2010;15:8082-97.
18. Otera J., Nishikido J. Esterification: Methods, Reactions, and Applications. John Wiley & Sons; 2009.
19. Rose J. B., Pacelli S., El Haj A. J., Dua H. S., Hopkinson A., White L. J., Rose F. R. Gelatin-Based Materials in Ocular Tissue Engineering. *Materials*. 2014;7:3106-35.
20. Wu W., Chen S., Hu Y., Zhou S. A Fluorescent Responsive Hybrid Nanogel for Closed-Loop Control of Glucose. *Journal of Diabetes Science and Technology*. 2012;6:892-901.
21. Su S., Ali M. M., Filipe C. D., Li Y., Pelton R. Microgel-Based Inks for PaperSupported Biosensing Applications. *Biomacromolecules*. 2008;8:935-41.
22. Chiu P. L. Microwave Enabled Dispersion of Highly Conductive Carbon Nanomaterials and Their Interfacial Assemblies. PhD thesis, the State University of New Jersey; 2013.

23. Hu L., Serpe M. J. Poly(*N*-Isopropylacrylamide) Microgel-Based Etalons for Optical Sensing. *J Anal Bioanal Techniques*. 2012;3.
24. Peters J. T., Verghese S., Peppas N. A. Surface hydrolysis mediated PEGylation for the passivation of pNIPAM Nanogels. *Society for Biomaterials*; 2014.
25. Farooqi Z. H., Khan H. U., Shah S. M., Siddiq M. Stability of poly(*N*isopropylacrylamide-co-acrylic acid) polymer microgels under various conditions of temperature, pH and salt concentration. *Arabian Journal of Chemistry*. 2013.
26. Chen H., Fang Y. Synthesis and characterization of temperature and pH responsive Poly(*N*-isopropylacrylamide) copolymer. China: MOE Key Laboratory of Food Colloids and Biotechnology, School of Chemical & Material Engineering, Jiangnan University.
27. Luo Q., Guan Y., Zhang Y., Siddiq M. Lead-Sensitive PNIPAM Microgels Modified with Crown Ether Groups. *Journal of Polymer Science: Part A: Polymer Chemistry*. 2010;48:4120–7.
28. Hu X., Hao X., Wu Y., Zhang J., Zhang X., Wang P. C., Zou G., Liang X. J. Multifunctional hybrid silica nanoparticles for controlled doxorubicin loading and release with thermal and pH dual response. *J Mater Chem B*. 2013;1:1109.
29. Hexen-1-ol. <http://www.sigmaaldrich.com/spectra/ftir/FTIR003303.PDF>. Accessed on 2nd of December, 2015.
30. Lambert J. B., Shurvell H. F., Lightner D., Cooks R. J. Introduction to organic spectroscopy. Verbit L., editor. New York/London: Macmillan Publishing Company/Collier Macmillan publishers; 1987.
31. Lide, D. R. Handbook of Chemistry and Physics, 83rd Edition. 2002, London/New York, CRC Press.
32. Haynes, W. M. Handbook of Chemistry and Physics, 91st Edition. 2010, London/New York, CRC Press.
33. Mathapa B. G., Paunov V. N. Cyclodextrin stabilised emulsions and cyclodextrinosomes. *Physical Chemistry Chemical Physics*. 2013; 15, 17903-14.

Chapter Six Conclusions and Future work

6.1 Conclusions

Four novel NIPAM based particles have been designed, synthesized and characterized. These are p(NIPAM)-*co*-5% VC, p(NIPAM)-*co*-5% AA-EDA-RhB, p(NIPAM)-*co*-5% LY and p(NIPAM)-*co*-5% AA-hex. This work aims at designing and synthesizing particles that have practical application in different fields that have been theoretically studied for years such as drug delivery (1-5), biomedical applications (6-9) and responsive surfaces (10-12).

Different synthesis techniques have been undertaken in this work; for incorporating comonomers with a pendant vinyl group (VC and LY), direct polymerization was used. For incorporating hexenol using the alcoholic OH (to synthesize a particle with a pendant vinyl group), a two-step procedure was used. Acrylic acid (AA) was directly incorporated in the NIPAM based particle and then the COOH of AA was esterified with the OH of hexenol using click chemistry. For incorporating RhB, a three-step procedure was used, where p(NIPAM)-*co*-5% AA was synthesized, COOH of AA was coupled to one of the amino groups of EDA and then the other amino group was coupled to the COOH of RhB using click chemistry. Comparing the PDI of the four particles suggest that using a one-step direct polymerization technique yields more uniform and mono-dispersed particles with PDI very close to zero. Increasing the number of synthesis steps and elongating the hairy layer around the particle yields less uniform and poly-dispersed particles with higher PDI values.

In the first results chapter, a novel fluorescent temperature-sensitive microgel particle (p(NIPAM)-*co*-5% VC) with a VPTT of 32-35°C was synthesized and characterized using DLS and fluorescence spectroscopy. At 15°C (below the VPTT), the particle size is 290 nm and deswells to 160 nm when the temperature exceeds the VPTT. The emission spectra of the novel microgel dispersion excited at 300 nm show a similar emission wavelength to that reported for VC (13). The emission (at 350 nm) of a known particle concentration (w/v) excited at 300 nm increases by increasing the temperature above the VPTT. This shows that both the size and fluorescence of the novel particle are temperature sensitive.

p(NIPAM)-*co*-5% VC was used to quantify the mass of microgel particles deposited on different solid surfaces, these are stainless steel, glass pre-treated with base, glass pretreated

with acid, quartz, gold, Teflon (the composition of the surfaces was determined using EDX). The results show that at 25°C, the highest net mass of microgel particles (adsorbed minus desorbed) was adsorbed on stainless steel, followed by glass pre-treated with base, glass pre-treated with acid, quartz, gold then Teflon. At 45°C, the mass of adsorbed microgel particles on all the previously mentioned surfaces increased. The order from the surface of highest net adsorbed mass of microgel particles is: stainless steel, glass pre-treated with base, gold, glass pre-treated with acid, quartz then Teflon.

The factors affecting the adsorption/desorption of cationic microgel particles on/from the solid surfaces were studied. These include the effect of solid surface charge, surface roughness (studied using AFM), temperature and hydrophilicity/hydrophobicity of the surface. Results show that the effect of the solid (substrate) surface charge is the most significant followed by that of surface roughness then temperature. On the other hand, the effect of hydrophilicity/hydrophobicity of the surface showed to be the least significant of the studied factors.

In the second results chapter, a fluorescent temperature/pH responsive particles (p(NIPAM)-*co*-5%AA-EDA-RhB) was presented. The synthesis of this particle was carried out using a three-step procedure. Step one was the synthesis of p(NIPAM)-*co*-5% AA. Step two was the coupling of the COOH of AA to one of the amino groups of EDA. Step three was coupling the second amino group of EDA to RhB using coupling chemistry. The particle is zwitterionic due to the presence of both negative (due to initiator and AA) and positive (due to EDA) charges on its surface. At 15°C, the particle size is 500 nm and deswells to 250 nm when the temperature exceeds the VPTT. The particles are more stable in highly alkaline pH media (pH 11.5). At lower pH values the particles tend to aggregate. This can be attributed to the presence of opposite charges due to unreacted moieties of AA and EDA. Changing the pH of the media changes the protonation state of these moieties which affects their reactivity and hence particle stability. The particles are negatively charged with an initial electrophoretic mobility of $-2 \mu\text{mcm/Vs}$ at 15°C. The microscopy images show that the particles are spherical in shape. It is also apparent from the pictures that there are bridges between the particles. This can be attributed to the long hairy structures on the surface of the particles due to the conjugation of two molecules (EDA and RhB). The suggested applications of the novel particles include the stabilization of emulsions and drug delivery.

In the third results chapter, p(NIPAM)-*co*-5% LY particle was synthesized, characterized and its toxicity on HeLa and Vero cells was studied *in vitro*. The fluorescent probe LY was chosen to be incorporated in p(NIPAM) particles due to the presence of a pendant vinyl group in its molecular structure which makes it easy to polymerize. Negatively charged fluorescent temperature/pH sensitive particles were produced. At 15°C and pH 7, the size of the particle was 250 nm particle size is smaller than p(NIPAM) due to incorporating a hydrophobic co-monomer), increasing the temperature to above the VPTT, the particle deswells to 100 nm. The electrophoretic mobility of the particles at 15°C is $-0.3 \mu\text{mcm/Vs}$ and increases to $-3.7 \mu\text{mcm/Vs}$ when the temperature exceeds the VPTT. The fluorescence spectroscopy data of the novel particles suggest the successful incorporation of LY. The fluorescence emission spectra of the new particles compares to that of LY (with a slight blue shift of the emission peak due to the change of the environment surrounding the fluorescent probe LY). The data also show that the fluorescence of the particles is affected by the change in temperature and pH. This can be due to the change in particle size and/or the change in LY properties with the environmental change. The microscopy studies show that the particles are fluorescent, spherical, mono-dispersed and their average size is 120 nm which is comparable to that shown by DLS at deswollen state.

A fluorescent temperature/pH sensitive system such as the one presented in this work (p(NIPAM)-*co*-5% LY) can be very useful in various biological applications such as diagnosis and drug delivery or both combined together. The use of these particles in biological applications have been frequently challenged because of their suggested toxicity problems especially that they include acrylamide. Also very few data have been reported in literature about this topic. Accordingly, the study hereby provides some data that aim to assess the toxicity of NIPAM based particles *in vitro*.

The toxicity of different concentrations of the novel particles (p(NIPAM)-*co*-5% LY, as well as the 100% p(NIPAM) and the main monomer NIPAM was tested on two cell lines (HeLa and Vero). The toxicity was tested in comparison to a positive control (dextran) and a negative one (poly(ethylenimine)) (PEI). The results show that the two particles show cell viability over 80% (for both cell lines HeLa and Vero) up to a concentration of 3 mg/mL while NIPAM monomer showed cell viability over 80% at a concentration equal to or less than 0.3 mg/mL. The comparison between the results of this study as well as some reported

data from the literature with some existing drugs in the market, suggests the need for further work to establish the viability of utilizing particles of this type for pharmaceutical applications.

The fourth chapter is about p(NIPAM)-*co*-5% AA-hex particle with a pendant vinyl group that enables further crosslinking of the particles to produce bigger structures referred to as “microgelloosomes”. Both the particles and the microgelloosomes (including hydrophilic and hydrophobic moieties) were used to stabilize oil-in-water emulsions. To polymerize hexenol and keep its vinyl group free (unreacted), a new synthesis method was carried out. This was the synthesis of p(NIPAM)-*co*-5% AA using surfactant free emulsion polymerization and then esterifying the COOH of AA to the alcoholic OH of hexenol.

The novel particle (p(NIPAM)-*co*-5% AA-hex) is negatively charged and is responsive to both temperature and pH having an initial particle size (at 15°C) of 680 nm. Increasing the temperature to above the VPTT, the particle deswells to 280 nm. At 15°C, the electrophoretic mobility of the particles is $-1.7 \mu\text{mcm/Vs}$ while above the VPTT it increases to reach $-3.3 \mu\text{mcm/Vs}$. The microscopy images show that the particles are spherical and mono-dispersed.

The new particles with a hydrophilic co-monomer (AA) as well as a hydrophobic one (hexenol) were used to stabilize emulsions. Oil-in-water emulsions using two different oils (tricaprylin and hexadecane) and different concentrations of the new particles were prepared. At lower concentrations of the particles (0.1% w/v), two different phases were observed. Increasing the particle concentration (to about 0.3% w/v for tricaprylin and 0.45% w/v for hexadecane) showed a significant increase in the emulsion stability (persistent for a week) suggesting that the particles were successfully adsorbed at the oil/water interface.

6.2 Future work

Research in the field of environmentally responsive colloidal polymeric particles is growing. This is because of the possibility of using these particles in different fields such as medical, pharmaceutical, industrial and environmental applications. Also, there are various factors that affect the synthesis, properties and applications of the particles. There are more than

one suggested area of research for future work to further understand the properties and possible applications of different colloidal particles such as the NIPAM based ones. These include:

- New fluorescent environmentally responsive NIPAM based particles may be designed by incorporating different kinds and concentrations of co-monomers. These can be temperature sensitive or other triggers such as pH and photosensitivity can also be added (synthesizing particles with more than one comonomer). Different fluorescent probes with different excitation and emission wavelengths as well as fluorescence intensities will also be tried as co-monomers, examples of suggested fluorescent probes can include fluorescein *isothiocyanate*. The use of the new particles in diagnostics, drug delivery as well as industrial applications will be studied.
- The deposition of new NIPAM based particles on different solid surfaces such as glass, gold, stainless steel and Teflon in response to different stimuli may be carried out. Surfaces responsive to different environmental triggers such as pH and light will be produced and studied. Such surfaces can have a lot of applications in the industrial field as well as diagnostics and biotechnology (control of protein and cell adhesion and bio-separation).
- The improvement of the pH sensitivity of p(NIPAM)-*co*-5% LY particles (chapter three), particles with more than one co-monomer (p(NIPAM) co-polymerized with both lucifer yellow and acrylic acid or other ionisable co-monomers) can be designed. This aims at improving the ability of the particles to differentiate between acidic and alkaline media and accordingly differentiate between the cancer cells (which normally have low pH) and the the normal cells.
- To support the suggestion of using NIPAM based particles in drug delivery and other biomedical applications, further toxicity studies should be carried out. This could include more *in vitro* testing than the ones presented in chapter three (p(NIPAM)-*co*-5% LY) and *in vivo* animal testing. Toxicity studies including other NIPAM

based particles such as p(NIPAM), p(NIPAM)-*co*-vinyl cinnamate and p(NIPAM)-*co*-acrylic acid might also be conducted.

- The uptake and release profiles of different drugs from NIPAM based particles will be studied. Drugs with different hydrophilicities/hydrophobicities will be tried. This will include the quantification (stoichiometric studies) of the weights of drugs absorbed and/or released by a specific weight of particles.
- The effect of time on the stability of NIPAM based particles should be studied. This includes the identification and quantification of degradation products of these particles.
- Study the possibility of attaching different co-monomers to NIPAM particles using different techniques such as coupling chemistry. This may make it more likely to increase the use of a wider range of co-monomers which can lead to the synthesis of particles responsive to different triggers. Accordingly, more applications to environmentally responsive microgel particles such as NIPAM based ones may then emerge.

6.3 References

1. Pinkrah V. T., Beezer A. E., Chowdhry B. Z., Gracia L. H., Cornelius V. J., Mitchell J. C., Castro-Lopez V., Snowden M. J. Swelling of cationic polyelectrolyte colloidal microgels: Thermodynamic considerations. *Colloids and Surfaces A- Physicochemical and Engineering Aspects*. 2005;262:76-80.
2. Ramkissoon-Ganorkar C., Liu F., Baudys M., Kim S. W. Modulating insulin release profile from pH thermosensitive polymeric beads through polymer molecular weight. *Journal of Controlled Release*. 1999;59:287-98.

3. Castro Lopez V., Hadgraft J., Snowden M. J. The use of colloidal microgels as a (trans)dermal drug delivery system. *International Journal of Pharmaceutics*. 2005;292:137–47.
4. Wu W., Chen S., Hu Y., Zhou S. A Fluorescent Responsive Hybrid Nanogel for Closed-Loop Control of Glucose. *Journal of Diabetes Science and Technology*. 2012;6:892–901.
5. Ravaine V., Ancla C., Catargi B. Chemically controlled closed-loop insulin delivery. *Journal of Controlled Release*. 2008;132:2-11.
6. Yasui M., Shiroya T., Fujimoto K., Kawaguchi H. Activity of enzymes immobilized on microspheres with thermosensitive hairs. *Colloids and Surfaces B-Biointerfaces*. 1997;8:311-9.
7. Kondo A., Oku S., Higashitani K. Adsorption of gamma-globulin, a model protein for antibody on colloidal particles. *Biotechnology and Bioengineering*. 1991;37:537-43.
8. Kitano H., Nakamura K., Hirai Y., Kaku T., Ise N. Restricted diffusion effect on the binding of proteins to porous polymer resins as studied by repetitive injection method. *Biotechnology and Bioengineering*. 1988;31:547-52.
9. Pelton R. Temperature-sensitive aqueous microgels. *Advances in Colloid and Interface Science*. 2000;85:1-33.
10. Alarcon C. D., Farhan T., Osborne V. L., Huckb W. T., Alexander C. Bioadhesion at micro-patterned stimuli-responsive polymer brushes. *Journal of Materials Chemistry*. 2005;15:2089–94.
11. Burkert S., Bittrich E., Kuntzsch M., Muller M., Eichhorn K. J., Bellmann C., Uhlmann P., Stamm M. Protein Resistance of PNIPAAm Brushes: Application to Switchable Protein Adsorption. *Langmuir*. 2010;26:1786–95.
12. Qin L., He X. W., Zhang W., Li W. Y., Zhang Y. K. Macroporous thermosensitive imprinted hydrogel for recognition of protein by metal coordinate interaction. *Anal Chem*. 2009;81:7206–16.
13. Torres J. M. Designing dual thermoresponsive & photoresponsive materials for biomedical applications: MSc. thesis. McMaster University: 2011.